Tuning the activity of supported metal catalysts

Thesis submitted in accordance with the requirement of Cardiff University for the degree of Doctor of Philosophy

Margherita Macino

School of Chemistry
Cardiff University

2019

APPENDIX 1 - STATEMENTS AND DECLARATIONS TO BE SIGNED BY THE CANDIDATE AND INCLUDED IN THE THESIS

STATEMENT 1 This thesis is being submitted in partial fulfilment of the requirements for the degree of PhD

Signed _(signature)_

Date _____

STATEMENT 2

This work has not been submitted in substance for any other degree or award at this or any other university or place of learning, nor is it being submitted concurrently for any other degree or award (outside of any formal collaboration agreement between the University and a partner organisation)

Signed _(signature)_

Date _____

STATEMENT 3

I hereby give consent for my thesis, if accepted, to be available in the University's Open Access repository (or, where approved, to be available in the University's library and for inter-library loan), and for the title and summary to be made available to outside organisations, subject to the expiry of a University-approved bar on access if applicable.

Signed _(signature)_

Date _____

DECLARATION

This thesis is the result of my own independent work, except where otherwise stated, and the views expressed are my own. Other sources are acknowledged by explicit references. The thesis has not been edited by a third party beyond what is permitted by Cardiff University's Use of Third Party Editors by Research Degree Students Procedure.

Signed _(signature)_

Date _____

Abstract

This research intends to explore strategies able to modify the activity of heterogeneous catalysts, in order to draw structure-activity relationships and gain an improved understanding of the catalytically active sites. Different approaches have been attempted, such as applying an activation treatment, modifying the metal loading, changing the support and adding organic ligands. These methods have been applied to supported noble metal nanoparticles of Pt, Pd and bimetallic AuPd, which have been previously found active for liquid-phase hydrogenation and oxidation reactions such as the reduction of nitro compounds and the oxidation of alcohols. Several characterisation methods were applied to study the structure and properties of these materials.

First, a Pt/TiO_2 catalyst for the selective hydrogenation of 3-nitrostyrene has been developed by optimising the effect of the variation of metal loading and heat treatment. In particular, a series of catalysts were prepared, tested and characterised, showing that combining the choice of metal loading (from 0.05 to 0.5%Pt) and activation treatment (reduction or calcination followed by reduction at 450 °C) leads to what shows to be the most active catalyst reported so far. The data acquired by several characterisation techniques such as STEM, XPS, XAS and CO adsorption led to the conclusion that particle size and distribution as well as the environment surrounding the active site affect the catalytic activity and a delicate balance between them needs to be achieved.

Then, the role of the support on the catalytic activity of AuPd nanoparticles for the oxidation of glycerol was investigated. Different hydrothermal carbon materials, which derive from biomass and presenting different structural and elemental characteristics were applied as supports. Overall, the amount of oxygen in the structure as well as the curvature of the surface of the hydrothermal carbons showed to have an effect on the glycerol conversion either due to the variation in electron mobility that would favour adsorption of the reactants, or to the strain arising from the lattice mismatch at the metal-support interface.

At last, N-heterocyclic carbene ligands were added to a 1% Pd/TiO_2 catalyst. The presence of the ligand on the surface of the catalyst has been confirmed and found to be in both a neutral and protonated form. The results obtained by testing these catalysts for the hydrogenation of 3-nitrostyrene and the direct synthesis of hydrogen peroxide suggest that catalytic performance can be affected by either a geometric effect, where active sites are blocked, or by an electronic effect, due to the electronic interaction of the ligands and the Pd nanoparticles.

Overall, to develop catalytic materials and improve industrial processes, the reactivity of nanoparticles needs to be maximised, by using strategies that tune their structural and electronic properties.

Acknowledgments

Glossary

3-EA	3-Ethylaniline
3-EN	3-Ethylnitrobenzene
3-NS	3-Nitrostyrene
3-VA	3-Vinylaniline
ATR	Attenuated total reflectance
BET	Brunauer Emmett Teller
CO	Carbon monoxide
DAD	Diode array detector
EXAFS	Extended X-ray absorption fine structure
FID	Flame ionisation detector
GC	Gas chromatography
GC-MS	Gas chromatography- Mass spectrometry
H_2O_2	Hydrogen peroxide
HAADF-TEM	High-angle annular dark-field scanning electron microscopy
HPLC	High performance liquid chromatography
HTC	Hydrothermal carbon
ICP	Inductively coupled plasma
IR	Infrared
PSD	Particle size distribution
RID	Refractive index detector
SEM	Scanning electron microscopy
TCD	Thermal conductivity detector
TEM	Transmission electron microscopy
TGA	Thermogravimetric analysis
TiO_2	Titania
TOF	Turnover frequency
XANES	X-ray near edge spectroscopy
XAS	X-ray absorption spectroscopy
XPS	X-ray photoelectron spectroscopy
XRD	X-ray diffraction

Table of Contents

Chapter

1

Introduction

1.1   Introduction to heterogeneous catalysis

From the ancient times, when the fermentation of the sugars contained in the grapes to produce alcohol was introduced, catalysis has been omnipresent in the development of our society. In the annual review of 1836, the Swedish chemist J. J. Berzelius was the first to use the term catalysis, indicating and correlating different homogeneous and heterogeneous systems where a catalytic phenomenon was indeed taking place but yet not described.[1] Since that definition, a lot of research has been carried out in order to develop processes able to supply goods to a growing population and an advancing society.

Some well-known examples of how catalytic processes have helped developing the chemical industry in the last century are the Haber-Bosch process for the synthesis of ammonia, which from the 1913 allowed a synthetic way to fixate nitrogen and opened up to the production of explosives but most importantly of fertilisers, necessary in a growing modern society. Later, in the 1920's, the development of fluid catalytic cracking in the treatment of heavy petroleum oils for the production of fuels permitted the use of the highly energetic fossil fuels that were found in nature. By the end of the 1960's the introduction of catalytic converters in the automotive industry for the control over atmosphere pollution became indispensable since the pollution in big cities had become a crucial issue and a direct consequence of the growth of modern society.

If the advances in catalysis and industrial development were at first answering the increasing request of growing economies and population, later they had to face the environmental issues that such intensive production involved. Waste emission leading to water, air and land pollution and uncontrolled use of limited natural resources resolving in what has been defined in recent years as global climate change. For this scope, scientific research has focussed in increasing the knowledge and the technology to address these problems and in the last 20 years the introduction of the concept of "green chemistry" has opened to a new field of research,[2] where overall specific attention is given to:

1. Decreasing waste.
2. Use of non-toxic solvents, reagents and auxiliaries.
3. Increase the atom economy of each reaction.

4. Use of renewable feedstocks.

5. Designing energetically efficient processes.

Nowadays catalysts are widely used in order to make the majority of the industrial processes feasible from a point of view of temperature and pressure. In fact, the most important characteristic of a catalyst is the ability to decrease the activation energy required to achieve the formation of the products, hence increasing the rate of a reaction (Figure 1.1). Though the reaction kinetics are modified, the equilibrium of the process remains unchanged, hence the thermodynamics are the same as for the uncatalysed reaction. More specifically, a catalyst is defined as a substance that participates in a particular chemical reaction, increasing its rate and without being itself modified during the process.[3]
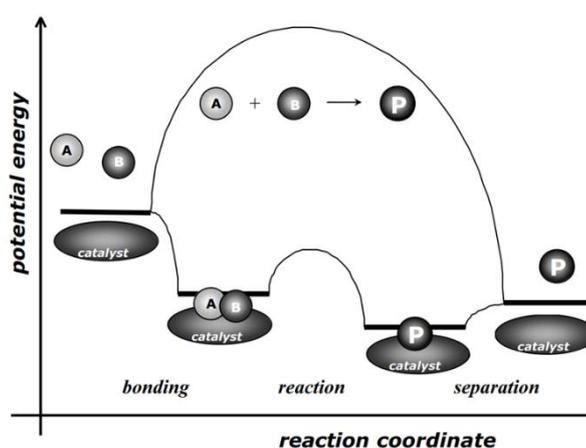
Figure 1.1 Schematic energy level diagram comparing a catalytic reaction to an un-catalysed reaction. Taken from reference [4].

The other important feature that makes a catalyst so appealing is the small quantity required (orders of magnitude smaller) compared to the reactants, avoiding non-catalytic stoichiometric amounts of additives in the reaction system. This point gains strong impact when considering the large volumes of reagents used in industrial processes and how unpractical would it be to deal with uncatalytic stoichiometric amounts of additives that would need to be recovered, separated or neutralised after the process. As we will discuss more in detail later, the possibility of using reduced amounts of catalytic substances is extremely economically convenient when the substances contain rare and precious metals such ruthenium, rhodium, palladium or platinum.

Different types of catalysis exist: homogeneous catalysis sees the interaction of a substrate with a catalyst, both in the same phase (usually liquid). Examples are organometallic complexes, which are synthesised with use of a metal atom centre, coordinated to specific ligands that not only stabilise the metal, but also direct the reacting molecules achieving the desired products. These catalysts are often applied in the synthesis of delicate compounds like pharmaceuticals, where large organic molecules undergo transformation and high selectivity is required. The

presence of both reactants and catalyst in the same phase makes it however difficult to use such technology in large scale, where separation becomes an issue.

The naturally occurring, extremely complex molecules and specific catalyst that are enzymes often inspire these organometallic systems. An enzyme could be described as a large protein, the structure of which is a highly shape-specific active site that interacts and guides the substrate towards the optimum orientation for reaction. Enzymes are extremely efficient and highly specific catalysts, fundamental for the numerous reactions taking place in every living organism and controlling the metabolism.

Both homogeneous and enzymatic catalysis are characterised by high structural specificity aimed at favouring the orientation of the substrate as it approaches the reactive site, as schematically shown in Figure 1.2. This feature does not only limit the interaction to specific reactants or group of molecules, but also leads to very high selectivity toward the desired products.[5]
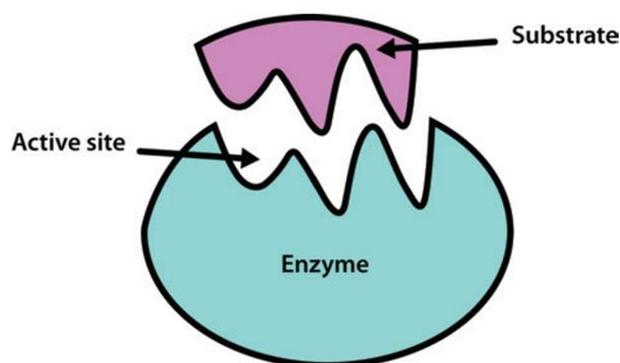
Figure 1.2 Schematic representation of the specific interaction between an enzyme and the substrate. Taken from reference [5].

In heterogeneous catalysis, generally solid materials favour the reaction between species in the liquid or gaseous phase. Hence, the reaction occurs at the surface of the solid, or in the pores if there are any. This type of catalysis is highly preferred in industrial applications, as easy separation of the catalytic material from the reaction mixture can be done after reaction.

In a typical heterogeneous process, the reactants approach the catalyst, adsorbing on its surface. The reaction takes place with formation of the products, which desorb form the catalyst, allowing the catalytic cycle to repeat (Figure 1.3). The interaction between the substrate and the catalyst should satisfy the Sabatier's principle. According to this principle, the adsorption is required to be strong as that the chemisorption of the molecules occur favourably. However, the strength of such interaction should not be too strong, otherwise no desorption after reaction would take place, obtaining low products selectivity as further reaction steps might take place, together with poisoning of the catalyst and blocking of the catalytic cycle.
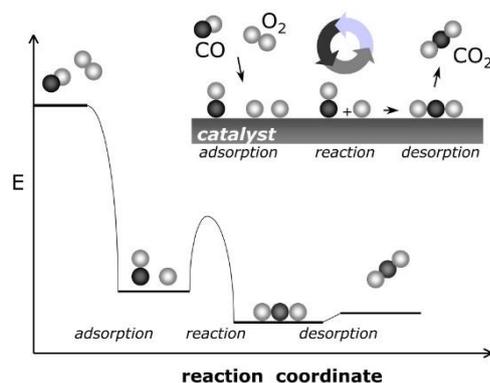
Figure 1.3 Schematic representation of the reaction cycle and potential energy for the catalytic oxidation of CO to CO_2 using O_2 as oxidant. Taken from reference [4].

These solid catalysts can be oxides or mixed metal oxides, however another large branch of heterogeneous catalysis is composed by nanometre-sized particles of expensive rare metal such as gold, palladium or platinum supported on an inert material whose function is to anchor the metal to its surface, avoiding sintering or loss of the precious metal during reaction. A catalyst's support should be characterised by properties such mechanical strength, resistance to dissolution or disintegration and show the ability to act as a carrier on the surface of which the catalytic species can be distributed as well and uniformly as possible in order to have a homogenously distributed catalyst where the surface area available for the reactants is maximised. The large request of chemicals at the global scale sees the necessity of using catalytic materials that are resistant to the reaction conditions, stable and reusable.

When using supported metal catalysts, small metal particles (generally in the nanometre range) need to be formed in order to increase at the maximum the amount of surface area of the metal available to the reactant and for this reason single atom heterogeneous catalysts are of great interest because of the high atomic efficiency of the metal (Figure 1.4).[6]

Total atoms: 10
Surface atoms: 10
Percent surface: 100%

Total atoms: 92
Surface atoms: 74
Percent surface: 80%

Total atoms: 792
Surface atoms: 394
Percent surface: 50%
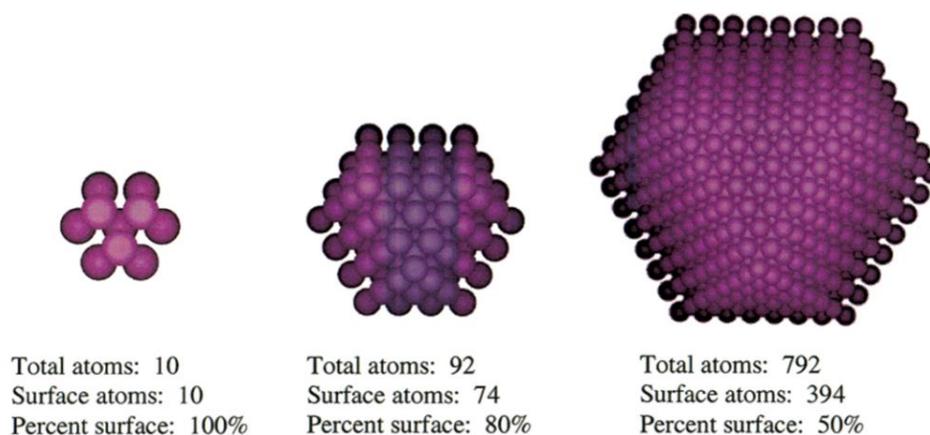
Figure 1.4 Schematic depiction of the variation of the fraction of surface atoms with increasing number of atoms in a nanoparticle. Taken from reference [7].

Another important reason for using small metal particles is that the intrinsic characteristics of the metal change deeply when comparing a bulk metal (especially in the case of noble metals, which are highly stable and unreactive materials), to the corresponding nanometre-sized particle (nanoparticle or NP). In fact, from the characteristic overlapping and continuous band of electronic structure in a solid metal, a separation and formation of discrete electronic energy levels occurs as the metal particles decrease in size, as depicted in Figure 1.5. If in the metal the electrons can easily move within the conduction band, once the material is broken down to form small particles, the electronic states separates and the electrons are confined, more similar to a molecular system than a bulk metal. Hence, small metal particles show different electronic and physical properties from their bulk counterparts.[8]
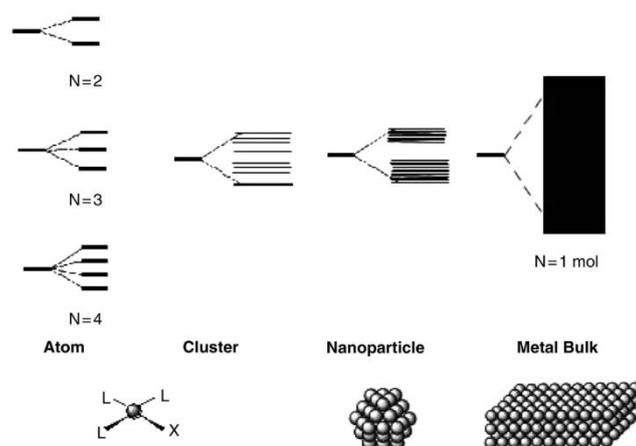
Figure 1.5 Electron levels of atoms, clusters, nanoparticles and bulk metal. Taken from reference [9].

Because metal species at the surface of a nanoparticle present fewer bonds compared to bulk atoms, they are defined as low-coordinated and are more reactive since they are prone to minimize the high surface free energy that characterises them by filling their coordination sphere. Therefore, as the surface energy increases with decreasing particle size, the melting point of small metal nanoparticle is significantly lower than the corresponding bulk solid. In fact, physicochemical variations occur because a large percentage of atoms appear on the surface. These exposed species tend to be very reactive due to their low coordination, leading upon others, to unexpected catalytic activity.[10-11]

In contrast to enzymes and homogenous catalysts where a specifically reactive centre is present, when using heterogeneous catalysts, a more complicated and inhomogeneous structure is present and needs to be investigated in order to fully understand how the system behaves. As mentioned before, some catalysts are formed of mixed metal oxides species, where crystalline complex structure are formed, such as in the example of the so called M1 structure of the $MoVTeNbO_x$ catalyst to be used in the ammoxidation or oxidation of propane to produce

acrylonitrile or acrylic acid respectively (Figure 1.6).[12] The point in the structure where the substrate interacts with the catalyst and is activated, allowing the chemical transformation to occur, is named catalytic active site. The identification of the active site for a specific reaction, taking place using a specific catalyst, is an important focus of research nowadays, since often these complex materials are not fully understood, while being found active for specific catalytic processes.
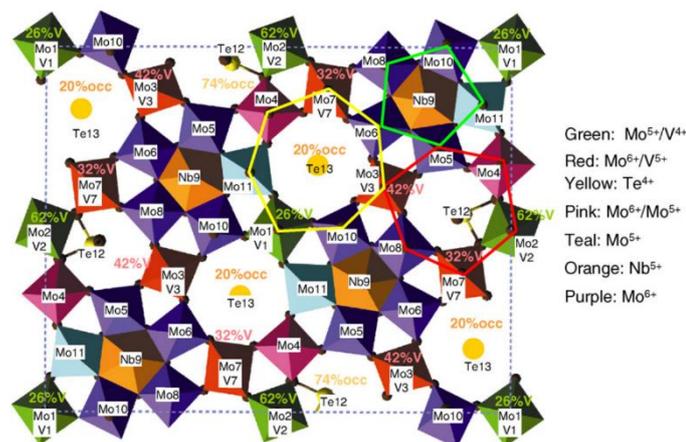
Figure 1.6 Rendering of the model M1 structure of MoVTeNb mixed metal oxide. Image taken from reference [13], based on data from reference [14].

As for mixed metal oxides, supported metal catalysts are widely applied in industrial processes and the complexity of the structure plays a crucial role in the final activity of these solids. As depicted in Figure 1.7, a variety of low coordination metal sites can be identified and not all have necessarily the same reactivity since some catalytic reactions show dependence on the type and amount of specific species.
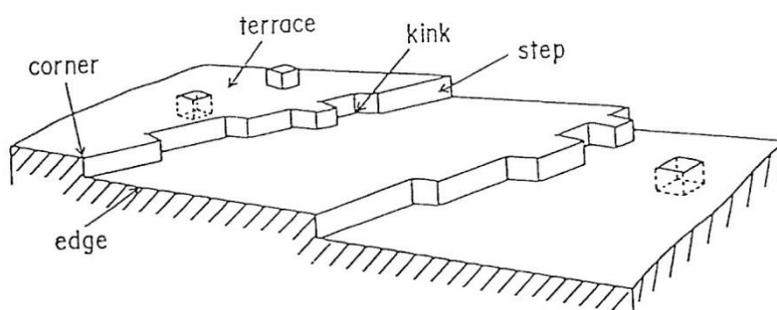
Figure 1.7 Schematic microscopic view of a metal surface. Taken from reference [15].

Because of the complexity of heterogeneous catalysts, one way of understanding how a real catalyst works, is to prepare a simplified material with known characteristics, such as uniform and defined structure or crystalline metal or support. In a similar fashion, by computational means, it is possible to design and develop simplified systems in which structural and electronic characteristics are known. In the last decades, computational chemistry has become a very useful tool in the design and prediction of materials with desired features, which in the future, could

possibly become a fundamental tool in the production of catalysts for real applications.[16] By this means, the preparation and thorough study of so-called "model" catalysts has helped in determining of specific structures and correlating them to the catalytic activity.[17]

For long time catalysis research was conducted on a basis of trial and error empirical method, however with improving theoretical methods and characterisation techniques, as well as *in-situ* and *in operando* analytical methods, it became easier to understand what is happening at the atomic level on the catalyst and in the presence of the reactants. Allowing a deeper understanding of how a catalyst works and giving the opportunity to improve the performance by selectively tune the final structure of the material.

Overall, without catalysis, many common reactions of the chemical industry would not be feasible and many other processes would not be economical. Still, more efforts need to be put in the research and development of materials that allow the production of chemicals in an efficient, economic and environmentally friendly way.

In a catalyst, complex structures can be found, but the active sites are the centre of interest, therefore a lot of research efforts are put towards their identification and improvement. In the following section will be presented some examples of the research that has been conducted in the field of heterogeneous supported metal catalysis for both oxidation and hydrogenation reactions. More specifically, the study of how the performance of such nanomaterials has been investigated, modified and tuned by tailoring electronic and geometrical characteristics by means of various method will be discussed.

1.2 Tuning the reactivity of supported metal catalysts by understanding the catalyst characteristics

Generally, a supported metal catalyst consists in large part of an inert carrier material (the support, that alone would not catalyse the reaction), whereas the active metal constitutes only a small percentage of the total. Therefore, most of the surface of a supported metal catalyst is inactive, while only few and possibly homogeneously distributed sites exhibit catalytic activity. At these sites, the reactant molecules interact with the catalyst through chemisorption.

From homogeneous catalysis, it is known that depending on how the substrate approaches the catalyst, a different side of the molecule could be facing the active site, as depicted in Figure 1.2, leading to differences in reactivity. The presence of ligands and the formation of metal-organic complexes play an extremely important role in homogeneous catalysis in the creation of a specific

geometric and electronic environment that overall directs towards the desired molecular configuration.

A similar consideration should be applied for supported metal catalysts. Although ligands are generally not present, the environment that the substrate should face when moving towards the active site should be designed in such way that the preferential adsorption of the desired reactive group should lead to its higher reactivity and favour a specific reaction pathway over an alternative other. To maximise the activity of the often-used noble metal catalysts, uniformity in the species present on the surface of the support is required. In fact, if species in different oxidation states, particle size and exposure are available, understanding which reaction occurs on a specific site is challenging due to the inhomogeneity of the system. In addition, the presence of potentially inactive but expensive material is not desirable. Therefore, it is preferred to develop a preparation procedure that allows primary formation of the ideal active site aiming to decrease the occurrence of unwanted side-reactions and increase products selectivity.

The nature of the active sites, the structure of the nanoparticles and the way a substrate interacts with the catalyst surface is still a debate for many catalytic transformations. Here, different approaches and strategies applied in the tuning of the activity of heterogeneous catalysts will be introduced. During this PhD work, three main projects have been developed around the study of the structure-activity relationships in materials for liquid phase catalytic reactions. The results of the three branches of the research work are reported in the discussion Chapters 3, 4 and 5. The work presented in Chapter 3 explores the effect that different heat treatments and metal loading have on Pt/TiO_2 catalysts used for the chemoselective hydrogenation of substituted nitro compounds. In Chapter 4, the effect of the use of a variety of carbonaceous supports has been investigated for the oxidation of glycerol. At last, in Chapter 5 the possible effect on the catalytic activity of palladium supported catalysts by addition of organic ligands has been studied.

The main topics and approaches applied during this research work will introduced more in detail in the following sections.

1.2.1   Tuning the catalytic properties by support effects and metal-support interactions

The support is inert in respect to the reaction, and it is chosen based on the stability that gives to the supported metal nanoparticles, avoiding leaching and sintering during reaction. When, during metal deposition or impregnation, the metal comes in contact with the support, a bond is formed, creating an electronic interaction between the two species which inevitably affects their electronic density. Since small quantities of nanometre-sized particles are bonded to a much larger amount of support material, the effect of the electronic change should be expected to be more evident on the former. This interaction is reflected in the variation in catalytic activity and

selectivity of metal nanoparticles supported on different materials.[18] For example, the use of different oxide supports has shown to lead to different catalytic activity and selectivity in the selective oxidation of benzyl alcohol to benzaldehyde (Figure 1.8).[19] It has been suggested that whereas an electronic effect is induced by the formation of a bond between a support and a nanoparticle,[20] also a shaping and faceting effect has been observed as consequence of the influence of the support on the nanoparticle formation.[21]
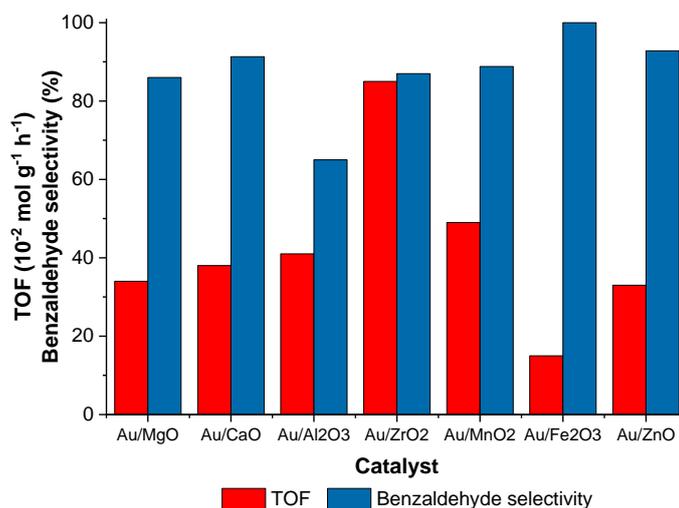
Figure 1.8 Effect of the support on the activity and selectivity of Au based catalysts for the oxidation of benzyl alcohol to benzaldehyde. Data redrawn from reference [19].

Not only the type of support, based on the acid-base properties, hydrophobicity and reducibility among others, but also the type of structure may have an effect on the supported nanoparticle characteristics. For example, it has been investigated how the support induces strain in the metal nanoparticles due to mismatch of the structural lattices at the metal-support interface.[22-23] In fact, often the presence of defect sites, oxygen vacancies and anchoring sites favours the dispersion, the formation and the adhesion of reactive metal nanoparticles on the support material.[24]

Although the bare support materials should all be considered inert and hence inactive if used as catalysts, some metal oxide supports such as TiO_2 and CeO_2, also considered as reducible, *i.e.* they can undergo structural changes during reductive treatments. This can lead to a strong interaction with the metal nanoparticles, affecting the catalytic behaviour of the metal. This property of reducible supports was first observed by Tauster, who noticed how a high temperature reductive treatment (500 °C) would markedly decrease the CO and H_2 chemisorption capacity of Pt/TiO_2 samples compared to the lower temperature treated (200 °C) samples.[25] This effect was later named Strong Metal-Support Interaction (SMSI).[26] In addition to these modifications in chemisorption properties, improved catalytic abilities were also observed for the hydrogenation

of acetaldehyde and phenylacetaldehyde.[27-29] This enhancement has been attributed to two main factors affecting the interaction of the support on the metal: an electronic and a geometric effect.

On one hand, during the reductive treatment, H_2 is adsorbed and dissociated on the metal particles, followed by the spillover effect that facilitates the mobility of H atoms from atop the nanoparticle to the support, leading to a partial reduction of the latter (Figure 1.9).[30] After the treatment, as the partly reduced metal oxide in the support attempts to return to the initial oxidised state, the supported metal will receive an additional electronic charge, affecting its electronic properties. This is usually detected by photoelectron shift in the binding energy.[31]
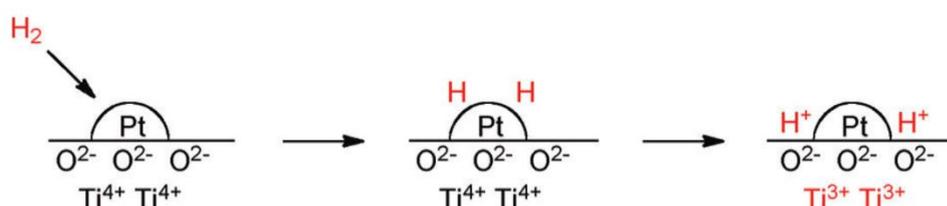
Figure 1.9 Schematic rapresentation of the adsoprtion of H_2 on Pt and spillover of H atoms to the TiO_2 support. Taken from reference [30].

On the other hand, the geometrical effect arises when a metal sub-oxide (MO_{2-x}) layer grows on the nanoparticle, covering it. During reduction, the reducible oxide is more mobile and undergoes restructuring, leading to the nanoparticle decoration and partial coverage. This may reflect in the decrease in chemisorption properties of these modified samples as well as in the detection of an oxide layer by high resolution electron microscopy.[32]

In a recent paper from our group, Freakley *et al.* reported that the addition of Sn to a Pd catalyst, followed by an appropriate activation treatment (oxidation- reduction- oxidation, Figure 1.10) would induce SMSI, and consequently switch off the decomposition and hydrogenation pathways during the direct synthesis of H_2O_2, by growing a SnO_x layer over small Pd-rich particles responsible for the undesired steps. Whereas larger nanoparticles composed of bimetallic PdSn alloy are believed responsible for the selective H_2O_2 synthesis.[33]
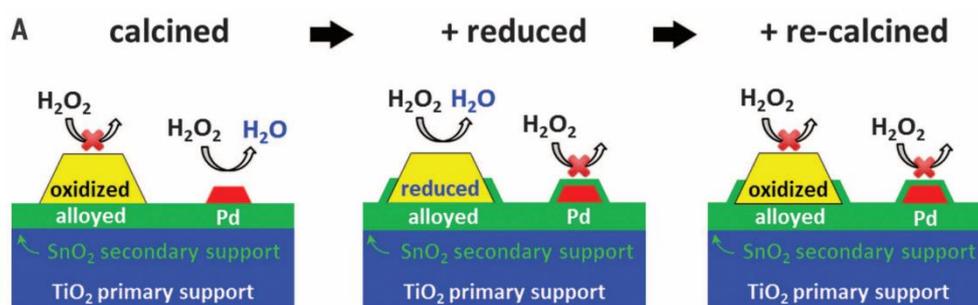
Figure 1.10 Schematic view of the growth of SnO_x through SMSI, encapsulation of the small Pd-rich nanoparticles is triggered during the reductive step. Taken from reference [33].

Since the electronic and geometric structures of metal nanoparticles are crucial for controlling the activity and selectivity of supported catalysts, the modification of the electron density and of the exposed species present in a catalytic material could lead to a variation in its reactivity.

1.2.2 Identification of the active site on Au-based catalysts for the chemoselective reduction of nitro aromatic compounds

Although for long time gold has been considered a noble and inactive metal, the discovery by Haruta that supported nanoparticulate gold could catalyse the oxidation of CO to CO_2 at low temperature,[34] opened up to new opportunities in the field of catalysis. Gold shows high stability under oxygen pressure, compared to the very poor stability of the other platinum group metals due to oxygen poisoning.[35] From here, supported gold NPs showed to be able to catalyse the oxidation of carbon monoxide, alcohols and polyols,[36-39] the epoxidation of alkenes,[40] the hydrochlorination of acetylene[41] and the direct synthesis of hydrogen peroxide.[42] However, subsequently gold was found to be an active catalyst also in hydrogenation reactions, such as the reduction of α, β-unsaturated aldehydes, acrolein and crotonaldehyde, where control over the intramolecular selectivity is required. While conventional hydrogenation catalysts would deliver the saturated aldehyde or the fully reduced product, Au-based catalysts were found to be able to reduce the C=O group, forming the corresponding allylic alcohol, [43-44] which is of interest in the synthesis of fine chemicals, such pharmaceuticals and cosmetics.[45]

In 2006, Corma *et al.* were the first to report the application of supported gold catalysts for the reduction of nitro compounds containing other reducible functional groups such as C=C double bonds, carbonyls and nitriles.[46] Two gold catalysts (Au/TiO_2 and Au/Fe_2O_3) as well as platinum and palladium catalysts and their bimetallic combinations AuPd and AuPt were tested for the hydrogenation of 3-nitrostyrene under 9 bar pressure of pure H_2 at 120 °C (see scheme in Figure 1.11). The results showed that the samples containing palladium and platinum were not selective towards formation of 3-vinylaniline, while the monometallic gold catalysts gave conversions >98% with selectivity of 96% to 3-vinylaniline. Similar results were obtained for the hydrogenation of 4-nitrobenzaldehyde and 4-nitrobenzonitrile.

3-vinylaniline (3-VA)

3-nitrostyrene (3-NS)

3-ethylnitrobenzene (3-EN)

3-ethylaniline (3-EA)
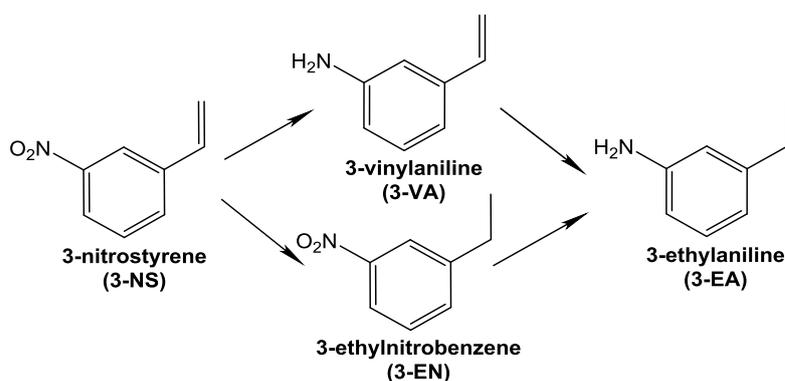
Figure 1.11 Reaction scheme of the hydrogenation of 3-nitrostyrene (3-NS).

After showing the unique catalytic behaviour of gold catalysts compared to palladium and platinum ones, in 2007 Boronat *et al.*[47] published a study of the interaction occurring at the molecular level between the substrate and the catalyst surface, focusing on the Au/TiO$_2$ system which had showed the best results. A combination of *in-situ* infrared (IR) spectroscopy, quantum mechanical modelling and kinetic experiments led to the conclusion that a synergistic effect between the metal and the support is present. More specifically, the H$_2$ is dissociated on the Au nanoparticle on low coordination metal sites,[48-49] while the substrate is adsorbed preferentially through the NO$_2$ group on the peripheral gold atoms located between the TiO$_2$ and the Au nanoparticle (Figure 1.12), explaining the high chemoselectivity. Direct interaction of the substrate and the bare support through the NO$_2$ group also takes place, however those species are considered to be only spectators. These results were in agreement with the intrinsic higher hydrogenation rate of the NO$_2$ versus the C=C group when using a gold catalyst and is also in agreement with the catalytic results obtained using different supports, showing that materials such TiO$_2$ and Fe$_2$O$_3$ show higher selectivity, while SiO$_2$ and C are more inert and their use leads to formation of by-products.
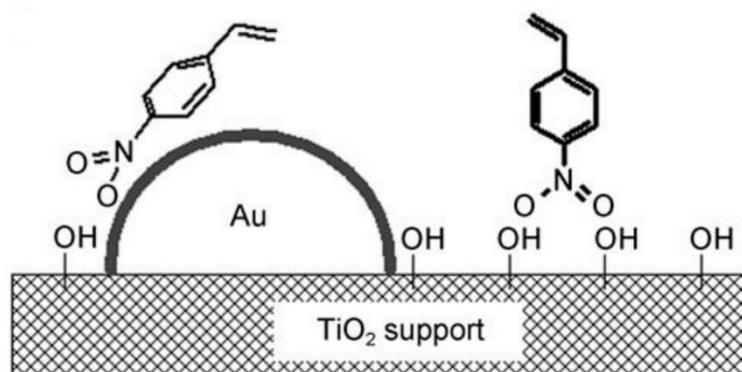
Figure 1.12 Schematic representation of adsorbed 4-nitrosyrene on Au/TiO$_2$. Taken from reference [50].

The gold catalysts here mentioned, although showing an extremely high selectivity towards the amino product, showed low activity and TOF. The reason for this has been attributed to the rate-determining step during the hydrogenation reaction. In fact, it has been found that a drawback of this system is the low capacity of gold to adsorb and dissociate the hydrogen molecules, concluding that the H$_2$ dissociation on the gold nanoparticles is the controlling step of the reaction.[44, 51]

Platinum is well known to be an exceptionally active metal for H$_2$ dissociation. By computational means, Boronat was able to determine that the presence of atomically dispersed Pt species atop of an Au nanoparticle could make the dissociative adsorption of H$_2$ exothermic and barrier less, facilitating its availability to the reactant and improving the overall reaction rate, while

not affecting the selectivity of the reaction as controlled by the interfacial Au-TiO$_2$ species.[52] Supported by these theoretical results, Corma *et al.* prepared a series of Au/TiO$_2$ catalysts with addition of small percentages (0.005 to 0.2 %, see Figure 1.13) of Pt observing that the rate of hydrogenation could be improved by one order of magnitude, while maintaining the high chemoselectivity. However, with increasing percentages of Pt, a substantial increase in TOF is achieved at disadvantage of a quick drop in the reaction selectivity.
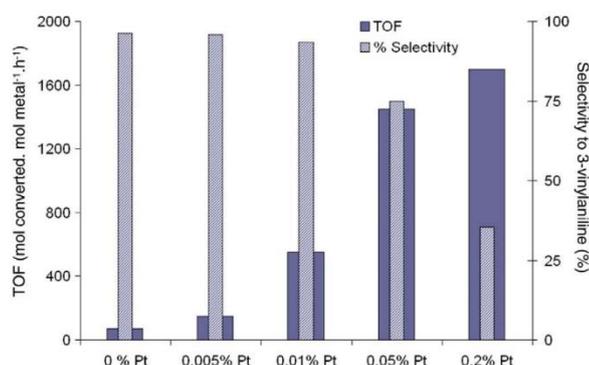
Figure 1.13 Effect of the Pt loading in the 1.5%Au/TiO$_2$ catalyst on the TOF and selectivity towards 3-vinyl aniline during the hydrogenation of 3-nitrosyrene. Taken from reference [51].

Overall, combining theoretical and experimental studies allowed to understand deeply how this hydrogenation reaction works and to design an ideal catalyst. Mixing and alloying different metals requires a delicate balance but, as it will be discussed later, it could also be of great advantage.

1.2.3   Tuning the chemoselectivity of active Pt-containing catalysts

Application of Pt in catalysis is well known. In fact, Pt is historically one of the key active components used in catalytic converters as it is a good oxidation catalyst and has good resistance to poisoning. In addition, because of its high activity in the oxygen reduction reaction, Pt based catalysts have been applied in the growing field of fuel cells research.[53] Commonly, Pt containing catalysts are known to be exceptional reduction catalysts due to the facile H$_2$ adsorption and bond dissociation that also leads to the hydrogen spillover effect.

As presented in the previous section 1.2.2, Pt based catalysts showed to be highly active also for the hydrogenation of substituted nitro aromatic compounds, but often show low chemoselectivity, this being defined as the preferential reaction of one of two or more functional groups present on a substrate.[3] With the addition of PbO or H$_3$PO$_2$ to supported Pt catalysts, the selectivity towards substituted aromatic amines could be improved but explosive hydroxylamines are formed as by-products. With the further addition of vanadium or iron salts that act as promoters, intermediates hydroxylamines could be converted and the overall activity and

selectivity could be improved.[54-57] However, together with the presence of metal ions in solution, which need careful separation, the preparation and formulation of these catalysts remains critical and the amount of modifiers and additives must be precisely controlled. Despite the encouraging results obtained with these catalytic systems, the process requires the use of a large amount of transitional metal salts in solution, which makes it not environmentally sustainable nor easily reusable. Ideally, a heterogeneous catalytic material able to reduce the substrate by using molecular hydrogen over multiple uses is highly desirable. For these reasons, the study and development of both a highly active and chemoselective heterogeneous system is required.

Catalytic studies on purely monometallic Pt catalysts reported that when comparing the TOF of nitrobenzene hydrogenation to the one of styrene, it was found that the former was very stable, indicating structure insensitivity, while the latter strongly increased as the Pt nanoparticle supported on Al_2O_3 increased in size, indicating the structure-sensitivity of the C=C double bond reduction.[58] This finding was supported by the adsorption of CO coupled with infrared (IR) spectroscopy analysis, showing that as the metallic particle grow in size, larger Pt(111) and Pt(100) plane surfaces and terraces are formed and become available to a favourable planar adsorption of the substrate inducing a more favourable styrene reduction. Whereas in small metal particles (~2 nm) the amount of low coordination Pt atoms at corners and edges was determined as higher, favouring the adsorption through the nitro group.[58] Similarly to the Au/TiO_2 catalyst, where the favourable adsorption of the NO_2 group took place at the interface between the metal and the support,[47] also the chemoselectivity of the highly active Pt/TiO_2 hydrogenation catalyst might be improved by favouring the Pt-Ti interface species. In a previous study by Coq *et al.* it was suggested that the increased amount of Pt-Ti species would favour the preferential adsorption of the NO_2 group when as other reducible functional group Cl is present.[59]

Based on previous knowledge of Au-based catalysts, Corma and co-workers demonstrated that small Pt crystallites were necessary for achieving high selectivity for the desired product and that the choice of support was crucial, with TiO_2 being the best support because no hydroxylamine derivatives are formed. No additive or promoter were needed but the way the catalyst is activated is crucial for obtaining the final desired selectivity. In particular, it was observed that by activating the catalyst at 450 °C instead of 200 °C in a reducing atmosphere, a strong enhancement in chemoselective reduction of the nitro group was achieved.[60] Similarly to the previous results reported in 1993 by Coq *et al* for the selective reduction of *p*-chloronitrobenzene.[59] Moreover, a similar influence of the catalyst activation temperature on the activity of Pt-based catalysts was observed before, for different reactions.[27-28] Such enhancement was explained with an increase in the metal-support interface and more in particular by the SMSI. This found evidence in the Pt crystallites decoration by mobile TiO_2. The growth of a TiO_2 layer on the metal nanoparticles increased the amount of Pt-Ti interface species and decreased the percentage of metal atoms in

terraces, which are found to be responsible for the unselective hydrogenation of the multiple functional groups present on the substrate. Moreover, since the activity of Pt/TiO_2 is comparable to the activity of the same Pt catalyst supported on C and Al_2O_3, where SMSI is not to be expected, the electronic effect due to the support interaction could be disregarded, leaving the geometric effect only playing a role in tuning the catalytic activity.[58] The increased amount of low coordination Pt species enhances the favourable adsorption of 3-NS through the NO_2 group, leading to its selective hydrogenation.

More recently, other metal oxide supports have been successfully applied as support materials for Pt nanoparticles. Kiwi-Minsker *et al.*[61-62] reported that alloying the platinum with zinc originating from the ZnO support during the catalyst activation at 300 °C led to a selectivity of 97% towards formation of 3-VA at nearly full 3-NS conversion. Such enhancement in selectivity could be explained by the high dispersion of the noble metal by the intercalation of zinc in the metal structure, which avoids formation of large platinum aggregates. Based on a similar principle, Zhang *et al.* have also shown how FeO_x could be the support of choice for Pt-based catalysts for the chemoselective hydrogenation of substituted nitro aromatic compounds [63-64] The proposed theory for which low coordination Pt species are the one responsible for the selective aniline formation was supported by preparation of single atom catalysts. Low loading $0.08\%Pt/FeO_x$ samples were prepared by co-precipitation method. The recovered solid sample was calcined at 400 °C for 5 h and reduced at 200-250 °C for 0.5 h, leading to aniline selectivity > 90% for a variety of substituted aromatic anilines at almost complete substrate conversion.

1.2.4   Alloying of metals to tune the formation of the catalytically active sites. The gold-palladium synergistic effect

Since the study and development of metallurgy, for the fabrication of widely used bronze and steel, it is known that the mixing of metals and other elements with different properties allows to produce new materials with combined or completely new characteristics. Similarly, although monometallic noble metals nanoparticles could act as good catalysts for a wide range of reactions, sometimes their properties could be further enhanced by mixing them with other metals. It has been reported that by nanoalloying, new catalytic properties arise. The addition of a second metal can induce a modification in the electronic characteristics of the first metal as well as modify the geometry of the metal nanoparticle. Moreover, the presence of a second metal facilitate the dilution and the dispersion of the first metal, overall having an effect on the chemico-physical properties of the final bimetallic material.[65-68]

Catalysts comprised of group 10 metals suffer from oxygen poisoning as the partial pressure of the gas increases. Therefore, when using these types of catalyst, low partial pressures of oxygen are applied, often using air as oxidant, in order to limit the oxygen concentration in the catalytic

system and avoid the strong adsorption (chemisorption) of oxygen species on the surface of the metal particles.[69] In contrast to other metals, gold does not suffer from oxygen poisoning. Hence higher oxygen partial pressures (3-6 bar O_2) could be applied when performing catalytic oxidations, without undergoing irreversible deactivation.[70]

The bimetallic AuPd catalytic system has shown improved performances in the oxidation of *n*-butanol to butyric acid,[71] in the oxidation of benzyl alcohol to benzaldehyde,[72] in the hydrogenation of levulinic acid to γ-valerolactone,[73] in the oxidation of D-sorbitol to gluconic acid [74] and in the oxidation of glycerol to glyceric acid (see Figure 1.14).[75]
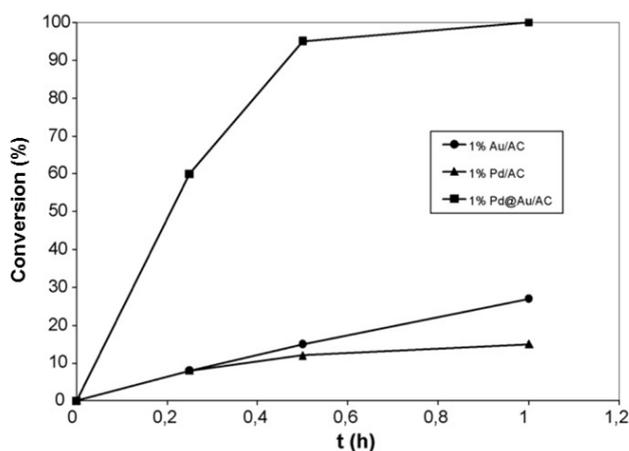
Figure 1.14 Activity comparison of monometallic gold and palladium catalysts versus bimetallic AuPd catalyst supported on carbon for the selective oxidation of glycerol. Taken from reference [75].

The reason behind the enhancement in performance observed in AuPd bimetallic catalytic systems has been researched. The addition of Pd to Au catalysts leads to a change in not only the geometry of the crystalline structure of the nanoparticle, affecting the strain and lattice parameters,[76] but also to the electronic density of the metal centres,[66] overall affecting the properties of the metal atoms. For example, it has been found that the oxygen binding energy with palladium decreases when the metal is in contact with gold, avoiding its deactivation.[77] Overall the improvement in activity is due to a combination of geometrical as well as electronic effects.[78]

1.2.5 Addition of N-Heterocyclic Carbenes over supported metal nanoparticles

Carbenes are a class of compounds characterised by a divalent carbon species R_2C: that have found application in organic synthesis and organocatalysis, among others.[79-82] Carbenes are very reactive intermediates, a feature that for long time has made them very difficult to isolate. In 1991 Arduengo *et al.* reported the first example of a not only isolable but also crystalline carbene, an N-heterocyclic carbene (NHC).[83] The same group was also the first to publish the formation of a

NHC-metal complex, with a zerovalent metal centre.[84] In contrast to the majority of the carbene species, the NHCs are an electronically and sterically stabilised class of carbenes, and as such it is possible to synthesise, isolate and store them as crystalline solids.[85] Due to the resonance effect, NHCs are electron rich, neutral σ-donor ligands and form strong bonds with most metals (Figure 15). Since their introduction, NHCs have been widely applied in organocatalysis as well as in transition-metal catalysis, for olefin metathesis, strong bond activation and many other reactions.[86-87] NHC-Pd complexes have been reported to be effective homogeneous transition metal catalysts, for Heck, Suzuki and Sonogashira C-C coupling, and aryl halides dehalogenation and amination reactions among others.[88-90] Homogeneous asymmetric organic synthesis has much expanded in the last decades, also thanks to the exploited use of NHC as ligands for the production of variously stabilised, functionalised and sterically hindered electron rich metal centres.
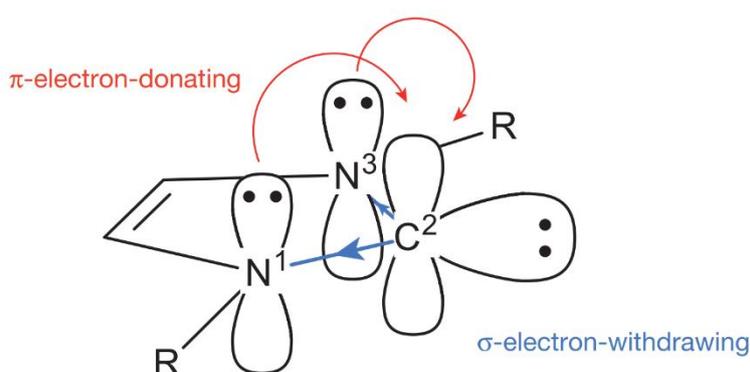
Figure 1.15 Schematic electronic structure of a general NHC. Taken from reference [85].

In recent years, a new field of interest has opened up towards the use of NHCs as surface ligands and modifiers, thanks to their simple synthesis method, structural diversity and interaction with a variety of metals such as Pd, Ir, Ru and Pt, which make them good anchoring groups to achieve surface modification. The use of NHCs as stabilising agents for monoatomic centres as well as metal nanoparticles was known and characterised since the 1990's.[84] The hypothesis of a direct bonding of the carbene carbon to the metal NP was advanced by Finke *et al.* in 2005, when studying metallic NPs suspended in ionic liquids composed of imidazolium cations.[91] Imidazolium cations are the stable protonated form of NHC, and it was found that the C-H oxidative addition of the imidazolium cation to Ir(0) took place. However, a deeper insight on the interaction between NHC and Ru metal NPs was given by the study in 2011 by Chaudret *et al.* using ^{13}C liquid and solid-state NMR spectroscopy, where the formation of a bond between the carbene carbon and the metal surface was proven.[92] After that, the study of the interaction between different metal NPs and NHCs has expanded. Stable and catalytically active NHC stabilised Pt nanoparticles were studied,[93] followed by the first report by Glorius and co-workers in 2014 of long-term stable NHC

Au and Pd NPs, with the latter being tested for the hydrogenation of olefins and demonstrating the influence of the NHC on the catalytic activity and selectivity of Pd nanoparticles.[94]

As mentioned previously, NHCs are efficient compounds able to act as anchoring sites, as well as ligands to metal centres. Many examples showed that NHC-metal systems are effective homogenous catalysts, however the possibility of anchoring the metal complexes on supports surfaces would give the advantages typical of heterogeneous catalysis: easy separation from the reaction mixture and reusability. Many efforts have been made towards supporting NHC-metal complexes on the surface of various materials, showing to form active and reusable catalysts. These supported complexes were characterised by means of NMR, XPS, IR and TGA techniques in order to determine and confirm the stability of the strong bond formed between the carbene carbon and the metal as well as the robustness of the whole system.[95-98]

In recent years, Glorius and co-workers have reported, for the first time, the use of NHCs as added ligands, decorating the surface of supported metal nanoparticles (Figure 1.16). In 2010, the group reported on Fe_3O_4 supported palladium nanoparticles decorated by use of chiral, enantiomerically pure NHC ligands. These were characterised by XPS, IR and electron microscopy and further tested for the asymmetric α-arylation of cyclic ketones with different phenyl halides, showing a notable improvement in stereoselectivity compared to the catalyst without any ligand as well as representative homogeneous palladium complexes.[99] Moreover, the use of a ferromagnetic support, allowed for an easy catalyst recovery after reaction. In 2016, the same group reported the addition of NHC ligands to ruthenium particles supported on alumina as well as their characterisation. These catalysts were tested for the chemoselective hydrogenation of substituted benzenes, where both the substituent and the aromatic ring could be reduced. The increase in NHC loading blocked active sites on the Ru particles, able to hydrogenate the less reactive benzene ring, favouring the selectivity to the terminal reducible functional group compared to the bulkier benzene ring .[100] More recently, the group of Glorius and co-workers reported the enhancement in catalytic activity of a Pd/Al_2O_3 heterogeneous catalyst modified by addition of NHC ligands.[101] Translating the knowledge from homogeneous catalysis, where an electron-donating ligand would be beneficial in the activation of bromobenzene, the electron donation from the ligand to the nanoparticle was confirmed to be necessary to increase the activity for the hydrogenolysis of bromobenzene.
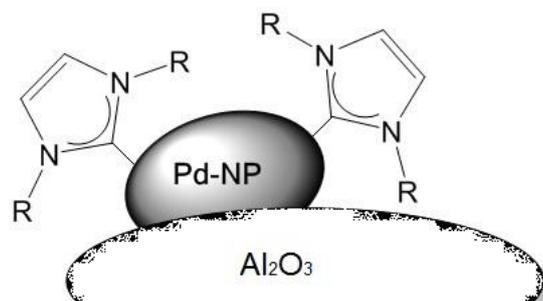
Figure 1.16 Graphic view of the decoration of metal nanoparticles by addition of NHC ligands. Redrawn image from reference [100].

This field of research could offer the possibility to expand the library of heterogeneous catalysts available, as the addition of ligands such as the NHC allows modification of the electronic characteristics of supported metal species. Similar to a formation of an alloy by mixing two or more metals, or by changing the support that inevitably interacts with nanometre sized particles, the presence of a ligand with a specific molecular structure could not only donate electronic density, but also add steric hindrance to the nanoparticle, allowing the reactants to access only determined active sites.

1.3   Thesis aims

Based on previous work, where knowledge was gathered on how a reaction proceeds or how a material behaves, it is possible to learn how to design and tune new catalytic materials. The aim of this PhD project has been to try different approaches to vary and modify catalytic systems in order to improve their catalytic activity for hydrogenation or oxidation liquid-phase test reactions. A range of characterisation techniques were employed to attempt and understand the properties of the variety of catalysts that were prepared, aiming to reach structure-activity correlations.

In this introductory chapter, the three topics studied and developed during the research work have been presented. From here, the discussion part of this thesis is composed of three chapters, each one of them focusing on a different approach, which was applied to modify mono- and bimetallic supported nanomaterials:

- - Chapter 3- the way supported catalysts are prepared has a strong influence on the final catalytic activity as different proportion of active sites can be formed, overall modifying the particle size as well as the distribution. In this chapter the effect of different heat treatments and metal loadings of Pt/TiO_2 catalysts have been studied, to determine the most active species for the chemoselective hydrogenation of 3-nitrostyrene and how to form it during catalyst synthesis.

- Chapter 4- the choice and type of support is known to have an effect on the reactivity of supported nanoparticles. In this chapter this effect has been studied using a variety of hydrothermal carbons presenting various surface and structural characteristics. They have been applied as supports for bimetallic AuPd nanoparticles and tested for the glycerol oxidation reaction.

- Chapter 5- in homogeneous catalysis, ligands play a fundamental role in stabilising the active metal centre and in forming the most suitable geometrical environment for a specific reaction. In this chapter the addition of NHC ligands to a Pd/TiO$_2$ catalyst was investigated. The presence of the NHC ligands, their effect on the supported metal nanoparticles and how this affects the activity in the reduction of 3-nitrostyrene and in the synthesis of H$_2$O$_2$ were studied.

1.4   References

1.   Berzelius, J. Quelques Idées sur une nouvelle Force agissant dans les Combinaisons des Corps Organiques. *Ann. Chim* **1836,** *61*, 146-151.

2.   Anastas, P.; Eghbali, N. Green chemistry: principles and practice. *Chem Soc Rev* **2010,** *39* (1), 301-12.

3.   Muller, P. Glossary of terms used in physical organic chemistry (IUPAC Recommendations 1994). In *Pure and Applied Chemistry*, 1994; Vol. 66, p 1077.

4.   I. Chorkendorff, J. W. N. *Concepts of Modern Catalysis and Kinetics*. WILEY-VCH Verlag GmbH & Co. KGaA: Weinheim, 2003.

5.   Robinson, P. K. Enzymes: principles and biotechnological applications. *Essays In Biochemistry* **2015,** *59*, 1-41.

6.   Liu, L.; Corma, A. Metal Catalysts for Heterogeneous Catalysis: From Single Atoms to Nanoclusters and Nanoparticles. *Chem Rev* **2018,** *118* (10), 4981-5079.

7.   Frenkel, A. I.; Hills, C. W.; Nuzzo, R. G. A View from the Inside: Complexity in the Atomic Scale Ordering of Supported Metal Nanoparticles. *The Journal of Physical Chemistry B* **2001,** *105* (51), 12689-12703.

8.   Okazaki, K.; Ichikawa, S.; Maeda, Y.; Haruta, M.; Kohyama, M. Electronic structures of Au supported on TiO2. *Applied Catalysis A-General* **2005,** *291* (1-2), 45-54.

9.   Karine Philippot, P. S. Concepts in Nanocatalysis. In *Nanomaterials in Catalysis*, Wiley-VCH Verlag GmbH & Co. KGaA: 2012.

10.   El-Sayed, M. A. Some interesting properties of metals confined in time and nanometer space of different shapes. *ACCOUNTS OF CHEMICAL RESEARCH* **2001,** *34* (4), 257-264.

11.   Das, S. K.; Marsili, E. Bioinspired metal nanoparticle: synthesis, properties and application. In *Nanomaterials*, InTech: 2011.

12.   Grasselli, R. K.; Burrington, J. D.; Buttrey, D. J.; DeSanto, P.; Lugmair, C. G.; Volpe, A. F.; Weingand, T. Multifunctionality of active centers in (amm) oxidation catalysts: From Bi–Mo–O x to Mo–V–Nb–(Te, Sb)–O x. *Topics in Catalysis* **2003,** *23* (1-4), 5-22.

13.   Shiju, N. R.; Guliants, V. V. Recent developments in catalysis using nanostructured materials. *Applied Catalysis A-General* **2009,** *356* (1), 1-17.

14.   DeSanto, P.; Buttrey, D. J.; Grasselli, R. K.; Lugmair, C. G.; Volpe, A. F.; Toby, B. H.; Vogt, T. Structural aspects of the M1 and M2 phases in MoVNbTeO propane ammoxidation catalysts. *Zeitschrift für Kristallographie-Crystalline Materials* **2004,** *219* (3), 152-165.

15.   Tamaru, K. *Dynamic processes on solid surfaces*. Springer Science+Business Media: New York, 1993; Vol. 3.

16.   Andersson, M. P.; Bligaard, T.; Kustov, A.; Larsen, K. E.; Greeley, J.; Johannessen, T.; Christensen, C. H.; Norskov, J. K. Toward computational screening in heterogeneous catalysis: Pareto-optimal methanation catalysts. *Journal of Catalysis* **2006,** *239* (2), 501-506.

17.   Henry, C. R. Surface studies of supported model catalysts. *Surface Science Reports* **1998,** *31* (7-8), 235-325.

18.   Mironenko, R. M.; Belskaya, O. B.; Gulyaeva, T. I.; Nizovskii, A. I.; Kalinkin, A. V.; Bukhtiyarov, V. I.; Lavrenov, A. V.; Likholobov, V. A. Effect of the nature of carbon support on the formation of active sites in Pd/C and Ru/C catalysts for hydrogenation of furfural. *Catalysis Today* **2015,** *249*, 145-152.

19.   Choudhary, V. R.; Dhar, A.; Jana, P.; Jha, R.; Uphade, B. S. A green process for chlorine-free benzaldehyde from the solvent-free oxidation of benzyl alcohol with molecular oxygen over a supported nano-size gold catalyst. *Green Chemistry* **2005,** *7* (11), 768-770.

20.   Argo, A. M.; Odzak, J. F.; Lai, F. S.; Gates, B. C. Observation of ligand effects during alkene hydrogenation catalysed by supported metal clusters. *Nature* **2002,** *415* (6872), 623-6.

21.   Jorg Radnik, C. M., Peter Claus. On the origin of binding energy shifts of core levels of supported gold nanoparticles and dependence of pretreatment and material synthesis. *Physical Chemistry Chemical Physics* **2003,** (5), 172–177.

22.   Mavrikakis, M.; Stoltze, P.; Norskov, J. K. Making gold less noble. *Catalysis Letters* **2000,** *64* (2-4), 101-106.

23.   Lopez, N.; Norskov, J. K.; Janssens, T. V. W.; Carlsson, A.; Puig-Molina, A.; Clausen, B. S.; Grunwaldt, J. D. The adhesion and shape of nanosized Au particles in a Au/TiO2 catalyst. *Journal of Catalysis* **2004,** *225* (1), 86-94.

24.   Wahlstrom, E.; Lopez, N.; Schaub, R.; Thostrup, P.; Ronnau, A.; Africh, C.; Laegsgaard, E.; Norskov, J. K.; Besenbacher, F. Bonding of gold nanoclusters to oxygen vacancies on rutile TiO2(110). *Phys Rev Lett* **2003,** *90* (2), 026101.

25.   S. J. Tauster, S. C. F., and R. L. Garten. Strong Metal-Support Interactions. Group 8 Noble Metals Supported on Ti02. *Journal of the American Chemical Society* **1978,** *100* (1), 170-175.

26.   S. J. Tauster, S. C. F., R. T. K. Baker, J. A. Horsley. Strong Interactions in Supported-Metal Catalysts. *Science* **1981,** *211* (4487), 1121-1125.

27.   Englisch, M.; Jentys, A.; Lercher, J. A. Structure Sensitivity of the Hydrogenation of Crotonaldehyde over Pt/SiO₂and Pt/TiO₂. *Journal of Catalysis* **1997,** *166* (1), 25-35.

28.   Poondi, D.; Vannice, M. A. The influence of MSI (metal-support interactions) on phenylacetaldehyde hydrogenation over Pt catalysts. *Journal of Molecular Catalysis a-Chemical* **1997,** *124* (1), 79-89.

29.   Vannice, M. A.; Sen, B. Metal Support Effects on the Intramolecular Selectivity of Crotonaldehyde Hydrogenation over Platinum. *Journal of Catalysis* **1989,** *115* (1), 65-78.

30.   Prins, R. Hydrogen spillover. Facts and fiction. *Chem Rev* **2012,** *112* (5), 2714-38.

31.   Sexton, B. XPS investigation of strong metal-support interactions on Group IIIa?Va oxides. *Journal of Catalysis* **1982,** *77* (1), 85-93.

32.   Dulub, O.; Hebenstreit, W.; Diebold, U. Imaging Cluster Surfaces with Atomic Resolution: The Strong Metal-Support Interaction State of Pt Supported on TiO₂. *Physical Review Letters* **2000,** *84* (16), 3646-3649.

33.   Freakley, S. J.; He, Q.; Harrhy, J. H.; Lu, L.; Crole, D. A.; Morgan, D. J.; Ntainjua, E. N.; Edwards, J. K.; Carley, A. F.; Borisevich, A. Y.; Kiely, C. J.; Hutchings, G. J. Palladium-tin catalysts for the direct synthesis of H(2)O(2) with high selectivity. *Science* **2016,** *351* (6276), 965-8.

34.   Haruta, M.; Kobayashi, T.; Sano, H.; Yamada, N. Novel Gold Catalysts for the Oxidation of Carbon Monoxide at a Temperature far Below 0 °C. *Chemistry Letters* **1987,** *16* (2), 405-408.

35.   Toste, A. S. K. H. a. F. D. *Modern Gold Catalyzed Synthesis*. First Edition ed.; Wiley-VCH Verlag GmbH & Co. KGaA: 2012.

36.   Herzing, A. A.; Kiely, C. J.; Carley, A. F.; Landon, P.; Hutchings, G. J. Identification of active gold nanoclusters on iron oxide supports for CO oxidation. *Science* **2008,** *321* (5894), 1331-1335.

37.   Abad, A.; Almela, C.; Corma, A.; Garcia, H. Unique gold chemoselectivity for the aerobic oxidation of allylic alcohols. *Chemical Communications* **2006,** (30), 3178-80.

38.   Abad, A.; Almela, C.; Corma, A.; Garcia, H. Efficient chemoselective alcohol oxidation using oxygen as oxidant. Superior performance of gold over palladium catalysts. *Tetrahedron* **2006,** *62* (28), 6666-6672.

39.   Carrettin, S.; McMorn, P.; Johnston, P.; Griffin, K.; Hutchings, G. J. Selective oxidation of glycerol to glyceric acid using a gold catalyst in aqueous sodium hydroxide. *Chemical Communications* **2002,** (7), 696-697.

40.   Sinha, A. K.; Seelan, S.; Tsubota, S.; Haruta, M. Catalysis by gold nanoparticles: epoxidation of propene. *Topics in Catalysis* **2004,** *29* (3-4), 95-102.

41.   Hutchings, G. J. Vapor-Phase Hydrochlorination of Acetylene - Correlation of Catalytic Activity of Supported Metal Chloride Catalysts. *Journal of Catalysis* **1985,** *96* (1), 292-295.

42.   Landon, P.; Collier, P. J.; Carley, A. F.; Chadwick, D.; Papworth, A. J.; Burrows, A.; Kiely, C. J.; Hutchings, G. J. Direct synthesis of hydrogen peroxide from H₂ and O₂ using Pd and Au catalysts. *Physical Chemistry Chemical Physics* **2003,** *5* (9), 1917-1923.

43.   Schimpf, S.; Lucas, M.; Mohr, C.; Rodemerck, U.; Brückner, A.; Radnik, J.; Hofmeister, H.; Claus, P. Supported gold nanoparticles: in-depth catalyst characterization and application in hydrogenation and oxidation reactions. *Catalysis Today* **2002,** *72* (1), 63-78.

44.   Claus, P. Heterogeneously catalysed hydrogenation using gold catalysts. *Applied Catalysis A-General* **2005,** *291* (1-2), 222-229.

45.   Lumbroso, A.; Cooke, M. L.; Breit, B. Catalytic Asymmetric Synthesis of Allylic Alcohols and Derivatives and their Applications in Organic Synthesis. *Angewandte Chemie International Edition* **2013,** *52* (7), 1890-1932.

46.   Corma, A.; Serna, P. Chemoselective hydrogenation of nitro compounds with supported gold catalysts. *Science* **2006,** *313* (5785), 332-4.

47.   Boronat, M.; Concepcion, P.; Corma, A.; Gonzalez, S.; Illas, F.; Serna, P. A Molecular mechanism for the chemoselective hydrogenation of substituted nitroaromatics with nanoparticles of gold on TiO₂ catalysts: a cooperative effect between gold and the support. *J Am Chem Soc* **2007,** *129* (51), 16230-7.

48.   Corma, A.; Boronat, M.; Gonzalez, S.; Illas, F. On the activation of molecular hydrogen by gold: a theoretical approximation to the nature of potential active sites. *Chem Commun (Camb)* **2007,** (32), 3371-3.

49.   Boronat, M.; Illas, F.; Corma, A. Active sites for H2 adsorption and activation in Au/TiO2 and the role of the support. *J Phys Chem A* **2009,** *113* (16), 3750-7.

50.   Hans-Ulrich Blaser, H. S., and Martin Studer. Selective Catalytic Hydrogenation of Functionalized Nitroarenes: An Update. *ChemCatChem* **2009,** *1*, 210-221.

51.   Pedro Serna, P. C., Avelino Corma. Design of highly active and chemoselective bimetallic gold–platinum hydrogenation catalysts through kinetic and isotopic studies. *Journal of Catalysis* **2009,** *265*, 19-25.

52.   Boronat, M.; Corma, A. Origin of the different activity and selectivity toward hydrogenation of single metal Au and Pt on TiO₂ and bimetallic Au-Pt/TiO₂ catalysts. *Langmuir* **2010,** *26* (21), 16607-14.

53.   Antolini, E. Formation, microstructural characteristics and stability of carbon supported platinum catalysts for low temperature fuel cells. *Journal of Materials Science* **2003,** *38* (14), 2995-3005.

54.   Baumeister, P.; Blaser, H. U.; Studer, M. Strong reduction of hydroxylamine accumulation in the catalytic hydrogenation of nitroarenes by vanadium promoters. *Catalysis Letters* **1997,** *49* (3-4), 219-222.

55.   Urs Siegrist, P. B., Hans Ulrich Blaser, Martin Studer. The selective hydrogenation of functionalized nitroarenes: New catalytic systems. *Catalysis of organic reactions (Dekker)* **1998,** 207-219.

56.   Studer, M.; Neto, S.; Blaser, H. U. Modulating the hydroxylamine accumulation in the hydrogenation of substituted nitroarenes using vanadium-promoted RNi catalysts. *Topics in Catalysis* **2000,** *13* (3), 205-212.

57.   Cisneros, L. O.; Rogers, W. J.; Mannan, M. S.; Li, X.; Koseki, H. Effect of Iron Ion in the Thermal Decomposition of 50 mass % Hydroxylamine/Water Solutions. *Journal of Chemical & Engineering Data* **2003,** *48* (5), 1164-1169.

58.   Corma, A.; Serna, P.; Concepcion, P.; Calvino, J. J. Transforming nonselective into chemoselective metal catalysts for the hydrogenation of substituted nitroaromatics. *Journal of the American Chemical Society* **2008,** *130* (27), 8748-53.

59.   Coq, B.; Tijani, A.; Dutartre, R.; Figueras, F. Influence of Support and Metallic Precursor on the Hydrogenation of P-Chloronitrobenzene over Supported Platinum Catalysts. *Journal of Molecular Catalysis* **1993,** *79* (1-3), 253-264.

60.   Serna, P.; Boronat, M.; Corma, A. Tuning the Behavior of Au and Pt Catalysts for the Chemoselective Hydrogenation of Nitroaromatic Compounds. *Topics in Catalysis* **2011,** *54* (5-7), 439-446.

61.   Berguerand, C.; Yarulin, A.; Cardenas-Lizana, F.; Murzin, D.; Kiwi-Minsker, L. Chemoselective liquid phase hydrogenation of 3-nitrostyrene over Pt nanoparticles: synergy with ZnO support. *Industrial and Engineering Chemistry Research* **2015,** *54*, 8659-8669.

62.   Yarulin, A.; Berguerand, C.; Alonso, A. O.; Yuranov, I.; Kiwi-Minsker, L. Increasing Pt selectivity to vinylaniline by alloying with Zn via reactive metal–support interaction. *Catalysis Today* **2015,** *256*, 241-249.

63.   Wei, H.; Liu, X.; Wang, A.; Zhang, L.; Qiao, B.; Yang, X.; Huang, Y.; Miao, S.; Liu, J.; Zhang, T. FeOx-supported platinum single-atom and pseudo-single-atom catalysts for chemoselective hydrogenation of functionalized nitroarenes. *Nature Communications* **2014,** *5*, 5634.

64.   Xu, G.; Wei, H. S.; Ren, Y. J.; Yin, J. Z.; Wang, A. Q.; Zhang, T. Chemoselective hydrogenation of 3-nitrostyrene over a Pt/FeOx pseudo-single-atom-catalyst in CO_2-expanded liquids. *Green Chemistry* **2016,** *18* (5), 1332-1338.

65.   Sinfelt, J. H. *Bimetallic catalysts: discoveries, concepts, and applications*. Wiley-Interscience: 1983; Vol. 7.

66.   Rodriguez, J. A.; Goodman, D. W. The nature of the metal-metal bond in bimetallic surfaces. *Science* **1992,** *257* (5072), 897-903.

67.   Veldurthi, S.; Shin, C. H.; Joo, O. S.; Jung, K. D. Promotional effects of Cu on Pt/Al2O3 and Pd/Al2O3 catalysts during n-butane dehydrogenation. *Catalysis Today* **2012,** *185* (1), 88-93.

68.   Sankar, M.; Dimitratos, N.; Miedziak, P. J.; Wells, P. P.; Kiely, C. J.; Hutchings, G. J. Designing bimetallic catalysts for a green and sustainable future. *Chem Soc Rev* **2012,** *41* (24), 8099-139.

69.   Michèle Besson, P. G. Selective oxidation of alcohols and aldehydes on metal catalysts. *Catalysis Today* **2000,** *57*, 127–141.

70.   Prati, L.; Rossi, M. Gold on carbon as a new catalyst for selective liquid phase oxidation of diols. *Journal of Catalysis* **1998,** *176* (2), 552-560.

71.   Gandarias, I.; Miedziak, P. J.; Nowicka, E.; Douthwaite, M.; Morgan, D. J.; Hutchings, G. J.; Taylor, S. H. Selective oxidation of n-butanol using gold-palladium supported nanoparticles under base-free conditions. *ChemSusChem* **2015,** *8* (3), 473-80.

72.   Enache, D. I.; Edwards, J. K.; Landon, P.; Solsona-Espriu, B.; Carley, A. F.; Herzing, A. A.; Watanabe, M.; Kiely, C. J.; Knight, D. W.; Hutchings, G. J. Solvent-free oxidation of primary alcohols to aldehydes using Au-Pd/TiO2 catalysts. *Science* **2006,** *311* (5759), 362-365.

73.   Wenhao Luo, M. S., Andrew M. Beale, Qian He, Christopher J. Kiely, Pieter C.A. Bruijnincx, Bert M. Weckhuysen. High performing and stable supported nano-alloys for the catalytic hydrogenation of levulinic acid to g-valerolactone. *Nature Communications* **2015,** *6*.

74.   Dimitratos, N.; Porta, F.; Prati, L.; Villa, A. Synergetic effect of platinum or palladium on gold catalyst in the selective oxidation of D-sorbitol. *Catalysis Letters* **2005,** *99* (3-4), 181-185.

75.   Prati, L.; Villa, A.; Porta, F.; Wang, D.; Su, D. S. Single-phase gold/palladium catalyst: The nature of synergistic effect. *Catalysis Today* **2007,** *122* (3-4), 386-390.

76.   Chen, M.; Kumar, D.; Yi, C. W.; Goodman, D. W. The promotional effect of gold in catalysis by palladium-gold. *Science* **2005,** *310* (5746), 291-3.

77.   Weissman-Wenocur, D. L.; Spicer, W. E. Comparison between the catalytic activities of Pd(111) and Pd-Au(111) for water synthesis. *Surface Science* **1983,** *133* (2-3), 499-515.

78.   Groß, A. Reactivity of Bimetallic Systems Studied from First Principles. *Topics in Catalysis* **2006,** *37* (1), 29-39.

79.   Enders, D.; Balensiefer, T. Nucleophilic carbenes in asymmetric organocatalysis. *Acc Chem Res* **2004,** *37* (8), 534-41.

80.   Enders, D.; Niemeier, O.; Henseler, A. Organocatalysis by N-heterocyclic carbenes. *Chem Rev* **2007,** *107* (12), 5606-55.

81.   Dotz, K. H.; Stendel, J. Fischer carbene complexes in organic synthesis: metal-assisted and metal-templated reactions. *Chem Rev* **2009,** *109* (8), 3227-74.

82.   Wanzlick, H. W. Aspects of Nucleophilic Carbene Chemistry. *Angewandte Chemie International Edition in English* **1962,** *1* (2), 75-80.

83.   Arduengo, A. J.; Harlow, R. L.; Kline, M. A Stable Crystalline Carbene. *Journal of the American Chemical Society* **1991,** *113* (1), 361-363.

84.   Arduengo, A. J.; Gamper, S. F.; Calabrese, J. C.; Davidson, F. Low-Coordinate Carbene Complexes of Nickel(0) and Platinum(0). *Journal of the American Chemical Society* **1994,** *116* (10), 4391-4394.

85.   Hopkinson, M. N.; Richter, C.; Schedler, M.; Glorius, F. An overview of N-heterocyclic carbenes. *Nature* **2014,** *510* (7506), 485-496.

86.   Vougioukalakis, G. C.; Grubbs, R. H. Ruthenium-based heterocyclic carbene-coordinated olefin metathesis catalysts. *Chem Rev* **2010,** *110* (3), 1746-87.

87.   Arduengo Iii, A. J.; Calabrese, J. C.; Davidson, F.; Rasika Dias, H. V.; Goerlich, J. R.; Krafczyk, R.; Marshall, W. J.; Tamm, M.; Schmutzler, R. C−H Insertion Reactions of Nucleophilic Carbenes. *Helvetica Chimica Acta* **1999,** *82* (12), 2348-2364.

88.   McGuinness, D. S.; Cavell, K. J. Donor-Functionalized Heterocyclic Carbene Complexes of Palladium(II): Efficient Catalysts for C−C Coupling Reactions. *Organometallics* **2000,** *19* (5), 741-748.

89.   Viciu, M. S.; Grasa, G. A.; Nolan, S. P. Catalytic dehalogenation of aryl halides mediated by a palladium/imidazolium salt system. *Organometallics* **2001,** *20* (16), 3607-3612.

90.   Cheng, J.; Trudell, M. L. Synthesis of n-heteroaryl-7-azabicyclo[2.2.1]heptane derivatives via palladium-bisimidazol-2-ylidene complex catalyzed amination reactions. *Org Lett* **2001,** *3* (9), 1371-4.

91.   Ott, L. S.; Cline, M. L.; Deetlefs, M.; Seddon, K. R.; Finke, R. G. Nanoclusters in ionic liquids: evidence for N-heterocyclic carbene formation from imidazolium-based ionic liquids detected by (2)H NMR. *J Am Chem Soc* **2005,** *127* (16), 5758-9.

92.   Lara, P.; Rivada-Wheelaghan, O.; Conejero, S.; Poteau, R.; Philippot, K.; Chaudret, B. Ruthenium nanoparticles stabilized by N-heterocyclic carbenes: ligand location and influence on reactivity. *Angew Chem Int Ed Engl* **2011,** *50* (50), 12080-4.

93.   Lara, P.; Suárez, A.; Collière, V.; Philippot, K.; Chaudret, B. Platinum N-Heterocyclic Carbene Nanoparticles as New and Effective Catalysts for the Selective Hydrogenation of Nitroaromatics. *ChemCatChem* **2014,** *6* (1), 87-90.

94.   Richter, C.; Schaepe, K.; Glorius, F.; Ravoo, B. J. Tailor-made N-heterocyclic carbenes for nanoparticle stabilization. *Chem Commun (Camb)* **2014,** *50* (24), 3204-7.

95.   Özdemir, I.; Gürbüz, N.; Seçkin, T.; Çetinkaya, B. Synthesis of silica-supported rhodium carbene complex as efficient catalyst for the addition of phenylboronic acid to aldehydes. *Applied Organometallic Chemistry* **2005,** *19* (5), 633-638.

96.   Li, P.; Wang, L.; Zhang, Y. SiO2–NHC–Cu(I): an efficient and reusable catalyst for [3+2] cycloaddition of organic azides and terminal alkynes under solvent-free reaction conditions at room temperature. *Tetrahedron* **2008,** *64* (48), 10825-10830.

97.   Movahed, S. K.; Esmatpoursalmani, R.; Bazgir, A. N-Heterocyclic carbene palladium complex supported on ionic liquid-modified graphene oxide as an efficient and recyclable catalyst for Suzuki reaction. *RSC Advances* **2014,** *4* (28), 14586-14591.

98.   Rostamnia, S.; Golchin Hossieni, H.; Doustkhah, E. Homoleptic chelating N-heterocyclic carbene complexes of palladium immobilized within the pores of SBA-15/IL (NHC–Pd@SBA-15/IL) as heterogeneous catalyst for Hiyama reaction. *Journal of Organometallic Chemistry* **2015,** *791*, 18-23.

99.   Kalluri V. S. Ranganath, J. K., Andreas H. Schaefer, Frank Glorius. Asymmetric Nanocatalysis: N-Heterocyclic Carbenes as Chiral Modifiers of Fe3O4/Pd nanoparticles. *Angew. Chem. Int. Ed.* **2010,** (49), 7786 –7789.

100.   Johannes B. Ernst, S. M., Fei Wang, Mizuki Tada, Frank Glorius. Tunable Heterogeneous Catalysis: N‑Heterocyclic Carbenes as Ligands for Supported Heterogeneous Ru/K-Al2O3 Catalysts To Tune Reactivity and Selectivity. *Journal of the American Chemical Society* **2016,** (138), 10718−10721.

101.   Ernst, J. B.; Schwermann, C.; Yokota, G. I.; Tada, M.; Muratsugu, S.; Doltsinis, N. L.; Glorius, F. Molecular Adsorbates Switch on Heterogeneous Catalysis: Induction of Reactivity by N-Heterocyclic Carbenes. *J Am Chem Soc* **2017,** *139* (27), 9144-9147.

Chapter

2

Experimental

2.1   Materials

- Titanium dioxide, TiO_2 (P25 Aeroxide®, Evonik))

- Carbon black, Vulcan VXC72R (Cabot)

- Hydrogen hexachloroplatinic acid aqueous solution, H_2PtCl_6 (assay 30.21 %, Johnson Matthey)

- Chloroauric acid, $HAuCl_4$ $3H_2O$ (99.99 %, Sigma Aldrich)

- Palladium chloride, $PdCl_2$ (99.9 %, Sigma Aldrich)

- 3-Nitrostyrene (96%, Sigma Aldrich)

- Toluene anhydrous (99.8%, Sigma Aldrich)

- *o*-Xylene (99 %, Sigma Aldrich)

- Glycerol (anhydrous >99.5 %, Sigma Aldrich)

- Sodium hydroxide, NaOH (pellets, anhydrous>98%. Sigma Aldrich BioXtra)

- Methanol, MeOH (HPLC grade, Fisher Scientific)

- Water, H_2O (HPLC grade, Fisher Scientific)

- Cerium (IV) sulfate, $Ce(SO_4)_2$ (> 98%, Sigma Aldrich)

- Ferroin indicator (0.025M, Sigma Aldrich)

- Oxygen (99.999 %, BOC gases)

- Hydrogen (99.999 %, BOC gases)

- Hydrogen in argon, $5\%H_2/Ar$ (BOC gases)

- Hydrogen in carbon dioxide, $5\%H_2/CO_2$ (BOC gases)

- Oxygen in carbon dioxide, $25\%O_2/CO_2$ (BOC gases)

2.2 Preparation of the catalysts

2.2.1 Modified impregnation

All the catalysts presented and discussed in this thesis have been prepared by the modified impregnation method, followed by reductive treatment in furnace, unless otherwise specified.[1-2] Metal precursors were dissolved in water and concentration was determined by ICP analysis. For the palladium solution, $PdCl_2$ was dissolved in 0.58 M HCl according to what reported in the literature to achieve a better mixing and alloying degree.[1] The addition of HCl increases the solubility of the solid in solution, but also the Cl^- acts as a ligand to the metal atoms in solution and in the preparation of bimetallic catalysts it leads to a better mixing and formation of bimetallic nano-alloyed particles.

For a typical preparation of 2 g of catalyst, the right amount of platinum, gold or palladium aqueous solution was added in a 50 ml round bottom flask and deionised water was added for a total volume of 16 ml of solution. The flask was fitted in an oil bath previously heated to 60 °C under vigorous stirring (800 rpm). After mixing for 10 min, the right amount of support was slowly added to permit complete and homogeneous mixing. Once a homogeneous slurry was obtained, heating was increased up to 95 °C and the preparation was left to dry overnight (*ca.* 16 h). The dry sample was recovered and ground with mortar and pestle to obtain a homogeneous powder.

After impregnation of the support, a heat treatment is required in order to form stable nanoparticles and to eliminate the chlorine excess. Moreover, the type of environment during this treatment in furnace allows achieving the desired oxidation state and dispersion of the metal. By reductive step in 5% H_2/Ar flow leads to formation of metallic nanoparticles. When developing this preparation method, it was found that the ideal reduction temperature was of 400 °C, which ensured reduction of the metal and led to the best balance between catalyst activity and stability over multiple reuses.[1] A 700 mg portion of the dried-only sample was transferred in a borosilicate calcination boat (15 cm x 2 cm) and heat treated in a furnace either in static air (for a calcination treatment) or under a steady flow of 5% H_2/Ar (for a reductive treatment). Heat treatments were carried at 400 °C, unless otherwise stated, for 4 h applying a ramp rate of 10 °C/min.

2.2.2 Preparation of the hydrothermal carbons (HTCs)

In Chapter 4, the AuPd catalysts studied were supported on a series of carbonaceous materials prepared by hydrothermal method by our collaborators from the Max-Planck Institute.

pH dependant synthesis and KOH treatment

A 20 wt. % sucrose (or as stated) solution was prepared and the pH adjusted with addition of HNO_3. The solution was loaded in a stainless steel autoclave and heated up to 220 °C for 6 h. The solid product was annealed in nitrogen atmosphere at 900 °C for 5 h.[3] In order to improve the surface area of the final material, the same procedure was used, but before annealing the solid was added to a 4 M KOH solution and cooked under reflux at 100 °C for 30 min. The solid was then annealed in argon flow at 900 °C for 5 h.

Oxygen-containing HTC

A 20 wt. % sucrose solution in deionised water was prepared and the pH adjusted to 6 with HNO_3, the hydrothermal synthesis followed as mentioned above, 220 °C for 6 h. The solid was then annealed in nitrogen at 900 °C for 5 h and named HTC pH6. In Figure 2.1 the set up used for the oxygen functionalisation is shown. Nitrosulfuric acid was prepared by mixing 500 ml of concentrated HNO_3 (65 %) and 500 ml of concentrated H_2SO_4 (98 %) and heated up in an oil bath set to 105 °C. Once the solution reached 80 °C, the HTC pH6 solid was slowly added to the acid solution and let to mix for 30 minutes. The reactor was purged with argon flow and cooled down with an ice bath. Ice cold water (3 l) was also slowly added to the mixture, which was then filtered and washed on vacuum with at least 10 l of water until neutral pH. The solid sample was let to dry in a vacuum oven at 80 °C overnight and named HTC pH6funct. As new oxygen functionalities were formed on the surface of the solid during the oxidation in acid. This is the sample containing up to 22 at. % oxygen, hence the corresponding catalyst was named AuPd/HTC 22%O. To decrease the amount of oxygen by eliminating specific oxygen functional groups from the carbon surface, heat treatments in nitrogen flow at increasing temperatures 510 and 800 °C were performed, achieving HTC 15%O and HTC 5%O respectively.
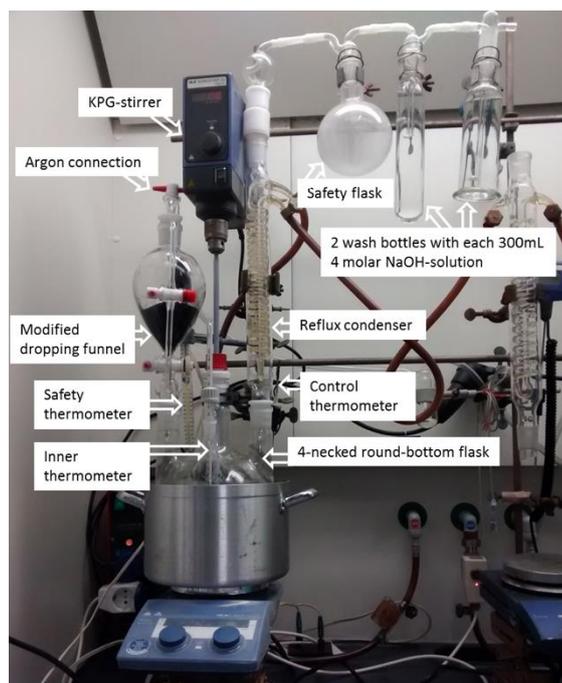
Figure 2.1 Picture of the set up used for the functionalisation of the HTC pH6 sample.

2.2.3   N-Hetrocyclic carbenes (NHCs) addition

The procedure for the catalyst modification was performed by our collaborators in the research group of Professor Glorius in Münster, following the method previously reported in literature.[4]

In the glovebox, the imidazolium salt and a strong base (KO*t*Bu) are added to a Schlenk flask. Outside the glovebox, working under inert atmosphere with the use of a Schlenk line, toluene was added to the flask and the reaction mixture was stirred for 2 h at room temperature so to deprotonate the cation and form the free N-heterocyclic carbene (Figure 2.2). The reaction mixture was filtered over *Celite* and the filtrate was added to the as prepared 1% Pd/TiO$_2$ sample supplied from Cardiff University. The suspension was stirred for 1 h after which it was allowed to settle. The supernatant was removed by syringe and the modified catalyst was dried *in vacuum*.
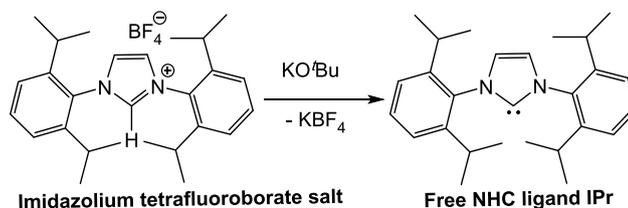
Figure 2.2 Formation of the free NHC ligand by addition of base.

2.3   Characterisation techniques

2.3.1   X-ray photoemission spectroscopy

The X-ray photoemission spectroscopy (XPS) is a widely used surface technique that makes use of the photoelectron effect, which was first studied and reported by Einstein.[5] It is based on the quantised energy necessary to eject a core or valence electron from a metallic surface. As it is nowadays well known, the Einstein's relation describes the energy of a photon of all types.

$$E = hv$$

With

h= Planck's constant, $6.62 \ 10^{-34}$ Js

v= photon frequency, Hz

XPS is based on the process for which one single photon with kinetic energy (KE) goes in the system and it is absorbed by one atom, which leads to ionisation and emission of a core electron from an inner shell (Figure 2.3).
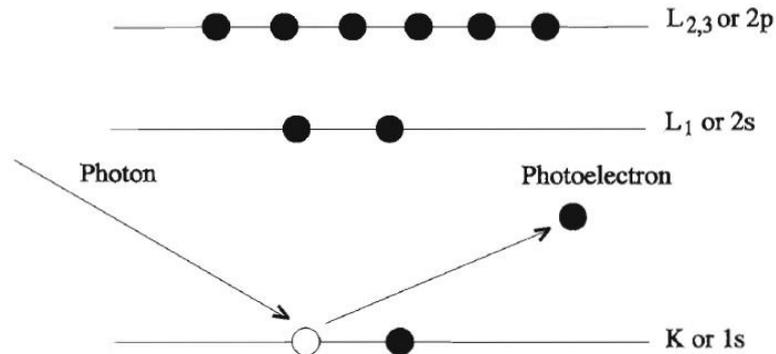
Figure 2.3 The XPS emission process. Taken from reference[6].

The kinetic energy of the electron is defined as:

$$KE = hv - BE$$

With

hv= the energy of the incoming photon, eV

BE= the binding energy of the electron, eV

For p, d and f electrons, two XPS peaks are observed with constant spin-orbit splitting. This is due to the Spin-Orbit interaction, which in multi electron atoms is named Russell-Saunders or

L-S coupling. The addition of all the orbital angular momenta of the individual electrons result in an orbital angular momentum (L) and the sum of the spin angular momenta give raise to S, the combination of the two gives a total angular momentum

$$J = L + S$$

With L=0…..s

1…..p

2…..d

3…..f

S=±1/2

For example Au4f will show two spin orbit components, 7/2 at lower binding energy and 5/2 at a distance of 3.7 eV.

The most important information that can be acquired by analysis of the XPS data is the oxidation state of the element considered. The relative binding energy values of a specific element change depending if a withdrawal (oxidation) or addition (reduction) of valence electron charge is taking place, reflecting in an increase or decrease in binding energy, respectively. By comparing with literature values is possible to assign the observed peaks to specific species.

During the experiment, a survey scan is performed, which covers a wide range of energies. However, for a better spectra resolution, repeated scans are ran for specific energy ranges, where desired elements are expected to give rise to photoelectron signals. During the analysis, photo induced reduction may take place, especially in the case of metals like Au and Pd. Hence, scans at the beginning and end of the analysis are performed for comparison.

XPS was performed using two systems; the first was a Kratos Axis Ultra DLD spectrometer using monochromatic Al Kα radiation (source power 140 W). An analyser pass energy of 160 eV was used for survey scans, and 40 eV for detailed acquisition of individual elemental regions. The second system was a Thermo Scientific K-Alpha+ spectrometer utilizing micro-focused monochromatic Al K_α radiation (source power 72 W), with analyser pass energies of 40 and 150 eV. Data was analysed with CasaXPS, using escape depth corrected sensitivity factors supplied by the instrument manufacturers. The binding energies were calibrated using the Ti2p binding energy (458.5 eV) or the C1s carbon (284.8 eV).

2.3.2 X-ray diffraction technique

X-ray powder diffraction (XRD) is a common analytical technique applied in the study of crystalline materials for phase identification and unit cell dimensions. Average bulk composition information can also be obtained. XRD is based on the constructive interference of monochromatic X-rays and a crystalline sample. When the interaction between the incident rays and the sample satisfy Bragg's law, constructive interferences and diffracted rays are produced.

$$n\lambda = 2d\sin\Theta$$

With

n= integer number

λ =wavelength of the X-ray beam, Å

d= inter-planar distance, Å

θ= diffraction angle, °

This relation connects the wavelength of the X-rays to the diffraction angle and the lattice spacing of the crystalline sample (Figure 2.4).
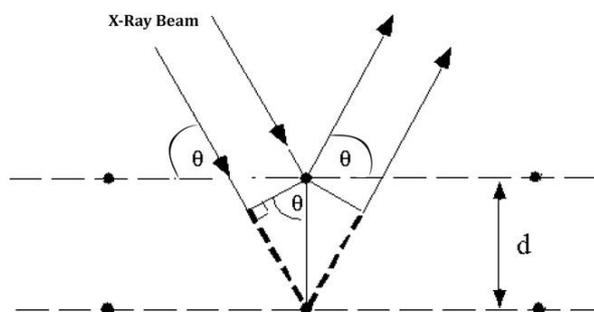
Figure 2.4 X-ray crystal diffraction scheme.

The production and use of monochromatic rays is required in order to obtain a good quality response that satisfy Bragg's law. The use of target materials is beneficial to produce monochromatic X-ray beams; copper is the most common target material for single-crystal diffraction, with CuKα radiation = 1.5418 Å. By varying the angle of the incident X-ray beam with constant wavelength a range of diffracted rays are detected (Figure 2.5), counted and processed to give a diffractogram. After converting the diffraction peaks into d-spacing values is possible to identify the crystal and elemental structure, by comparing the d-spacing with standard reference patterns.
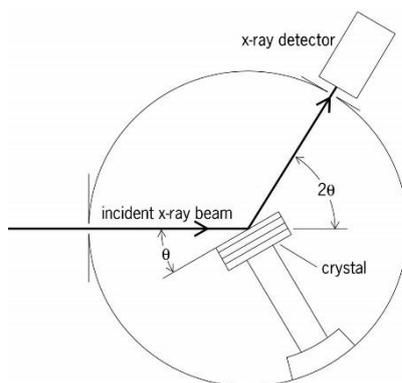
Figure 2.5 Schematic arrangement of XRD diffractometer components. Taken from reference [7].

From XRD analysis, various information can be obtained. Comparing the diffractogram with reference standards and literature data is possible to identify a material, as well as assess the composition, purity, crystalline structure and unit cell dimensions of a powder sample. Moreover, by use of the Scherrer equation the average particles size (L) of crystallites can be calculated from the broadening (β) of the diffraction line corresponding to the diffraction angle (θ) using the constant wavelength radiation (λ).[8-10] Long range crystal order is necessary to obtain diffraction signals, therefore nanoparticles can be difficult to detect if their size is below *ca.* 5 nm.

$$L = \frac{K\lambda}{\beta \cos \theta}$$

With

K= constant close to unity

λ = the radiation wavelength, Å

β= the full width at half maximum of the reflection, °

Θ= diffraction angle of a line maximum, °

XRD analysis was conducted using a PANanalytical X'pert pro diffractometer fitted with an X'Celerator detector and a CuKα X-ray source operated at 40 kV and 40 mA, 2θ = 5-80 °, since some carbon show a peak at low angles around 10 °.

2.3.3   Attenuated total reflectance infrared spectroscopy

Infrared (IR) spectroscopy is a useful characterisation method, thanks to its well-recognised fingerprint features.The IR spectra of liquids, gases and solid can usually be measured by transmitting the IR radiation through the sample. The signal that reaches the detector is dependent on the sample thickness, as the energy of the radiation will decrease the longer is the interaction

with the sample. Hence, preparation of the sample is crucial, and generally reproducibility issues between different users and samples occurs. Attenuated Total reflectance IR spectroscopy (ATR IR) uses a beam with energy in the IR region passing through an ATR crystal with high refractive index. The incoming radiation undergoes multiple reflection in the crystal, which is in close contact with the sample. Finally the beam exiting the crystal is collected by a detector (Figure 2.6).
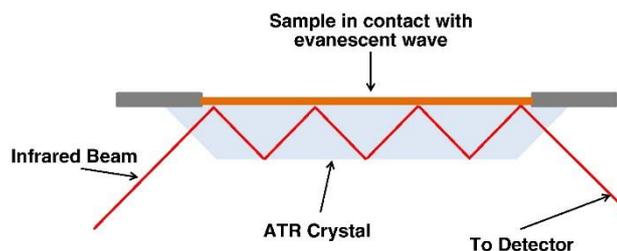
Figure 2.6 Scheme of an ATR-IR experiment. Taken from reference [11].

Molecular vibration give rise to infrared bands only if they produce a variation in the dipole moment of the molecule. For this reason diatomic molecules such N_2 or O_2 could not be detected by IR spectroscopy, whereas the asymmetric bond stretching of CO_2 gives rise to a characteristic band at 2400 cm^{-1}.
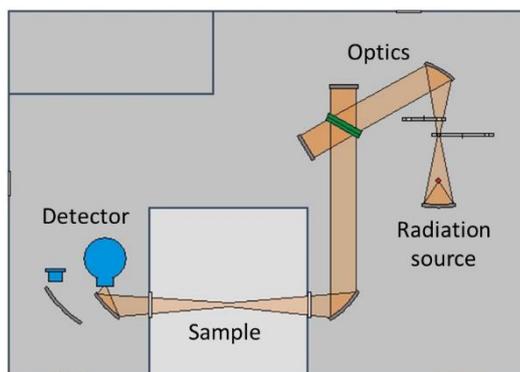
Figure 2.7 Scheme of the ATR spectrometer instrument setup used.

A Bruker Platinum ATR Vertex 70 was used to collect the ATR-IR spectra of the solid samples (Figure 2.7). Transmittance was measured between 4000 and 500 cm^{-1} with a resolution of 2 cm^{-1} using a MIR source, a Liquid Nitrogen cooled Mercury Cadmium Telluride (LN-MCT) detector and a KBr beam splitter.

2.3.4 Brunauer Emmett Teller surface area analysis

The ability to determine the surface area and pore volume of a material is very useful in the study and development of materials. The technique used to obtain such information is based on the physisorption properties of gases, in particular of N_2. When interacting with a surface at standard temperatures, N_2 condenses, forming a liquefied monolayer of the size of the N_2

molecule itself. The method requires the treatment of the sample under vacuum, to clean the surface from adsorbed molecules, such as water. After that, the sample undergoes additions of the adsorbate gas (usually N_2, at -196 °C) at different pressures. The adsorption isotherm represents the volume of N_2 that has been adsorbed, against the relative pressure.

The Brunauer Emmett Teller (BET) method is the most widely used for the determination of the surface area of finely ground and porous materials, and makes use of the corresponding isotherm equation.[12-13]

$$\frac{p}{v(p_0 - p)} = \frac{1}{v_m c} + \frac{(c-1)p}{v_m c \, p_0}$$

With

v_m= volume of gas required to form a monolayer

v= volume of gas adsorbed at the relative pressure p/p_0

c= value exponentially related to the enthalpy of adsorption in the first layer.

The plot of $p/v(p_0 - p)$ against p/p_0 should give a straight line, whose intercept is $1/v_m c$ and whose slope is $(c-1)/v_m c$, from which is possible to determine the surface area of the sample.

Surface area analysis was performed on the hydrothermal carbon samples. Initial experiments counted 20 points of adsorption and desorption of N_2. However, as these extended measurements were not giving clear results, and many of the HTCs showed extremely low surface areas, shorter experiments were conducted using 5 adsorption points to obtain a linear trend. Nitrogen adsorption isotherms were collected using a Quantachrome Quadrasorb instrument after evacuating the samples at 120 °C overnight. Analyses was carried out at -196 °C with p_0 measured continuously.

2.3.5   Metal surface area pulse titration using carbon monoxide

Carbon monoxide (CO) has a very strong affinity to transition metals and it is a known strong poison to some noble metals, as it binds very strongly blocking the access to other gasses and reactants. CO bonds to transition metals *via* a partial triple bond, depicted in Figure 2.8 and composed by:

1. A σ-bond between a sp-hybridised electron pair of the carbon with the orbitals of the metal.

2. A pair of π-bonds formed from the overlapping of π-antibonding orbitals of the carbon atom in the CO molecule and the filled d-orbitals on the metal. For this bonding, the metal needs to have d-electrons and be in a low oxidation state, in order to make the back donation as strong as possible.

σ bond   π back-bond
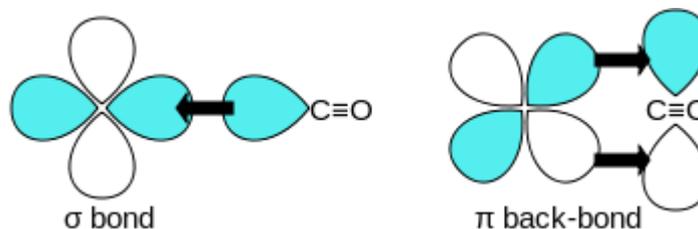
Figure 2.8 Orbitals representation showing the M-CO bond formation.

Taking advantage of the strong interaction between CO and metals such as Pd, Pt, Rh, Ir and Ni, CO can be used as probe molecule to analyse and measure the metal surface area of a sample containing such reactive elements. A fixed amount of gas is flushed through the sample, the CO will bind to the metal, blocking a site. By repeating the procedure the surface of the metal is saturated with CO and no more gas will be adsorbed.

By this method it is possible to determine the exposed surface area of the target metal, as well as its dispersion on the support, knowing the total amount of metal.

Metal dispersion is defined as

$$D(\%) = \frac{N_S}{N_T} 100$$

With

N_S = atoms on the surface

N_T = total amount of atoms.

The specific surface area, S_{SP} calculated with the following formula

$$S_{SP} = a_m \frac{N_A}{M} D$$

With

a_m = surface area occupied by a metal atom

N_A = Avogadro's number

M = atomic mass of the metal

The metal surface area of the Pt/TiO_2 catalysts has been measured by use of CO as probing molecule. The amount of CO adsorbed on the platinum surface was measured using a chemisorption measuring system. To do this, *ca.* 50 mg of sample was loaded in a U-shaped Quarts cell, packed between two quartz wool layers. Accurate weight was noted, and the tube was set up in a ChemBet Pulsar (Quantachrome) analyser attached with a thermal conductivity detector (TCD). In order to clean the surface of the catalyst and ensure metallic platinum was present, the sample was pre-treated in 10% H_2/Ar flow at 150 °C for 30 min before the titration. Then an automated CO pulse titration program was used to flush the sample with 70 µl of 10% CO/Ar at room temperature. Pulses of CO were flushed through the sample until saturation of the platinum surface was achieved. The amount of CO adsorbed on the platinum surface (stoichiometry 1:1) was calculated from the change in the peak area of CO due to its adsorption on the catalyst. Depending on the sample, 8 to 10 pulses were necessary to achieve saturation of the surface. Calibration was based on the biggest peak areas.

2.3.6   Thermogravimetric analysis

Thermogravimetric analysis (TGA) measures the change in weight of a sample, by applying a temperature gradient. From this experiment, it is possible to determine the stability of a material in a desired temperature range, the water or residual solvent content, or the amount of functional groups (such as hydroxyls or carbonyls). Usually a gas flow is present, determining the environment under which the temperature treatment is performed: helium, nitrogen or air. An empty crucible is tared at the beginning of the experiment, then the sample is loaded in the crucible and the exact weight of the sample is noted as 100 %. The amount of sample being around 50 mg. The crucible is then hooked and connected to a high precision balance that tracks the variation in mass as the temperature raises. For a better understanding of the species formed during decomposition of the sample, the analysis can be coupled with spectroscopic or spectrometric analysis of the outcoming gas flow. At the end of the experiment, a plot of mass % *vs.* temperature can be obtained. Calculating the first derivative as the change of mass as a function of temperature can give a better indication of the change in weight, since it is more sensitive to slope changes.

Experiments under an inert atmosphere of flowing He were carried out using a Perkin Elmer Thermogravimetric Analyzer Pyris 1 TGA. Whereas the controlled combustion of the samples in air was performed using a Perkin Elmer Thermogravimetric analyser TGA 4000. For both type of experiments, a gas flow of 20 ml/min was applied and a 10 °C/min temperature ramp rate up to 800 °C was used to study the thermal stability of the samples.

2.3.7 Electron microscopy

In the first half of the 1900s electron microscopy started to develop, thanks to Ernst Ruska and Maximillian Knoll. This is a very useful and still expanding characterisation technique that allows to look at the structure, composition and morphology of nanomaterials, such as heterogeneous catalysts.[14] In light-based optical microscopes, visible light interacts with a sample and glass lenses control magnification of the image with, a resolution of ca. 0.5 μm, not allowing looking at smaller objects, due to the limit of visible light wavelength. However, since electrons are particles, but also behave like waves, with very short wavelength (<1 Å), in electron microscopes a high-energy electron beam interacts with the specimen, allowing for much higher (near atomic) resolution. Different type of electron microscopes exist, during this work, scanning electron microscopy (SEM) and transmission electron microscopy (TEM) have been used.

In general, electron microscopes work under vacuum, to prevent loss of electrons. The electron beam is produced by a field emission gun, emitted by the cathode and then formed and concentrated by a system of magnetic lenses. It is then directed through the specimen, where the electrons may interact with it and be deflected. In Figure 2.9 a TEM and SEM set up are depicted. Similar features are found in both instruments, however in the SEM, the electron beam is reflected and scattered to the detector that is located aside and not below the specimen.
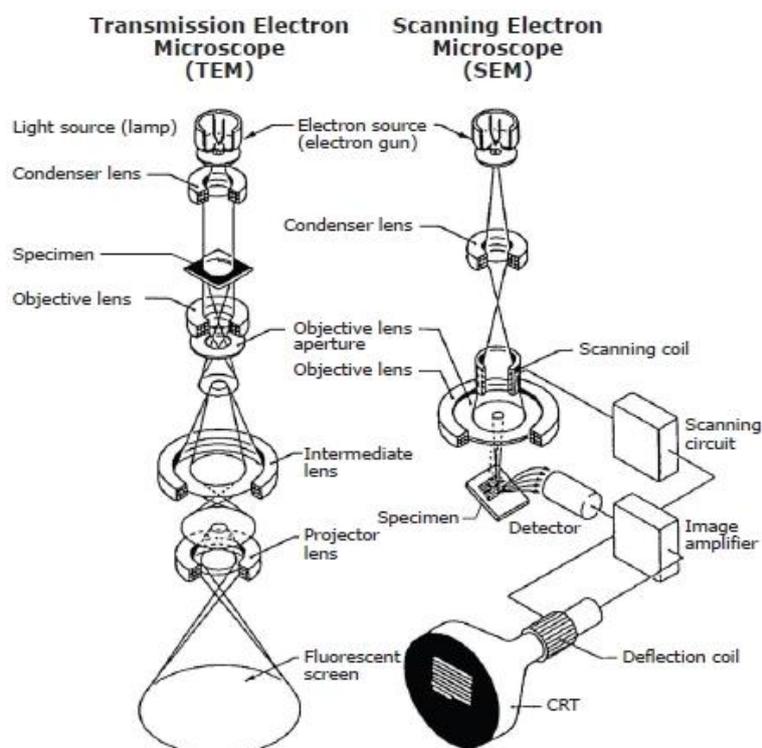
Figure 2.9 Schematic representation of a transmission and a scanning electron microscope. Taken from JEOL website.

Spatial resolution is controlled by the penetration and spreading of the electron beam in the sample. Using ultra-thin specimens, in which the penetration of the beam is limited, can allow obtaining a better spatial resolution.

Scanning Electron Microscopy

During a scanning electron microscopy analysis, an electron beam scans rapidly over the surface of the sample specimen, obtaining an image of the topography of the surface at high magnifications by collecting the secondary and backscattered electrons. The resolution of a SEM is about 10 nm. The resolution being limited by the width of the exciting electron beam and the interaction volume of electrons in a solid. Therefore from SEM analysis is possible to obtain information on the morphology, topology and composition of the area considered. Since electrons irradiate and interact with the sample, if X-rays are generated from the sample, they can be detected to give elemental information by X-Ray energy dispersive (EDX) analysis.

To analyse the catalysts supported on HTC materials, a Hitachi-TM3030 Plus Tabletop Microscope was used. Observation mode was set to standard back scattering electron (BSE), while the voltage setting and lens conditions were set to the analysis mode EDX. Elemental analysis (EDX) – was applied using Quantax 70 program for the element determination and quantification.

Transmission Electron Microscopy

Instead of bouncing the electron beam off the sample as occurs during SEM analysis, with TEM the electron beam travels across the specimen, and information is obtained by looking at beam electrons transmitted by the sample.

Transmitted beam electrons that have been scattered through a relatively large angle are detected using a high angle annular dark field (HAADF) detector (Figure 2.10). The image intensity arising from these inelastically scattered electrons is dependent on the square of the atomic number Z^2 of the element in the specimen. Therefore, HAADF images are easier to interpret and are informative of the elements present in the specimen as heavier elements will look brighter.
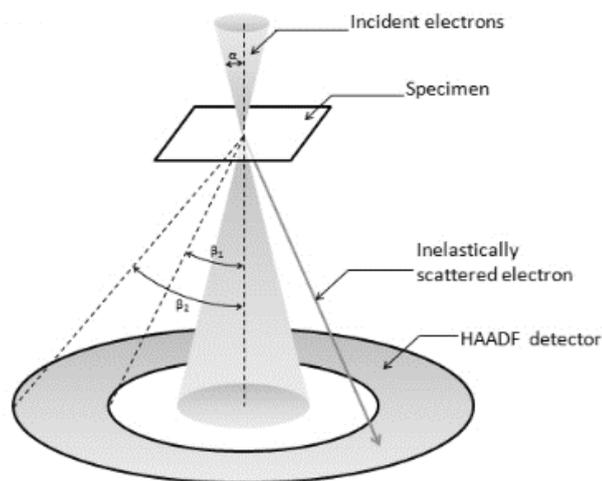
Figure 2.10 Schematic representation of the electron beam detector used in TEM. Imagine taken from JEOL website.

Samples for examination by STEM were prepared by collaborators, by dry dispersing the catalyst powder onto a holey carbon film supported by a 300-mesh copper TEM grid. Bright field (BF) and high angle annular dark field (HAADF) STEM images were taken using an aberration corrected JEM ARM-200CF microscope operating at 200kV. This instrument was also equipped with a JEOL Centurio silicon drift detector for X-ray energy dispersive spectroscopy (XEDS). Particle size distribution analysis was performed from analysis of the HAADF electron micrographs using Image J.

2.3.8   X-ray absorption spectroscopy

X-Ray absorption spectroscopy (XAS) is a powerful and useful technique that allows the study of the local structural environment of a specific element contained in a sample. It requires use of a synchrotron radiation as source of energetic X-ray beams and the incoming photons are tuned using a specific binding energy of a core electron of the element of interest. In Figure 2.11 is shown an absorption spectra as example, where the intense first peak at low binding energy values is the edge that defines the ionisation threshold to continuum states of the excited electron.[15] A wide range of information can be obtained from XAS experiments, from oxidation state and geometry to neighbouring atoms.[16]

As shown in Figure 2.11, two regions of interest can be identified from an X-ray absorption spectrum: X-ray absorption near edge structure and extended X-ray absorption fine structure.
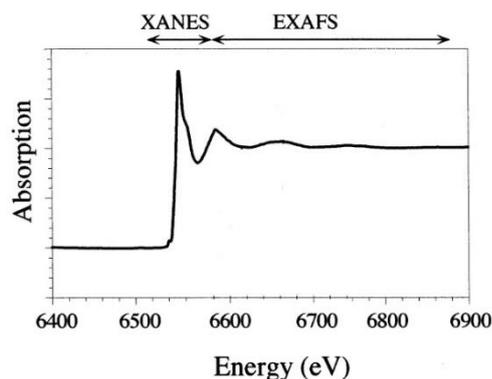
Figure 2.11 Scheme showing the different energy regions considered in the XANES and EXAFS measurements for the X-ray absorption spectrum at the Mn K edge. Taken from reference [16].

X-Ray Absorption Near Edge Structure

XANES is the region of the X-ray absorption spectrum within ~50 eV just before and after the adsorption edge (white line). The energy of the photon is enough to excite a core electron to unfilled orbitals.[17] From this measurement is possible to obtain information about the oxidation state and the coordination geometry of the specific element analysed. The edge position (binding energy) depends on the oxidation state of the element, with a shift to higher binding energy as the oxidation state increases. The intensity of the signal depends on the transition probability and the density of the unoccupied states.

By XANES analysis is possible to probe the angular momentum of the unoccupied electronic states, hence dipole selection rule applies:

$\Delta l=\pm1, \Delta j=\pm1, \Delta s=0$

Possible transitions are:

$s\rightarrow p$ for K and L_1 edges of $1s$ and $2s$ core electron initial state respectively.

$p\rightarrow d$ for L_2 and L_3 edges for $2p_{1/2}$ and $2p_{3/2}$ core electrons.

For group VIII metals, the L_3 absorption edge of the XANES is called white line. The electrons transit from $2p_{3/2}$ to $5d$ states. The more unoccupied $5d$ states are on the atoms, the more intense is the white line intensity (see Figure 2.12). In the case of platinum, the L_3 edge can be measured and the more unfilled are the 5d states, so the more oxidised is the platinum, the stronger is the intensity of the white line.
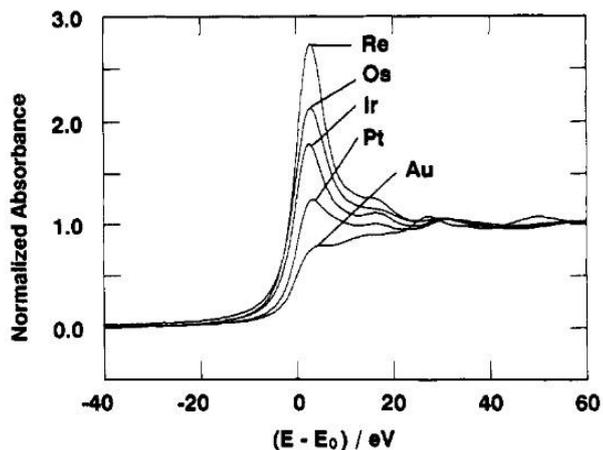
Figure 2.12 Spectra comparing the L_3 adsorption edge of the group VIII metals. Taken from reference [18].

Extended X-Ray Absorption Fine Structure

EXAFS is a technique that looks at the oscillatory structure after the electron has been ejected. It is a powerful probe, which provides a local structural model, without the need of a periodic long-range order. By this absorption technique, it is possible to determine the chemical environment of a specific element, the number and type of neighbours, interatomic distances and structural disorder. This determination is confined to a distance given by the mean free path of a photoelectron in the condensed matter, ~5-10 Å. The fine structure arises from the interference effects between the outgoing and backscattered photoelectron waves. The EXAFS spectrum is constituted of different sine waves, each representative of the different scattering paths taken by the photoelectron wave (Figure 2.13).
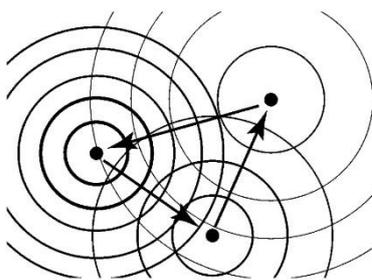
Figure 2.13 Simplified representation of the interference effect arising from the multiple scattering of a wave between neighbouring atoms. Taken from reference [15].

Because EXAFS is an interference effect that arises from the photoelectron rather than the X-ray, it is convenient to think of EXAFS in term of photoelectron wavenumber k (Å^{-1}) instead of X-ray energy (eV). For this reason the EXAFS analysis data comprises of a series of steps, here briefly summarised:

The absorption data $\mu(E)$ are first normalised, so to obtain a straight baseline $\mu(E)_{norm}$. The signal, a function of energy, is then transformed into a function of wavenumber $\mu(k)_{norm}$. The EXAFS oscillations $\chi(k)$ can be extracted from $\mu(k)_{norm}$ by subtraction of the background of the isolated atom and normalising.

$$\chi(k) = \frac{\mu(k) - \mu_0(k)}{\mu_0(k)}$$

Eventually the Fourier transformation allows to see the contribution representative of the different scattering of the photoelectron, giving a radial distribution function $FT(\chi(k))$.

XAS measurements were performed on stations B18 and I20 at the Diamond Light Source (Harwell, Oxon) operating at 3 GeV in multi-bunch mode with a current of 200 mA. The experiments and data analysis were carried out by collaborators at Harwell and UCL.

Both B18 and I20 stations are equipped with a Si(111) double crystal monochromator, ion chambers for measuring incident and transmitted beam intensities and/or a multi-element Ge (fluorescence) detector for recording X-ray absorption spectra. The measurements were carried out in air on self-supporting wafers (approximately 100 mg) at the Pt L_3 edge, with the respective foil (10 μm) used as a calibrant for the monochromator. Measurements were performed at room temperature in normal step scanning mode. To improve the signal-to-noise ratio, multiple scans were taken. All data were subjected to background correction using Athena (*i.e.* IFEFFIT software package for pre- and post-edge background subtraction and data normalisation). XAFS spectra were normalized from 30 to 150 eV above the edge energy, while the EXAFS spectra were normalized from 150 eV to the last data point using the Autobk algorithm. Normalisation was performed between $\mu(E)$ and $\mu_0(E)$ via a line regression through the data in the region below the edge and subtracted from the data. A quadratic polynomial was then regressed to the data above the edge and extrapolated back to E_0. The extrapolated value of the post edge polynomial at E_0 was used as the normalisation constant. This threshold energy (E_0) is normally determined using either the maximum in the first derivative, approximately 50 % of the rising absorption edge, or immediately after any pre-edge or shoulder features. The isolated EXAFS spectra were analysed using the DL-EXCURV programme. Data were analysed using a least squares single or dual shell EXAFS fitting analyses performed on data that had been phase corrected using muffin-tin potentials. Amplitude reduction factors (S_o^2) of 0.94 obtained from fitting a Pt metal foil, was also used in the analysis.

2.4 Catalysts testing

2.4.1 3-Nitrostyrene hydrogenation

Catalytic testing was performed in a 50 ml glass round bottom Colaver® reactor fitted in an oil bath. For each reaction, 3-NS (0.2 ml) and toluene (8 ml) were added in the reactor, together with the catalyst (0.05 g). Once the reactor was loaded with reactant and solvent, it was purged with nitrogen flow before addition of pure hydrogen. After fitting the reactor in the oil bath previously heated at 40 °C, it was purged by flushing three times with 3 bar of H_2 under stirring at 500 rpm. After sealing the reactor, the reaction was set to start. After a specific time, the reaction stirring was stopped and the reactor was immersed in an ice bath to quench the reaction. After releasing the pressure from the reactor, two 1.5 ml centrifuge tubes were filled with the reaction mixture (1 ml) and centrifuged using a mini bench centrifuge for 10 min to separate the catalyst from the liquid reaction mixture. After separation, a GC vial was prepared by adding the reaction solution (1 ml) and the external standard *o*-Xylene (0.1 ml), accurately added and weighted. The determination of the conversion was performed by GC analysis (see Product analysis Section 2.5.1).

2.4.2 Glycerol oxidation

The glycerol oxidation test reaction was performed in a 50 ml glass round bottom Colaver® reactor fitted in an oil bath. For each reaction 0.5%AuPd/C catalyst (0.0455 g), NaOH 1.2 M (5 ml) and glycerol 0.6 M (5 ml) solutions were added and stirred at 900 rpm at 60 °C. For all the test reactions, the substrate to metal ratio was 4000:1 (glycerol: metal, mol: mol) and the substrate to base ratio was 1:2 (glycerol: NaOH, mol: mol).

After purging three times the reactor with 3 bar O_2, the reaction was set to start. Aliquots of 0.5 ml were collected after 15, 30, 60 and 120 min and the reaction was quenched by diluting 10 times in 4.5 ml deionised water. The catalyst was separated by filtration on a PTFE syringe filter (0.45 μm pores, 13 mm diameter, Fisherbrand) and the solution was analysed by HPLC (see Product analysis Section 2.5.2).

2.4.3 Hydrogen peroxide synthesis and hydrogenation

Tests were carried out using a Parr Instruments stainless-steel autoclave. The autoclave was equipped with an overhead stirrer (0– 2000 rpm) and provision for measurement of temperature and pressure. For each reaction, H_2O (2.9 g, HPLC grade), MeOH (5.6 g) and catalyst (0.01 g) were added in a PTFE 100 ml liner. The autoclave was then pressurised with 5% H_2/CO_2 (420

psi) and 25% O_2/CO_2 (160 psi). The autoclave was then cooled at 2 °C and stirred at 1200 rpm for 30 min. The amount of hydrogen peroxide formed during reaction was determined by titration using a diluted $Ce(SO_4)_2$ solution acidified with 2% H_2SO_4 and using ferroin as indicator. Productivity [mol/kg*h] was calculated as moles of H_2O_2 formed/mass of catalyst*time.

Hydrogenation experiments were performed by following the same procedure as above, but in the absence of oxygen and by addition of H_2O_2. Exact measurements of H_2O_2 concentration before and after reaction allowed to determine the decrease in H_2O_2 due to a combination of hydrogenation and decomposition processes.

2.4.4 Reusability tests

The catalyst used for the glycerol oxidation and for the hydrogenation of 3-nitrostyrene were tested over multiple uses, to study whether they are stable materials and can be used for multiple runs of the same reaction.

To do so, two 50 ml round bottom Colaver® glass reactors were used and loaded with the usual amount of substrate and solvent. Then, in one of the reactors (denominated A), the usual amount of catalyst was added, while in the second reactor (denominated B) a larger amount of catalyst weight (about five times more) was added. The catalytic testing was then ran as usual. After stopping and quenching the reaction in a bath of ice and water, the mixture from reactor A was analysed following the procedure, while the mixture B was filtered on a filter paper, washed with deionised water and acetone and let to dry in air in order to be used in a second reaction. The procedure was repeated multiple times.

2.5 Products analysis

2.5.1 Gas chromatography

Chromatographic techniques are highly applied methods to separate liquid mixtures into their components. The general concept is that a liquid sample is put in contact with a solid (stationary) phase. Then, a mobile phase (a gas or a liquid) is added to elute the sample along the stationary phase. The favourable interaction (physical or chemical) between the various components of the sample and the stationary phase makes it possible to elute and separate the mixture.

Gas chromatography (GC) is an analytical method where the sample is vaporised at high temperature prior to injection into a capillary column contained into an oven in order to maintain the vaporised species into gaseous phase (Figure 2.14). Usually, a temperature gradient

is applied, to facilitate the separation of the compounds based on their boiling points. The vapours are carried through the column and, at the end of the column, are analysed by a flame ionisation detector (FID). The combustion of the eluted organic molecules in hydrogen flame leads to the formation of ions that are detected by a pair of electrodes. The signal is proportional to the amount of ions formed and detected, therefore quantitative results can be obtained after calibration of the instrument. By this technique, mainly volatile hydrocarbons can be detected and quantified, whereas inorganic molecules cannot be studied.
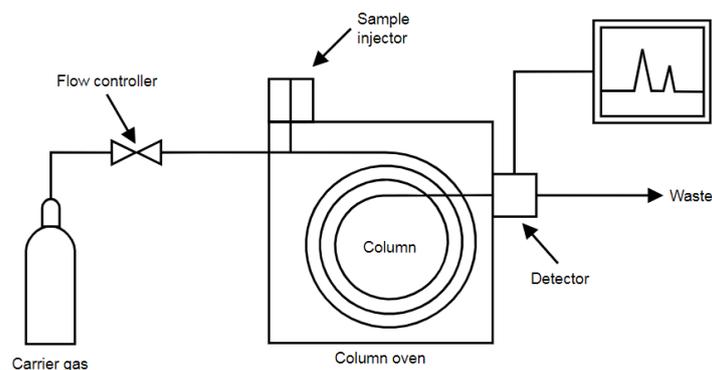
Figure 2.14 GC apparatus scheme.

Analysis were carried out using a Varian 450GC Gas Chromatograph with a fitted CP-Sil 5CB boiling point column and an FID detector and a CP8400 Autosampler. The sample was injected at 70 °C with a split ratio of 20 and using He as carrier gas. The oven temperature was set to reach 250 °C with a ramp rate of 5 °C/min and keep the set temperature for 1 min before the analysis was completed. The conversion of 3-NS was calculated as the percentage of moles of 3-NS converted to the initial amount of moles of 3-NS, while the selectivity was calculated as the percentage of moles of 3-VA to the moles of hydrogenated products.

2.5.2   High Performance Liquid Chromatography

High performance liquid chromatography (HPLC) similarly to GC, separates analytes along a column generally made of silica-based microporous materials, polymers or gels. With this method, poorly volatile liquid samples are injected, maintained under pressure, separated along the column and eluted at different retention times in the presence of a liquid eluent. A scheme of a HPLC system is reported in Figure 2.15. Usually aqueous solutions are analysed by HPLC and many different detectors can be used to analyse their components. In this work, two detectors were fitted in the HPLC system, a refractive index detector (RID) and a diode array detector (DAD). The former is a universal detector for HPLC, where the column effluents pass through a flow-cell over which the change in refractive index is determined. The latter is a spectrophotometric method where the eluted solution is analysed at a specific wavelength (where maximum absorption of the components is expected) in the UV range. The RID was used to

study the compounds containing hydroxyl groups (glycerol), while the DAD could detect compounds presenting carbonyl groups (glyceric and glycolic acid).
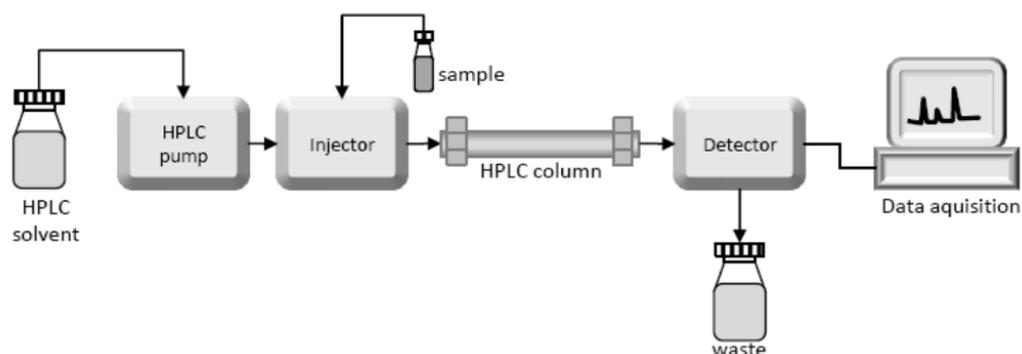
Figure 2.15 Schematic of a HPLC system. Taken from reference [19]

Samples were quenched and diluted 1:10 in 4.5 ml deionised water before filtration and analysis by HPLC. Product analysis was carried out using an Agilent 1260 Infinity HPLC with a Metacarb 67H column with a 0.1% wt solution of phosphoric acid as mobile phase.

2.6 Data analysis and quantification

The reaction liquid solutions from the 3-nitrostyrene hydrogenation and the glycerol oxidation reactions were analysed by chromatography, followed by a data analysis based on calibration curves and response factors.

Substrate conversion was calculated as

$$Conversion = \frac{mol_0 - mol_t}{mol_0} * 100$$

With mol_0 and mol_t being the amount of moles of substrate at reaction time 0 and end reaction time t.

Reaction rates of the initial stage of a reaction, when equilibrium is not yet reached, allow to estimate the velocity of a reaction under specific conditions. As the reaction time-on-line shows a linear trend, and the substrate conversion is below 20-30%, it can be determined as the negative of the slope of the plot of substrate concentration against time. Or as

$$Initial\ rate = -\frac{mol_t - mol_0}{vol * time_t}$$

Another crucial parameter of a chemical reaction is the selectivity of the products formed during the process. Because substrates containing multiple reactive functional groups were used during this project, which may lead to a mixture of products if the transformation of one

functional group is not energetically favourable compared to the other functionalities, selectivity for each possible product has been calculated as

$$Selectivity \; _A = \frac{moles \; of \; A}{tot \; moles \; of \; products} * 100$$

At last, the capacity of adsorbing and desorbing of reactants and products from the surface of the catalyst determines the velocity at which one catalytic cycle takes place, hence the activity of a catalyst, which could in turn be correlated to the Turn Over Frequency, which is defined as

$$TOF \; [h^{-1}] = \frac{moles \; of \; substrate \; converted}{moles \; of \; metal * time}$$

This is a valuable method to compare catalysts that might contain different amount of metal or might have been tested under different reaction conditions, especially when comparing data from literature.

Catalytic reactions were repeated multiple times (between two and five, depending on the reproducibility of the data). Standard deviation values were calculated from the catalytic data and used to produce error bars.

2.7 References

1. Sankar, M.; He, Q.; Morad, M.; Pritchard, J.; Freakley, S. J.; Edwards, J. K.; Taylor, S. H.; Morgan, D. J.; Carley, A. F.; Knight, D. W.; Kiely, C. J.; Hutchings, G. J. Synthesis of stable ligand-free gold-palladium nanoparticles using a simple excess anion method. *ACS Nano* **2012,** *6* (8), 6600-13.

2. Hutchings, G. J.; Kiely, C. J. Strategies for the synthesis of supported gold palladium nanoparticles with controlled morphology and composition. *Acc Chem Res* **2013,** *46* (8), 1759-72.

3. Reiche, S.; Kowalew, N.; Schlögl, R. Influence of synthesis pH and oxidative strength of the catalyzing acid on the morphology and chemical structure of hydrothermal carbon. *Chemphyschem* **2015,** *16* (3), 579-87.

4. Johannes B. Ernst, S. M., Fei Wang, Mizuki Tada, Frank Glorius. Tunable Heterogeneous Catalysis: NHeterocyclic Carbenes as Ligands for Supported Heterogeneous $Ru/K-Al_2O_3$ Catalysts To Tune Reactivity and Selectivity. *Journal of the American Chemical Society* **2016,** (138), 10718−10721.

5. Einstein, A. Über die von der molekularkinetischen Theorie der Wärme geforderte Bewegung von in ruhenden Flüssigkeiten suspendierten Teilchen. *Annalen der Physik* **1905,** *322* (8), 549-560.

6. Moulder, J. F.; Stickle, W. F.; Sobol, P. E.; Bomben, K. D. *Handbook of X-ray Photoelectron Spectroscopy*. Perkin-Elmer Corporation: Norwalk, CT, 1992.

7. McGraw-Hill. *Concise Encyclopedia of Physics*. 2002.

8.   Jacques Lemaitre, G. M., Francis Delannay. *Characterisation of heterogeneous catalysts*. Dekker: New York, 1984; Vol. 15.

9.   Scherrer, P. Estimation of the size and internal structure of colloidal particles by means of röntgen. *Nachr. Ges. Wiss. Göttingen* **1918,** *2*, 96-100.

10.   Dorofeev, G. A.; Streletskii, A. N.; Povstugar, I. V.; Protasov, A. V.; Elsukov, E. P. Determination of nanoparticle sizes by X-ray diffraction. *Colloid Journal* **2012,** *74* (6), 675-685.

11.   Shai, Y. ATR-FTIR studies in pore forming and membrane induced fusion peptides. *Biochim Biophys Acta* **2013,** *1828* (10), 2306-13.

12.   Sing, K. S. W.; Everett, D. H.; Haul, R. A. W.; Moscou, L.; Pierotti, R. A.; Rouquerol, J.; Siemieniewska, T. Reporting Physisorption Data for Gas Solid Systems with Special Reference to the Determination of Surface-Area and Porosity (Recommendations 1984). *Pure and Applied Chemistry* **1985,** *57* (4), 603-619.

13.   Brunauer, S.; Emmett, P. H.; Teller, E. Adsorption of gases in multimolecular layers. *Journal of the American Chemical Society* **1938,** *60* (2), 309-319.

14.   Liu, J. Y. Advanced Electron Microscopy of Metal-Support Interactions in Supported Metal Catalysts. *ChemCatChem* **2011,** *3* (6), 934-948.

15.   Rehr, J. J.; Albers, R. C. Theoretical approaches to x-ray absorption fine structure. *Reviews of Modern Physics* **2000,** *72* (3), 621-654.

16.   Penner-Hahn, J. E. X-ray absorption spectroscopy in coordination chemistry. *Coordination Chemistry Reviews* **1999,** *190*, 1101-1123.

17.   Brown, M.; Peierls, R. E.; Stern, E. A. White Lines in X-Ray Absorption. *Physical Review B* **1977,** *15* (2), 738-744.

18.   Meitzner, G.; Via, G. H.; Lytle, F. W.; Sinfelt, J. H. Analysis of X-Ray Absorption-Edge Data on Metal-Catalysts. *Journal of Physical Chemistry* **1992,** *96* (12), 4960-4964.

19.   Czaplicki, S. *Chromatography in Bioactivity Analysis of Compounds*. 2013; p 99-122.

Chapter

3

Study the effect of metal loading and heat treatment of Pt/TiO₂ catalysts for the chemoselective hydrogenation of 3-nitrostyrene to 3-vinylaniline

3.1   Introduction

3.1.1   Synthesis of substituted aromatic anilines

Production of anilines is of interest as they are intermediates for the production of industrially important products such as fertilizers, pharmaceuticals, dyes and plastics.[1-2] They can be obtained by the reduction of corresponding nitro compound precursors, but in the case of organic molecules with more than one functional reducible group, the selective hydrogenation is of fundamental importance.[3-4] In fact, not only products of unselective reaction could be formed, but also unstable intermediates such as hydroxylamines could be produced, leading to low yield of the desired aniline. In particular, hydroxylamine are intermediates formed during the subsequent reduction of the nitro group (Figure 3.1). If these toxic intermediates accumulate in the reaction mixture, they can not only decompose exothermically, but also condensate, leading to product quality problems.
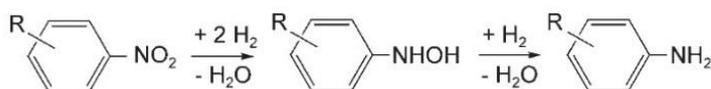
Figure 3.1 Proposed reaction scheme for the hydrogenation of a substitute aromatic nitro compound to the corresponding aniline. Taken from reference [5].

On one hand, selective reduction could be performed using stoichiometric amounts of inorganic salts such as stannous chloride $(SnCl_2)$[6], samarium iodide (SmI_2)[7] or zinc in ammonium hydroxide $(Zn(OH)_2+2NH4^+)$[8] as reducing agents in solution. These methods are not catalytic and reaction conditions and waste production are a major drawback. On the other hand, the use of environmentally friendly gaseous dihydrogen (H_2) as reducing agent and the activation by an appropriate heterogeneous catalyst would be the ideal solution towards a greener synthetic production, as it would be a cleaner and more atom efficient way to reduce organic molecules. Although this reaction could take place very efficiently, starting materials bearing multiple reducible functional groups may lead to unselective reduction products, which is a major problem

that involves additional purification and separation steps after synthesis. Therefore, it is necessary to develop catalysts able to enhance the reaction and to promote the formation of the desired product (chemoselective), hence catalyst designing, modification and implementation is required.

Gold-based catalysts have shown the ability to adsorb substituted nitro aromatic compounds *via* the nitro group, at the metal-support interface, favouring the hydrogenation of the adsorbed group to the corresponding aniline, avoiding formation of undesired by-products. Although very selective, the activity of monometallic Au/TiO$_2$ catalysts could not reach high turnover frequencies (TOF of 173 h^{-1} as reported by Corma *et al.* for a 1.5 % Au/TiO$_2$ catalyst) due to the low ability of gold to adsorb and dissociate H$_2$.[9-10]

Platinum-based catalysts are extremely active in the dissociation of H$_2$, to form reactive hydride species, making them good hydrogenation catalysts.[11] However, it has been reported that often these very active catalysts are not selective for the reduction of nitro groups when other functionalities are present on the substrate, hence addition of modifiers and additives is required to enhance the formation of the amino product. The hydrogenation of 3-nitrostyrene (3-NS) is often used as test reaction for the study and development of selective catalysts towards the reduction of substituted nitro aromatic compounds. In particular, the formation of the corresponding aniline, 3-vinylaniline (3-VA), while maintaining the C=C group, is of interest (Figure 3.2).
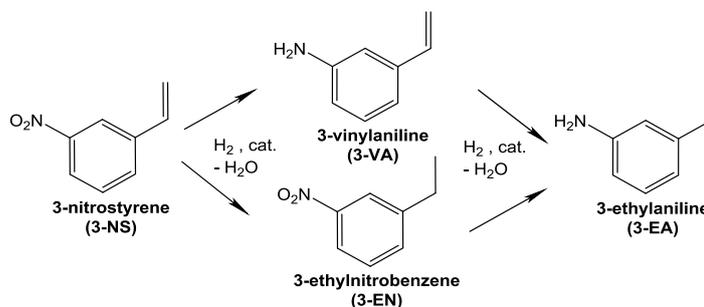
Figure 3.2 Reaction scheme of the hydrogenation of 3-NS.

It has been reported that the reduction of the C=C group is sensitive to the Pt particle size, with the rate of hydrogenation increasing with increasing metal particle size. Whereas, the hydrogenation of the NO$_2$ group is size insensitive.[12] The preparation of small Pt nanoparticles or even single atom catalysts with extremely high dispersion onto the metal oxide support have been the approach of choice of various research groups. Zhang and co-workers have studied the formation of clusters and single atoms on the surface of FeOx, which led to active catalysts delivering high selectivity towards the desired aromatic aniline.[13] Moreover, based on previous reports where Zn showed to inhibit the C=C hydrogenation,[14-17] Kiwi-Minsker and co-workers have studied the use of ZnO as support and showed that the dilution of Pt by Zn alloying led to the preferential formation of the substituted aniline.[18-19] In a similar way, Corma and co-workers

have determined that Pt species in close vicinity to the TiO₂ support would preferentially adsorb and hydrogenate the NO₂ group.[20] The same group showed how an appropriate activation step could substantially enhance the selectivity of monometallic Pt/TiO₂ catalysts, by favouring the formation of Pt-Ti interfacial sites, through a TiO₂₋ₓ encapsulation of the supported metal particles.[12]

3.1.2 Metal sintering and dispersion

After synthesising heterogeneous catalysts, it is of general practice to perform an activation step prior to use, in order to remove ligands and clean the surface of the supported metal, to achieve the desired oxidation state of the active species and to obtain a uniform distribution of the active sites. The temperature and the environment (inert, oxidising or reducing), under which the activation treatments are performed, are important parameters for achieving a stable and active material. One effect that the temperature and atmosphere could have on the supported metal species is to induce their agglomeration or dispersion, achieving large particles or favouring the formation of small homogeneous metal aggregates, respectively.[21]

Numerous studies have focussed on the effect that a calcination or reduction treatment has on the metal nanoparticle size of platinum catalysts supported on Al₂O₃ and TiO₂,. When samples were treated in oxidative atmosphere at temperatures >400 °C, platinum particles as big as 17 nm have been observed.[22-24] Such particles enlargement has been explained with the volatility of PtO₂, which is formed under oxidising atmosphere and that leads to facile interparticle transport.[23] However a similar argument was used to describe the redispersion observed in calcined Pt/TiO₂ samples, where Pt agglomerates were barely visible by TEM.[25] When a reductive heat treatment is performed, platinum could undergo reduction and small nanoparticles grow through migration and coalescence.[23, 25] Whereas, especially samples supported on alumina have shown that under reductive conditions, strong sintering and enlarging of metallic nanoparticles takes place.[26-27] An agreement is found in literature when supported platinum catalysts undergo a combination of oxidative and reductive treatments. It is generally found that this procedure would overall favour formation of small particles < 3 nm and narrow particle size distributions.[22, 24, 26-27] But since both treatments separately have been seen to lead to metal agglomeration, it is not completely understood which step helps in the metal dispersion on the support, finally favouring good distribution of the active sites.

3.1.3 Aim of the project

Different supports and preparation methods have been investigated in order to obtain active, selective and stable Pt-based catalysts,[28-29] however, in this work we aimed to study the effect that

the activation step could have on the final catalytic performance of Pt/TiO₂ catalysts prepared via a simple impregnation method. The majority of the research reported here indicates that the low selectivity of platinum-based catalysts could be improved by mean of the right preparation or activation method, which consequently leads to a different amount of highly active noble metal active sites.

With the knowledge of previous work on the topic, we decided to further explore the Pt/TiO₂ system for the chemoselective reduction of 3-NS to 3-VA. Moreover, the improvement of the efficiency of the metal used was of interest, since platinum is a rare and expensive metal. For this reason, it was aimed to studying the effect that a combination of various metal loadings, and post-preparation heat treatments, could have on the population of supported metal species and how that correlated with the final catalytic performance of these Pt/TiO₂ catalysts.

To do this, a series of samples with various metal loading were prepared and reductive or oxidative heat treatments were performed in order to affect the characteristics of the metal. All the catalysts were tested for the 3-NS hydrogenation reaction. In order to be able to draw a structure-reactivity correlation, a series of characterisation techniques have been applied to study the structural and electronic features of these catalytic materials. The catalysts were characterised by X-ray photoelectron spectroscopy (XPS), scanning transmission electron microscopy (STEM), X-ray absorption spectroscopy (XAS) and CO chemisorption.

3.2   Results

3.2.1   Catalytic testing

Previous studies carried out in our research group showed that noble metal based catalysts prepared by the modified impregnation method were active in the hydrogenation reaction of substituted nitro compounds.[30] To try comparing the results with the previous work by Corma *et al.*, we decided to test a platinum based catalyst prepared following the same procedure. A 0.2 %Pt/TiO₂ sample reduced at 450 °C was prepared by modified impregnation and tested for the hydrogenation of 3-NS at 40 °C under 3 bar H₂ pressure.[12] A good activity and complete selectivity towards the chemoselective reduction of the nitro group, forming 3-VA with a selectivity up to 100% was achieved, with no other undesired by-products being formed, such as the product of C=C double bond reduction 3-ethilnitrobenzene (3-EN) or the formation of hydroxylamine derivatives.

To study how an oxidative heat treatment rather than a reductive one could affect the catalytic activity, the as-prepared 0.2 %Pt/TiO₂ sample was calcined in static air under the same conditions

and tested, showing that the catalysis was completely switched off. To prove whether the catalytic performance could be re-established *via* a reductive treatment, which was initially shown to lead to formation of an active catalyst, a reductive heat treatment in furnace was performed under the same conditions. The 0.2% calcined and reduced sample was tested, achieving higher 3-NS conversions compared to the reduced only catalyst under the same reaction conditions and a constant 100% selectivity towards 3-VA. At longer reaction times, when higher 3-NS conversions are achieved, a slight decrease in 3-VA selectivity was observed as the formation of the product of over-reduction 3-ethylaniline (3-EA) occurred (Figure 3.3b).

To study the effect of the amount of metal impregnated onto the support, a series of samples with higher (0.5 %Pt) and lower (0.05 and 0.08 %Pt) metal loading were prepared. All samples underwent calcination in static air, reduction in hydrogen flow and both consecutive treatments (calcination and reduction) at 450 °C for 4 h. These samples have then been tested for the hydrogenation of 3-NS at 40 °C under 3 bar H$_2$ pressure. As observed before, we could confirm that no substrate conversion was obtained when testing the calcined only samples. For this reason, in Figure 3.3 as well as in the following catalytic results, only the data obtained testing the reduced only, and calcined and reduced samples are reported. In Figure 3.3a the initial rates of conversion of 3-NS are plotted for the series of catalysts with increasing platinum content. It is possible to see that the two reduced samples with metal loading 0.2 and 0.5%Pt show a substantially lower activity compared to the calcined and reduced counterparts (1.5 and 2.8 10^{-3} mol$_{3NS}$ L^{-1} min^{-1} rate the former, 6.0 and 10.4 10^{-3} mol$_{3NS}$ L^{-1} min^{-1} the latter). Opposite behaviour was observed for the low metal loading catalyst 0.05%Pt, where the reduced only sample is more active than the calcined and reduced one (8.3 and 1.6 10^{-4} mol$_{3NS}$ L^{-1} min^{-1} respectively). In contrast to the other samples, the 0.08%Pt sample does not show major variation in catalytic activity when comparing the reduced only and the calcined and reduced sample, both showing very comparable hydrogenation rate of 1.8 10^{-3} mol$_{3NS}$ L^{-1} min^{-1}, suggesting that a possible volcano plot peak has been identified.

It can be observed that by changing the activation step, the activity for the 3-NS hydrogenation reaction changes, while the selectivity for all of the catalysts is exclusively towards the formation of 3-VA. The only change in selectivity is observed when the 3-NS conversion reaches 70% and further hydrogenation of 3-VA towards the fully reduced 3-EA starts taking place, showing an overall decrease in 3-VA selectivity, as clearly seen in Figure 3.3b. It should also be noticed that apart from the substrate 3-NS and the desired and by-product 3-VA and 3-EA respectively, no formation of unstable and toxic hydroxylamines nor other undesired products were formed. In all the GC analysis of the reaction mixtures, only the chromatogram peaks assigned to the substrate and to the two products 3-VA and 3-EA were observed. This indicates not only the extremely high selectivity of the process but also suggests that a consecutive step

reduction is taking place, where the nitro group is preferentially hydrogenated at first, followed by the hydrogenation of the C=C double bond only when the concentration of 3-VA exceeds the concentration of 3-NS.
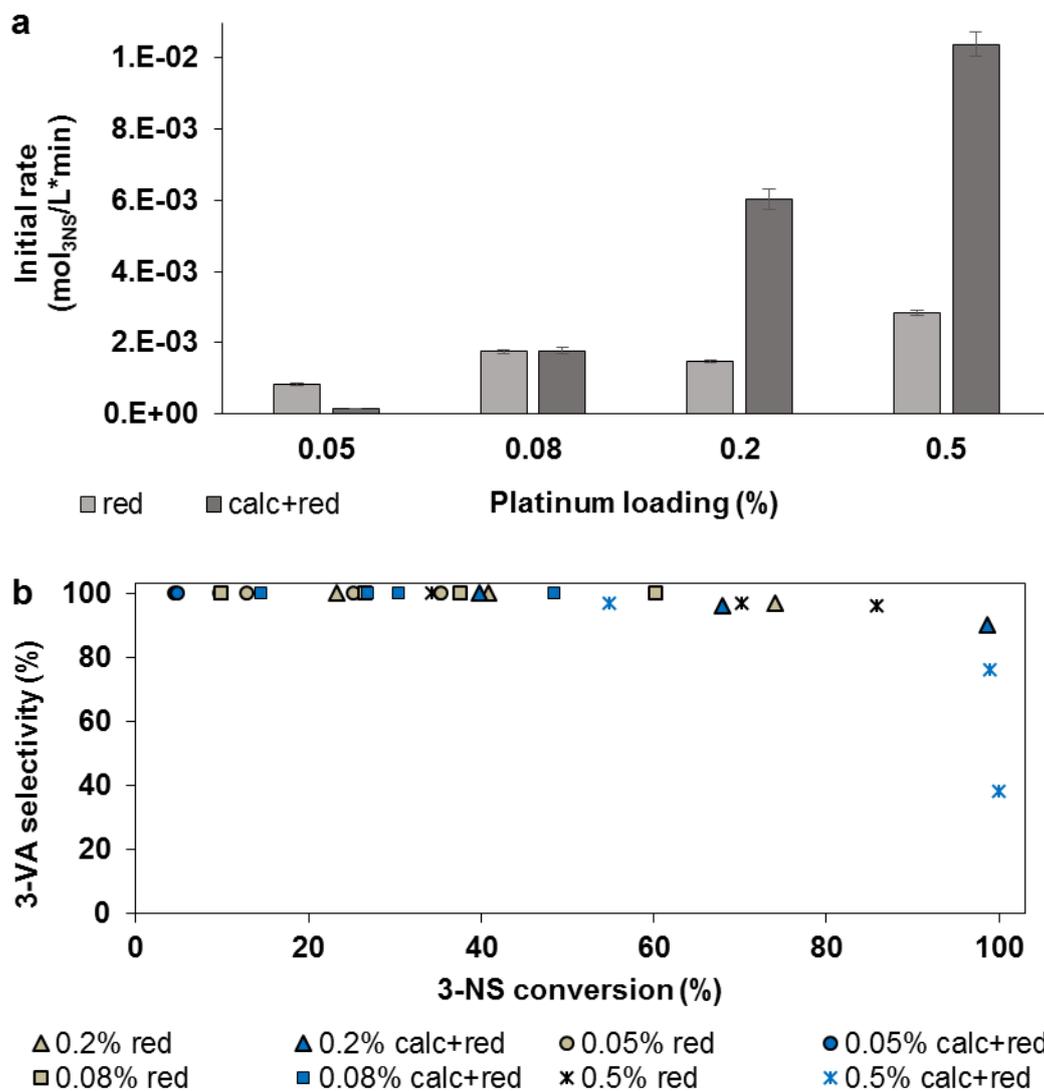
Figure 3.3 a) Comparison of the initial rates of the 3-NS hydrogenation reaction using catalysts with increasing metal loading. b) Variation of 3-VA selectivity with the 3-NS conversion. Reaction condition: 3-NS 0.2 ml, toluene 8 ml, catalyst 0.05 g, 40 °C, 3 bar H₂, 500 rpm.

3.2.2   Intrinsic catalytic activity

Because the catalytic screening was performed using the same reaction conditions, including the amount of catalyst mass, whereas the metal loading did change depending on the sample tested, a normalisation of the results obtained was necessary. The Turnover Frequency (TOF) is calculated dividing the number of moles of substrate that are converted during the reaction by the

amount of moles of metal in the catalyst divided by time (hours). In this manner, normalised catalytic activity values are obtained and could be used to compare samples containing different amount of metal. To be able to compare at best the results obtained in this work with previous literature, we assumed that all Pt atoms were accessible to the reactants.[13] By using the nominal metal values, an indication of the proportion of active sites, compared to the metal used during preparation is obtained. The rate values, where the initial change in 3-NS concentration gives a linear trend with time, were used to calculate the TOFs. Comparing TOF values of different catalysts gives indication about the relative amount of catalytically active species.

The TOF values are plotted in Figure 3.4. Similar to the trend observed in the rates data in Figure 3.3a, the higher metal loadings 0.2 and 0.5% Pt show that the reduced samples are less active than the calcined and reduced ones, whereas the lowest metal loading 0.05% Pt follows the opposite trend. Moreover, the catalysts containing 0.08% Pt seem to be independent on the heat treatment. However, overall, in the TOF plot in Figure 3.4, a different trend to the one seen for the rate data can be found and two plots with different maxima could be fitted.
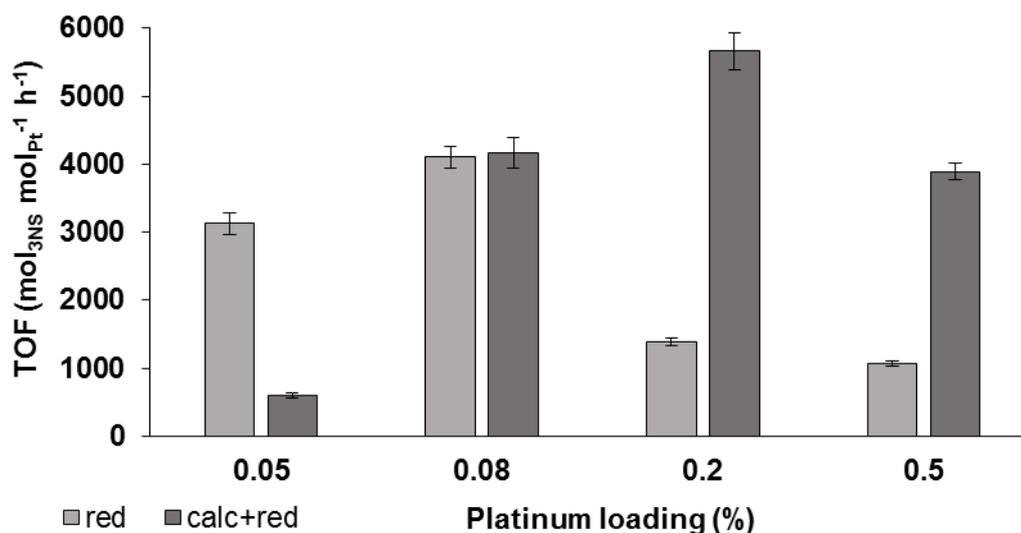
Figure 3.4 Turnover frequencies from Table 1 for the 0.05 to 0.5 %Pt/TiO₂ catalysts that underwent reduction and calcination+reduction treatments. Reaction condition: 3-NS 0.2 ml, toluene 8 ml, catalyst 0.05 g, 40 °C, 3 barH₂, 500rpm.

The TOF values of reduced only samples show a first increase from 3127 to 4101 h^{-1} between 0.05 and 0.08 %Pt catalysts, followed by a decrease in activity as the metal loading increases, with values of 1384 and 1065 h^{-1} for the 0.2 and 0.5 %Pt samples respectively. These results indicate that the amount of active species strongly depends on the metal loading and that a volcano plot rather than a constant trend is found, where the 0.08 %Pt reduced sample is the top of the volcano, with the highest percentage of catalytically active sites.

The TOF values of the calcined and reduced samples show a similar trend to the reduced only samples. The very low activity of the 0.05 %Pt sample is confirmed by a TOF value of 596

h^{-1} followed by 0.08 %Pt calcined and reduced catalyst showing a very comparable activity to the reduced only one (4164 h^{-1}). The relative amount of active species is at its most in the 0.2 %Pt sample with a TOF of 5659 h^{-1}, followed by a decrease in the 0.5 %Pt catalyst. In this way for the calcined and reduced samples, a second trend is identified, where the 0.2 %Pt sample is positioned at the maximum.

Overall the TOF values here discussed show that there is not a general trend, because both the metal loading and the type of heat treatment must be leading to formation of different proportion of active sites. However, the 0.2 %Pt calcined and reduced catalyst has the highest intrinsic activity of 5659 mol$_{3NS}$.mol$_{Pt}^{-1}$ h^{-1} and hence it is possible to conclude that it contains the largest percentage of active species.

The catalyst containing the lowest platinum content, 0.05%Pt, is an extreme case that behaves differently. After reduction only, the intrinsic activity is comparable if not higher than samples with higher metal loading. When the same metal loading sample undergoes both calcination and reduction treatments, the catalysis is strongly diminished. This result underlines again the importance of not only the metal content but also the activation step, the effect of which should not be generalised as will be presented in more detail in the following sections. However, from the catalytic results discussed so far, it should be possible to suggest that the combination of deposited metal and heat treatment plays a crucial role in the formation of the nanoparticles structure and in the metal dispersion onto the support. Once the lowest metal loading is reached, the combination of two heat treatments might negatively affect the exposure of the active metal, which might indicate that a limit in the metal content necessary for an optimal dispersion and formation of the active species has been reached. This could be confirmed by the very similar activity observed so far for the 0.08 %Pt samples, where both heat treatments have led to similarly active catalysts. It is possible that the amount of metal deposited is low enough to avoid sintering during the only reductive step, forming well-dispersed metal aggregates similar to the case of calcined and reduced samples. If the effect of the heat treatment environment on the metal dispersion is as reported by Koninsberger *et al.*, where agglomeration of the platinum was observed when only a reductive treatment was performed on the as prepared catalysts,[26] the behaviour of the 0.2 and 0.5% Pt catalysts could be explained based on the final metal exposure due to poor distribution. The more metal sintering occurs during reductive treatment, the larger are the final nanoparticles, which leads to a larger ratio of metal atoms in the bulk and hence not available to the reactants during the reaction. In contrast to, if from calcination followed by reduction a higher dispersion of the metal is achieved,[24] a higher proportion of low coordinated active Pt species should be present on the surface. In contrast to the higher metal loadings, the 0.08 and 0.05% Pt catalysts may contain a too low amount of metal to lead to substantial platinum

agglomeration, whereas the combination of heat treatments may actually affects negatively the final catalyst.

3.2.3 Comparison with previous works

Comparing TOF values with other data reported in literature (see data in Table 3.1), Zhang *et al.* reported a maximum TOF of 1514 $mol_{conv.}mol_{Pt}^{-1}$ h^{-1} for the single-atom 0.08%Pt/FeO$_x$ catalyst reduced at 250 °C and to 88 $mol_{conv.}mol_{Pt}^{-1}$ h^{-1} 0.2%Pt/TiO₂ reduced at 450 °C under comparable reaction conditions.[13] Results reported by Kiwi-Minsker,[18] Polshettiwar,[31] and Corma[12] are difficult to compare because of the difference in reaction conditions or in the way the results are reported, hence it is challenging to compare TOF values. However, from our understanding, the catalysts discussed here show extremely high activity together with an almost complete selectivity towards the desired product.

Table 3.1 Comparison of the activity and selectivity of the most active 0.2%Pt/TiO₂ calc+red catalyst and the values found in literature for the same reaction.

Catalyst	Treatment	Reaction conditions	3-NS conv (%)	3-VA sel (%)	TOF (h⁻¹)	Ref.
0.2%Pt/TiO₂	calc+red 450 °C	3-NS/Pt = 1000 Temp= 40 °C Pressure = 3 bar Time = 60 min	99	90	5659	This work
0.08%Pt/FeO$_x$	red 200 °C	3-NS/Pt = 1250 Temp= 40 °C Pressure = 3bar Time = 49 min	96	98	1494	13
0.08%Pt/FeO$_x$	red 250 °C	3-NS/Pt = 1250 Temp= 40 °C Pressure = 3bar Time = 50 min	97	99	1514	13
0.08%Pt/FeO$_x$	red 250 °C	3-NS/Pt = 1250 Temp= 80 °C Pressure = 10 bar Time = 7 min	89	91	11064	13

Catalyst	Treatment	Reaction conditions	3-NS conv (%)	3-VA sel (%)	TOF (h⁻¹)	Ref.
0.2Pt/TiO₂	red 450 °C	3-NS/Pt = 323 Temp= 40 °C Pressure = 3 bar Time = 390 min	95	93	-	12
0.2%Pt/TiO₂	red 450 °C	3-NS/Pt = 1250 Temp= 40 °C Pressure = 3 bar Time = 840 min	97	94	88	13
1.4%Pt/ZnO	red 300 °C	3-NS/Pt = 150 Temp= 75 °C Pressure = 10 bar Time = -	~99	97	44640	18
0.1%Pt/TiO₂	red 300 °C	3-NS/Pt = 150 Temp= 75 °C Pressure = 10 bar Time = -	~99	53	24120	18
2%Pt/ZnO	red 300 °C	3-NS/Pt = 100 Temp= 75 °C Pressure = 10 bar Time = -	~99	97	3840	19
1%Pt/SiO₂		3-NS/Pt = 2000 Temp= 25 °C Pressure = 10 bar Time = -	90	70		31

From here, catalyst characterisation is crucial for understanding, which is the active site for this reaction, how to achieve it and how it is modified during the heat treatments.

To further study and understand the effect of metal loading and heat treatment, electron microscopy and particle size analysis could give detailed information regarding the microscopic characteristics of the supported metal particles. The results of these analyses are discussed in the following section.

3.2.4 Study of the platinum particle size

From the catalytic performances discussed in the previous section, we could conclude that different population of active catalytic species could be present on the platinum samples prepared using a combination of various amount of metal precursor and heat treatment. One important parameter that is considered when studying noble metal supported heterogeneous catalysts is the metal particle size. In fact, the peculiar catalytic properties of nano-sized metal particles seem to arise from the modified electronic properties compared to the bulk material, which makes them more reactive. Moreover, because each metal atom is a potential active site, the maximal metal exposure needs to be achieved. The sphere is the most energetically favourable shape for an aggregate and the high surface area to volume ratio that could be reached by extremely small metal aggregates can strongly affect the final catalytic performance. For this reason, to try finding a correlation between the different catalysts and their hydrogenation activity, the study of the type, shape and size of platinum particles has been performed using a powerful method of mapping samples in a Scanning Transmission Electron Microscope (STEM) using High-Angle Annular Dark-Field (HAADF) imaging. This tomography technique is very sensitive for detecting variation in the atomic number Z of the atoms present in the sample, giving images with good contrast. HAADF-STEM tomography finds large application in the characterisation of nanostructured heterogeneous catalysts, where very small length scales, overlapping morphologies and large difference in average Z between the metal particles and the support combine. By HAADF-STEM imaging and analysis, we were not only able to look at the samples but also to study how much dispersed is the metal, the particle size distribution and in which form and structure the platinum is organised on the surface of the support. Our collaborators from the Department of Materials Science and Engineering at Lehigh University in Pennsylvania conducted the electron microscopy analysis of the samples, collected the images and performed the Particle Size Distribution (PSD) analysis on the 0.05, 0.08, 0.2 and 0.5 %Pt reduced only as well as calcined and reduced samples. In Figure 3.5 are shown representative images, whereas in Figure 3.6 are reported the results of the particle size distribution.
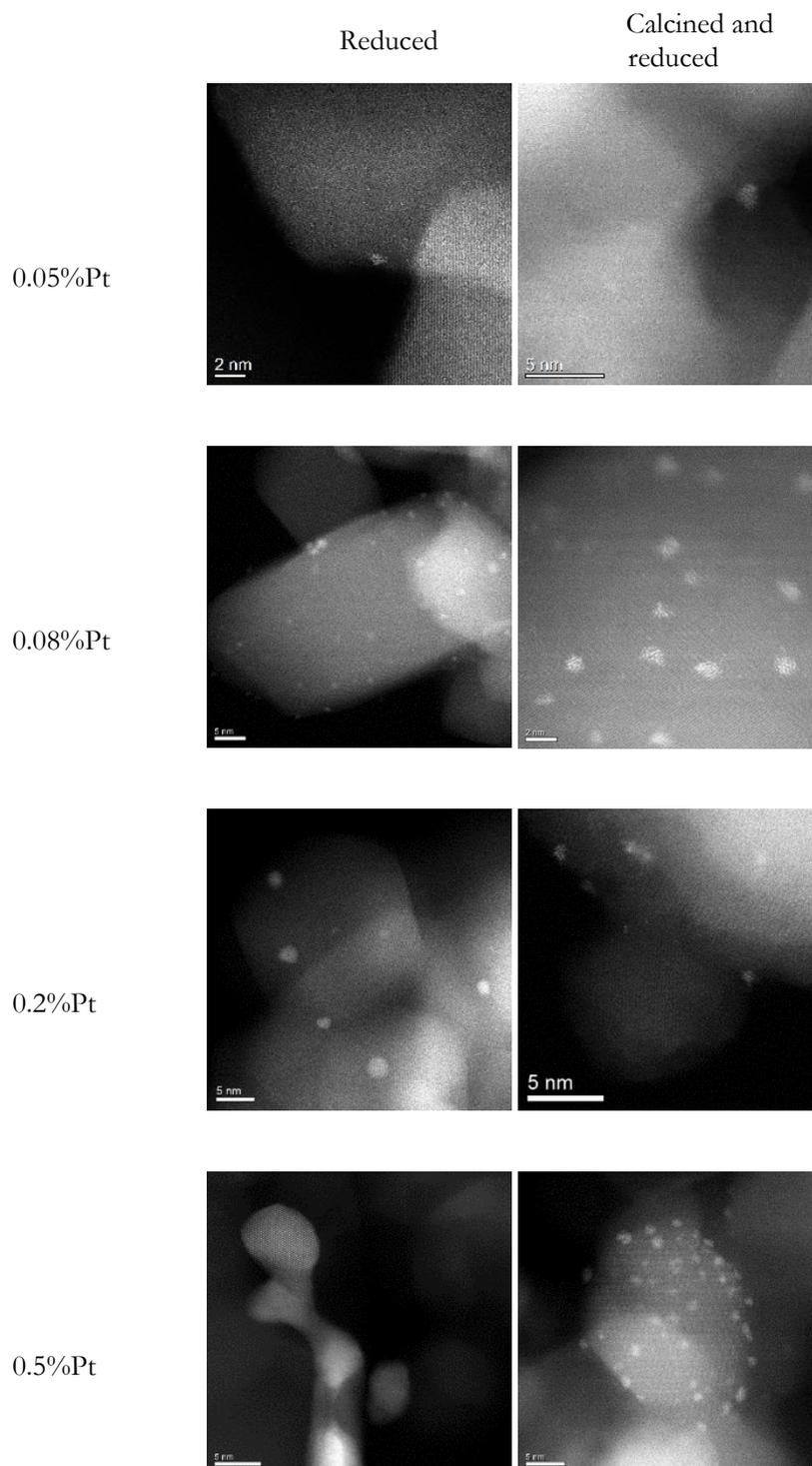
Figure 3.5 STEM-HAADF images of reduced only (left hand side column) and calcined and reduced (right hand side column) 0.05, 0.08, 0.2 and 0.5%Pt samples (top to bottom).

Reduced   Calcined and reduced
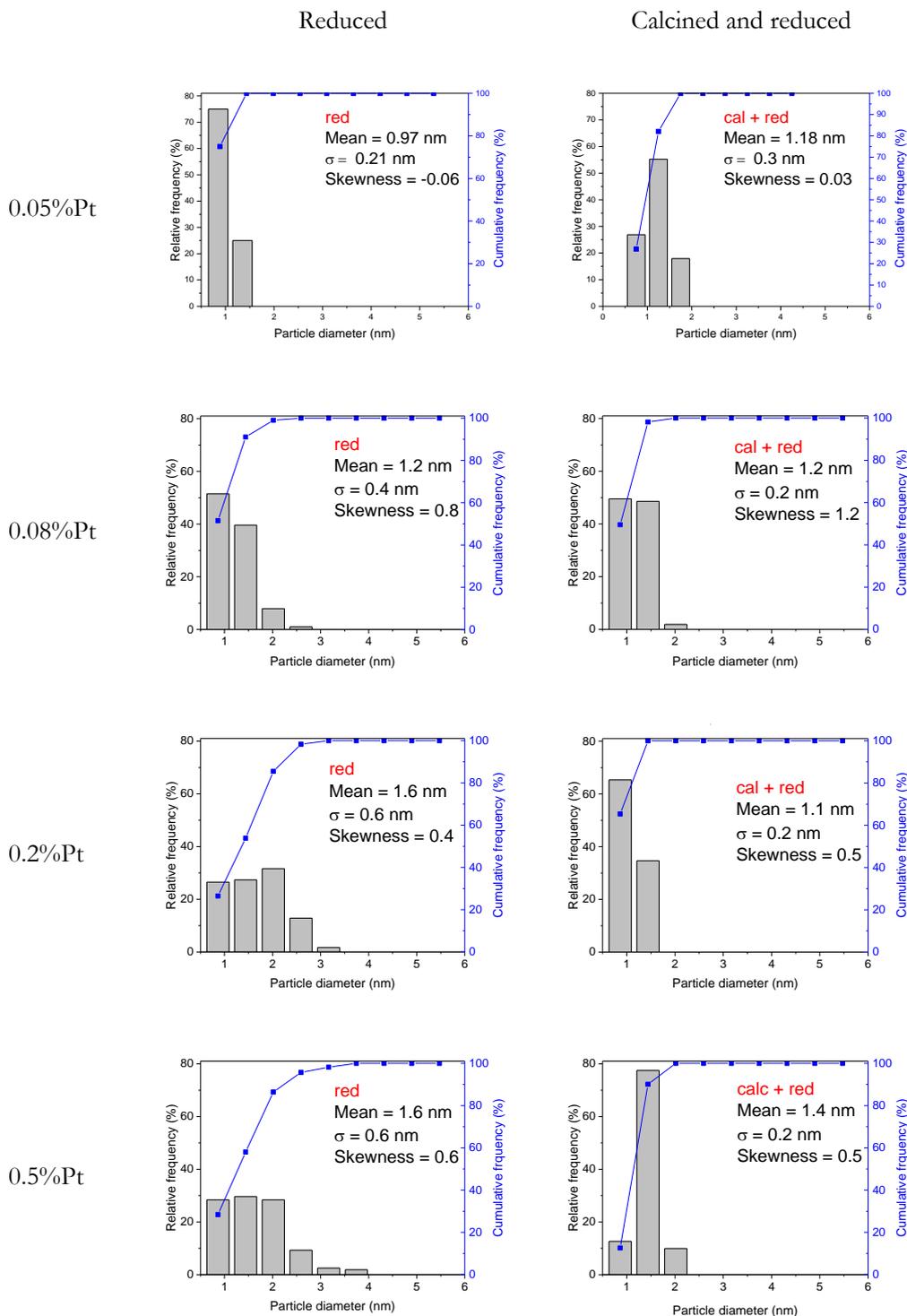
Figure 3.6 Particle size distribution plots of reduced only (left hand side column) and calcined and reduced (right hand side column) 0.05, 0.08, 0.2 and 0.5%Pt samples (top to bottom).

By mean of STEM and particle size analysis, looking at the higher loading reduced only samples similar observation could be made. In fact, it is revealed that on the surface of the 0.2% Pt reduced sample a quite broad particle size distribution with a mean particle size of 1.6 nm is present. The presence of relatively big nanoparticles of size greater than 3 nm and crystalline

structure as well as some disordered particles smaller than 1 nm is found. Similar behavior is observed for the 0.5% Pt reduced only sample, in which there is a variety of small and big particles. Large Pt particles with particle size greater than 3 nm are present as well as even larger particles and nanorods showing well-defined crystalline structure. Some small particles with particle size smaller than 1 nm are also present. These results should be seen in light of the fact that the metal loading here considered is relatively small compared to the more commonly used 1-5 wt% metal for studying supported metal catalysts. Consequently, although the average particle sizes are to be considered small as in the range of nanometres, what should take the attention is the broad and inhomogeneous distribution of such particles. In fact, as mentioned in the Introduction chapter, the homogeneity and reproducibility of the same catalyst relies on the presence of constant species, rather than formation of various mixtures.

Different characteristics are found in the higher loading calcined and reduced samples. The HAADF-STEM images reveal that Pt particles on the 0.2%Pt calcined and reduced sample show a uniform distribution of the metal over the support and a very narrow particle size distribution with a mean particles size of 1.1 nm. In a similar way, the 0.5%Pt calcined and reduced sample shows metal nanoparticles homogeneously distributed over the support with good dispersion and a mean particle size of 1.4 nm, often having a disordered looking structure. Very few dispersed Pt atoms and no larger Pt particles are present anymore.

For the two higher metal loading series of catalysts (0.2 and 0.5%Pt), it is possible to suggest that, on one side, the reduction step leads to agglomeration of the metal as the reduction takes place. This has been explained as that during the reductive annealing the metal species are very mobile as the chlorine ligands from the metal precursor salt leave the surface, allowing sintering and formation of bigger nanoparticles.[32] Consequently, the formation of a range of nanoparticles sizes (> 1 nm) showing crystalline and facetted structures takes place, which could be associated to the overall lower intrinsic activity determined for these samples. On the other side by performing the calcination followed by reduction, a more homogeneous dispersion of the metal is achieved, with narrower particle size distributions. It should be possible to suppose that the calcination step allows the metal to first anchor onto the metal oxide support, which prevents the aggregation during the later reductive step, hence forming well dispersed (sub-nanometer) reduced and more active metallic species. Confirmation of this was obtained by analysis of the calcined only samples. In Figure 3.7 a representative micrograph of the 0.5%Pt calcined sample reveals the presence of atomically dispersed platinum species and disordered clusters, showing that the calcination treatment allows dispersion of the metal, probably by anchoring the platinum to the oxide support as the chloride ligand leaves the sample during the heat treatment. Although a PSD analysis was not performed on this sample, it would appear that the metal distribution is similar to the correspondent calcined and reduced sample.
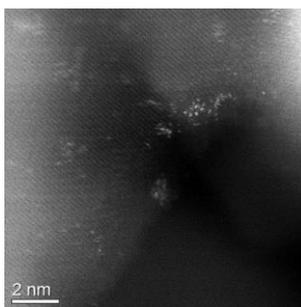
Figure 3.7 Representative STEM-HAADF image of 0.5%Pt calcined sample, where high metal dispersion can be observed as bright dots.

The similar activity of the 0.08%Pt samples (Figure 3.4) reflects their very similar catalyst morphology. In fact, both reduced only and calcined and reduced samples show a homogeneous distribution of the metal with the mean particle size for both samples being 1.2 nm and good dispersion, with only few –if any- individual Pt atoms. Also in this case, particles smaller than 1 nm (clusters) look less ordered than the 2 nm ones.

The analysis of the lowest metal loading samples reveal that, as the metal content decreases, it becomes more challenging to pinpoint the metal particles, because they are either rare or small. The particle size analysis of 0.05%Pt reduced only sample showed a mean particle size of 0.98 nm and a narrow distribution, whereas a slightly larger mean particle size and distribution were detected in the calcined and reduced sample. Compared to the previous catalysts, this finding does not completely agree with the catalytic activity determined for the 3-NS hydrogenation reaction. This could be explained with the aforementioned limitations that such low metal loading sample has. In contrast to the higher loading catalysts, the 0.08 and 0.05% Pt samples might contain a limited amount of metal, such that during support impregnation and catalyst activation, the metal particles are well separated, and coalescence is strongly limited. Therefore, the treatments in furnace should be able to influence only partially the metal distribution.

Overall, by comparing the particle size distribution plots is possible to notice that the sample giving the highest intrinsic catalytic activity, 0.2%Pt/TiO₂ calcined and reduced (TOF 5659 h⁻¹), shows the highest contribution from particles of sub-nanometre size. Whereas the 0.5%Pt/TiO₂ calcined and reduced sample that shows lower activity (TOF 3890 h⁻¹), presents mainly particles with size between 1 and 2 nm. The presence of clusters and particles of 1 nm or smaller with disordered structure is crucial for the observation of high turnovers. In fact, the most active catalysts (0.08 red, 0.08 calc+red and 0.2 calc+red) show a majority of platinum aggregates with such characteristics.

With the help of our collaborators from Lehigh University, the estimation of the surface and of the peripheral platinum atoms was performed. The Mackay icosahedral model was applied for the calculation of the different surface sites. Assuming that the nanoparticles have a shape of half

Mackay icosahedrons with various shell numbers depending on their size, the diameter of the particles can be determined. The portion of peripheral sites to the total amount of platinum atoms can be calculated based on the particle size distribution of each sample. This number could then be used to calculate the absolute number of platinum atoms on the surface or at the interface using the nominal metal loading. These two series of values (total surface and perimeter atoms, expressed as the weight percentage of the total catalyst) have been plotted in Figure 3.8 against the initial rates of 3-NS conversion.
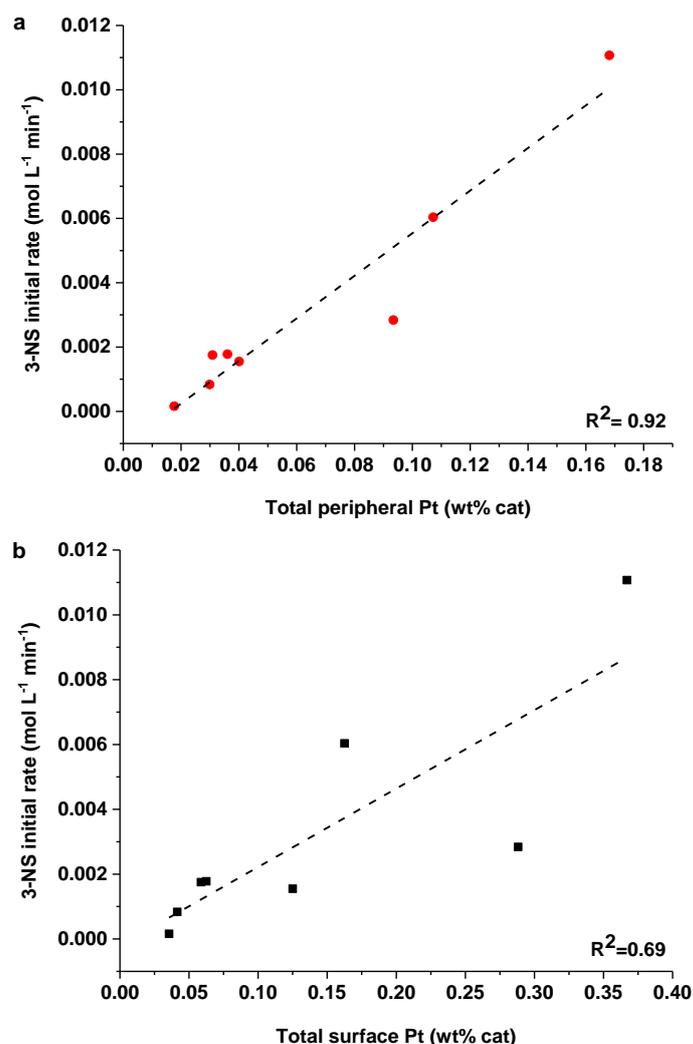
Figure 3.8 The correlation between the 3-NS initial rates and total amount of (a) peripheral and (b) surface Pt atoms for different Pt/TiO$_2$ catalysts as determined from HAADF-STEM analysis and expressed as weight percentage of the total catalyst.

The plot in Figure 3.8a shows a very good correlation between the number of peripheral atoms and the initial rate values (R-squared = 0.92), which is in good agreement with the previous finding from Boronat *et al.* that the Pt-TiO$_2$ interfacial sites are crucial for the chemoselective hydrogenation of nitrocompounds.[33] A poorer correlation (R-squared = 0.69) is found between the metal atoms that are exposed to the surface and the initial rate data, supporting the theory that

exposed platinum planes are not very active reaction sites. The combination between the metal loading and the heat treatment has a strong influence on the ratio of metal species present at the peripheral line that the platinum forms when interacting with the TiO₂ support, which consequently has shown to deeply affect the final catalytic activity.

3.2.5   Study of the platinum surface area

Another way to study metal nanoparticles is the use of carbon monoxide as probing molecule. This simple diatomic molecule is a strong poison to some noble metals because it binds very strongly, blocking and hindering the metal sites that become unavailable to hydrogen (or oxygen) and the reactants. A way to take advantage of the properties of CO is to perform a titration of the metal surface area, by pulsing fixed volumes of gas, which allow the calculation of the surface area of the metal present on the catalyst once the surface of the metal is saturated by the probing molecule, as well as the metal dispersion (see Experimental Chapter 2, Section 2.3.5).

During this study, CO pulse titration was performed to estimate the amount of metal exposed and available to the reactants. In Figure 3.9, the platinum surface area and dispersion are plotted together with the catalytic activity. The quality of the data reported here is subject to some error due to the low metal loading present on the samples as well as to the error of the instrument. Nevertheless, the results reported here are to be considered qualitatively accurate. In fact, we observed that, in good accordance with other characterisation techniques, the dispersion of the metal with two consecutive heat treatments (calcination followed by reduction) was higher compared to the sample that underwent only one reductive treatment. The dispersion values oscillate between 5% and 45%, with the lower dispersion observed for the reduced values, independently of their metal content. As could be expected, the metal surface area does increase with the metal loading, since it is a density of metal per mass of catalyst. Unfortunately as all the samples contain a low metal content, it is difficult to determine accurately its surface area, but it is possible to assume that the trend is qualitatively accurate.

According to the studies performed by Tauster and co-workers, no CO adsorption was observed on a 2 wt. % Pt/TiO₂ sample after a reduction at 500 °C, as the adsorption properties of the metal are modified when a strong metal-support interaction is present. On the contrary, the same 2 wt. % Pt/TiO₂ sample reduced at 200 °C could adsorb CO and a metal dispersion of 65% was calculated.[22, 34] Hence, a method to determine whether our system is in a strong metal-support interaction state could be the determination of CO adsorption on the sample. Taking into account that the catalysts here discussed have a metal loading as high as 0.5 wt. % Pt with a maximum metal dispersion of 44% after both calcination and reduction, the results indicate that CO adsorption occurs and suggest that no SMSI is to be taking place.
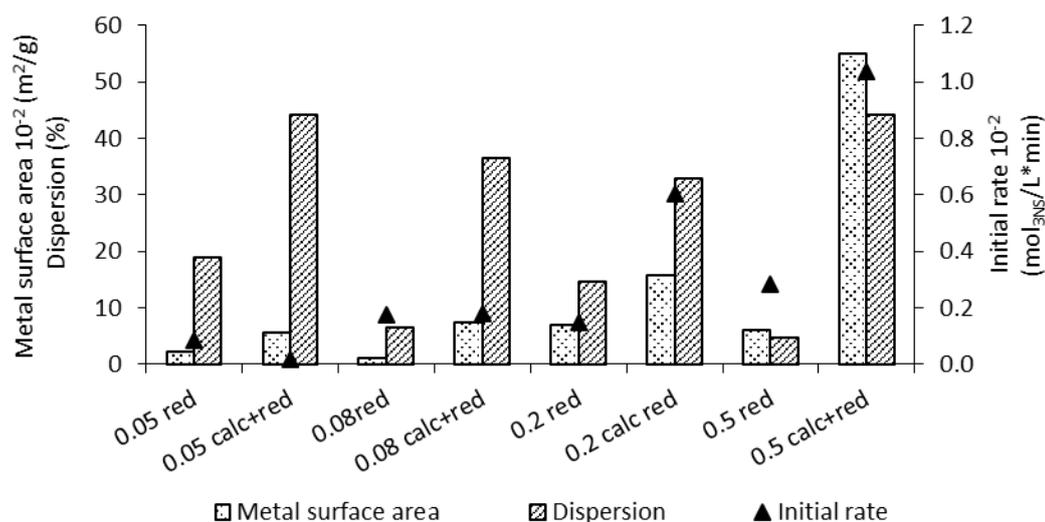
Figure 3.9 CO chemisorption and activity data for all reduced only and calcined+reduced samples.

The results determined by CO titration of the platinum surface were confirmed from the quantitative analysis of the XPS data, which are presented and discussed in the following Section 3.2.6. In Table 3.2, the platinum atomic concentration in the variously treated 0.2 and 0.5 %Pt/TiO₂ samples are tabulated. The two series of samples show identical trend, with lower metal concentration for the 0.2 %Pt samples, as could be expected. Focussing the attention on the results calculated for the 0.5 %Pt samples, the as-prepared material, after impregnation of the metal precursor on the surface of the support, shows a concentration of 0.21%. When the as-prepared material is calcined in air, the concentration of platinum remains in the same order of magnitude and an only slightly higher value of 0.28% was calculated, meaning that the dispersion of the metal is very comparable between the two samples. If the as-prepared 0.5%Pt/TiO₂ sample is reduced in H₂/Ar flow, a strong decrease in platinum percentage is determined, the surface concentration becoming 0.07%, which is a third of the dispersion present in the starting material. Because the XPS technique is a surface analysis, as the platinum aggregates, less metal surface is exposed to the X-ray beam, resulting in a decrease in the photoelectron signal. This low platinum concentration calculated for the reduced sample is in accordance with the electron microscopy results previously discussed, where a strong metal agglomeration and formation of bigger nanoparticles has been observed, possibly due to a higher mobility of the platinum atoms when exposed to a reducing environment. When the before mentioned 0.5 %Pt calcined sample is also reduced, the platinum content calculated from the XPS analysis is 0.24%, which is a value in between the as-prepared sample and the calcined one. This indicates that the platinum dispersion is almost as high as it was in the starting material, but also that the reductive treatment only slightly affects the platinum dispersion achieved during the oxidative step.

Table 3.2 Platinum atomic concentration as calculated from XPS analysis for the 0.2 and 0.5 %Pt/TiO₂ samples.

	At%	
	0.5%Pt	**0.2%Pt**
Calcined and reduced	0.24	0.09
Reduced	0.07	0.02
Calcined	0.28	0.09
As-prepared	0.21	0.1

From these results is possible to deduce that during the support impregnation, the metal is dispersed well and homogeneously onto the surface of the support material. The oxidative step is crucial in anchoring the metal atoms onto the oxide support, as the oxygen takes place of the ligand of the metal precursor, while maintaining the good metal dispersion. At last, the reductive step is necessary to activate the catalyst by forming the catalytic sites.

To study how consecutive treatments would affect the highest loading sample 0.5 %Pt, which could be more accurately measured by CO chemisorption compared to the lower metal loading samples, two cycles of calcination and reduction were performed. The 3-NS hydrogenation testing as well as the CO pulse titration of the final sample were performed. The results of these experiments are shown in Table 3.3 and it is possible to notice how the catalytic results are very well comparable, although a change in the metal surface area and related quantities would suggest a modification of the catalyst. Because the titration experiments were subject to errors, we believe the catalytic results are strong evidence of stability of the catalyst upon a second calcination-reduction cycle, especially in light of the strong variation in activity observed between the catalysts discussed in this chapter that show how small variation in particle size affects the conversion of 3-NS.

Table 3.3 Results of CO titration of 0.5%Pt/TiO$_2$ variously treated [a] Reaction conditions: 0.2 ml 3-NS, 8 ml toluene, 0.05 g catalyst, 40 °C, 3 bar H$_2$, 500 rpm, 15 min.

	0.5%Pt/TiO$_2$	
	C+R	**C+R+C+R**
Metal surface area [m^2/g]	0.7	0.9
Average crystallite size [Å]	7	5
Dispersion [%]	56	76
3-NS conversion [%][a]	55	56

These results seem to confirm that our system is most certainly not controlled by SMSI. If it were, more metal oxide support would have grown on the metal particles during the second cycle of heat treatments, decreasing the surface area of the metal by covering it and showing a variation in catalytic performance, both evidence are missing from what reported in Table 3.3.

Although a reduction treatment was found to be necessary in order to have an active catalyst, an ordered metallic platinum nanoparticle has proved not to be the most active catalytic structure. Hence, a detailed study of the oxidation state of the metal present on the surface of the samples discussed so far is necessary.

3.2.6 Platinum oxidation state study

Because a strong difference in catalytic activity was obtained from the series of samples tested, understanding the properties of the supported metal is fundamental. As mentioned before, the calcined samples did not show any catalysis, indicating that the species formed upon calcination are not active for the hydrogenation reaction. While the samples that underwent a reductive treatment showed hydrogenation products, hence presence of catalytically active sites.

One surface analytical technique that gives an insight into the oxidation state and chemical environment of a specific element is the X-ray Photoelectron Spectroscopy (XPS). By means of this technique, the platinum samples prepared during this work and discussed in this chapter could be analysed.

In Figure 3.10 the platinum photoelectron spectra for each metal loading are reported. The stacked plots help in the comparison of the different treated samples with the same metal loading, and the photoelectron spectra of the as-prepared (a), calcined (b), reduced only (c) followed by the calcined and reduced (d) samples are shown. In this way, formation of different platinum

species upon the three different heat treatments could be evaluated. It needs to be considered that the XPS technique is a surface technique and that the metal concentration affects the quality of the data, as the intensity of the peaks becomes sensibly lower, making the analysis challenging. Moreover, the titanium Ti3s satellite peak at *ca.* 75 eV (blue fitted line) falls in the same energy range of platinum Pt4f [35] partially covering the platinum signals, which could be more clearly identified only after peak fitting.

The as-prepared samples, after drying the aqueous solution of hexachloroplatinic acid precursor mixed with the support and before performing any heat treatment, shows mainly presence of Pt(II) species (fitted red line), presumably associated with hydroxide or chloride species, with the Pt $4f_{7/2}$ and Pt $4f_{5/2}$ photoelectron peaks at 72.4 and 75.4 eV respectively.[36-39] The peaks are symmetrical and the two spin-orbit components are separated by a difference of *ca.* 3.3 eV. Because the metal precursor is a Pt(IV) chloride acid, a Pt $4f_{7/2}$ signal at higher binding energies *ca.*75 eV would be expected.[36] This feature has been observed before,[40-41] and a possible explanation for the absence of such peak could be the partial reduction of Pt(IV) to Pt(II) as a consequence of the X-ray beam exposure.[38] However, it is also possible that the metal partially reduces during impregnation onto the titania surface, or as it bonds to surface oxygen.[42]

During the calcination treatment, most of the samples do not show change in oxidation state, whereas the 0.5% Pt calcined sample does show presence of Pt(IV) contribution (green fitted line in Figure 3.10). The Pt $4f_{7/2}$ peak is positioned below the broad peak at *ca.*75 eV and the second spin-orbit component Pt $4f_{5/2}$ can be found as expected at a distance of $\Delta=3.3$ eV at 77.6 eV.[37]

When an as-prepared sample undergoes reduction at 450 °C for 4 h, the metal is reduced forming metallic Pt(0) nanoparticles (grey fitted line). The platinum photoelectron peaks shift to lower binding energies, with the lower energy peak Pt $4f_{7/2}$ at *ca.*71 eV and the second spin-orbit component Pt $4f_{5/2}$ at *ca.* 74 eV.

The samples that undertook both calcination and reduction treatments, show maijor presence of metallic platinum. However, especially in the case of higher metal loading samples 0.2 and 0.5% Pt, the intensity of the peaks is more comparable to the intensity of the corresponding calcined only samples, whereas the reduced only samples show sensibly smaller photoelectron peaks, as discussed in the previous Section 3.2.5.
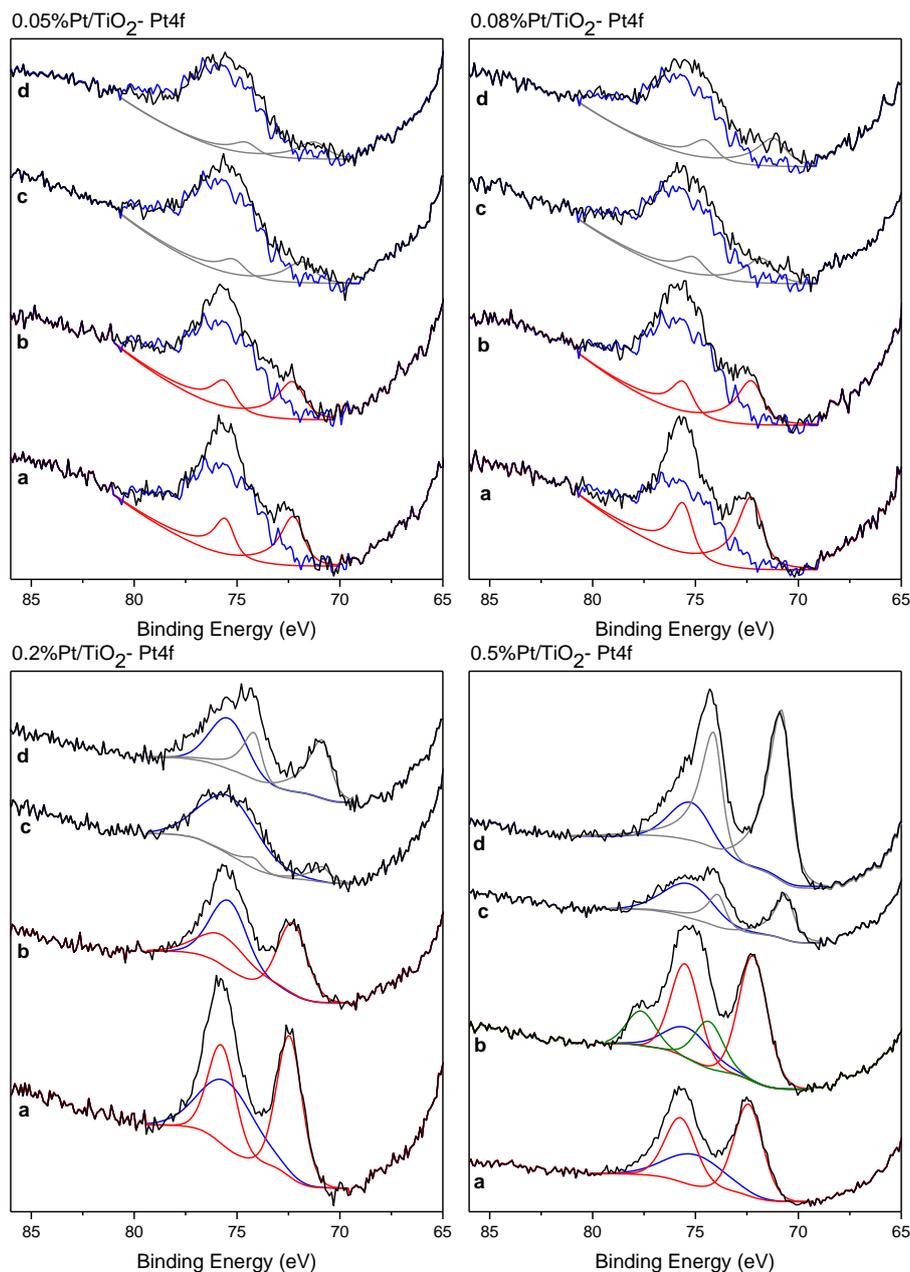
Figure 3.10 XPS spectra of the platinum region of the 0.05, 0.08, 0.2 and 0.5%Pt/TiO₂ samples. From bottom to top the treatments are: as-prepared (a), calcined (b), reduced (c), calcined and reduced (d). colour key: Pt(0) grey, Pt(II) red Pt(IV) green and Ti satellite peak blue.

In light of the electron microscopy results, the defined and intense platinum peaks could be correlated to a better metal dispersion and overall smaller nanoparticles, which in the surface of the catalyst would reflect in a higher percentage of platinum detectable by the X-ray beam. On the contrary, less intense peaks of sample with the same metal loading could be due to the agglomeration of the metal and formation of rather large metal nanoparticles during the reductive treatment. To support this conclusion are the results discussed in the previous section, where electron microscopy analysis showed the formation of larger (>3 nm) metallic platinum particles,

particularly in the case of 0.2 and 0.5%Pt reduced samples, compared to the small (< 2nm) agglomerates found in the 0.5% Pt calcined only sample as well as in the calcined and reduced materials.

The comparison of the different heat-treated 0.2 and 0.5% Pt catalysts seems to lead to the conclusion that during calcination of the as-prepared catalysts, the metal achieves good dispersion on the oxide support, possibly anchoring through the oxygen. During reduction, when the chloride ligand dissociates from the platinum centre, a mobile metallic species is more prone to interact with neighbouring platinum atoms, forming large metallic aggregates. Another possible explanation for the attenuated platinum peaks could be found in a possible growth of the titania support as it covers the metal during the reductive heat treatment and hence to a strong metal support interaction (SMSI).[43] It is generally reported that SMSI arise when Pt group metals supported on reducible oxide supports are treated in H$_2$ at temperature above 500 °C.[22] The reduction of bare TiO$_2$ has been reported to take place at temperatures above 600 °C.[44-45] However after addition of platinum, possible reduction of TiO$_2$ to TiO$_{2-x}$ by effect of the hydrogen spillover from platinum particles in contact with the support might take place at lower temperature.[46-47] The encapsulation ability is one of the two features that have been related to the presence of the SMSI, the other property being the electronic modifications that takes place between the metal and the support, affecting the final material.[22, 48-49] Metals in SMSI state could show increased electron richness, which is reflected in decreased binding energy values, due to the formation of oxygen vacancies, Ti^{3+} species and electrons during reductive treatment.[50] However, in the system discussed here such change in XPS peaks was not observed. Since the XPS signals are defined and intense when both calcination and reduction treatments are performed on the same sample, and the lower metal loadings samples do not show any substantial variation in the photoelectron signals, such encapsulation seems to take place only when the reductive treatment alone is performed on catalysts with metal loading higher than 0.2%Pt. It has been observed that the titania growth takes place at already relatively low temperature (~200 °C) when treating the samples in reductive flow,[51] and that the titania covering has been shown to be detectable with TEM.[52-53] After extensive electron microscopy analysis of the samples discussed in this chapter, the presence of titania decoration on the platinum particles was not confirmed. Moreover, the model applied for the determination of the peripheral and surface atoms indicates that good accuracy has been achieved, as it worked well for both high and low metal loadings, reduced only and calcined and reduced samples. Whereas some discrepancy should have been expected for the reduced only 0.2 and 0.5% Pt if encapsulation was present but not detected. An experiment discussed in Section 3.2.5 shows that two cycles of calcination and reduction on the 0.5%Pt/TiO$_2$ catalyst did not affect the activity of the catalyst, nor the surface area of the metal, suggesting that a support decoration is not taking place, otherwise a decrease in metal surface area should have been measured.

Overall, TiO$_2$ decoration may take place, as suggested by the strong decrease in XPS signal and Pt surface area in the reduced only 0.2 and 0.5% Pt/TiO$_2$ samples, however from XPS binding energy values, electron microscopy and multiple heat treatments cycles a definite proof is missing. Moreover, the calcined and reduced samples show a very different behaviour, with clear and intense photoelectron peaks. Whether the calcination step could prevent the titania covering during the subsequent reductive treatment is not to be excluded, however a definitive understanding and explanation would probably require a more extensive study.

In conclusion, the choice of support is known to influence and affect the final catalytic performance by modifying the characteristics of the supported metal. However, these series of catalysts have been prepared by the same method, using the same support and heating temperature, hence the metal-support interaction should be considered the same for all of the catalysts taken into account. From the results presented so far, it is possible to deduce that the size of the nanoparticles and the population of peripheral atoms is crucial for achieving exceptional 3-NS conversions and high 3-VA selectivity. From the microscopy study discussed in the previous section, we were able to determine the generally small size (< 2 nm) of the particles deposited on the surface of the TiO$_2$, where not only nanoparticles were present, but also sub nanometre particles or clusters were found.

From the analysis of a different energy region, it was possible to study the chlorine photoelectron signal, which is shown in Figure 3.11. The Cl2p XPS spectrum of the as-prepared 0.2% Pt/TiO$_2$ sample shows a peak at lower binding energy assignable to the Cl2p$_{3/2}$ component of a metal chloride, positioned at 198.3 eV. Separated by 1.6 eV at higher binding energy, the second Cl2p$_{1/2}$ component is at 200.0 eV.[36] From the atomic quantification performed using the CasaXPS analysis program, it was possible to determine the percentage of chlorine on the surface of the as-prepared 0.2% Pt sample, which was calculated as 1.49%. After either calcination or reduction, the plots in Figure 3.11b and 3.11c show a strong decrease in chlorine signal, whose content is not determinable. This result suggests that during treatment at 450°C the chlorine present in the platinum precursor leaves the sample and depending on the environment is replaced around the platinum by oxygen or enhances the mobility of the metal as it is reduced.
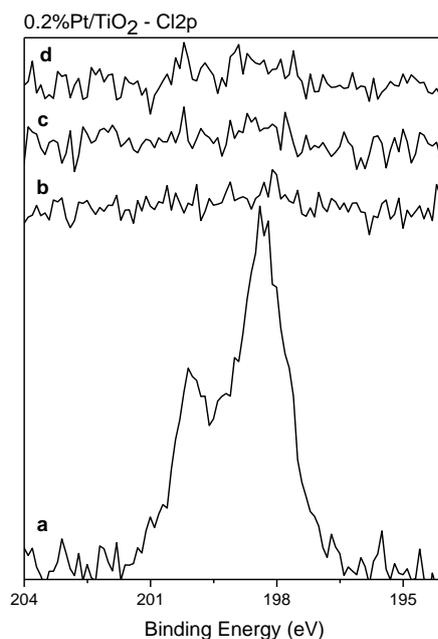
Figure 3.11 XPS spectra of the chlorine region of the 0.2%Pt/TiO₂ samples. From bottom to top the treatments are: as-prepared (a), calcined (b), reduced (c), calcined and reduced (d).

During this project, we had the opportunity to apply and gain access to the synchrotron beam lines B18 and I20 of the Diamond complex in Harwell, UK and be able to perform X-Ray Absorption Spectroscopy (XAS) analysis. Multiple experiments were performed in order to analyse the 0.05 to 0.5% Pt reduced only as well as the calcined and reduced samples. The two extreme metal loading samples 0.5 and 0.05% Pt calcined samples were also analysed.

The XAS analysis gives the opportunity to collect both XANES and EXAFS information. The platinum white line, which corresponds to the L3 edge XANES, indicates the allowed $2p_{3/2}$ → $5d_{5/2}$ transition of a core electron.[54] By XANES analysis of the platinum samples, it should be possible to study the average oxidation state of the metal present on the surface of the catalysts. In contrast to, the EXAFS technique examines the waves emitted by the ejected photoelectron that interacts with the neighbouring atoms, giving information regarding the interatomic distances and the chemical environment of the specific element analysed.[55, 56] Moreover, it is possible to gain information about the particles size, as the stronger the intensity of a contribution, the bigger is the particle. During the experiments, multiple spectra were collected for each sample, which were later merged and normalised by our collaborators working at the synchrotron Research Complex at Harwell.

In Figure 3.12 and 3.13, the XANES energy plots and the Fourier Transform EXAFS plots of all the samples measured are reported according to increasing metal loading (a) 0.05% Pt, (b) 0.08% Pt, (c) 0.2% Pt and (d) 0.5% Pt. From the energy XANES spectra of all the samples is possible to notice that the average oxidation state of platinum is +2, characterised by a white line height with a normalised absorption value between 1.5 and 2. The presence of such slightly

oxidised platinum speciation is reflected in the Pt-O contribution at *ca.* 1.6 Å as seen in the corresponding EXAFS FT plots.[57-58]

The only exception is the 0.5 % Pt reduced sample, which shows a strong decrease in white line intensity, which is only slightly higher than the normalised intensity of the standard platinum foil indicating that the majority of the platinum on this sample is in the lowest oxidation state (Figure 3.12d). The formation of Pt metallic nanoparticles during reductive treatment and hence the metallic nature of the sample could also be confirmed by the large and defined peak assignable to Pt-Pt distance at 2.5 Å in the EXAFS spectrum of the 0.5% Pt reduced catalyst (Figure 3.13d).[59]

The abundance in Pt-O speciation in most of the samples discussed here should be seen in light of the characteristics of the XAS analysis compared to the previously discussed XPS. Since the bulk rather than the surface is probed, a different kind of environment is studied. As concluded from the electron microscopy study, disordered nanoparticles and clusters are often present in the samples, which would require a direct interaction of the metal atoms with the support, possible through an oxygen bonding. Moreover, it has been previously reported that 1% Pt/TiO₂ catalysts reduced at 200 and 400 °C and analysed by EXAFS would show Pt-O contribution.[41] Such presence has been explained as small platinum particles can easily interact not only with the oxide support, but also with the atmospheric oxygen during the experiment. Whereas larger metallic nanoparticles can more easily show Pt-Pt contribution, as they are less affected by both the bonding with the support and with the chemisorbed oxygen present in the air. This theory is in agreement with the finding that the 0.5% Pt reduced sample only showed a clear Pt-Pt interatomic distance, together with a percentage of rather larger metallic platinum particles as seen by TEM. While samples characterised by major presence of 1 nm particles and clusters, are closely interacting with the TiO₂ or could easily chemisorb O₂.

The 0.5 and 0.05 %Pt calcined samples were also measured and showed a very high white line comparable to that of the PtO₂ standard (Figure 3.12a, d) and a very intense peak at 1.69 Å assignable to Pt-O distance (Figure 3.13a, d), indicating that the majority of the metal is in the Pt(IV) state. This result is partly in contradiction with the results reported in the XPS discussion, where calcined samples showed mainly presence of Pt(II) species. The different result could be due to the reducing effects of the experimental conditions during the XPS analysis.

The relative intensity of an atomic pair contribution in the FT plot can give qualitative information regarding the size of the considered agglomerate in samples with the same metal loading.[60] Since most of the samples contain signals assignable to the Pt-O pair, it is possible to say that the higher the contribution, the larger are the PtOₓ particles. In Figure 3.13d, the 0.5%Pt calcined and reduced sample shows only a less intense peak at 1.68 Å compared to the calcined sample, indicating that the PtOₓ particles become smaller as they are partially reduced. In a similar

way to the fine structure analysis reported in Figure 3.13a of the three heat treated 0.05 % Pt/TiO₂ samples, it is possible to say that qualitatively the biggest PtO₂ particles are found in the calcined only sample, smaller in the calcined and reduced sample, while in the reduced only sample are the smallest. Overall oxidation state as determined from the XANES fitting in Figure 3.12a confirms this trend, with the platinum oxidation state lowering down as the sample is only calcined in static air, calcined and reduced in hydrogen flow or only reduced.

As during the catalytic screening and the electron microscopy analysis, also by XAS technique the two 0.08%Pt samples are very similar, with an average metal oxidation state of +2. The small peak at 1.65 Å in the Fourier transform spectra in Figure 3.13b indicates the presence of the atomic pair Pt-O aggregated in small particles.
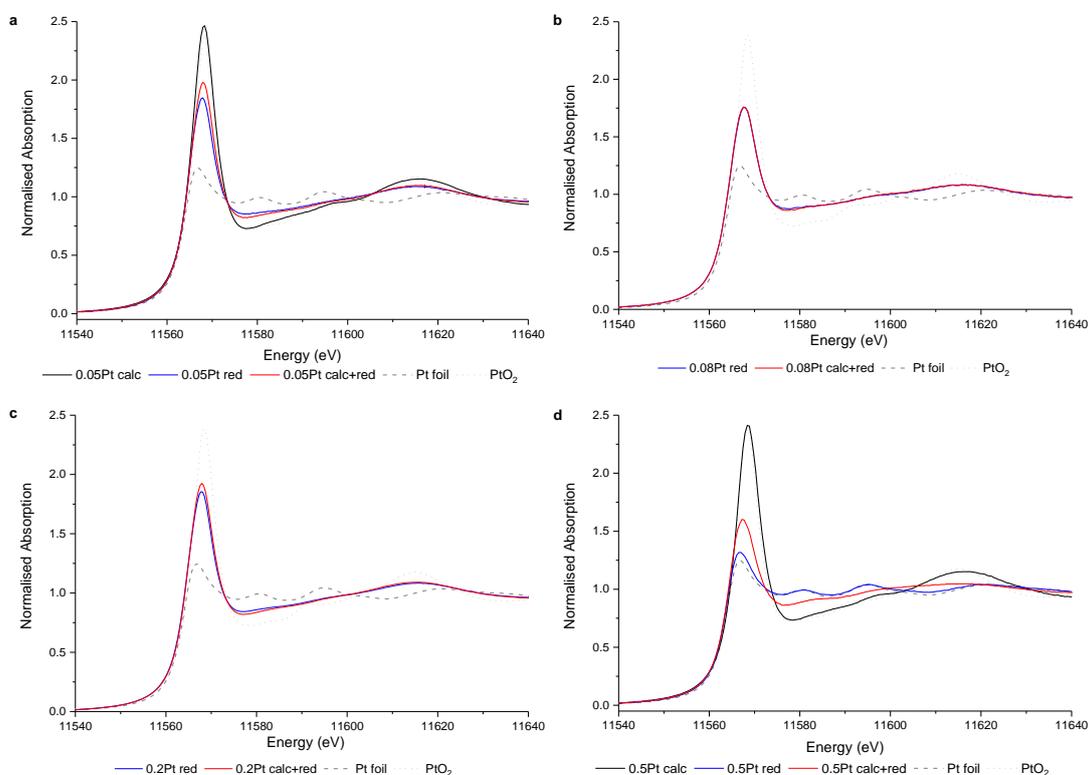
Figure 3.12 XANES data of the Pt L3-edge of (a) 0.05, (b) 0.08, (c) 0.2 and (d) 0.5% Pt/TiO₂ samples that underwent different heat treatments.
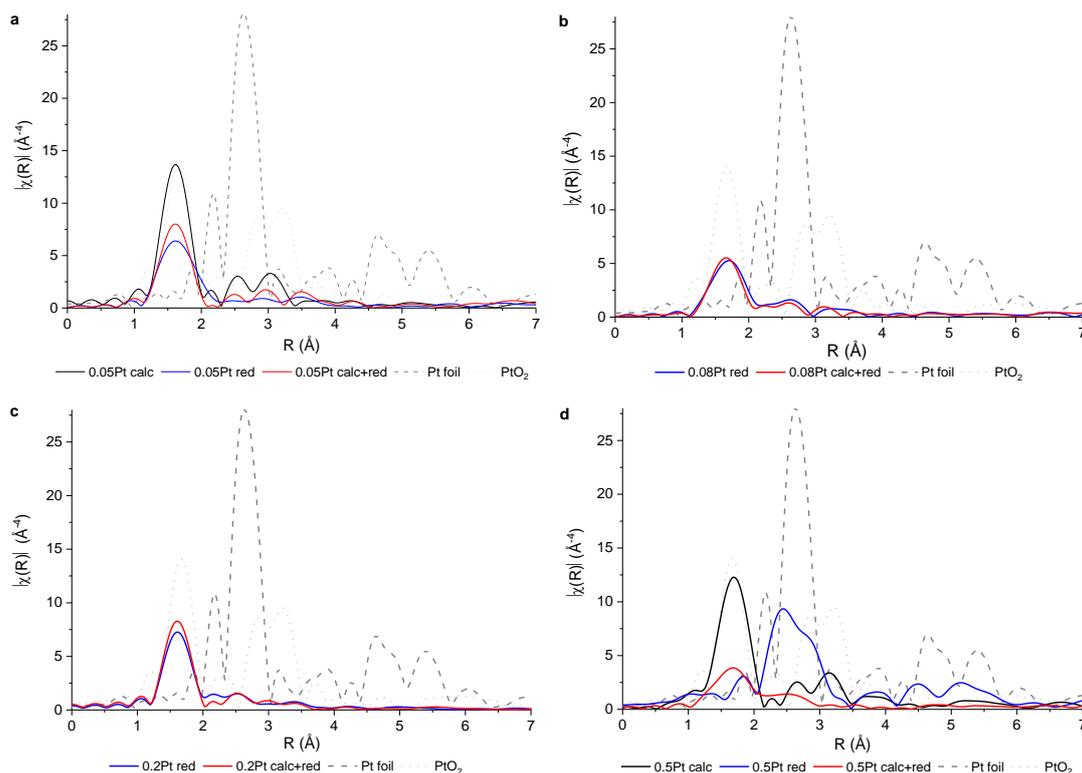
Figure 3.13 EXAFS data of the Pt L₃-edge of (a) 0.05, (b) 0.08, (c) 0.2 and (d) 0.5% Pt/TiO₂ samples that underwent different heat treatments.

Correlating these spectroscopic results with the catalytic performances previously discussed, it is possible to conclude that the highly oxidised Pt species present in the calcined samples are not active. Also the formation and presence of metallic crystalline Pt(0) surfaces lead to not very active materials, while samples containing in average Pt(II) species, probably at the boundary between more metallic atoms and the oxide support, show the best catalytic performances. The amount of these species needing to be optimised by the correct heat treatment.

To conclude this section, a surface and a bulk analysis technique were applied to study the platinum speciation on the variously loaded and treated samples. Some discrepancies in the results have been observed, relatable to the difference in experimental procedures and information achievable by means of the two different analysis. Overall, it is possible to confirm that during oxidative calcination large aggregates composed of Pt-O species are formed as seen in the XPS and XANES spectra and the final samples are not catalytically active. When performing a reduction after the calcination, partial reduction of the Pt-O agglomerates occurs, shifting to lower binding energy and decreasing the white line height. When performing solely a reductive treatment, agglomeration and formation of Pt-Pt species are found more easily in the high metal loading sample (0.5%Pt), while for low metal loadings ones (< 0.5%Pt) the concentration is too low to favour agglomeration, leading to formation of few nanometres particles or clusters where the Pt-O contribution is strongly present. Although in some samples the metal does not exhibit

proper metallic characteristics as major interaction with the oxide support is present, it cannot be neither defined as oxidised.

These results are in agreement with previous literature as well as our characterisation techniques, pointing to the conclusion that platinum species located at the interface with the oxide support are mostly prone to be active catalytic sites. A higher proportion of peripheral atoms, more than metallic surface species have proven to be mainly present in samples showing higher intrinsic catalytic activity.

From this, it is possible to conclude that 0.05% Pt calcined and reduced and 0.5% Pt reduced only are the two extreme cases, where the former has too low metal concentration showing rather oxidised Pt-O characteristics, while the latter has high concentration of reduced Pt-Pt metallic species, both poorly active. Activity lays in balance between the amount of Pt-O sites and agglomeration of metallic platinum.

3.2.7 Effect of hydrogen environment on the catalysts

Because the catalytic tests are conducted under pure hydrogen pressure, it could be supposed that compared to the *ex-situ* analysis, different platinum species would arise under reaction conditions. To study how the features of the catalysts may change, some semi *in-situ* XAS experiments were performed, aiming to study how the platinum oxidation state and chemical environment varies after flushing the palletised samples with 10 % H₂/Ar for 30 min.
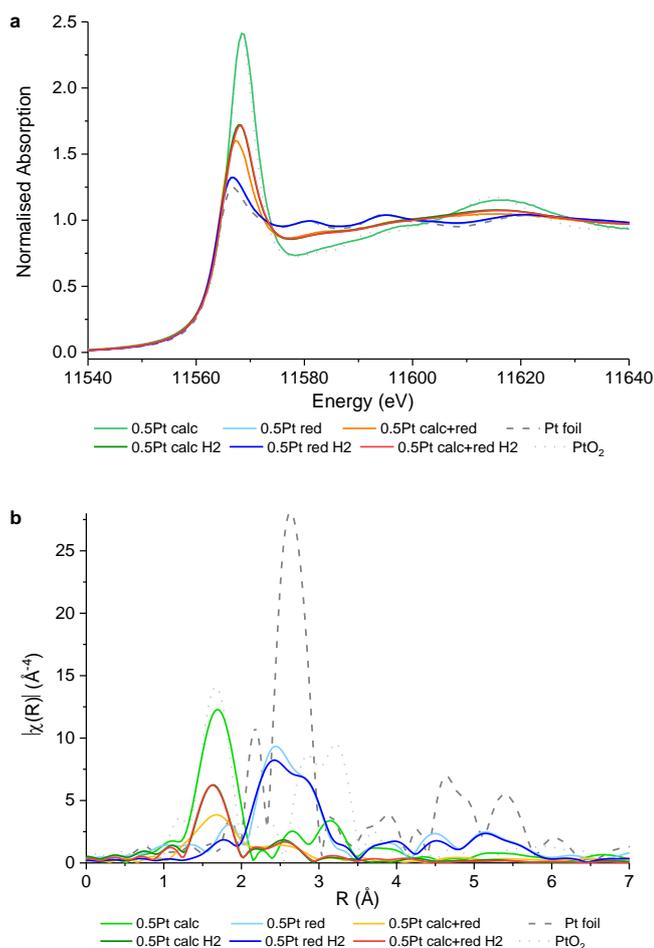
Figure 3.14 XANES (a) and EXAFS (b) spectra of the 0.5 %Pt calcined, reduced and calcined+reduced samples before and after flushing with H_2.

In Figure 3.14a, the XANES energy plots of the 0.5 %Pt/TiO₂ samples before and after flushing with H_2 are shown. The 0.5 %Pt calcined samples show quite a lowering in oxidation state, where the white line height decreases from 2.4 to 1.7, indicating possible reduction of the Pt(IV) particles to Pt(II). In Figure 3.14b are shown the EXAFS R-space plots of the same 0.5 %Pt samples. The 0.5% Pt calcined samples spectra show a strong decrease in Pt-O particle size as the $|\chi(R)|$ intensity at 1.6 Å decreases after the flushing in H_2, confirming the reduction of the surface PtO₂ species.

By comparing the energy plot of the reduced samples it is possible to notice that they are stable and the surface of the metal particles does not change upon H_2 flushing. This is further confirmed by the EXAFS results that show very comparable Pt-Pt contribution at around 3.5 Å. During the same treatment in hydrogen flow, the calcined and reduced samples have opposite trend, with a slight increase in white line height from 1.6 to 1.7. This unusual behaviour is seen also in the R-space plot, where the Pt-O contribution at 1.6 Å does increase after the sample flushing in hydrogen, which might indicate an increase in Pt-O particles, an unexpected behaviour

under reducing atmosphere. Should be noted that the analysis of these samples was performed at different experiments, therefore variation in the samples may have occurred.
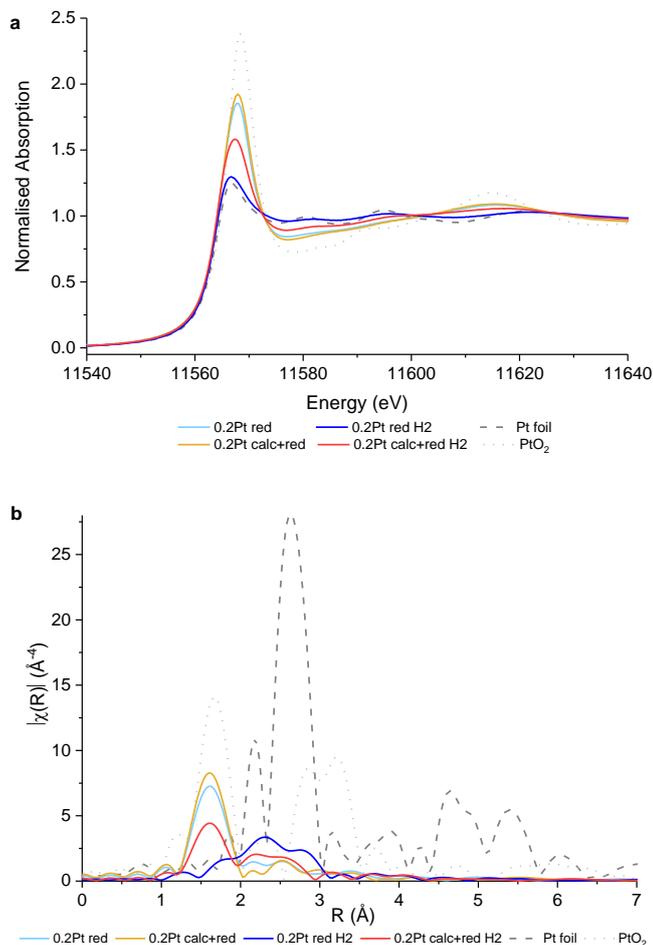
Figure 3.15 XANES (a) and EXAFS (b) spectra of the 0.2 %Pt reduced only and calcined+reduced samples before and after flushing with H_2.

In Figure 3.15a, the XANES energy plots of the 0.2 %Pt/TiO₂ samples before and after being flushed in a hydrogen flow are shown. The white line height of the 0.2 %Pt reduced samples decreases from 1.8, assignable to Pt(II), to 1.3 after hydrogen flushing, which can be assigned to Pt(0) formation, suggesting that a reduction of the platinum species is occurring. This is confirmed by the fine structure analysis, plotted in Figure 3.15b. The Pt-O contribution at 1.6 Å strongly decreases and the peak shifts to longer R distances upon hydrogen flushing with a significant formation of Pt-Pt metal contribution just below 3 Å.

The 0.2 %Pt calcined and reduced samples show a similar trend to the reduced only samples with a small decrease in white line height from 1.9 to 1.6 in the energy plot. From the EXAFS data in Figure 3.15a, it is possible to conclude that a significant decrease in Pt-O particles size occurs as the intensity of the signal decreases and that likely formation of Pt-Pt metal contribution is taking place.
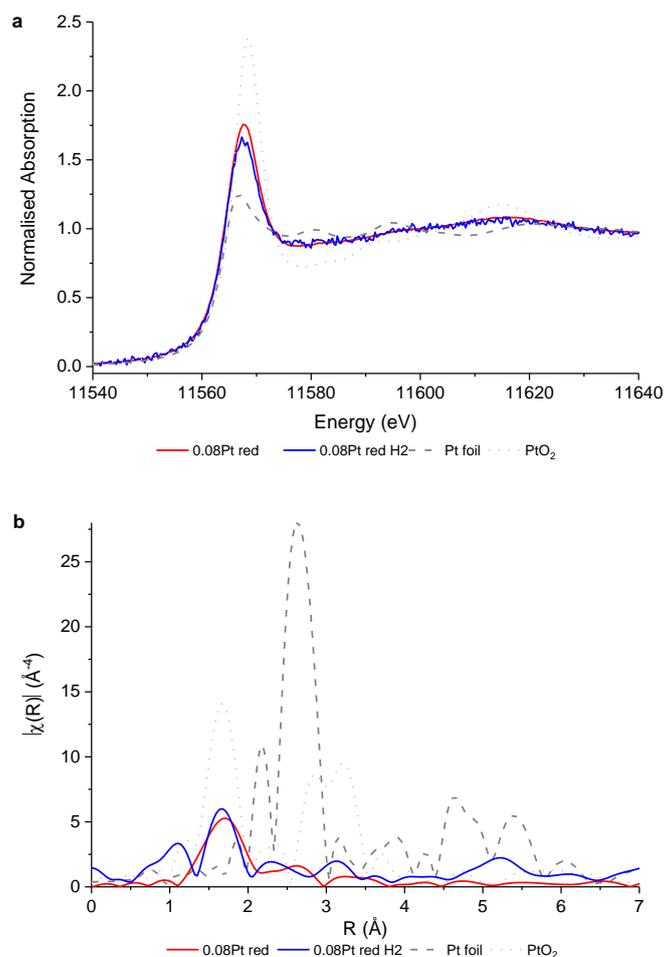
Figure 3.16 XANES (a) and EXAFS (b) spectra of the 0.08 %Pt reduced samples before and after flushing with H₂.

In Figure 3.16a and b, the XAS analysis of the 0.08% Pt/TiO₂ reduced samples are shown. The white line height as seen in the energy plot shows a slight decrease as the sample is treated in a flow of H₂, with the normalised adsorption changing from 1.8 to 1.6, which is a possible indication of a partial reduction. Unfortunately, the EXAFS analysis seem to be noisy, as the hydrogen treated sample was analysed during a different experiment, in a beamline where the low loading may have affected the quality of the results. Nevertheless, the main contribution at 1.6 Å confirms the presence of small PtO₂ particles, hence good metal dispersion that is not affected by the reductive environment.
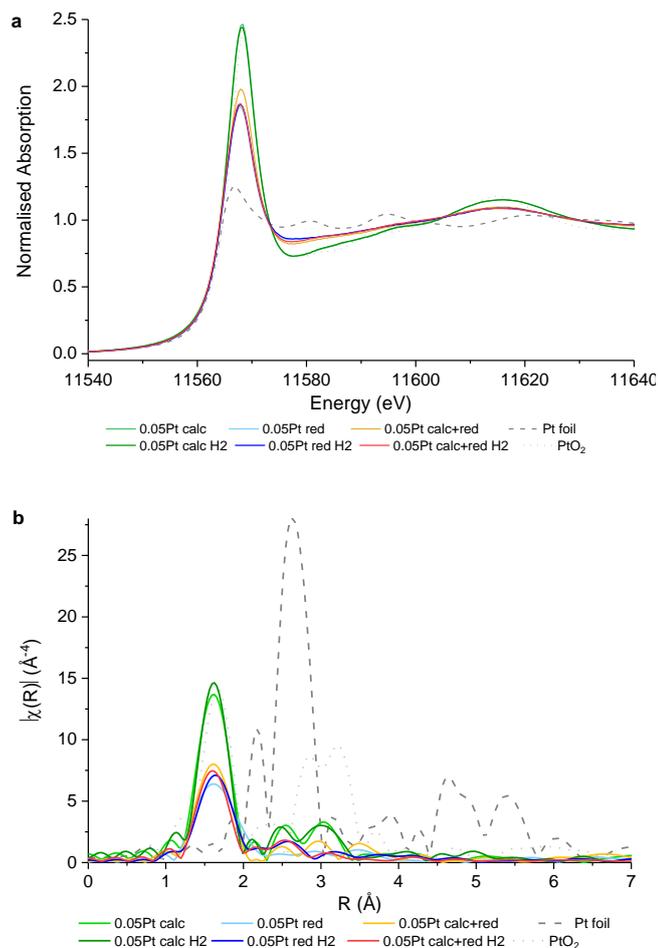
Figure 3.17 XANES (a) and EXAFS (b) spectra of the 0.05 %Pt calcined, reduced and calcined+reduced samples before and after flushing with H_2.

In Figure 3.17a and b, the XAS analysis of the lowest metal loading 0.05 % Pt/TiO₂ samples before and after flushing the pellets for 30 min with 10% H_2/Ar flow are reported. In particular, the XANES plot of the 0.05 % Pt calcined samples show the presence of stable oxidised Pt(IV) species that do not change upon hydrogen flushing. In fact, no difference is found between the samples recorded in and out of H_2 atmosphere. The main peak in the Fourier Transform plot (Figure 17b) can be assigned to Pt-O contribution. In particular, the strong intensity of the peak at 1.8 Å suggests the presence of large PtO₂ particles.

The 0.05 %Pt reduced sample is slightly affected by the hydrogen flushing, with a change in height line from 2 to 1.8 as seen in the energy plot. When comparing the R-space plots of the samples before and after the H_2 flushing, it is possible to confirm the slight reduction of the small Pt particles, as likely formation of Pt-Pt metal contribution arises at just below 3Å. The white line height of the 0.05 % Pt calcined and reduced samples before and after treatment in hydrogen atmosphere show a small decrease, which in the R-space plot reveals the possible presence of Pt-Pt distance.

These experiments were carried out in order to partially mimic the reaction conditions and allow us to study whether the catalysts change during the catalytic hydrogenation of 3-NS. By use of a powerful technique such XAS, we could look at the changes in the oxidation state of platinum as well as the variation in the platinum environment.

Overall, it is possible to observe a partial reduction of the samples during the mild treatment in H₂. This is especially true is the case of the higher metal loading 0.2 and 0.5 %Pt samples and in particular for the reduced only samples, which have a broader particle size distribution, with a presence of large particles (>2 nm) with exposed crystalline Pt(0) facets. A possible explanation for this behaviour is that once the samples are prepared, they are handled and exposed to air, and slight oxidation of the metallic platinum nanoparticles can occur. Because flushing the samples with hydrogen is a mild treatment, this behaviour could be seen as a reduction of a passivated metallic surface. Since the higher metal loading 0.2 and 0.5 %Pt reduced samples show also the lowest catalytic performance in the reduction of 3-NS, it could be possible to confirm once again the inactivity of extended metallic platinum surfaces.

With a different behaviour, the lower metal loading 0.08 and 0.05 %Pt samples show only slight changes when comparing the samples before and after flushing hydrogen at room temperature, suggesting a higher stability and a lower tendency to reduction. This could be explained by the strong intimacy between the metal and the oxygen from the support. Of interest, it is the case of 0.05 %Pt samples, where it can be seen that as the PtO₂ particle size decreases (calcined > calcined and reduce> reduced sample) the reduction during exposure to hydrogen takes place more easily.

During these semi *in-situ* series of experiments discussed in this section, it was possible to establish that the catalysts might change their surface characteristics during the catalytic reaction; nevertheless, the catalytic trend previously observed is confirmed.

3.2.8 Effect of reduction temperature

The samples prepared, tested and discussed in this chapter achieved constant *ca.* 100 % selectivity towards the formation of the desired 3-NS chemoselective hydrogenation product 3-VA, thus it was decided to examine the effect of the reduction temperature on the catalytic performance. To confirm what reported before regarding the effect of the reduction temperature on the catalytic activity,[12] the as-prepared 0.2 % Pt/TiO₂ sample was reduced at three different temperatures (200, 300 and 450 °C) and the resulting materials were tested for 1 h under standard reaction conditions. The results in Table 3.4 show that the three catalysts achieved a lower 3-NS conversion as the reduction temperature decreased, with the sample reduced at 200 °C achieving 14 % less 3-NS conversion. Moreover, as the reduction temperature decreased, selectivity to 3-

VA decreased of less than 10 %, counting that the by-product 3-EA should be considered as a further hydrogenation product of 3-VA. These results are in good accordance with the work published by Corma *et al.* that showed how the temperature at which the samples are activated is crucial for achieving the final high catalyst chemoselectivity.[12] In this way, we could confirm that we have worked at the conditions that permit to achieve the highest selectivity, as in this work, we have aimed at studying how to change and improve the catalytic activity by varying the proportion of active sites present on the catalyst.

Table 3.4 Effect of the temperature of the reductive heat treatment on the activity and selectivity of 0.2%Pt/TiO₂ catalysts. Reaction conditions: 0.2 ml 3-NS, 8 ml toluene, 0.05 g catalyst, 40 °C, 3 bar H₂, 800 rpm, 1h.

Sample	Reduction temperature (°C)	Conversion (%)	Selectivity (%)	
			3-VA	3-EA
	450	74	97	3
0.2%Pt	300	67	96	4
	200	64	93	7

At high temperatures and under reductive conditions, SMSI may be triggered. The samples considered in this work were treated at a maximum temperature of 450 °C, so that the SMSI effect might take place and be the cause of such catalytic improvement. In fact, this strong interaction has previously shown to enhance the performance of catalysts.[61] In the work by Corma *et al.* mentioned before, it was claimed that a geometric effect only is present, where the TiO₂ support decorates the platinum particles partly encapsulating them and leading to an increase in the active Pt-TiO₂ interface. TEM images confirmed this, showing a Pt particle covered by a thin layer of TiO₂.[12] However, it should also be noted that based on the same work, it is possible to confirm that by using carbon as support (a non-reducible, inert material), the platinum led to the chemoselective hydrogenation product 3-VA if the metal particles were small enough. This indicates that the metal particle size plays a fundamental role in the achievement of high selectivity, while the type of support most probably controls the overall catalytic activity.

In our research, we have not come across platinum particles showing support encapsulation but using a variety of characterisation techniques, we have demonstrated how the close interaction between the metal and the oxide support is crucial for the chemoselective catalytic activity in the reduction of substituted nitroaromatic compounds such as 3-NS.

3.2.9   Catalyst reusability

After determining and establishing the high activity of these catalysts, it was necessary to assess whether they were also reusable over multiple reaction tests. In fact, together with activity, the stability of catalytic materials is a fundamental feature, especially required for industrial applications. The 0.2% Pt/TiO_2 reduced sample was chosen for these tests. The reaction was performed three times and already after the first reuse it was clear that the oxidation of the supported metal occurred, because the colour of the catalyst changed from grey to yellow after reaction. Simultaneously to this colour variation, a decrease in 3-NS conversion was reached after the first reuse (Figure 3.18). This is possibly a consequence of the recovery, washing and drying procedure. The oxidation of the platinum nanoparticles could also be explained by their size. In fact, the smaller the metal agglomerate, the more easily it is oxidised.[62-63] It is possible to notice that although the 3-NS conversion decreases after multiple catalyst reuses, the selectivity to 3-VA is constantly as high as 100 %, which is a possible indication that no metal agglomeration, but only oxidation or loss of some active species is taking place.
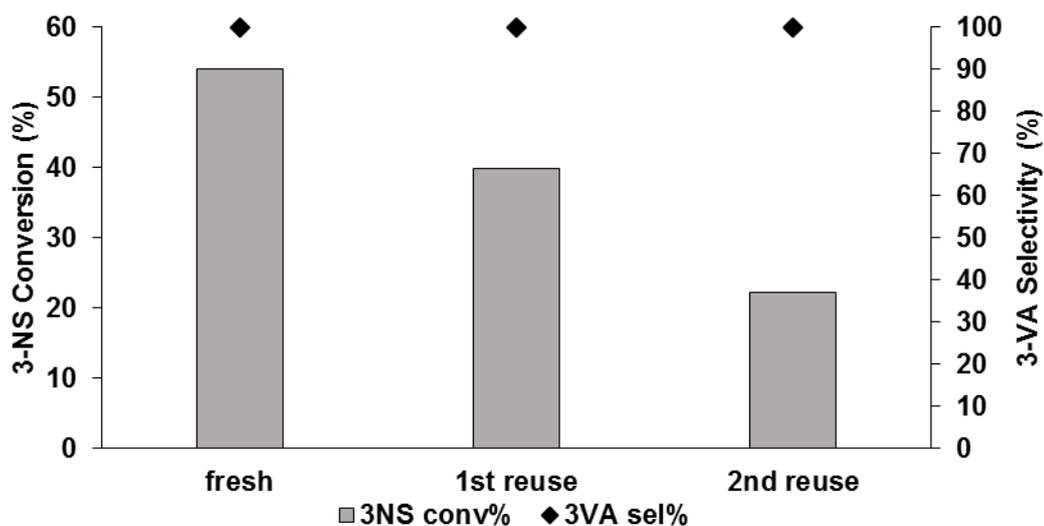
Figure 3.18 Catalyst reusability data for the 0.2%Pt/TiO₂ reduced. Reaction condition: 3NS 0.2 ml, Toluene 8 ml, catalyst 0.05 g, 40 °C, 3 barH₂, 500 rpm.
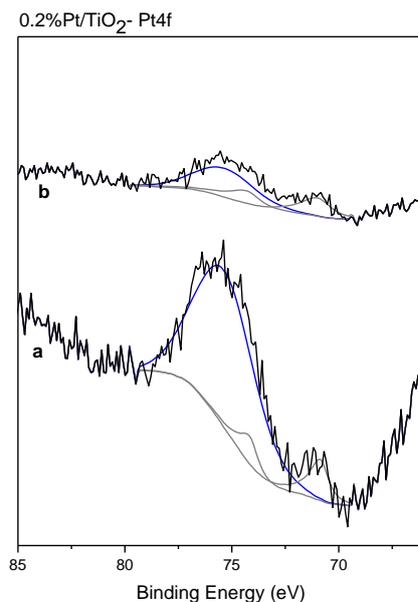
Figure 3.19 XPS Pt4f analysis of the 0.2 %Pt reduced samples, before (a) and after (b) use in the 3-NS hydrogenation reaction.

The platinum XPS spectrum of the 0.2 %Pt/TiO₂ reduced sample (Figure 3.19a) shows the presence of metallic platinum, with the two Pt4f$_{7/2}$ and Pt4f$_{5/2}$ components at *ca.* 71 and 74 eV respectively. After using the catalyst for multiple consecutive test reactions, the XPS spectrum of the 0.2 %Pt reduced used sample (Figure 3.19b) still presents reduced platinum species. Although the peaks intensities are different, the platinum atomic percentages, determined with CasaXPS, are of 0.01% for both samples. Moreover, confirmation that the platinum is retained on the surface of the support was obtained by a leaching test on the reaction mixture after 30 min reaction. The platinum content determined by ICP was 0.8 % of the total platinum contained in the catalyst used. Which suggest a negligible loss overall.

It is not clear why the catalyst achieves lower 3-NS conversion over multiple reuses. It might be possible that the recovery procedure is detrimental. A more in-depth study could be something to be considered as a future work.

3.3   Conclusions

In this work it has been shown how the preparation method and the activation of a catalyst is crucial for achieving not only high selectivity but also extraordinary activity for the chemoselective hydrogenation of nitro compounds. In particular, a series of Pt/TiO₂ catalysts were studied for the selective hydrogenation of 3-NS to 3-VA at low pressures and temperatures. As platinum was found to be a very active catalyst for this process, previous studies focussed on the improvement of the reaction selectivity, a major problem when formation of 3-EN and highly undesired toxic hydroxylamines may take place.[13, 20]

Small platinum nanoparticles (< 3 nm) that contain mainly low coordinated Pt species, often at the interface with the support material, were defined responsible for the increase in selectivity towards the reduction of the NO_2 group and formation of the desired 3-VA.[12] The procedure for the activation of the catalyst has shown to be particularly important when platinum is supported on TiO_2. By increasing the temperature of the reductive step from 200 °C to 450 °C, a substantial decrease in by-products was obtained and formation of 3-VA with a selectivity higher than 90 % was achieved.[12]

With this knowledge in mind, one of the aims of this work has been to study how the performance of the catalysts could change upon different heat treatments, so of two portions of the as-prepared 0.2 % Pt/TiO₂ sample, one was reduced at 450 °C for 4 h and the other was calcined followed by a reduction under the same conditions. After testing the materials for the hydrogenation of 3-NS, the 0.2 %Pt calcined and reduced catalyst was found to be substantially more active compared to the 0.2 %Pt reduced catalyst, while the selectivity of the products was almost completely for 3-VA (> 95%).

From this observation, the other focus of this work has been to investigate how the activity of the Pt/TiO₂ catalysts could vary with the metal loading. Therefore, 0.05, 0.08, 0.2 and 0.5 %Pt reduced as well as calcined and reduced samples were prepared, tested and characterised in order to achieve a structure-activity correlation.

During the project, *via* XPS, STEM, CO chemisorption and XAS analysis it was possible to conclude that when TiO₂ is impregnated with an amount of platinum higher than 0.2%, metal agglomeration takes place under reductive atmosphere, leading to a broad particle size distribution. However, performing a calcination followed by a reduction permits to form homogeneous and small Pt nanoparticles, well distributed on the surface of the support and leading to high intrinsic catalytic activities. By mean of some approximation and with the particle size distribution resulting from TEM analysis it was possible to draw a strong correlation between the platinum peripheral atoms located at the interface between the nanoparticle and the support and the catalytic results. Whereas, a similar approach using the amount of surface metal would lead to a less accurate correlation.

From these results is clear how the heat treatment required for the formation of the right proportion and type of active site is strongly dependent on the metal loading. Higher loadings require multiple heat treatments in order to first anchor the small metal particles on the support by the oxidative calcination and then achieve the right oxidation state by reductive treatment (see Figure 3.20). By decreasing the metal loading, good dispersion of small clusters is obtained already at the impregnation step and only a reductive treatment is required, in order to achieve the most active oxidation state.
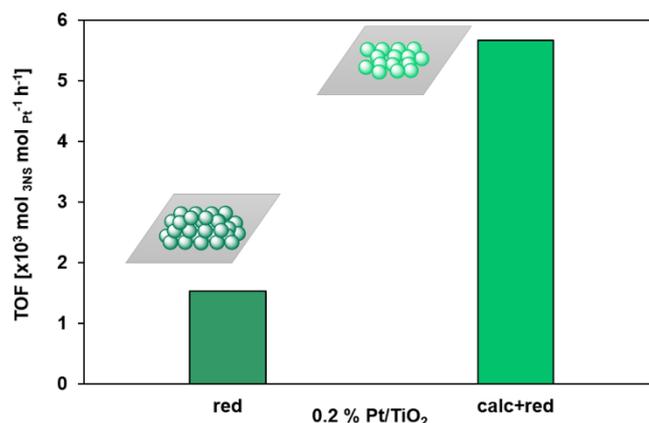
Figure 3.20 Graphical representation of the effect of agglomeration on the intrinsic activity in the 0.2 %Pt/TiO₂ catalysts.

Most importantly, in this study previously reported knowledge on how to achieve high selectivity in supported platinum catalysts for the chemoselective hydrogenation of nitro compounds has been applied. However, it was also possible to expand such knowledge by exploiting the full activity of platinum and increase the availability of active sites, hence preparing extremely active Pt/TiO₂ catalysts.

The reusability of the 0.2% Pt/TiO₂ reduced catalyst has shown to be poor. Deactivation took place already at the first reuse, where conversion decreased while the selectivity remained constant. Leaching studies did not reveal substantial loss of metal from the surface of the catalyst, suggesting that a modification of the active sites took place, maybe during sample recovery, with consequent loss of activity. Because some samples showed extraordinary turn over frequencies, together with a constant high selectivity, it could be of interest to test these samples in a flow system instead of a batch reactor. Hence, a deactivation study of the catalyst under reaction condition could give better information regarding the catalytic system.

3.4   References

1.   Blaser, H. U.; Steiner, H.; Studer, M. Selective Catalytic Hydrogenation of Functionalized Nitroarenes: An Update. *ChemCatChem* **2009,** *1* (2), 210-221.

2.   Song, J. J.; Huang, Z. F.; Pan, L.; Li, K.; Zhang, X. W.; Wang, L.; Zou, J. J. Review on selective hydrogenation of nitroarene by catalytic, photocatalytic and electrocatalytic reactions. *Applied Catalysis B-Environmental* **2018,** *227*, 386-408.

3.   Rylander, P. N. *Hydrogenation Methods.* Academic Press: New York, 1990.

4.   Nishimura, S. *Handbook of Heterogeneous Catalytic Hydrogenation for Organic Synthesis.* Wiley-VCH: New York, 2001.

5.   Corma, A.; Concepcion, P.; Serna, P. A different reaction pathway for the reduction of aromatic nitro compounds on gold catalysts. *Angew Chem Int Ed Engl* **2007,** *46* (38), 7266-9.

6.   F. D. Bellami, K. O. Selective reduction of aromatic nitro compounds with stannous chloride in non acidic and non aqueous medium. *Tetrahedron Letters* **1984,** *25* (8), 839-842.

7.   Basu, M. K.; Becker, F. F.; Banik, B. K. Ultrasound-promoted highly efficient reduction of aromatic nitro compounds to the aromatic amines by samarium/ammonium chloride. *Tetrahedron Letters* **2000,** *41* (30), 5603-5606.

8.   Burawoy, A.; Critchley, J. P. Electronic spectra of organic molecules and their interpretation-V*. *Tetrahedron* **1959,** *5*, 340-351.

9.   Pedro Serna, P. C., Avelino Corma. Design of highly active and chemoselective bimetallic gold–platinum hydrogenation catalysts through kinetic and isotopic studies. *Journal of Catalysis* **2009,** *265*, 19-25.

10.   Claus, P. Heterogeneously catalysed hydrogenation using gold catalysts. *Applied Catalysis A-General* **2005,** *291* (1-2), 222-229.

11.   Rylander, P. *Catalytic hydrogenation over platinum metals*. Elsevier: 1967.

12.   Corma, A.; Serna, P.; Concepcion, P.; Calvino, J. J. Transforming nonselective into chemoselective metal catalysts for the hydrogenation of substituted nitroaromatics. *Journal of the American Chemical Society* **2008,** *130* (27), 8748-53.

13.   Wei, H.; Liu, X.; Wang, A.; Zhang, L.; Qiao, B.; Yang, X.; Huang, Y.; Miao, S.; Liu, J.; Zhang, T. FeOₓ-supported platinum single-atom and pseudo-single-atom catalysts for chemoselective hydrogenation of functionalized nitroarenes. *Nature Communications* **2014,** *5*, 5634.

14.   Sarkany, A.; Zsoldos, Z.; Furlong, B.; Hightower, J. W.; Guczi, L. Hydrogenation of 1-Butene and 1,3-Butadiene Mixtures over Pd/ZnO Catalysts. *Journal of Catalysis* **1993,** *141* (2), 566-582.

15.   Semagina, N.; Grasemann, M.; Xanthopoulos, N.; Renken, A.; Kiwi-Minsker, L. Structured catalyst of Pd/ZnO on sintered metal fibers for 2-methyl-3-butyn-2-ol selective hydrogenation. *Journal of Catalysis* **2007,** *251* (1), 213-222.

16.   Campo, B. C.; Volpe, M. A.; Gigola, C. E. Liquid-Phase Hydrogenation of Crotonaldehyde over Platinum- and Palladium-Based Catalysts. *Industrial & Engineering Chemistry Research* **2009,** *48* (23), 10234-10239.

17.   Tew, M. W.; Emerich, H.; van Bokhoven, J. A. Formation and Characterization of PdZn Alloy: A Very Selective Catalyst for Alkyne Semihydrogenation. *Journal of Physical Chemistry C* **2011,** *115* (17), 8457-8465.

18.   Berguerand, C.; Yarulin, A.; Cardenas-Lizana, F.; Murzin, D.; Kiwi-Minsker, L. Chemoselective liquid phase hydrogenation of 3-nitrostyrene over Pt nanoparticles: synergy with ZnO support. *Industrial and Engineering Chemistry Research* **2015,** *54*, 8659-8669.

19.   Yarulin, A.; Berguerand, C.; Alonso, A. O.; Yuranov, I.; Kiwi-Minsker, L. Increasing Pt selectivity to vinylaniline by alloying with Zn via reactive metal–support interaction. *Catalysis Today* **2015,** *256*, 241-249.

20.   Serna, P.; Boronat, M.; Corma, A. Tuning the Behavior of Au and Pt Catalysts for the Chemoselective Hydrogenation of Nitroaromatic Compounds. *Topics in Catalysis* **2011,** *54* (5-7), 439-446.

21.   Edwards, J. K.; Pritchard, J.; Piccinini, M.; Shaw, G.; He, Q.; Carley, A. F.; Kiely, C. J.; Hutchings, G. J. The effect of heat treatment on the performance and structure of carbon-supported Au–Pd catalysts for the direct synthesis of hydrogen peroxide. *Journal of Catalysis* **2012,** *292*, 227-238.

22.   S. J. Tauster, S. C. F., R. T. K. Baker, J. A. Horsley. Strong Interactions in Supported-Metal Catalysts. *Science* **1981,** *211* (4487), 1121-1125.

23.   Datye, A. K.; Xu, Q.; Kharas, K. C.; McCarty, J. M. Particle size distributions in heterogeneous catalysts: What do they tell us about the sintering mechanism? *Catalysis Today* **2006,** *111* (1-2), 59-67.

24.   Kim, G. J.; Kwon, D. W.; Hong, S. C. Effect of Pt Particle Size and Valence State on the Performance of Pt/TiO₂ Catalysts for CO Oxidation at Room Temperature. *Journal of Physical Chemistry C* **2016,** *120* (32), 17996-18004.

25.   Huang, H. B.; Leung, D. Y. C.; Ye, D. Q. Effect of reduction treatment on structural properties of TiO₂ supported Pt nanoparticles and their catalytic activity for formaldehyde oxidation. *Journal of Materials Chemistry* **2011,** *21* (26), 9647-9652.

26.   de Graaf, J.; van Dillen, A. J.; de Jong, K. P.; Koningsberger, D. C. Preparation of Highly Dispersed Pt Particles in Zeolite Y with a Narrow Particle Size Distribution: Characterization by Hydrogen Chemisorption, TEM, EXAFS Spectroscopy, and Particle Modeling. *Journal of Catalysis* **2001,** *203* (2), 307-321.

27.   Matos, J.; Ono, L. K.; Behafarid, F.; Croy, J. R.; Mostafa, S.; DeLaRiva, A. T.; Datye, A. K.; Frenkel, A. I.; Roldan Cuenya, B. In situ coarsening study of inverse micelle-prepared Pt nanoparticles supported on gamma-Al₂O₃: pretreatment and environmental effects. *Phys Chem Chem Phys* **2012,** *14* (32), 11457-67.

28.   Beier, M. J.; Andanson, J. M.; Baiker, A. Tuning the Chemoselective Hydrogenation of Nitrostyrenes Catalyzed by Ionic Liquid-Supported Platinum Nanoparticles. *ACS Catalysis* **2012,** *2* (12), 2587-2595.

29.   Cardenas-Lizana, F.; Berguerand, C.; Yuranov, I.; Kiwi-Minsker, L. Chemoselective hydrogenation of nitroarenes: Boosting nanoparticle efficiency by confinement within highly porous polymeric framework. *Journal of Catalysis* **2013,** *301*, 103-111.

30.   Qu, R.; Macino, M.; Iqbal, S.; Gao, X.; He, Q.; Hutchings, G. J.; Sankar, M. Supported Bimetallic AuPd Nanoparticles as a Catalyst for the Selective Hydrogenation of Nitroarenes. *Nanomaterials (Basel)* **2018,** *8* (9).

31.   Dhiman, M.; Polshettiwar, V. Ultrasmall nanoparticles and pseudo-single atoms of platinum supported on fibrous nanosilica (KCC-1/Pt): engineering selectivity of hydrogenation reactions. *Journal of Materials Chemistry A* **2016,** *4* (32), 12416-12424.

32.   Sankar, M.; He, Q.; Morad, M.; Pritchard, J.; Freakley, S. J.; Edwards, J. K.; Taylor, S. H.; Morgan, D. J.; Carley, A. F.; Knight, D. W.; Kiely, C. J.; Hutchings, G. J. Synthesis of stable ligand-free gold-palladium nanoparticles using a simple excess anion method. *ACS Nano* **2012,** *6* (8), 6600-13.

33.   Boronat, M.; Corma, A. Origin of the different activity and selectivity toward hydrogenation of single metal Au and Pt on TiO₂ and bimetallic Au-Pt/TiO₂ catalysts. *Langmuir* **2010,** *26* (21), 16607-14.

34.   S. J. Tauster, S. C. F., and R. L. Garten. Strong Metal-Support Interactions. Group 8 Noble Metals Supported on TiO₂. *Journal of the American Chemical Society* **1978,** *100* (1), 170-175.

35.   Zimmermann, R.; Steiner, P.; Claessen, R.; Reinert, F.; Hufner, S.; Blaha, P.; Dufek, P. Electronic structure of 3d-transition-metal oxides: on-site Coulomb repulsion versus covalency. *Journal of Physics-Condensed Matter* **1999,** *11* (7), 1657-1682.

36.   Moulder, J. F.; Stickle, W. F.; Sobol, P. E.; Bomben, K. D. *Handbook of X-ray Photoelectron Spectroscopy.* Perkin-Elmer Corporation: Norwalk, CT, 1992.

37.   Knecht, J.; Stork, G. Röntgenphotoelektronen spektroskopische Untersuchung der Thallium-Oxidelektrode. *Fresenius' Zeitschrift für analytische Chemie* **1978,** *289* (3), 206-206.

38.   Katrib, A. The reduction of Pt(IV) to Pt(II) by X-ray and argon-ion bombardment; evidence from X-ray photoelectron spectroscopy. *Journal of Electron Spectroscopy and Related Phenomena* **1980,** *18* (2), 275-278.

39.   Riggs, W. M. X-ray photoelectron spectrometry of platinum compounds. *Anal Chem* **1972,** *44* (4), 830-2.

40.   Jackson, S. D.; Willis, J.; McLellan, G. D.; Webb, G.; Keegan, M. B. T.; Moyes, R. B.; Simpson, S.; Wells, P. B.; Whyman, R. Supported Metal Catalysts: Preparation, Characterization, and Function. *Journal of Catalysis* **1993,** *139* (1), 191-206.

41.   Alexeev, O. S.; Chin, S. Y.; Engelhard, M. H.; Ortiz-Soto, L.; Amiridis, M. D. Effects of reduction temperature and metal-support interactions on the catalytic activity of Pt/gamma-Al₂O₃ and Pt/TiO₂ for the oxidation of CO in the presence and absence of H₂. *Journal of Physical Chemistry B* **2005,** *109* (49), 23430-43.

42.   Lee, J.; Ryou, Y.; Chan, X.; Kim, T. J.; Kim, D. H. How Pt Interacts with CeO₂ under the Reducing and Oxidizing Environments at Elevated Temperature: The Origin of Improved Thermal Stability of Pt/CeO₂ Compared to CeO₂. *Journal of Physical Chemistry C* **2016,** *120* (45), 25870-25879.

43.   Pan, C. J.; Tsai, M. C.; Su, W. N.; Rick, J.; Akalework, N. G.; Agegnehu, A. K.; Cheng, S. Y.; Hwang, B. J. Tuning/exploiting Strong Metal-Support Interaction (SMSI) in Heterogeneous Catalysis. *Journal of the Taiwan Institute of Chemical Engineers* **2017,** *74*, 154-186.

44.   Sexton, B. XPS investigation of strong metal-support interactions on Group IIIa-Va oxides. *Journal of Catalysis* **1982,** *77* (1), 85-93.

45.   de Resende, N. S.; Eon, J.-G.; Schmal, M. Pt–TiO₂–γ Al₂O₃Catalyst. *Journal of Catalysis* **1999,** *183* (1), 6-13.

46.   Zhang, C. B.; He, H.; Tanaka, K. Catalytic performance and mechanism of a Pt/TiO₂ catalyst for the oxidation of formaldehyde at room temperature. *Applied Catalysis B-Environmental* **2006,** *65* (1-2), 37-43.

47.   Epling, W. S.; Cheekatamarla, P. K.; Lane, A. M. Reaction and surface characterization studies of titania-supported Co, Pt and Co/Pt catalysts for the selective oxidation of CO in H₂-containing streams. *Chemical Engineering Journal* **2003,** *93* (1), 61-68.

48.   Englisch, M.; Jentys, A.; Lercher, J. A. Structure Sensitivity of the Hydrogenation of Crotonaldehyde over Pt/SiO₂and Pt/TiO₂. *Journal of Catalysis* **1997,** *166* (1), 25-35.

49.   Poondi, D.; Vannice, M. A. The influence of MSI (metal-support interactions) on phenylacetaldehyde hydrogenation over Pt catalysts. *Journal of Molecular Catalysis a-Chemical* **1997,** *124* (1), 79-89.

50.   Haerudin, H.; Bertel, S.; Kramer, R. Surface stoichiometry of 'titanium suboxide' Part I Volumetric and FTIR study. *Journal of the Chemical Society, Faraday Transactions* **1998,** *94* (10), 1481-1487.

51.   Pesty, F.; Steinruck, H. P.; Madey, T. E. Thermal-Stability of Pt Films on TiO₂(110) - Evidence for Encapsulation. *Surface Science* **1995,** *339* (1-2), 83-95.

52.   Bowker, M.; Stone, P.; Morrall, P.; Smith, R.; Bennett, R.; Perkins, N.; Kvon, R.; Pang, C.; Fourre, E.; Hall, M. Model catalyst studies of the strong metal–support interaction: Surface structure identified by STM on Pd nanoparticles on TiO₂(110). *Journal of Catalysis* **2005,** *234* (1), 172-181.

53.   Freakley, S. J.; He, Q.; Harrhy, J. H.; Lu, L.; Crole, D. A.; Morgan, D. J.; Ntainjua, E. N.; Edwards, J. K.; Carley, A. F.; Borisevich, A. Y.; Kiely, C. J.; Hutchings, G. J. Palladium-tin catalysts for the direct synthesis of H₂O₂ with high selectivity. *Science* **2016,** *351* (6276), 965-8.

54.   Brown, M.; Peierls, R. E.; Stern, E. A. White Lines in X-Ray Absorption. *Physical Review B* **1977,** *15* (2), 738-744.

55.   Koningsberger, D.; Prins, R. *X-ray absorption: principles, applications, techniques of EXAFS, SEXAFS, and XANES*. Wiley: 1988.

56.   Penner-Hahn, J. E. X-ray absorption spectroscopy in coordination chemistry. *Coordination Chemistry Reviews* **1999,** *190*, 1101-1123.

57.   Hyde, T. I.; Ash, P. W.; Boyd, D. A.; Randlshofer, G.; Rothenbacher, K.; Sankar, G. X-Ray Absorption Spectroscopic Studies of Platinum Speciation in Fresh and Road Aged Light-Duty Diesel Vehicle Emission Control Catalysts. *Platinum Metals Review* **2011,** *55* (4), 233-245.

58.   Kim, M. Y.; You, Y. S.; Han, H. S.; Seo, G. Preparation of highly dispersive platinum catalysts impregnated on titania-incorporated silica support. *Catalysis Letters* **2008,** *120* (1-2), 40-47.

59.   Beale, A. M.; Weckhuysen, B. M. EXAFS as a tool to interrogate the size and shape of mono and bimetallic catalyst nanoparticles. *Phys Chem Chem Phys* **2010,** *12* (21), 5562-74.

60.   Hashimoto, N.; Takahashi, Y.; Hara, T.; Shimazu, S.; Mitsudome, T.; Mizugaki, T.; Jitsukawa, K.; Kaneda, K. Fine Tuning of Pd(0) Nanoparticle Formation on Hydroxyapatite and Its Application for Regioselective Quinoline Hydrogenation. *Chemistry Letters* **2010,** *39* (8), 832-834.

61.   Hsieh, B. J.; Tsai, M. C.; Pan, C. J.; Su, W. N.; Rick, J.; Chou, H. L.; Lee, J. F.; Hwang, B. J. Tuning metal support interactions enhances the activity and durability of TiO₂-supported Pt nanocatalysts. *Electrochimica Acta* **2017,** *224*, 452-459.

62.   Xu, Y.; Shelton, W. A.; Schneider, W. F. Effect of particle size on the oxidizability of platinum clusters. *J Phys Chem A* **2006,** *110* (17), 5839-46.

63.   Wang, C. B.; Yeh, C. T. Effects of particle size on the progressive oxidation of nanometer platinum by dioxygen. *Journal of Catalysis* **1998,** *178* (2), 450-456.

Chapter

4

Hydrothermally prepared carbons as supports for AuPd nanoparticles

4.1   Introduction

4.1.1   Carbon as catalyst support

A heterogeneous catalyst support can be designed to contain desirable characteristics such as inertness, high stability under reaction conditions, high surface area, porosity and the presence of anchoring and nucleation sites such as surface defects.[1]

Graphite is a stable unreactive material composed of stacked sheets of graphene;[2] however, microcrystalline carbon, so called "activated carbon", consists of a more disordered structure with more defective sites that favour metal nanoparticle deposition and nucleation. In fact, the number of basal plane edges in crystalline graphite is much lower than in the microcrystalline carbon, where the presence of unsaturated carbon atoms at the edge of the aromatic structure is much higher. These sites are characterised by high concentrations of unpaired electrons and show strong chemisorption properties.[1, 3]
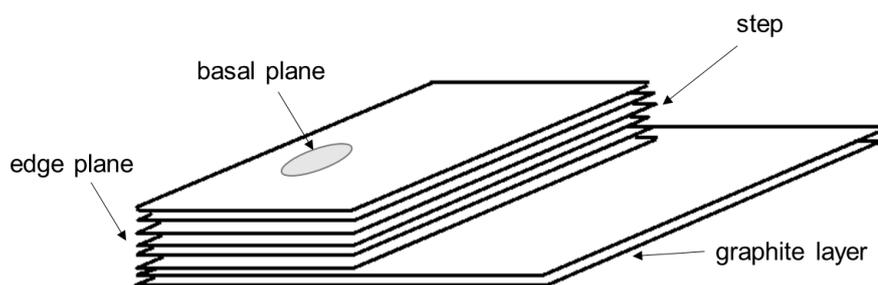
Figure 4.1 Schematic diagram of the condensed aromatic structures formed during the HTC synthesis. Redrawn from reference [4].

Activated carbon and carbon black are graphitic materials that have been used in a wide range of applications ranging from medical purposes to air purification and chemical applications as catalyst supports and electrodes. The main characteristic that makes carbon materials rather appealing is their extremely high surface area associated with the presence of microporosity, which

helps to generate strong interactions to adsorb small molecules.[5] The high electrical conductivity of graphitic carbon is also very valuable in the production of anode electrodes for lithium-ion batteries. Overall, in the fields of energy storage, chemical conversion and environmental pollution, carbon materials play an important role. The stability, availability and the possibility to tune the characteristics of these solids make them appealing for a variety of applications.

Commercially, these materials are prepared by controlled carbonisation or thermal decomposition of carbonaceous source materials such as coal, petroleum pitch and natural gas, however, also renewable feedstocks like bamboo and coconut husk are commonly used.[6] Due to the thermal treatments used to produce activated carbon being energy demanding together with the fact that environmental issues concerning the utilisation of fossil feedstocks are becoming more stringent, finding alternative ways to produce activated carbon is of interest in both the research and industrial community.

4.1.2   Hydrothermal carbons

During the dehydration of sugars for the synthesis of 5-hydroxymethyl furfural (HMF), solid by-products are formed, called "humins". These solids, also called hydrochar, are the products of a series of cyclisation, aromatisation and condensation reactions of organic molecules taking place during the high temperature and pressure conversion of HMF.[7] In fact, the formation of the hydrochar takes place when carbohydrates are loaded in an autoclave together with water, followed by prolonged thermal treatment under autogenous pressure.[8] Three main steps characterise the hydrothermal carbonisation process:[9]

1. Dehydration of the carbohydrate to HMF
2. Polymerisation towards polyfurans
3. Carbonisation due to intermolecular dehydration.

Because of the formation of furan species during the dehydration of the starting biomass material, the final solids feature the furan ring as main structural motif (see Figure 4.2).[10]
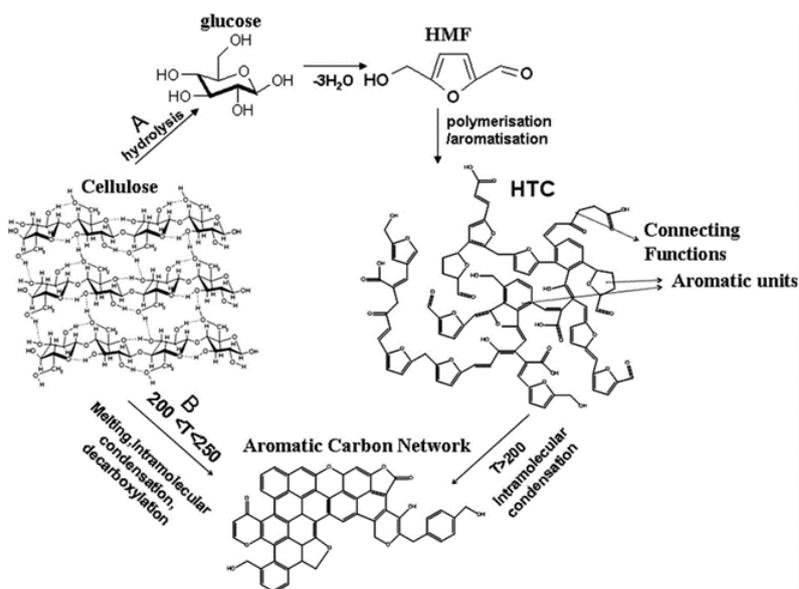
Figure 4.2 Biomass condensation into HTC. Taken from reference [11].

These carbonaceous solids formed upon hydrothermal treatment of carbohydrates could be promising candidates for the production of activated carbons.[12-13] From undesired by-products, the synthesis of carbonaceous solids has become an active field of study and the autoclave based high temperature preparation of hydrothermal carbons (HTC) has expanded in recent years.[11] The possibility of using various sources of renewable feedstocks, from pure carbohydrates to crop waste, would allow to a more economical and energetically viable preparation method.[8, 14] Moreover, one drawback of current activated carbon is the indiscriminate presence of a variety of impurities, arising from either the precursor or the preparation method. Whereas, the controlled hydrothermal processes can obtain precise elemental compositions, using simple carbohydrates.[15]

Together with the wide range of uses mentioned before, carbon materials have proved to be desirable catalyst supports for metal nanoparticles, due to their stability in liquid and gas phase catalytic reactions and over a broad range of pH values. Moreover, the possibility of metal recovery via combustion and surface functionalization by addition of heteroatoms such like nitrogen or oxygen in the structure is very appealing. In particular, carbon materials have shown to be the support of choice for the deposition of AuPd nanoparticles to be applied in the selective oxidation of glycerol to glyceric acid.[16] As discussed in the Chapter 1, AuPd bimetallic supported catalysts have been reported to show a synergistic effect when applied in various oxidation or hydrogenation reactions, including the oxidation of glycerol.[16-19]

4.1.3 Glycerol oxidation using supported AuPd catalysts in alkaline environment

As presented in Chapter 1- Sections 1.2.4, bimetallic AuPd catalysts have shown enhanced activity in a range of reactions, among which is the glycerol oxidation reaction.

Glycerol is a highly functionalised molecule obtained as a by-product of the manufacture of biodiesel. It can be used to further produce synthesis gas, but the functionality present on the short carbon chain molecule make it preferable to be used to synthesise products with higher chemical value such as esters, ethers, epoxides and diols that can be used in the production of pharmaceuticals, solvents, surfactants, resins and polymers.[20] As depicted in the reaction scheme in Figure 4.3, the oxidation of glycerol shows a complex reaction pathway by which a wide range of possible products could be obtained.[20-21] Stoichiometric processes that use mineral acids to achieve the oxidation of glycerol are known but environmentally harmful, hence undesired. Whereas the catalytic oxidation by use of molecular oxygen under mild conditions is a highly desired alternative.

During the oxidation of glycerol, the first reaction step is the oxidation of one of the terminal C-O bonds of the alkoxide, which has been found to require the presence of a base. The initial dehydrogenation *via* H-abstraction from one of the hydroxyl groups of glycerol is facilitated by the presence of the base.[22] In alkaline conditions, also the interconversion between hydroxyacetone and glyceraldehyde is favoured, with the further oxidation of the aldehyde to acid being very fast. Overall, this promotes substantial formation of glycerate (Figure 4.3). This product is stable in the alkaline aqueous environment,[22] whereas other by-products may undergo base-catalysed transformations.

It should be noted that during the reaction, the formation of hydrogen peroxide H_2O_2 takes place in presence of gold catalysts,[23-24] and this has been associated with C-C bond cleavage leading to C1 and C2 products such as glycolate, oxalate and formate.[25] Once formed, H_2O_2 is stable in the presence of gold catalysts, but unstable in an alkaline environment. Therefore, the addition of base is not only beneficial to the selectivity of glycerate, but also to the enhanced decomposition of peroxide formed during the process.
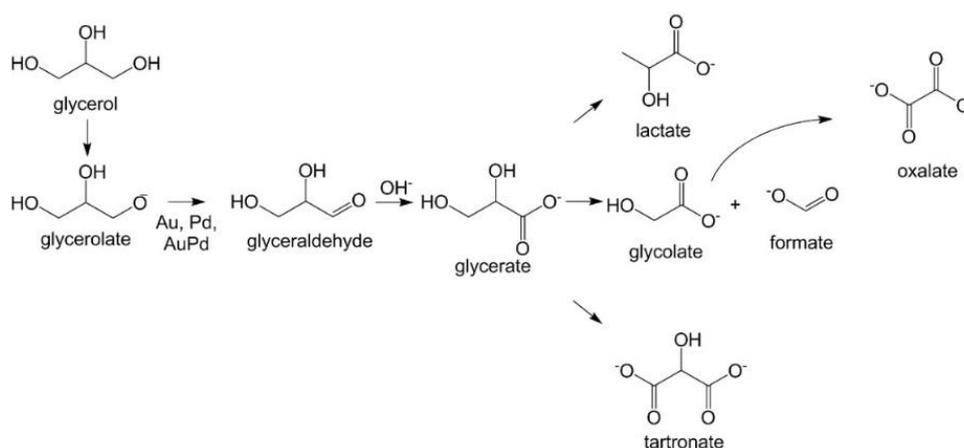
Figure 4.3 Reaction scheme for the liquid phase glycerol oxidation in alkaline environment. Taken from reference [26].

Prati and co-workers have long studied the oxidation of alcohols with addition of sodium hydroxide as base.[27-29] Carrettin *et al.* first reported the application of gold for the oxidation of glycerol to glycerate in the presence of sodium hydroxide, showing 100 % selectivity either using charcoal or graphite as support.[30] The addition of sodium hydroxide was fundamental for achieving high conversion and improving the selectivity by avoiding formation of C1 products, but the presence of gold metal was confirmed to be necessary when bare carbon was tested in a blank reaction in presence of sodium hydroxide. They observed a correlation between the glycerol to sodium hydroxide ratio, showing that high concentration of base led to exceptionally high selectivity to glycerate. With increasing sodium hydroxide to glycerol molar ratio an increase in substrate conversion and glycerate selectivity are observed, with a base to substrate ratio of 2 being a reasonable reaction condition counting that strong basic solution would need further neutralisation.[31] It was also noted that decreasing the amount of substrate, while increasing both the amount of catalyst and oxygen pressure led to formation of tartronic acid, which is the product of over-oxidation of glycerate.

The addition and choice of a second metal does affect not only the final catalytic activity but could also influence the selectivity of the reaction. For example, the addition of platinum to gold would direct the oxidation reaction towards the formation of dihydroxyacetone,[32] while AuPd bimetallic catalysts show improved selectivity towards glycerate.[33-34] Whether in the form of a bimetallic particle or in a physical mixture, the addition of Pd to the monometallic Au catalyst has an important influence on the reaction selectivity. This has been correlated to the ability of palladium to decompose H_2O_2 and hence decrease the amount of this by-product formed during reaction, and whose presence has been correlated to the formation of C-C cleavage products, overall leading to an increased selectivity towards glyceric acid.[35]

Because metal segregation and multiple phases could take place during catalyst preparation, making it difficult to find a direct correlation between catalytic activity and active species, a catalyst preparation method that could form alloyed bimetallic nanoparticles has been employed to study the synergistic effect between Au and Pd for glycerol oxidation.[34] By a subsequent sol nanoparticles formation and immobilisation onto the carbon support, narrow AuPd particles size distribution, centred around 3.4 nm and homogenous nanoalloy structure were observed, showing an overall enhanced activity for the glycerol oxidation reaction and higher glycerate selectivity, compared to the monometallic catalysts.[36]

The effect of the particle size of monometallic gold on carbon has been reported, showing that on one side high and constant selectivity (~80 %) from the beginning to the end of the reaction were obtained when large metal particles (~20 nm) were present, though having low activity. While on the other side, smaller nanoparticles (~ 6 nm) showed higher substrate turnover with the selectivity of the oxidation products changing as the reaction proceeded.[37-39] In a study

of AuPd bimetallic catalysts with increasing particles size from 2 to 6 nm showed how the catalytic activity of the catalyst with an average particles size of 6 nm was 5 time lower than the sample with 2 nm average particle size, while the selectivity to glycerate was slightly increased.[40] With similar results being obtained upon multiple catalyst reuses, which led to a slight enlargement of the bimetallic nanoparticles.[41]

Impregnation method has been applied to synthesise AuPd/C catalysts, which showed good catalytic activity as well as high and constant selectivity towards formation of glycerate of *ca.* 75%.[16, 31,] The particles size was found to be in between 3-8 nm, with 20% of the metal forming much larger particles (>20 nm). In contrast to the catalysts supported on TiO_2, on carbon bimetallic alloy nanoparticles were formed.[42] Also by electroless deposition, monometallic Au and Pd and bimetallic AuPd/C catalysts were prepared, characterised and tested in alkaline condition, confirming that the bimetallic system shows a strongly enhanced activity compared to the monometallic ones and the increased activity was ascribed to the existence of bifunctional Au-Pd bimetallic active sites.[26]

4.1.4   Aim of the work

The aim of this work is to use HTC materials as supports for metal nanoparticles. Few studies have been reported using such tuneable and environmental friendly carbonaceous materials as supports for supported nanocatalysts.[43-44] Gold-palladium nanoparticles have been shown to be active catalysts for various oxidation and hydrogenation reactions and when supported on carbon, have been reported to reach high activity and selectivity in the oxidation of glycerol to glycerate in aqueous basic solution. In previous works, the use of different commercial carbon supports has shown to lead to variations in catalyst activity, suggesting an influence of the support characteristics on the final performance.[45-46]

During this project, the HTC samples used as supports, were synthesised by our collaborators at the Max-Planck Institute for Chemical Energy Conversion (CEC) in Mülheim Germany. The materials feature various physical and chemical characteristics and the aim of this study is to investigate the effect that the various supports may have on the final catalytic performance in the oxidation of glycerol to glycerate, under alkaline reaction conditions. The AuPd catalysts have been prepared by a modified impregnation method using excess chloride.[47] The characterisation of the HTC before addition of the metals consisted in the elemental and surface area analysis, followed by XPS, XRD and SEM analysis of the supported catalysts. All catalytic samples were tested for the glycerol oxidation reaction and the data analysis aiming to define a structure-reactivity correlation has been reported in the following discussion.

4.2 Results and discussion

4.2.1 General discussion

4.2.1.1 Hydrothermal carbons used in the project

The HTC samples applied as supports in this chapter were received from our collaborators from the research group Carbon Synthesis and Applications of the Department of Heterogeneous reactions led by Dr. Saskia Heumann at the Max Planck Institute for Chemical Energy Conversion in Mülheim, Germany. The carbon materials were prepared via a hydrothermal synthesis as described in Chapter 2. The HTC discussed here were prepared by changing synthesis parameters such as initial pH, annealing conditions, oxygen and nitrogen content. The elemental analysis of these solids was performed by the collaborators, while in house instruments at Cardiff University were used to determine the surface areas. As a comparison, a commercial carbon black Vulcan VXC72R was also used.

In the following Table 4.1, the carbon materials used in the following discussion are listed with a short description of the preparation method.

Table 4.1 List of carbons discussed in this chapter, with some description on the preparation method.

Support name	Preparation characteristics
VXC72R	Commercial carbon black
Glu pH6	Initial glucose solution at pH6, annealed in nitrogen flow
Glu pH6 KOH	Initial glucose solution at pH6, activated by refluxing in KOH solution, annealed in N_2 flow
HTC pH6 Ar	Initial sucrose solution at pH6, annealed in Ar flow
HTC pH6 N_2	Initial sucrose solution at pH6, annealed in N_2 flow
HTC pH6 H_2O	Initial sucrose solution at pH6, annealed in humid N_2 flow
HTC pHX	Initial sucrose solution at pHX (0, 1, 3, 6), annealed in N_2 flow
HTC pHX KOH	Initial sucrose solution at pHX (0, 1, 3, 6), activated by refluxing in KOH solution, annealed in Ar flow
S:U=1:1	N-doped HTC. Sucrose and urotropine solution, annealed in Ar flow

Support name	Preparation characteristics
HTC 22%O	HTC pH6 washed in nitrosulphuric acid solution
HTC 15%O	HTC pH6 washed in nitrosulphuric acid solution and annealed in N_2 flow at 510 °C
HTC 5%O	HTC pH6 washed in nitrosulphuric acid solution and annealed in N_2 flow at 800 °C

These carbon materials were applied as supports for metal catalysts. A total metal loading of $0.5_{wt}\%$AuPd was used for all catalysts, with the two metals being in equal molar amounts. The AuPd/C samples discussed in this chapter were prepared following the modified impregnation method followed by reduction in furnace[47]. The so-prepared catalysts were then tested for the glycerol oxidation reaction according to literature[16] and characterised by means of XPS, XRD and SEM analysis.

4.2.1.2 X-ray photoelectron spectroscopy

XPS was used to analyse the samples and study the oxidation state of the deposited metals in addition to the oxygen, carbon and nitrogen species present on the surface of the materials. Overall, the gold and palladium deposited on all the carbon samples discussed in the following sections exist in the metallic Au(0) and Pd(0) state. In Figure 4.4 representative Au and Pd XPS spectra of the 0.5%AuPd catalyst supported on the hydrothermal carbon prepared using an initial aqueous sucrose solution of pH 6, annealed in N_2 flow (HTC pH6 N_2) are reported. The XPS spectra of the Au 4f region are characterised by two spin-orbit components, the $4f_{7/2}$ peak at 84.0 eV and the $4f_{5/2}$ signal at 88 eV.[48] Also the XPS spectra of the Pd region features two slightly asymmetric peaks, where the $3d_{5/2}$ photoelectron peak is centred at 335.2 eV and shows the secondary spin-orbit component $3d_{3/2}$ at a distance of 5.3 eV, at 340.3 eV.[49,50]
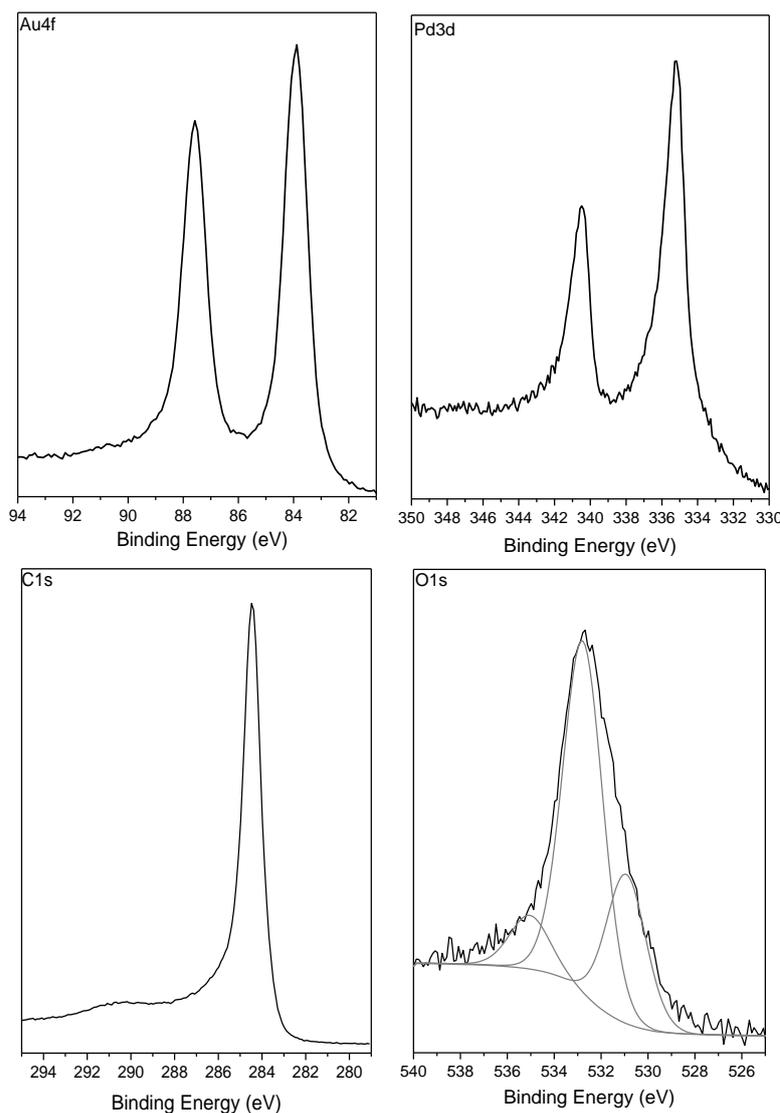
Figure 4.4 Representative XPS spectra of the Au, Pd, C and O region. Data from AuPd/HTC pH6 N_2.

The reference catalyst, AuPd/VXC72R, shows extremely low signals in both Au and Pd XPS regions. This reflects in low XPS normalised area values, as it can be seen in the tables discussed in the following sections. This behaviour can be explained with the fact that the metal deposited within cavities and defects of the support material, which hinders it from the X-ray beam. It should also be noticed that this commercial carbon is characterised by a very fine powder, compared to the hydrothermal carbons that have a more granular structure. Such XPS signal shielding has been reported before for other activated carbon supporting Au, which was not always clearly detectable by XPS analysis, suggesting that this is a common feature when using carbon supports.[46] However, confirmation of the presence of the metal is given by the catalytic activity for glycerol conversion, which is absent in the case of blank reactions. As will be discussed later in the chapter, XRD analysis gave information about the bulk composition of the reference sample, being able to determine the presence of AuPd nanoparticles, with an average size

comparable to the other samples. In addition, because all the catalysts discussed in this chapter are prepared by impregnation of the support, without filtration or washing of the solid, no loss of the metal added during preparation is expected.

The analysis of the oxygen O1s photoelectron region is of interest since this element is present in various percentages in all carbon samples. However, apart from the samples specifically prepared to achieve high content of oxygenated species, all samples show a broad photoelectron peak at 532.5 eV, where C=O (~531 eV), C-O-C and C-OH (~ 533 eV) species are expected to be present, whereas the peak fitted at higher binding energy (~ 535 eV) can be assigned to chemisorbed water or molecular oxygen (Figure 4.4).[51-52]

The photoelectron analysis of the C1s region is required as the carbon peak is used in the data analysis to calibrate the binding energy values. The area of the carbon peak was also used to calculate the normalised intensity of the other elements in the samples. All the carbon samples discussed here showed a defined and intense photoelectron peak at *ca.* 284 eV (Figure 4.4). According to literature, from the asymmetric shape of the peak, together with the presence of a small and broad satellite peak at higher binding energies around 290 eV, it is possible to assume that a substantial amount of sp^2 graphitic carbon species are present in the samples.[52-53] Confirmation of this is also found in a detailed study performed by Baccile *et al.* on the same materials and based on a combination of solid-state ^{13}C NMR techniques, were the majority of carbon species were characterised as in the form of sp^2 C=C carbons.[10]

4.2.1.3 X-ray diffraction analysis

A characterisation technique useful in studying an ordered bulk structure is X-ray diffraction (XRD). Even if the HTCs are mostly amorphous materials, they have a distinctive diffraction pattern. All the XRD spectra of the AuPd/HTC samples show broad reflections at *ca.* 23 and 43 ° as seen in Figure 4.5, which have been reported to correspond to the (002) and (100) planes of graphene, respectively. In particular, the diffraction peak at 23 ° arise from the stacking of multiple graphene sheets, while the reflection at 43 ° indicates the presence of a short-range order in stacked graphene layers in spherical structures formed by sp^2 carbon atoms, confirming the XPS findings.[54-56]

Crystalline metallic Au and Pd show characteristic X-ray diffraction patterns [57-58] and when they form an alloy, a new series of diffraction signals arises,[59] positioned at 2Θ values in between those of Au and Pd, depending on the composition of the bimetallic system. The highest diffraction signal is given by the (111) plane, which is at 38.2, 40.1 ° and at an in-between value around 39 ° for Au, Pd and their alloy, respectively. In Figure 4.5 a representative diffraction

pattern of the AuPd/HTC pH6 N_2 is shown. Together with a diffraction due to alloy AuPd particles, it is possible to notice the presence of also some isolated Pd.
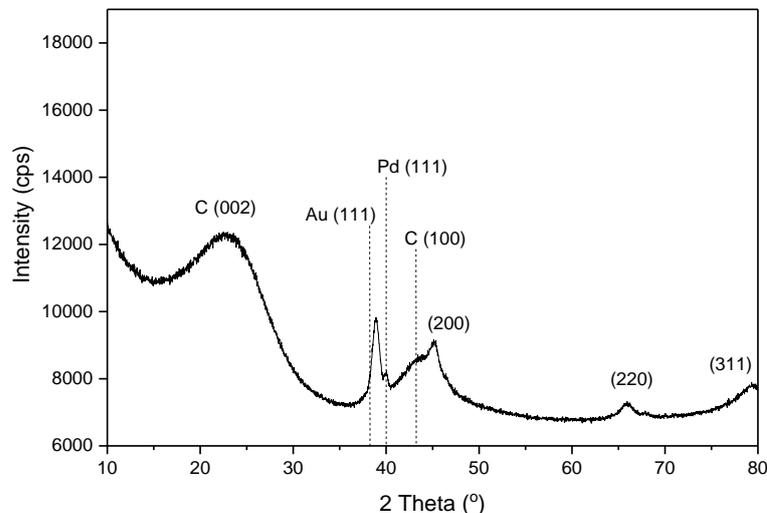
Figure 4.5 Representative XRD diffraction pattern of the catalyst AuPd/HTC pH6 N_2.

Defined diffraction patterns can be obtained from samples having a long-range crystalline structure, whereas the detection of small disordered particles in the nano-metre range is not always possible as it is dependent on the wavelength of the incident X-ray beam. In literature a limit of 3 nm is usually reported,[60-61] while the smallest metallic nanoparticle calculated from the XRD data of all the catalysts discussed here showed an average crystallite size of 6 nm. Once the supported metallic nanoparticles are big enough to be analysed by XRD, it is possible to analyse not only their composition, but also determine the average particle size of their crystallites. Using the Scherrer equation and the width of the (111) diffraction peak, it was possible to determine the average crystallite sizes, that were calculated in the range of 6 to 40 nm, with the majority of the samples having particle size around 13 nm.

4.2.1.4 Scanning electron spectroscopy

In order to study the different materials discussed in this chapter and study variations in the morphology of the carbon supports, Scanning Electron Microscopy (SEM) has been used. From previous works is known that similar carbon materials to those discussed here feature spherically shaped agglomerates, whose size varies depending on the preparation method. Moving from the commercial carbon black VXC72R[62] to the glucose-based HTCs[54, 63] and the sucrose-based HTCs,[15] carbon spheres with increasing particle size are observed and will be discussed in more detail in the following sections. As a general observation, during SEM analysis of all samples, metal agglomerates were often visible as bright areas, independently of the support characteristics. Considering that SEM has a limit of detection of few μm, it should be reasonable to say that some

rather large particles are formed on all samples, supporting the results obtained from the XRD analysis and overall indicating a low dispersion of the metal.

4.2.1.5 Catalytic testing

The catalytic activity of the AuPd/C samples was evaluated for the glycerol oxidation test reaction. The catalytic reactions were performed in basic conditions with addition of sodium hydroxide as reported in literature. The presence of base is known to enhance the activity as well as the selectivity of the oxidation products, favouring the formation of glycerate and reducing the amount of C2 and C1 undesired products.[16, 31] When testing the AuPd/C samples for the catalytic oxidation of glycerol, a variety of catalytic activities were observed, whereas it was possible to notice that the overall product selectivity was very comparable between the samples considered. The main glycerol oxidation product formed during reaction is glycerate, with selectivity between 72-81%, depending on the sample (see Figure 4.7). Other minor products are tartronate (whose selectivity only slightly increases during reaction, possibly indicating the further oxidation of the glycerate), oxalate, glycolate (whose formation could be explained by the oxidative degradation of hydroxypyruvic acid), lactate and formate, each with a selectivity between 1-8%, the products distribution being overall constant as the reaction proceeds. Previous data reported in the literature have often shown that the selectivity of AuPd/C catalysts towards glycerate decreased during the reaction, due to overoxidation of the products. Some reports indicated that the catalyst preparation method could have an effect. For example, bimetallic AuPd catalysts prepared by a wet impregnation method have shown to lead to a constant and high selectivity to glycerate over the entire reaction time,[16] supporting our findings, whereas sol-immobilised catalysts led to decreasing glycerate selectivity as the glycerol conversion increased.[16, 33] In the literature, when considering bimetallic AuPd particles, independently of the Au:Pd molar ratio, high selectivity (70-80%) to glycerate have always been achieved compared to a monometallic Au catalyst,[41, 64-65] which goes along with the results determined during the catalytic testing in this work.

Although the glycerate selectivity is very comparable between samples, the activity changed between the different AuPd/C catalysts discussed in this work. To identify a trend and understand what could give raise to a different catalytic performance, the nanoparticle size and composition as determined by XRD have been plotted against the initial glycerol conversion as shown in Figures 4.6-4.8).

The size of the nanoparticles has often been related to the catalytic activity, due to the amount of metal atoms that are exposed to the surface and hence available to the reactants.[40-41] Since the size of the HTC supported AuPd nanoparticles (as calculated from XRD data) varied, an attempt to find a correlation between the size of the metal agglomerates and the initial glycerol conversion is shown in Figure 4.6.
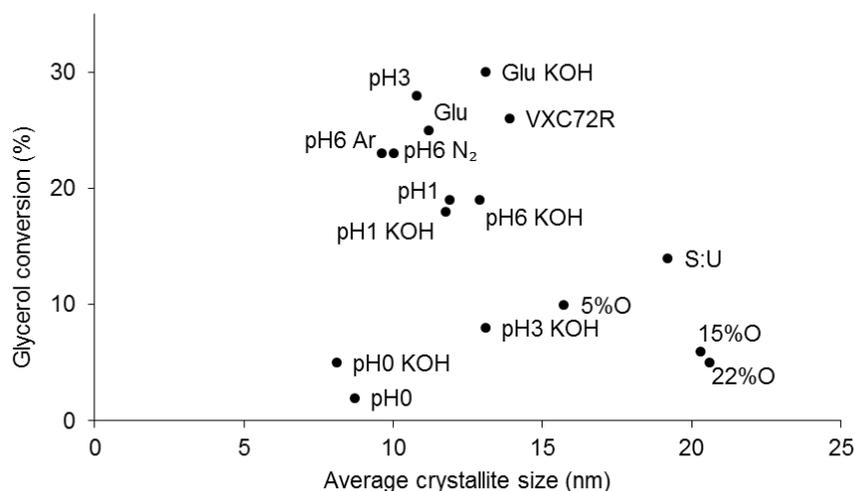
Figure 4.6 Correlation between the mean particle sizes calculated from XRD analysis and initial glycerol conversion.

The results plotted in Figure 4.6 show that independently on the nanoparticle crystallite size, the glycerol conversion after 15 min from the start of the oxidation reaction varies between *ca.* 2 and 30 %. A trend between the size of the AuPd nanoparticles and the glycerol oxidation activity was not found, it should be possible to say that a direct correlation between the size of the supported metallic particle and the catalytic performance is not present. Therefore, the metal particle sizes will not be considered responsible for the variation in catalytic activity.

As mentioned in Section 4.1.3, the size of the supported metal particles has sometimes been related to the products selectivity during the glycerol oxidation reaction.[40] In Figure 4.7, the glycerol oxidation selectivity results are reported for the AuPd/HTC discussed in this chapter. In particular, the glycerate selectivity is plotted against the crystallite size of the nanoparticles. Overall, the selectivity towards glycerate formation is quite comparable between samples, with all catalysts showing the formation of glycerate as main product, with a selectivity of *ca.* 80 % and the size of the nanoparticles does not seem to have an effect on the product formation.
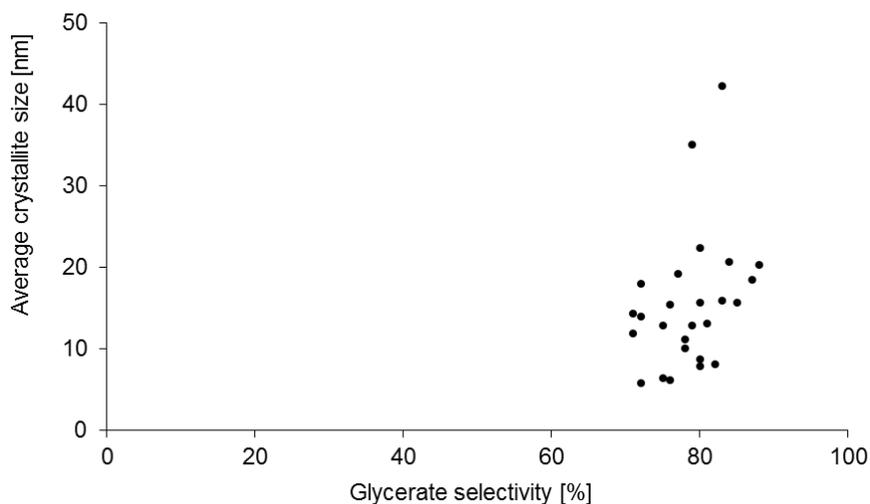
Figure 4.7 Dependence of the average crystallite size on the glycerate selectivity.

When considering bimetallic systems, another parameter that has been linked with catalytic activity is the composition of the nanoparticles. In previous AuPd/C studies, the presence of AuPd alloy has been related to a higher activity of the catalysts used for the glycerol oxidation reaction.[34, 64-65] Hence, the composition of the supported metal particles on the HTC described here could be influencing the catalytic glycerol conversion. In fact, although the catalysts were prepared by addition of equimolar amounts of Au and Pd during support impregnation, segregation occurred and Au-rich as well as Pd-rich and AuPd alloy aggregates have formed. In Figure 4.8, the analysis of the XRD data of all the 0.5% AuPd/C samples showed a heterogeneous presence of separate Au and Pd, as well as bimetallic alloy nanoparticles. The position of the signal arising from the (111) plane are plotted against the initial glycerol conversion. The dotted lines indicate the 2Θ values at which Au and Pd are expected to give rise to a diffraction peak (38.2, 40.1 ° respectively). Whereas peaks falling at intermediate values can be considered a mixture of the two monometallic structures, hence an alloy.[57-58] Some catalysts show two peaks, indicating that two crystal structures are present on the surface of the support, while some catalysts have only one diffraction pattern. Because the variation in composition does not reflect in a trend in initial glycerol conversion, it should be possible to assume that no direct relationship is present between the composition of the various AuPd/C samples and their catalytic activity. The presence of AuPd alloy nanoparticles or the segregation of Au and Pd regions have been detected, however catalytic activity shows to be independent from such catalyst characteristics.
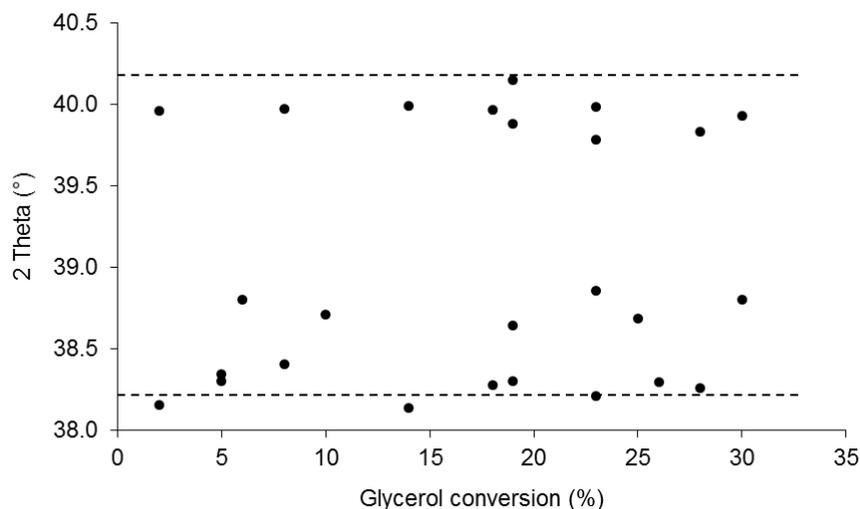
Figure 4.8 Position of the diffraction signal of the (111) plane and corresponding initial glycerol conversion of the 0.5% AuPd/C catalysts.

By use of the BET method to study the data obtained during the N_2 physisorption experiments, the surface areas of the HTC samples were determined. As can be seen in Figure 4.9, and it will be reported more in detail in the following sections, the majority of the HTC revealed to have very limited surface areas, with most values below 20 m²/g. It should be noted that together with a low surface area, rather dense materials are formed. This characteristic goes in contrast with the general feature of commercial carbons, which have large surface areas (up to 1000 m²/g) due to the small size of the carbon agglomerates that form the fine powders, as well as to the large presence of porosity. Because this parameter could be beneficial to the dispersion of the metal and hence positively affect the catalytic capacity of the materials, a plot of the HTC surface area values and the glycerol conversions of the corresponding supported catalysts is reported in Figure 4.9.
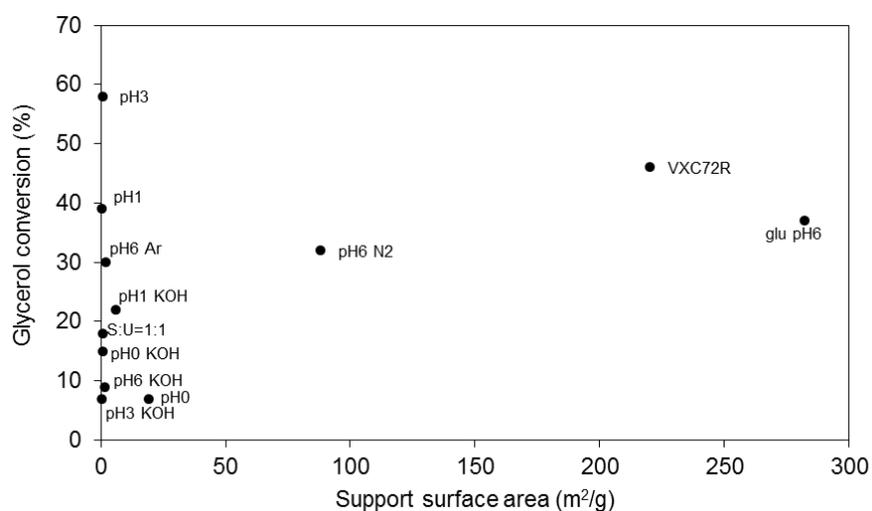
Figure 4.9 Correlation between the surface area of the HTC supports and the conversion of glycerol after 30 min reaction at standard conditions.

With most of the support samples having a surface area near zero, while a variety of glycerol conversions are achieved by the corresponding AuPd/C catalysts, it can be overall deduced how the extension of the surface of the support is not crucial. Moreover, as these materials do not seem to be porous, all the metal should be readily available on the external surface of the carbonaceous agglomerates.

In conclusion, in this first section the general and common characteristics of the AuPd/C samples discussed in this chapter have been introduced. In particular, all the catalysts present metallic AuPd nanoparticles, with variable particle size and composition. The particles size and composition data determined by XRD were plotted against the catalytic results, where a clear structure-activity correlation was not found. Therefore, it is possible to exclude the influence of the nature of the nanoparticles on the performance in the glycerol oxidation reaction. This finding suggests that although particle size effect have been reported for the system considered here, our catalytic results show to be independent from such characteristics of the metal nanoparticles. This is probably because rather large particles are present in these samples, where the effect of particle size can be neglected. Hence, independently on the composition and the size of the AuPd particles, the final catalytic activity should be controlled by other factors. Since the metals are impregnated on a range of HTC materials showing different elemental composition, surface functionalisation, surface area and morphology, it seems possible to hypothesize that an influence of the structural and elemental characteristics of the carbon supports on the final nanoparticles catalytic properties might be present.

In the following sections the catalysts will be presented and discussed depending on the preparation method of the hydrothermal carbons and final characteristics, focusing the discussion on the support effect.

4.2.2 Influence of the HTC synthesis method

One of the parameters investigated in the preparation of the HTC samples was the carbon source, which in the majority of cases is a simple sugar precursor. Initially, carbons were prepared from commercially available glucose (indicated as Glu) sourced from Sigma Aldrich, however in some cases the presence of iron impurities were identified in the precursor. To avoid the presence of hetero-elements that could bring an extra degree of complexity, it was decided to use a commercially, easily available, purer and everyday used table sugar as a sucrose source (indicated as Sucr). In a study where a variety of hexose-based sugars were applied for the synthesis of HTCs, Baccile *et al.* concluded that no substantial differences are observed between these carbon materials and same elemental composition and functional groups were identified in the final materials.[15]

Additionally, the synthesis of nitrogen doped HTC was performed. The addition of nitrogen in the carbon matrices of materials used in fuel cells and batteries is a highly studied modification, since it has shown very similar electrocatalytic properties to the Pt-based materials.[66-69] Addition of heteroelements such nitrogen could be performed following two ways: in-situ doping or post doping. This means that the introduction of nitrogen could take place during the synthesis of the carbon materials or *via* a post treatment of the carbon structures. Post treatments generally require procedures using HNO_3, NH_3 or HCN, which may not be easy to control and resulting in poorly homogeneous and irreproducible samples, or even disruption of the carbon structure. In order to dope the materials with nitrogen, our collaborators added a second compound during the initial step: urotropine (U), in equimolar amounts to the sucrose (S: U=1: 1). The addition of this secondary component not only contributes to the overall carbon content in the final product, but also introduces a significant amount of nitrogen (Figure 4.10).
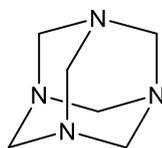
Figure 4.10 Molecular structure of urotropine.

In the process of preparing the HTCs, following the hydrothermal synthesis step, a high temperature annealing process is required in order to form stable materials. In fact, the initial use of catalysts supported on HTC samples that did not undergo such annealing step, eventually leached organic species during reaction. The analysis of the leached component revealed the presence of humins, organic molecules arising from the incomplete condensation of the sugar used for the hydrothermal preparation and that are not embedded within the condensed framework, hence thermal treatment of these compounds is necessary prior to any further application. Different annealing processes have been used in the preparation of the HTCs. However, after the hydrothermal step performed adding the initial sugar solution with pH6 in an autoclave, and treated at 220 °C for 6 h, the samples discussed here were annealed up to 900 °C in a flow of N_2. As for comparison, a fraction of the Sucr pH6 sample was also treated in Ar.

These hydrothermal carbon materials prepared from both sugar sources as well as the commercial VXC72R were used to deposit equimolar amount of Au and Pd and were further tested for the glycerol oxidation reaction.
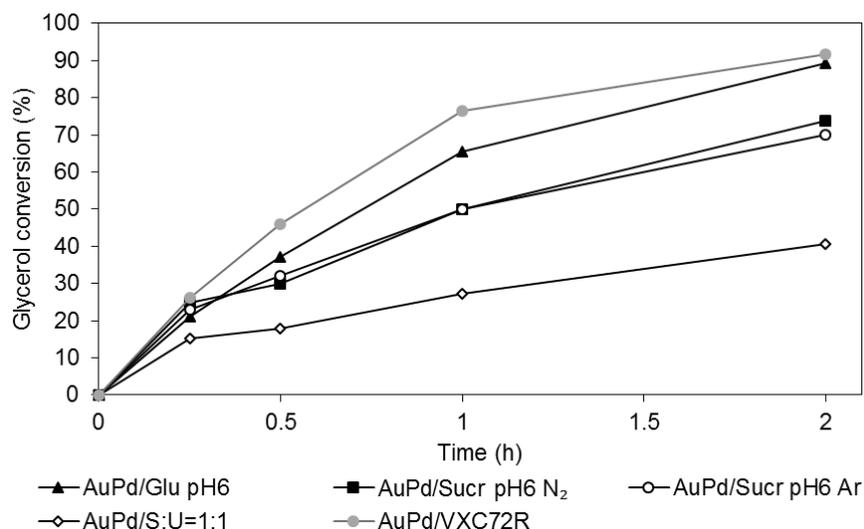
Figure 4.11 Time-on-line profile for the oxidation of glycerol over 0.5%AuPd/HTCs prepared at initial pH6 glucose and sucrose or nitrogen-doped. Reaction conditions: 0.0455 g catalyst, 5 ml NaOH 1.2 M, 5 ml glycerol 0.6 M, 60 °C, 3 bar O_2, 900 rpm, 2 h.

In Figure 4.11 the time-on-line of AuPd on Glu pH6, Sucr pH6 N_2, Sucr pH6 Ar and S: U= 1: 1 are plotted and compared to AuPd/VXC72R. The catalysts show a trend, in which the glucose-based catalyst is more active than the sucrose-based catalysts for the catalytic oxidation of glycerol. The glucose-based material supports a catalyst that achieves high conversions, only slightly less active than the sample supported on the commercial carbon, which achieves glycerol conversion of *ca.* 90 % after 2 h reaction, compared to the sucrose-based material that reaches a maximum glycerol conversion of *ca.*70 % after the same reaction time. The HTC support containing nitrogen shows a substantially lower glycerol conversion of 40 % after 2 h. It should be noted that no variation is observed in the time-on-line plot of the catalysts supported on the two HTC Sucr pH6 annealed in different atmospheres (N_2 and Ar), suggesting that the choice of inert gas has no impact on the final support material.

The elemental analysis of the HTCs is reported in Table 4.2 and shows that the two Sucr pH6 samples have the same elemental composition, whereas the HTC sample S: U=1: 1 synthesised by mixing sucrose and urotropine exhibits a nitrogen weight percentage substantially higher than that in the HTCs prepared with sucrose, with values of 9.3 and 0.01 % respectively. What is particularly noticeable in Table 4.2, is the variation of the HTCs surface areas. The HTC Glu pH6 exhibits a surface area of 280 m²/g, which is larger than that of the commercial carbon black. While on the other extreme, for the N-doped HTC S: U=1:1 an extremely low surface area of 0.6 m²/g was found. Moreover, changing the inert gas from Ar to N_2 increases the final surface area of the HTC (from 2 to 88 m²/g). Relating this last result with the very similar catalytic activities of the two HTCs Sucr pH6 indicates that the area of the support might have little effect on the metal nanoparticle dispersion and hence on the final catalytic activity for the glycerol oxidation reaction.

Table 4.2 Hydrothermal carbons characteristics and glycerol conversion after 0.5 h reaction.

Support description	C [%]	H [%]	N [%]	O [%]	SA [m²/g]	Conv. [%]
Glu pH6	94	0.7	0.1	4.8	282	37
Sucr pH6 N₂	94	1.7	0.1	4.2	88	30
Sucr pH6 Ar	94	1.7	0.1	4.2	2	32
S:U=1:1	89	1.1	9.3	0.6	0.6	18
VXC72R	94.2	0.1		5.7	220	46

To study the size of the supported AuPd nanoparticles, XRD analysis was performed,[59, 70] and the mean crystallite size was calculated for all samples and the resulting values are reported in Table 4.3.

Table 4.3 XRD diffraction peaks position and corresponding mean nanoparticle dimensions of the glucose and sucrose-based HTC materials as well as the reference AuPd/VXC72R catalyst.

Name	Crystallite size [nm]
Glu pH6	11.2
Sucr pH6	10.0
Sucr pH6 Ar	9.6
S: U=1:1	19.2
VXC72R	13.9

The Sucr pH6 samples annealed in Ar and N₂ show only a minor particle size variation (9.6 and 10 nm respectively), confirming that the increased area (from 2 to 88 m²/g) of the support does not influence the dispersion of the metal, nor the final catalytic activity. In the same way, the analysis of the AuPd catalyst supported on Glu pH6 indicates the presence of slightly larger nanoparticles (11 nm), however impregnated on a surface three times larger than the Sucr pH6 N₂ sample, confirming again that the extension of the support area available during impregnation does not affect the nanoparticles size. However, the catalyst supported on Glu pH6 reveals a higher glycerol conversion than the catalysts supported on the sucrose-based HTCs. At last, for

the N-doped sucrose HTC S: U=1: 1 quite larger crystallites, with an average size of 19 nm were determined, supported on a material showing very limited surface area (< 1 m²/g), overall leading to the least active catalyst. The reference catalyst supported on VXC72R presents AuPd crystallites with an average of 14 nm, which forms the most active catalyst of the series discussed here. This result supports what mentioned in the General discussion (Section 4.2.1.5), where was reported that the size of the metallic nanoparticles did not play a crucial role in the final catalytic activity towards the glycerol oxidation.

When analysing the data acquired during the XPS analysis, it was possible to calculate a normalised intensity value for each of the other elements analysed, using the carbon signal as reference element. These values could then be used to qualitatively compare elements from different samples. From the normalised values reported in Table 4.4, it is possible to see that for the Sucr pH6 N_2 and Ar samples with very similar AuPd crystallite sizes and decreasing surface areas, the normalised peak intensities increase from 0.16 to 0.35 respectively. This result supports the hypothesis that as the surface available for nanoparticle formation decreases and the metal loading is constant for all the samples, the metal particles are more densely localised on the support, giving rise to higher XPS signals. Although XPS is a surface analysis that can give partial information on the samples, it can still give indicative information about the metal distribution, especially when one of parameters such surface area, metal loading and particle size is comparable.

Table 4.4 Normalised XPS areas of the glucose and sucrose-based HTC materials.

Sample	Au/C	Pd/C
Glu pH6	0.03	0.04
Sucr pH6 N_2	0.15	0.17
Sucr pH6 Ar	0.35	0.35
S: U=1:1	0.10	0.86

It is noticeable the strong variation in metal intensity in the sample supported on the N-doped HTC S: U=1:1, because this support has an extremely low surface area (0.6 m²/g), high metal normalised area values would be expected. From XRD analysis, both Au and Pd crystallites are present in the bulk, whereas on the surface analysed by XPS, a Pd richness is detected, possibly indicating that some surface segregation has occurred.

Nitrogen gives rise to one photoelectron peak; whose position depends on the oxidation state of the element. In Figure 4.12, the N1s XPS spectrum of the N-doped HTC support is shown, and two peaks are identified; the first at lower binding energy at *ca.* 398 eV could be assigned to

pyridinic-N, and the second one at slightly higher binding energy positioned at *ca.* 401 eV assignable to quaternary (graphitic)-N species.[71-72] These results indicate that the nitrogen is incorporated during the condensation of the sucrose, becoming part of the graphitic structure and taking part to the formation of the final solid product. In contrast to the modification performed as a post-treatment, nitrogen is present not only on the surface of the HTC but also within the structure. In a work from Titirici *et al.* it was shown how the formation of the two nitrogen speciation took place upon the heat treatment, where at first only a peak attributed to primary amines was present, while both quaternary and pyridinic nitrogen species exist after annealing.[73] Previously, Prati *et al.* reported that the presence of nitrogen in the support leads to higher basicity of the support itself and enhances the activity for the glycerol oxidation reaction.[74] However it has also been reported that when a HTC is heat treated at high temperature, leading to incorporation of the nitrogen within the aromatic carbonaceous structure, the basic character of the element is strongly decreased, possibly affecting the final catalytic performance.[75]
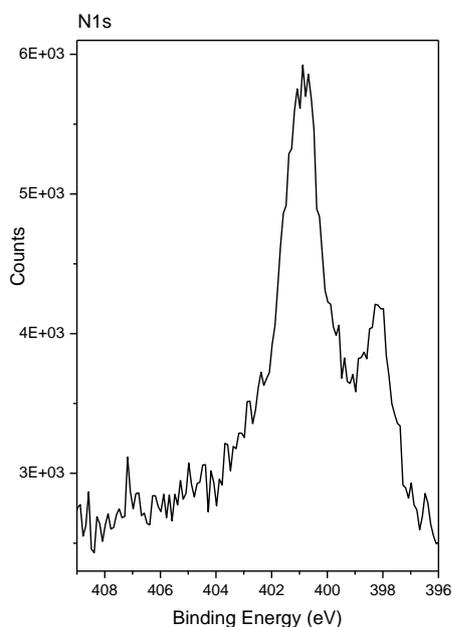
Figure 4.12 XPS spectra of the nitrogen region.

One last characterisation technique applied in the study of these samples was SEM. By the use of SEM, it is possible to study the morphology of the support, however also some rather large bright metal particles are visible. In Figure 4.13, representative micrographs of the AuPd supported on HTC prepared using glucose, sucrose or a sucrose-urotropine mixture, annealed in humid N_2 are shown. For comparison, a micrograph of the sample supported on the commercial carbon VXC72R is also shown. By looking at the images, it is possible to notice that the glucose-based and the reference carbons have similar powdery fine morphology, while the sucrose-based carbon have well defined spherical morphology. The microscopy analysis performed with SEM revealed that the N-doped materials have a very different morphology characterised by large

carbon agglomerates with various shapes and sizes, exposing plane surfaces as well as some rounded globular structures. Staykov *et al.* have reported that as the curvature of the support is higher, less mobility of the metal particle is observed during heat treatment. Whereas on more planar carbon surfaces the agglomeration and enlargement of metal aggregates takes place more easily.[76] This finding supports the observation that larger AuPd nanoparticles were detected by XRD on the catalyst supported on HTC S: U=1: 1 compared to the catalyst supported on commercial VXC72R. A deviation in morphology from the reference materials prepared using glucose was also reported by Titirici *et al.* when preparing HTC using N-containing carbohydrates such as glucosamine and chitosan.[73] In that study, the morphology of the HTCs featured spheres fused together forming a continuous network presenting interstitial macroporosity. It might be possible to suggest that the incorporation of nitrogen within the graphitic structure strongly influences the spatial organisation of the condensation product, leading to a final different morphology.
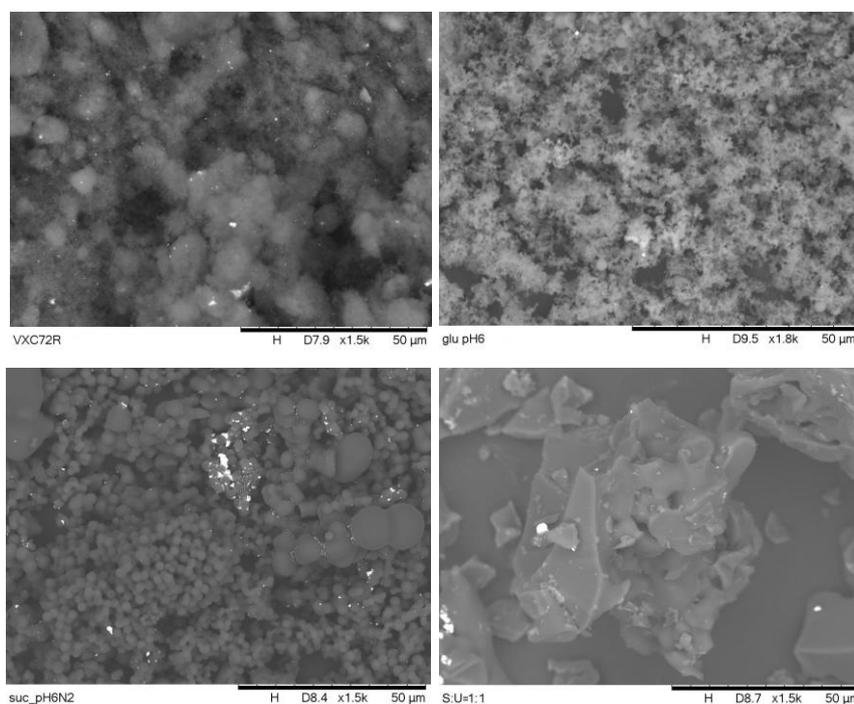
Figure 4.13 HTC synthesised following the same preparation method, but using different initial carbon source.

Since the SEM images of the reference and Glu pH6 carbons have low definition, information regarding their particle size was found in the literature. In previous studies, the morphology of the commercial Vulcan XC72R carbon black was studied and reported,[62, 77] showing that this material consists of spherical particles with size between 30-60 nm. Similar glucose-based materials prepared at initial pH6 and annealed in dry N_2 have shown to contain carbonaceous agglomerates of about 500 nm.[63] The SEM analysis has a spatial resolution of few μm, reason why the micrographs of the VXC72R and the glucose-based materials show to be

indistinct and cloudy. Based on this, it should be possible to confirm the presence of relatively small carbon particles. The particle size of both Sucr pH6 N2 and Ar HTCs were analysed, showing particles in the micrometre range, with an average particle size of 2-2.5 μm as well as larger particles. The different annealing atmosphere does not lead to major variation in the external diameter of the spherical agglomerates, which is governed mainly from the initial pH of the sugar solution (as will be described more in detail in Section 4.2.3). The smaller size of carbon agglomerates observed in the glucose-based HTCs and the larger particles formed using sucrose as starting material were previously observed and reported by Baccile et al.[15] They concluded that, the elemental composition, functionalisation and morphology of these materials was vary comparable, which is overall in agreement with our findings.

From the discussion of the samples considered here, a correlation between the total surface area of the HTC support and the catalytic conversion of glycerol by the supported AuPd nanoparticles was not found. The HTC pH6 Ar and N_2, showing same characteristics but substantially different surface areas, led to the same substrate conversion. Whereas the catalyst supported on Glu pH6, which is the largest surface area sample, led to lower conversions compared to the sample supported on commercial VXC72R that shows a lower surface area (280 and 220 m²/g respectively).

However, based on the information regarding the size of the carbon agglomerates, it is possible to find a trend, where the smaller the carbon spheres, the higher is the catalytic activity of the supported AuPd nanoparticles. Whereas on the other extreme, the N-doped HTC featuring a rock-like shape, with planes and sharp edges and corners, leads to a substantially lower glycerol conversion. In particular, the trend follows:

VXC72R > Glu pH6 > Sucr pH6 N_2 = Sucr pH6 Ar > S: U=1: 1

A correlation can be proposed, linking the curvature of the surface of the support and the way the metallic nanoparticles adhere to it and act as catalysts. A possible explanation could be found in the way the metal nanoparticles interact with a more curved surface of the HTC support and how the strain induced to adhere to the surface affects the reactivity of the nanoparticles. The increased presence of defects, edges and corner on highly curved surfaces is generally expected, and this difference in structure conformation seems to have an effect on the final catalytic activity of the supported catalysts. It has been reported that carbon fibres with various diameters supporting Pt nanoparticles of the same size, showed decreasing glucose oxidation ability as the diameter increased. By electrochemical means, it was possible to determine that the metal exposure was higher when supported on highly curved surfaces.[78] Another example of the modification in catalytic performance was also found for Pt nanoparticles supported on a variety of TiO_2 supports featuring a range of crystallite sizes (10-500 nm). The geometrical and electrical

properties of the supported metal particles changed as the support size decreased, favouring the formation of low coordinated Pt site, which led to an enhanced reaction selectivity for the hydrogenation of 3-nitrostyrene.[79] Extending this theory, it might be possible to assume that in the more flat, planar surfaces formed by addition of urotropine to the initial sucrose solution, the exposure of the metal nanoparticles is low, affecting negatively the glycerol turnovers. In conclusion, not the surface area of the support, but the type of exposed support surface plays a crucial role in the final catalytic activity. Where more spherical and possibly more defects are present, which may affect the interaction between the nanoparticles and the support, and hence the catalytic activity of the nanoparticles.

It is difficult to find previous literature on this topic, however from the results obtained during this project it seems that a possible feature explaining the final activity of these variously supported AuPd catalysts is the geometry of the surface. To study this further, a series of HTC samples prepared at different initial pH and showing variable size of the carbonaceous spheres are presented in the following section.

4.2.3 Influence of the initial pH during HTC preparation and KOH post treatment

The hydrothermal preparation method by which the HTCs are synthesised is catalysed by presence of acid. In fact, the dehydrogenation of sugars is enhanced by low pH values as the HMF intermediate is formed, followed by its condensation and formation of the solid humins. In a previous study, our collaborators have reported the effect of pH on the synthesis of HTCs.[63] The solid materials formed during the hydrothermal synthesis show different aggregates size and density, depending on the acid strength at the beginning of the preparation procedure. Based on this finding, it was observed that by increasing the pH of the initial sugar solution from 0 to 6, the larger (4-15 μm) and fused spherical particles became smaller (0.5 μm) and more homogeneous in morphology. This could be explained by the decreasing kinetics of nucleation and growth of the agglomerates that lead to particle formation. In this way, as the pH of the starting solution increases, the process of dehydrogenation of the sugar becomes slower and consequently the nucleation and growth of the particles is more homogeneous.

The study conducted in 2015 used glucose as starting material, while in this work the HTC samples exchanged with the collaborators were prepared with an initial sucrose aqueous solution. The preparation of these materials has been performed by adjusting the pH of the initial sugar solution by addition of HNO_3 to a final value varying from 0 to 6. These samples being name HTC pHX.

Once the HTC pHX samples were prepared, their properties could be further improved by an activation step. Activated carbons are generally produced by a treatment performed using KOH as activator, which does lead to formation of porosity within the carbonaceous structure, enhancing the surface area of the HTC, as well as its surface oxygen functional groups.[12, 14, 80] With this aim in mind, another series of samples was prepared using the same procedure, followed by a treatment in 4 M KOH solution at 100 °C for 30 min for the samples prepared at various initial pH, obtaining the HTC pHX KOH series. As discussed in the previous section, after the hydrothermal step, a high temperature treatment is necessary in order to form stable samples. For this reason the HTC pHX materials were annealed in a nitrogen flow and the HTC pHX KOH samples were treated in Ar, both at 900 °C.[54]

In Table 4.5, the elemental analysis and surface area as calculated by the BET method of the two series of samples HTC pHX and HTC pHX KOH are reported. As the preparation of these samples required addition of HNO_3 before the hydrothermal treatment in autoclave, the presence of nitrogen in the final solid material was expected. Indeed, the samples prepared with a lower initial pH 0, showed a higher N wt. % compared to the samples prepared at pH 6. After the activation in KOH is possible to confirm how the washing in alkaline solution leads to an increase in the content of hydroxyl groups on the surface of the materials, with up to six fold more oxygen species after the KOH treatment and the annealing. Also, the surface area increases slightly after the step in alkaline solution, even if it should be noted that all these samples show to have extremely low surface areas, with results as low as 0.2 m^2/g and, in general, below 10 m^2/g. The only exception being the HTC pH6 sample, which has a BET surface area of 88 m^2/g.

Table 4.5 Characteristics of the HTC materials prepared with increasing initial pH and corresponding series of materials that underwent washing in KOH. *Glycerol conversion after 15 min reaction, using the 0.5%AuPd/HTC catalysts prepared using these samples as support.

Support description	C [%]	H [%]	N [%]	O [%]	SA [m²/g]	Conv [%]*
HTC pH0	93.6	2.1	2.1	2.2	0.2	2
HTC pH1	95.7	1.3	0.6	2.3	0.4	19
HTC pH3	95	1.9	0.7	2.4	0.6	28
HTC pH6	94	1.7	0.1	4.2	88	23
HTC pH0 KOH	82	2.1	1.1	13.2	0.7	5
HTC pH1 KOH	83.5	2	0.2	13.5	6	18
HTC pH3 KOH	83.8	1.6	0.1	13.7	1.5	8
HTC pH6 KOH	84.6	1.5	0.9	12.3	2.2	19

The glycerol oxidation reaction time-on-line results of the catalytic testing of the catalysts supported on the HTC pHX (a) and on the HTC pHX KOH series (b) are shown in Figure 4.14 with the addition of AuPd/VXC72R for comparison.

For the HTC pHX series, the catalysts supported on HTCs prepared at initial pH 1, 3 and 6 showed substrate conversions higher than 20% after 0.25 h, while the AuPd sample supported on HTC prepared at initial pH 0 showed a very low activity throughout the reaction. The catalyst supported on HTC pH3 showed the best performance, with glycerol consumption results comparable if not slightly higher than the reference catalyst supported on VXC72R. While the least active sample was AuPd/HTC pH0, with a 20 % glycerol conversion after 2 h reaction.

By looking at the catalytic data of the samples supported on the HTC pHX KOH series, a general lower activity is observed compared to the previous series of samples. If the highest substrate consumption reached 92% after 2 h reaction with AuPd/HTC pH 3, the highest conversion using the HTC pHX KOH series of supports was 66% when testing AuPd/HTC pH1 KOH for 2 h. Samples supported on HTC pH3 KOH and pH0 KOH had very similar conversion profiles, with a glycerol consumption of *ca.* 40 % after 2 h. The catalyst supported on the HTC pH1 KOH was found to be the most active catalyst of this second series of samples, with a maximum glycerol conversion of 66% after 2 h. In both series of samples, the support prepared with initial pH0 showed low if not the lowest activity.
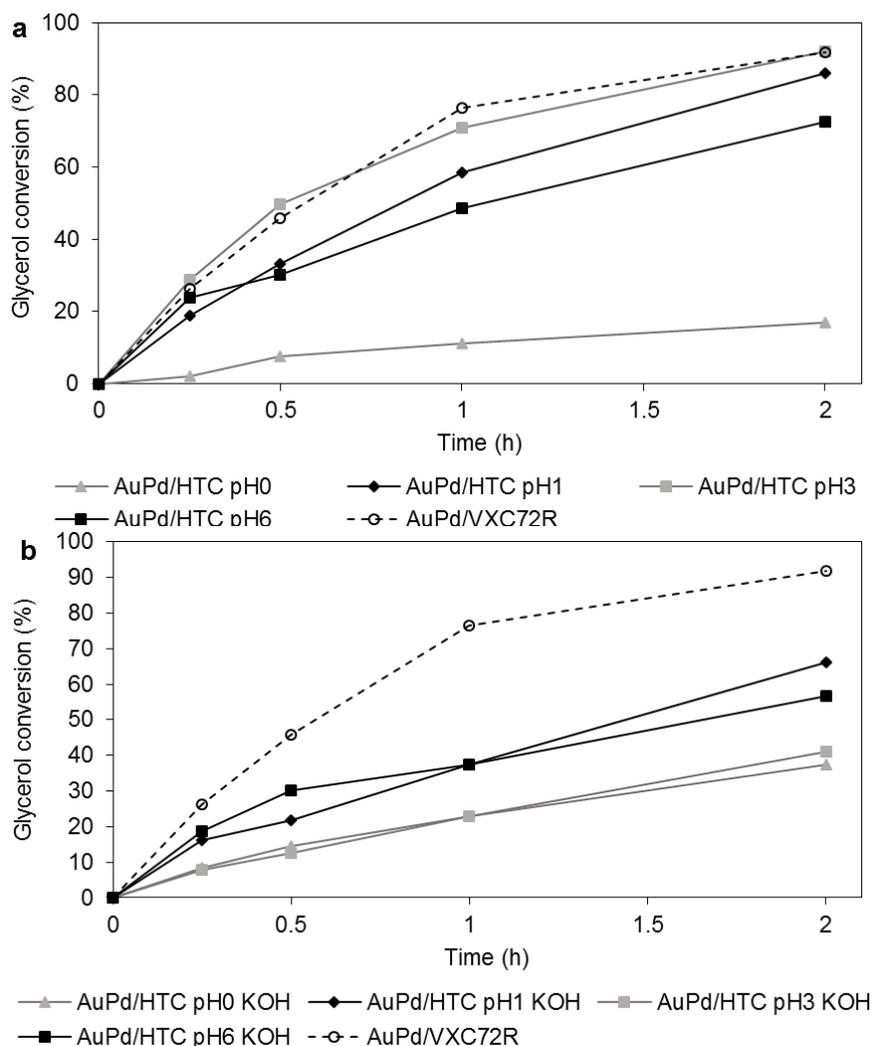
Figure 4.14 Time-on-line data of the glycerol oxidation tests performed with the two series of samples HTC pHX (a) and HTC pHX KOH (b). Reaction conditions: 0.0455 g catalyst, 5 ml NaOH 1.2 M, 5 ml glycerol 0.6 M, 60 °C, 3 bar O_2, 900 rpm, 2 h.

The average crystallites size of the supported metallic particles was calculated from the XRD data collected for all samples and are reported in Table 4.6. Catalysts supported on the series of carbons HTC pHX seem to present slightly more comparable crystallites size (10 to 16 nm), compared to the activated HTC pHX KOH series that shows a variety of AuPd nanoparticles sizes (8-27 nm). The analysis of the two samples showing the highest glycerol conversions, AuPd/HTC pH3 and AuPd/HTC pH1 KOH, show crystallite of 10.8 and 15.6 nm respectively, however less active catalysts contain both larger and smaller particles. Therefore, as mentioned in the General discussion (Section 4.2.1.5), the activity of these materials is not strongly governed by the metal particle size, and other parameters seem to influence the glycerol conversion.

Table 4.6 XRD diffraction peaks position and corresponding mean nanoparticle dimensions.

Name	Crystallite size [nm]
HTC pH0	15.5
HTC pH1	11.9
HTC pH3	10.8
HTC pH6	10
HTC pH0 KOH	8.1
HTC pH1 KOH	15.6
HTC pH3 KOH	27.2
HTC pH6 KOH	23.2

As previously reported by our collaborators, the particle size of the HTC decreases with increasing initial synthesis pH.[63] This is because the dehydrogenation of sugars is acid catalysed, hence the lower the pH the faster and more uncontrolled is the polymerisation taking place. This leads to formation of not only bigger spherical particles but also to big agglomerates. In Figure 4.15, some representative SEM micrographs are shown and in Figure 4.16 the corresponding particle size distributions (PSD) determined from the SEM micrographs are reported. On the left-hand side is the HTC pHX and on the right-hand side is the HTC pHX KOH series of catalysts. In the images is also possible to see the presence of large bright agglomerates, recognisable as AuPd particles.
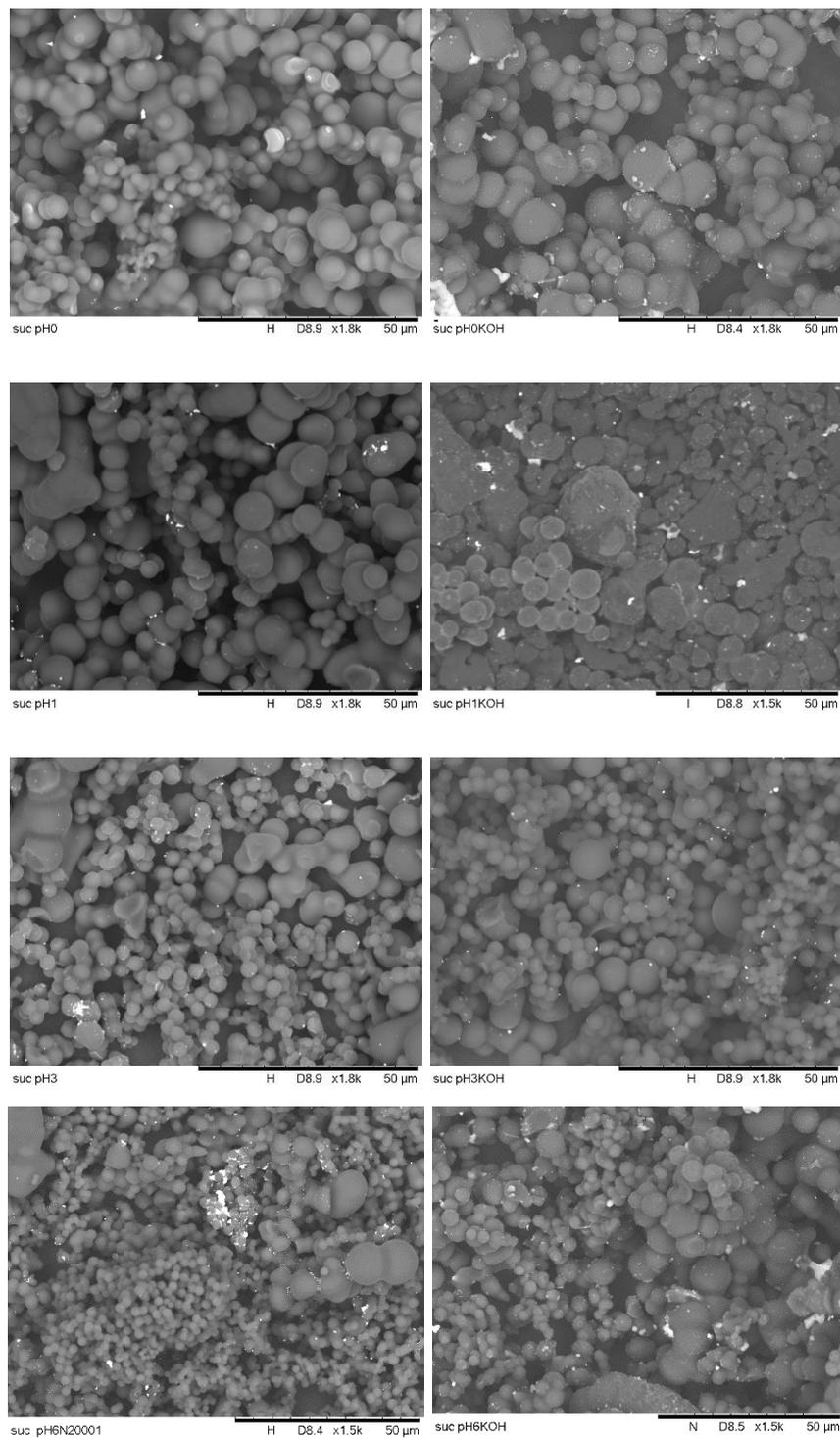
Figure 4.15 SEM micrographs of the HTCs prepared with increasing pH (top to bottom). Annealed in N_2 atmosphere (left column) or treated in KOH and then annealed in Ar (right column).
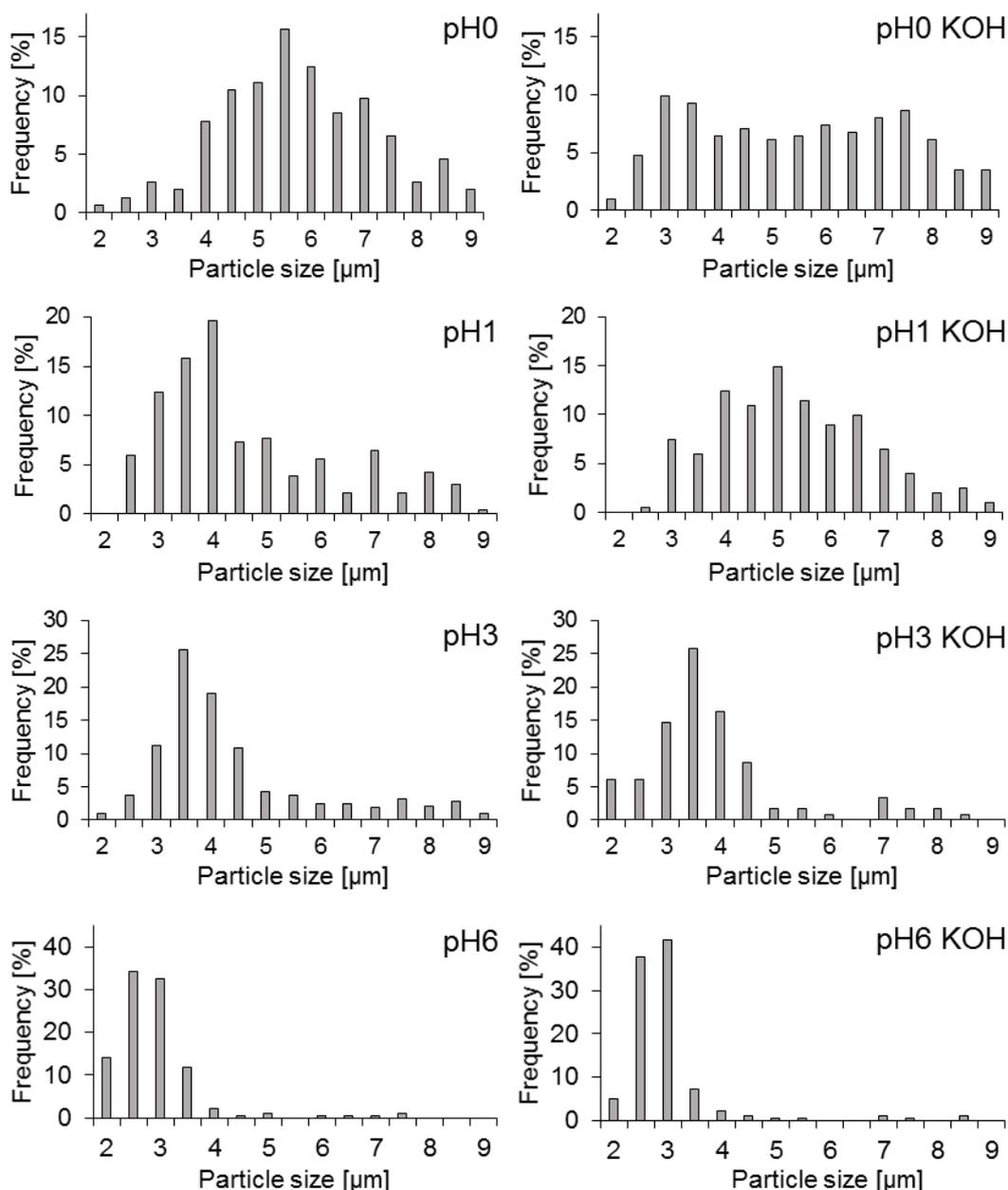
Figure 4.16 PSD as determined from the SEM micrographs of the HTC prepared at different initial pH (left side) and post treated in KOH solution (right side).

The samples prepared with initial pH0, 1, 3 and 6 confirmed the previously reported trend. The HTC prepared at initial synthesis pH 0, shows a very broad PDS (Figure 4.16 left side) with an average particle size of 5.5 µm. When the sample was post-treated in KOH solution under heat the PSD indicated, quite unexpectedly, that both a narrowing and a broadening of the particles has taken place at the same time, now showing two distribution with peaks at 3 and 7.5 µm. It is quite difficult to find an explanation for this behaviour, as it seems that the hydrothermal carbon underwent both dissolution and agglomeration when in the alkaline environment. When prepared with initial pH1, the HTC had a mean particle size of 4 µm. Also for this sample, the activation in KOH led to slightly larger particles and a broader distribution. The tendency of particle

broadening became less evident for the samples prepared at pH3 and pH6. At the same time, as the preparation pH was closer to neutral, the carbon particles were more homogeneous and sensibly smaller, achieving a mean particle size of 2.5-3.5 μm and the "cooking" treatment in KOH did not affect the size or distribution of the particles. Overall the preparation that led to less homogeneous materials (pH <3), also varied the most upon activation with KOH

In contrast to what expected, the results of the surface area analysis revealed that the two series of samples HTC pHX and HTC pHX KOH showed only a small enhancement in the surface area after the KOH activation (Table 4.5). However, as mentioned before, the major effect of the KOH treatment on the samples is the strong increase in oxygen content, which increases up to five times from an average 2 % in the HTC pHX series to an average of 13% in the HTC pHX KOH series. Therefore, the change in surface area could be neglected and the overall decrease in catalytic activity should be attributed to the increased amount of oxygen on the surface of the support. An exception being the catalysts supported on HTC pH6 and HTC pH6 KOH samples, where a decisive decrease in surface area and enlargement of the average crystallite size coincide with a deactivation of the corresponding catalyst after KOH treatment.
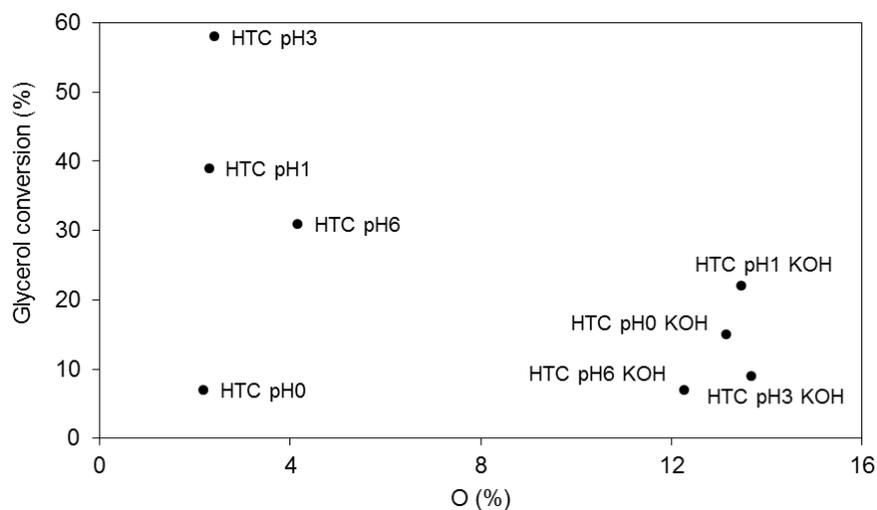
Figure 4.17 Plotted values of HTC oxygen content as determined by elemental analysis and corresponding glycerol conversions after 30 min oxidation reaction.

In Figure 4.17 is possible to notice how the catalysts supported on HTC prepared at different initial pH and activated in KOH reach generally lower glycerol conversions compared to the catalysts supported on materials that did not undergo such activation step. Previous works on catalysts supported on carbon have shown correlation between the amount of oxygen in the support and the catalytic activity for the glycerol oxidation reaction. In particular, it was reported that oxidised carbons (generally treated with strong acids) lead to less active catalysts, when supporting metallic nanoparticles.[51, 81] The reason behind this catalytic deactivation is attributed to a decrease in isoelectric point of the carbon surface, hence to a higher acidity of the material.

A change in isoelectric point of the support affects the surface charge that the support will present under reaction condition, which in turn, could have an influence on how reactants and products interact with the catalyst.

Although the particle size analysis based on XRD data gives an indication of the average particle size, another technique that should be considered for the metal dispersion on the surface of the support is XPS. In Table 4.7, the normalised XPS peak areas are reported and the most active samples AuPd/HTC pH3 and AuPd/HTC pH1 KOH seem to have the highest amount of metal in each corresponding series of samples.

Table 4.7 Normalised XPS peak areas of Au, Pd and oxygen of the AuPd samples supported on HTC pHX and HTC pHX KOH.

Sample	Au/C	Pd/C
AuPd/HTC pH6	0.15	0.17
AuPd/HTC pH3	0.55	0.53
AuPd/HTC pH1	0.41	0.43
AuPd/HTC pH0	0.13	0.11
AuPd/HTC pH6 KOH	0.22	0.13
AuPd/HTC pH3 KOH	0.32	0.19
AuPd/HTC pH1 KOH	0.46	0.28
AuPd/HTC pH0 KOH	0.26	0.20
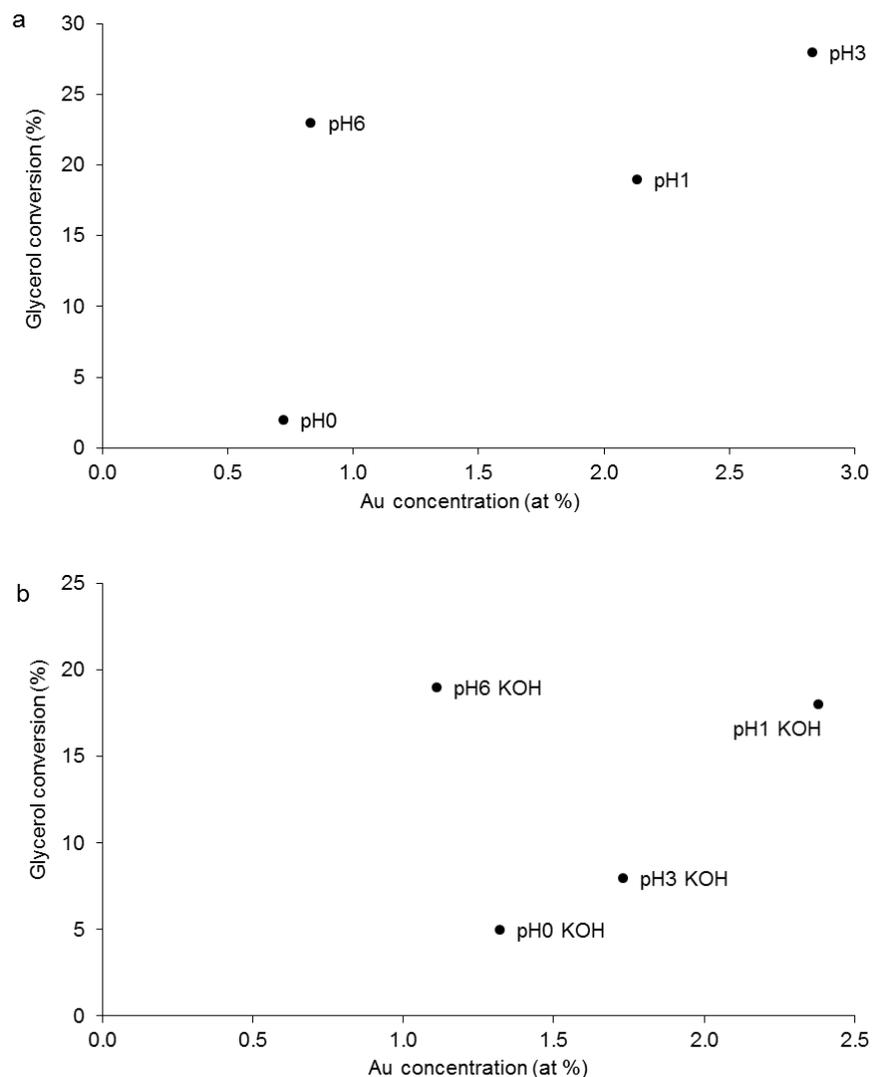
Figure 4.18 Plotted values of Au concentration as calculated from XPS analysis and 15 min glycerol conversion during oxidation reaction using AuPd/HTC pHX (a) and AuPd/HTC pHX KOH (b).

Because the surface area values are comparatively low (apart from the higher surface area HTC pH6, which should be discarded), it is possible to consider the photoelectron signals as informative of the metal dispersion on the support. Although crystallites are detected by XRD, the presence of smaller and not detectable particles should be expected. From Figure 4.18a, a linear positive trend is found between the Au concentration and the glycerol conversion, where is possible to see how the sample supported on HTC pH3 has the highest metal signal and the highest glycerol conversion, which supports the hypothesis of a higher metal dispersion. In Figure 4.18b a similar trend is found also for the pHX KOH supported catalysts. However, since the supports now have more comparable surface areas, the samples prepared at initial pH0 and pH6 and activated with KOH are more interesting. In fact, while they present Au concentration in a similar range of values, the activity for the glycerol conversion changes strongly, with the pH6 KOH sample being more active than the pH0 one. It should be reminded that the HTC prepared

at pH0 and pH6 show the strongest variation in terms of carbon particle size and distribution, with the higher synthesis pH leading to a more controlled condensation (see Figure 4.15 and 4.16). In a similar manner to the results discussed in the previous section, it might be possible to find a correlation between the curvature of the surface of the support and the catalytic activity of the final catalyst. On support of this hypothesis, it has been reported in literature that the curvature of carbon nanotubes does affect the binding of metal clusters, with stronger interactions when the curvature is higher. Whereas on flat surfaces, like graphene, weaker interaction between the metal particle and the surface takes place.[76] From this, it should be possible to hypothesise that the curvature of the support may interfere in other ways during the glycerol oxidation reaction, for example favouring more or less the adsorption of the reactants. In a previous study by Wang *et al.* on Au/C catalysts for the selective glycerol oxidation, it was shown that different degree of graphitisation and order of the support surface influenced the final shape of the deposited metal nanoparticles. This was related to a change in product selectivity as different facets of the metal nanoparticles were preferentially exposed.[82] Although the selectivity towards glycerate is comparable between the various catalysts tested here, an effect of the support on the catalytic properties is still present.

In conclusion, we see that even if these HTC materials reveal to be composed of highly dense carbonaceous particles, with extremely low surface area, still can be utilised as supports for metal deposition and lead to formation of active catalysts.

As for the previous sections, the hydrothermal synthesis and the steps that follow until the sample preparation is completed are crucial and each of them needs to be studied and optimised to achieve the desired material features.

The correlation between the size of the HTC agglomerates and the glycerol conversion data goes in accordance with the results reported in a previous section where, as for the HTC made of glucose and sucrose the size increased, the catalytic activity of the corresponding AuPd catalysts decreases.

The activation step in KOH solution may actually lead to an improved surface area, but to demonstrate this, we would need to prepare a starting material with a higher surface area, to avoid working around the lowest instrumental detection limit.

Another important effect observed by treating the samples in base is the increase in oxygen content, which is to be ascribed to presence of oxygen containing functional groups formed on the surface of the HTCs. This substantial variation in the elemental composition of the support materials seem to have a direct effect on the final catalysis, this result being in agreement with previous ones where increasing oxidation of the activated carbon materials led to less active Au/C catalysts.[81] The increased amount of oxygen groups has been reported to correlate with an increase

in the acid character of the support,[51, 83] which in turns has a negative effect on the glycerol oxidation reaction. To study this effect further, a series of HTCs were prepared aiming to contain increasing amount of oxygen and will be discussed in the next section.

4.2.4   Influence of oxygen content

All the carbon materials discussed so far presented a certain amount of oxygen, as determined not only by elemental analysis but also by XPS. Its presence is expected since it is a component of the carbon source. However, the samples that underwent an activation step in KOH solution showed a decisive increase in oxygen content, which was correlated to the formation of oxygenated functional groups on the surface of the final HTC materials.

High oxygen containing carbons are characterised by low isoelectric point values, since the oxygen functional groups, which are electron withdrawing, destroy and replace the basic surface sites, which are associated with the π electron-rich regions of the graphitic carbon structure.[3, 84,] Moreover, the presence of oxygenated functionalities is correlated with helping in the deposition of the metal catalyst as anchoring centres,[46] but it has also been reported that depending on the acid and base characteristics of these groups, they could enhance metal aggregation or help its dispersion, respectively.[85] Importantly, surface oxygen groups are believed to decrease the hydrophobic nature of carbon, which would be beneficial in a reaction ran in aqueous environment, like the glycerol oxidation.[1]

A research work published by our collaborators in Mülheim, reports the thermal stability of different oxygen species within the structural framework of Multi-Walled Carbon Nanotubes (MWCNT). By thermogravimetric mass spectrometry (TG-MS), carboxyl, lactone, anhydride, phenol ether and carbonyl groups were separately decomposed from the carbon structure, achieving not only a decrease in the oxygen amount, but also a selective elimination of specific oxygen-containing functional groups.[86] Overall, a correlation between the surface functionalities and the point of zero charge of activated carbons has been found, and while thermal treatments selectively remove the oxygen-containing surface functionalities, decreasing the overall amount of oxygen, and increasing in the isoelectric point of the resultant material.[81]

As described in the Chapter 2, starting from the Sucr pH6 N_2 annealed sample, a series of HTC samples containing oxygen functionalities were prepared. The aforementioned sample was oxidised in a nitrosulfuric acid mixture, increasing substantially the oxygen species (HTC 22%O). By heat-treating in a flow of nitrogen the highly oxygen functionalised HTC sample at specific temperatures (510 and 800 °C) and selectively decomposing the functional groups present on the surface, it was possible to achieve HTC materials with lower oxygen content (HTC 15% and 5%O respectively) and more specific functional group present in the material framework. The

temperature of the treatments and the corresponding expected functional oxygenated groups present in the HTC after treatment were based on the previous work by Heumann *et al.*[86]

In Table 4.8, the elemental and surface area analysis of the high oxygen containing HTC are reported together with the list of oxygen-containing functional groups expected to be present. It is possible to see that after the reaction with nitrosulfuric acid, the surface area of the starting material increases from 88 to 417 m²/g and then by performing subsequent treatments at increasing temperatures, the surface area increases up to 639 m²/g. This behaviour could be explained as that the high amount of oxygen introduced in the initial HTC material, coupled with the increasing temperature treatments, lead to combustion of the HTC itself, forming more porous structures and hence higher surface areas materials.

Table 4.8 Characteristics of the high oxygen containing HTC materials and catalytic conversions after 15 min glycerol oxidation reaction.[a] The temperature applied in the thermal treatment for the subsequent elimination of the oxygen functionalities.[86]

Support description	T[°C][a]	C [%]	H [%]	N [%]	O [%]	SA [m²/g]	Conv [%]	Functional groups
Sucrose pH6 N₂		94	1.7	0.13	4.2	88	23	Nearly none
HTC 22%O		75.2	2.29	0.22	22	417	5	Carboxylic, zigzag lactone, anhydrides, armchair lactones, phenol/ether, quinone
HTC 15%O	510	82.9	1.63	0.38	14.8	562	6	Armchair lactones, phenol/ether, quinone
HTC 5%O	800	94.4	0.66	0.1	4.68	639	10	Quinone

For consistency, the following discussion will focus on the three catalysts supported on HTC 22, 15 and 5%O as the AuPd/HTC pH6 N₂ was discussed before and was prepared by a different method. In Figure 4.19, the time-on-line results of the three catalysts are reported and it is possible to see how the carbon support containing the lowest amount of oxygen leads to the most active catalyst for the oxidation of glycerol to glycerate in presence of base. Whereas the AuPd catalyst supported on the highly oxygenated HTC 22%O shows very low conversion, if any.

These results goes well in accordance with a previous work from Órfão *et al.*, where a similar study to the one reported here was performed.[81] An activated carbon was treated with strong acid and subsequently a series of heat treatments at different temperatures were performed to selectively remove the oxygenated functional groups formed during the oxidation step. The resulting carbons were used as support to Au nanoparticles and tested for glycerol oxidation, showing that the higher the amount of oxygenates, the higher the acidity of the support, the lower the activity of the catalyst.
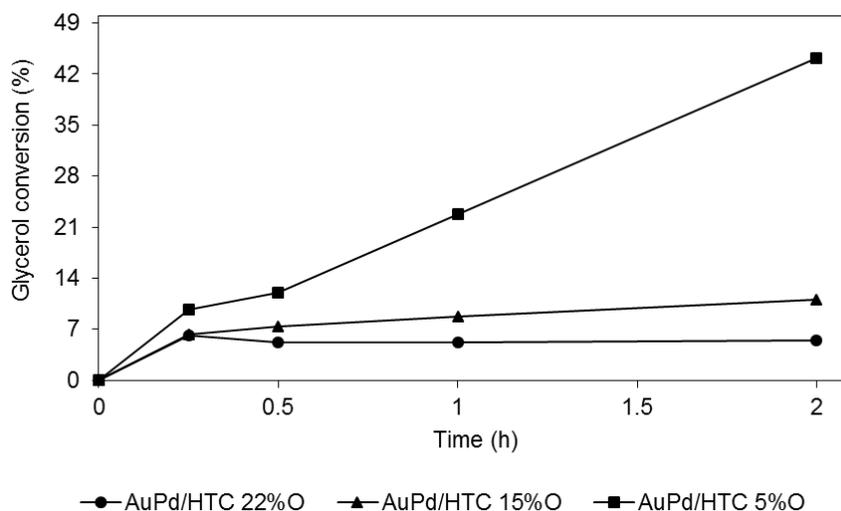
Figure 4.19 Time on line of the HTC with decreasing amount of oxygen functionalities. Reaction conditions: 0.0455 g catalyst, 5 ml NaOH 1.2 M, 5 ml glycerol 0.6 M, 60 °C, 3 bar O_2, 900 rpm, 2 h.

By plotting the glycerol conversion after 15 min and the oxygen content of the HTC as determined by elemental analysis, a linear and negative slope is found, as shown in Figure 4.20. A very similar trend would be observed when using the oxygen percentage values determined from XPS analysis, suggesting that both the surface and bulk elemental analysis lead to very comparable trends.
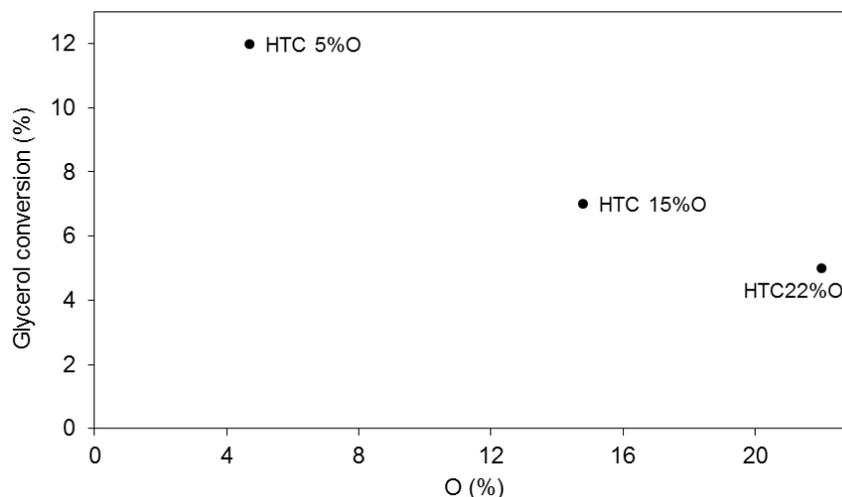
Figure 4.20 Dependency of the glycerol conversion after 15 min reaction, on the amount of oxygen present in the catalysts support.

From the analysis of the O1s XPS region was possible to confirm and study the presence of different O species. In particular, two peaks could be identified, positioned at 531.5 and 533.4 eV and depending on the oxidation level of the HTC, the lower binding energy peak is more or less intense (see Figure 4.21). Therefore, on the HTC 5% mainly C-O-C from ethers, esters and anhydrides exist as part of the graphitic structure, while in the HTC 22% and 15%O the before mentioned groups as well as C-O-C of furan-like aromatic structures and C=O carbonyl groups are present.[51-52]
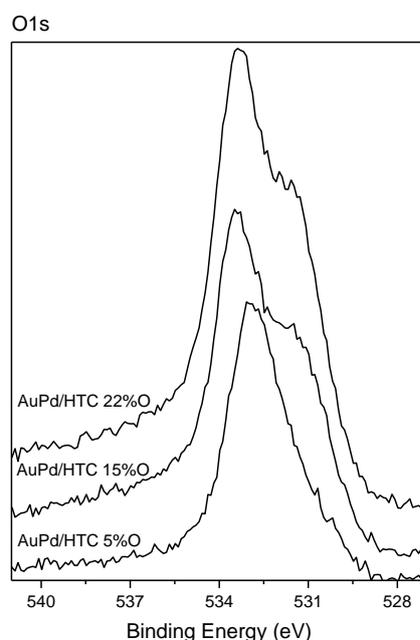
Figure 4.21 XPS spectra of the O region of high oxygen containing HTC.

The XPS analysis of the Pd region gave very noisy and unclear results even after a large number of scans (200). A possible reason for this behaviour is the poor distribution of Pd on the

surface of the support, or possible infiltration/coverage of the metal within the porous structure of the carbon. The Pd signal seems to improve only slightly as higher thermal treatments are performed and the amount of O diminishes. In any case, the peak at 335 eV is only slightly visible, confirming also for this series of catalysts the presence of Pd(0). A similar behaviour was observed for the reference catalyst, supported on VXC72R, where XPS analysis barely indicated presence of Au and Pd photoelectron peaks.

By calculating and reporting the XPS normalised intensity values of the Au and O peak areas in Table 4.9, is possible to see that as the O decreases and the surface area of the support increases, the Au detected on the surface is higher. Comparing the normalised XPS peaks of Au with previous samples from previous sections (for example Sucr pH6 N_2, with Au/C of 0.15) is possible to see that the values reported here are a magnitude of order smaller. It should, in fact, be noticed that after the acid treatment that leads to the HTC 22% O sample, a strong increase in surface area from 80 to up to 600 m^2/g is detected. Consequently, the metal is dispersed and diluted more and more on the support surface, possibly leading to such small XPS signals.

Table 4.9 XPS normalised area of Au and O.

Sample	Au/C	O/C
AuPd/HTC 22% O	0.003	0.30
AuPd/HTC 15% O	0.005	0.22
AuPd/HTC 5%O	0.012	0.16

From the XPS analysis of the Au region, it was also possible to determine a linear trend between the atomic percentages of Au detected by the analysis and the initial glycerol oxidation conversions determined during time-on-line experiments (Figure 4.22). More specifically, it was found that the lower the O amount in the support, the higher the Au detected by XPS and the higher the catalytic conversion of glycerol.
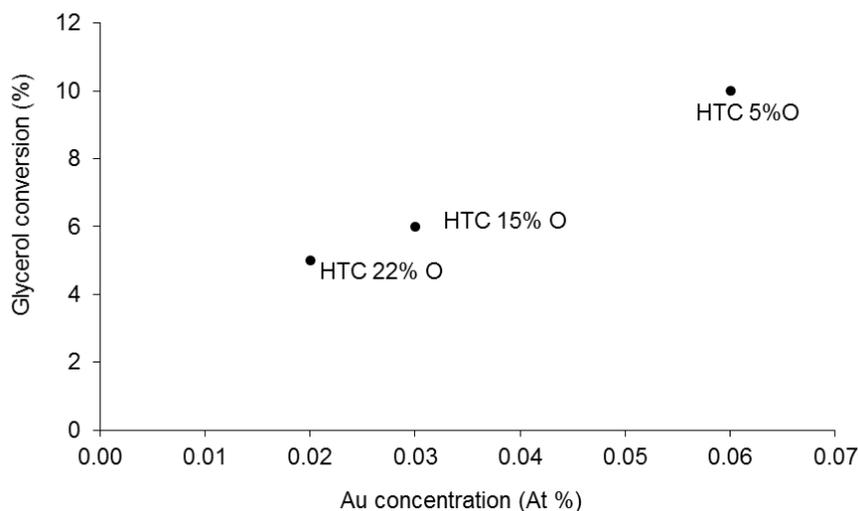
Figure 4.22 Plot of Au concentration as determined by XPS analysis and the glycerol conversion after 15 min reaction, using AuPd/HTC catalysts containing decreasing amount of oxygen.

The XRD analysis of the three AuPd catalysts supported on HTC containing 22 to 5% O gave rise to a set of diffraction patterns, revealing the presence of only one metallic phase. The most intense peak assigned to the (111) plane had a diffraction angle of ~ 38.7 °, which is indication of an AuPd alloy [59] and a confirmation of the presence of Pd in the catalyst. The particles size reported in Table 4.10 show that although the extremely large surface area the metals still aggregate in rather large nanoparticles with the average crystallites size of around 20 nm.

Table 4.10 Average crystallite size of the AuPd nanoparticles supported on the HTC with decreasing amount of O.

Name	Crystallite size [nm]
HTC 22%O	20.6
HTC 15%O	20.3
HTC 5%O	15.7

Although oxygen functionalities are generally considered anchoring site for metal deposition, they have also been related to an increased acid character of the support, which leads to a negatively charged surface over a wide range of pH values. Because the metals precursors used in this work are metal chloride anions, the more basic character the support has, the more positively charged the carbon surface will be over different pH values, facilitating the electrostatic interaction between the anchoring sites on the carbon surface and the metal precursors.[1] Therefore, less nucleation sites could be expected to be present on the surface of the O-rich supports, explaining the rather large AuPd nanoparticles detected by XRD.

The oxidative treatment in strong acid does not change the morphology of the initial HTC pH6 N_2 sample, nor do the heat treatments performed to reduce the O content. After the hydrothermal synthesis with initial pH6, the HTC particle size remains constant at $\sim$ 2.5 μm. However, as mentioned at the beginning of this section, the strong oxidation of the carbon material leads to higher surface area thanks to formation of pores as determined by surface area analysis. In contrast to the activation performed with KOH, it seems that the treatment in nitrosulfuric acid might be more suitable for successfully expanding the HTC surface area.

From the results reported and discussed here, it is possible to confirm that oxidised carbons are not the support of choice for catalysts to be applied in the oxidation of glycerol. In light of the results presented here, it is also possible to better understand the low activity of the AuPd catalysts supported on the KOH activated pHX series of HTCs discussed in Section 4.2.3. The presence of high percentages of oxygen and consequent increase in acidity of the HTC supports are detrimental to the catalytic activity for the glycerol oxidation reaction. Órfão *et al.* suggested that the free π-electrons system widely present in low oxygen carbon materials, allows electron mobility as the hydroxyl groups of glycerol adsorb on the electron-rich metal nanoparticles, enhancing the very first step of the glycerol oxidation process, which sees the dehydrogenation *via* H-abstraction from one of the hydroxyl groups of glycerol.[22, 81]

4.2.5 Catalyst stability

After determining that the various carbon materials presented and discussed in this chapter are potentially good supports for metal nanoparticles, the stability of the catalysts has been studied. Two parameters that are generally considered when talking about the stability of a catalytic material are the catalyst leaching and reusability. In fact, it is often observed that a fraction of metal dissolves into the reaction medium, leading to a loss of active metal, which is a major drawback since it is often an expensive element, as well as to a decrease in activity in case of reuse of the same material for more than one reaction. Hence, leaching tests were performed on some samples of choice to assess the stability under reaction conditions of the catalysts discussed here. For the leaching test, four catalysts supported on HTCs showing a range of characteristics, leading from high to low glycerol conversions were chosen. The aqueous reaction solutions of the aliquots collected at 30 and 120 minutes during the time-on-line experiments were analysed by Inductively Coupled Plasma (ICP). During the analysis presence of Pd was detected, whereas no Au was found in solution, confirming the higher stability to leaching of Au compared to Pd.[64] In Table 4.11 are reported the concentrations of palladium as detected in the reaction mixture solutions after separation of the solid catalyst, compared to a blank reaction.

Table 4.11 ICP results for palladium leaching in solution during the test reaction. Data at 0.5 and 2 h reaction time.

Sample name	Time [h]	Pd conc. [mg/l]	Glycerol conv. [%]
Blank	0	0.07 10^{-3}	
AuPd/Sucr_pH6Ar	0.5	0.03	25
	2	0.04	82
AuPd/Glu_pH6_KOH	0.5	0.02	30
	2	0.03	99
AuPd/Sucr_pH6_KOH	0.5	0.02	19
	2	0.03	57
AuPd/Sucr_pH6N$_2$	0.5	0.03	25
	2	0.05	74

It is possible to estimate that a maximum of 3% of Pd leached from the supported catalysts over a 2 h reaction. This being a negligible amount for the overall stability of the catalyst. It should be noticed that the values of Pd concentrations in solution over time reported in Table 4.11 seem quite stable, with the leaching process taking place at the very beginning of the reaction (after already 15 min from the beginning) and remaining quite stable over the duration of the test (values after 2 h). The amount of metal in solution remains quite stable over time, suggesting that after a first dissolution of a fraction of Pd, no more substantial amount of metal is lost in solution, with the remaining species anchored on the HTC support. Moreover, the AuPd/Glu_pH6KOH and AuPd/Sucr_pH6KOH show to be the most and the least active catalysts considered here, but both also show the lowest metal leaching over a 2 h reaction, indicating that there is no direct correlation between the amount of metal in solution and the overall activity. For the same reason it is also possible to say that no homogeneous but only heterogeneous catalysis is taking place.

After discussing in this chapter the effect that the HTC supports have on the catalytic activity of the AuPd catalysts for the glycerol oxidation reaction, it is possible to see that after deposition of the metal, although some loss of Pd, the metal nanoparticles are stable on the support. More importantly, the stability of the metal nanoparticles is not dependant on the structural characteristics such as morphology, elemental composition and surface area of the support.

After assessing the possibility that metal leaching could take place during reaction, the overall stability of some of these catalytic materials has been tested by performing a series of reusability tests. These were conducted on the materials prepared at initial pH6 and later treated in various ways. The AuPd catalyst supported on commercial carbon VXC72R was tested as well, for comparison. The results plotted here in Figure 4.23 show that all four catalysts are stable over up to three cycles. Not only the glycerol conversion after 1 h reaction is comparable between consecutive reuses, but also the selectivity to glycerate is stable and constantly as high as 80%. This stable behaviour suggests that the Pd leaching does not affect the overall catalytic activity and that the active species are not modified upon recovery and reuse of the materials. Previous works already observed good reusability of bimetallic AuPd/C catalysts up to 11 times in 30 min reactions under similar conditions.[36]
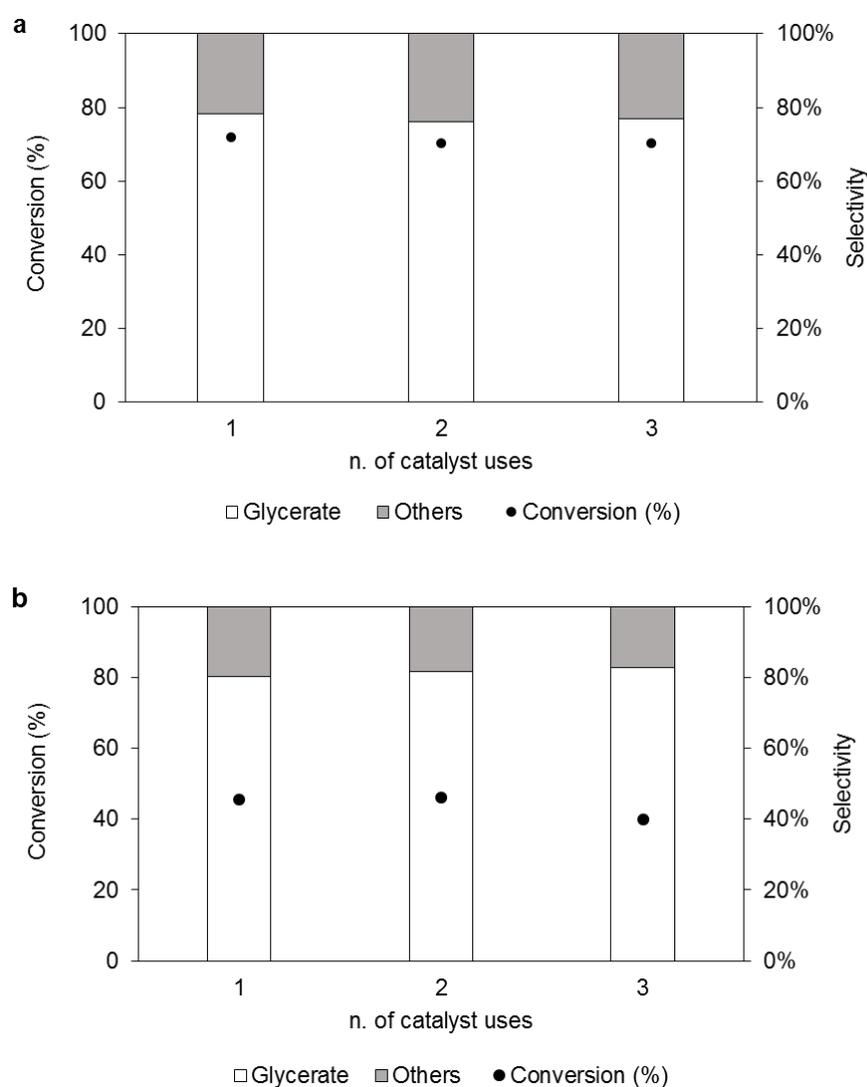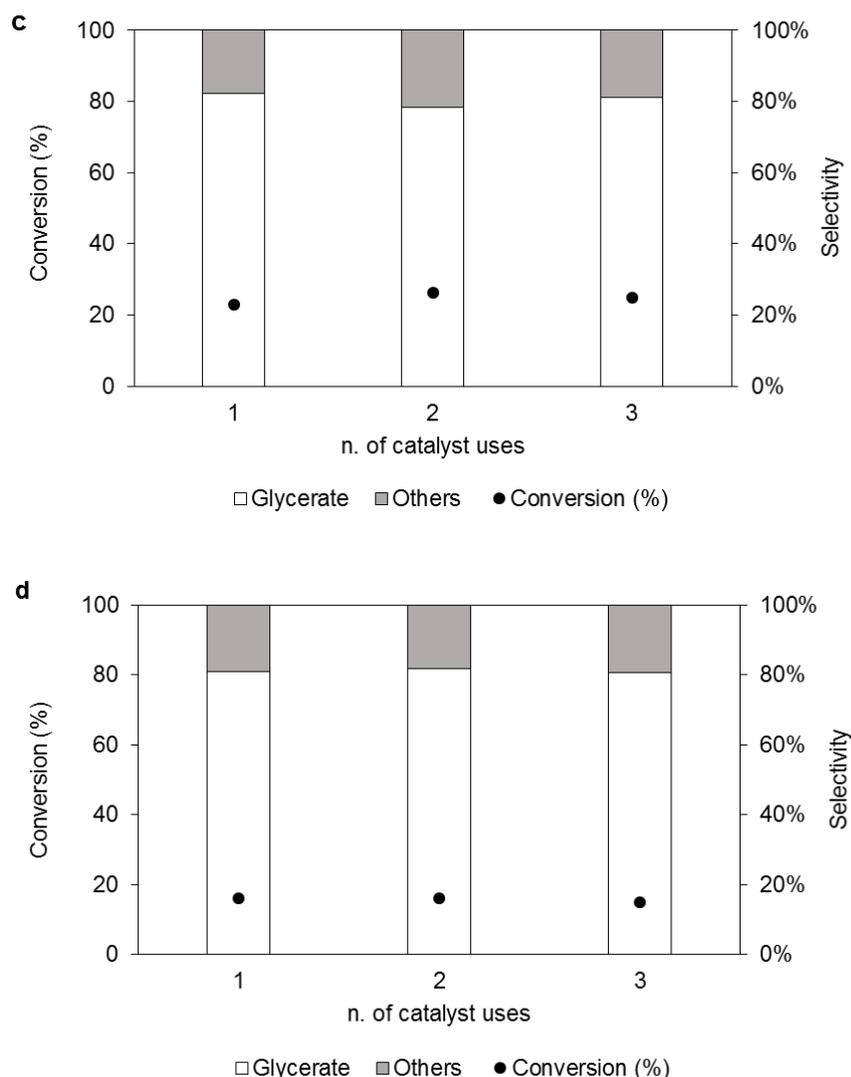
Figure 4.23 Glycerol conversion and glycerate selectivity over multiple catalyst reuses, using AuPd/VXC72R (a), AuPd/HTC pH6 (b), AuPd/HTC pH6 KOH (c), AuPd/HTC pH6 H2O (d). Reaction conditions: 0.0455 g catalyst, 5 ml NaOH 1.2 M, 5 ml glycerol 0.6 M, 3 bar O_2, 60 °C, 1 h.

From these catalyst reusability results, quite comparable results are achieved, the AuPd/C materials used for the oxidation of glycerol have overall good stability. The glycerol conversions after 1h reaction reach the same values and the selectivity to glycerate is extremely reproducible and constantly at 80%, with glycolic, tartronic, lactic, oxalic and formic acid taking up the residual 20% of the products formed.

Previous stability studies have reported how the catalyst preparation affects the stability and reusability of the materials. Catalyst preparation methods that favour the direct interaction between the deposited metals and the support seem to lead to more stable samples compared to immobilisation methods of preformed sols, where the use of organic stabilisers may affect the results over multiple catalytic tests as the stabilising agents are lost in the reaction medium and the nanoparticle collapse.[81]

The catalysts studied in the reusability tests were analysed by XPS to check whether the surface compositions changed upon use in consecutive reactions. The sample supported on the commercial carbon VXC72R also after use does not exhibit strong defined Au and Pd photoelectron peaks, suggesting that the metal particles are embedded within the carbon support and this condition is maintained during the catalytic reaction. For the other catalysts, the XPS analysis confirms the presence of metallic Au and Pd, with the lower binding energy peaks at *ca*. 84 and 335 eV respectively. This is noticeable since the reaction is ran under 3 bar of pure O_2 and the post reaction treatments are performed in contact with air, therefore overall oxidising conditions. The data reported in Table 4.12 should be treated carefully. In fact, the Au and Pd normalised signals before and after catalyst use do not show a general trend. The XPS peaks of AuPd/HTC pH6 vary substantially, whereas the AuPd/HTC pH6 H_2O changes only slightly. At last, the Pd content of AuPd/HTC pH6 KOH remains constant, while Au is halved. From the leaching test, we are aware of the possible loss of Pd in the reaction medium, while no Au loss was detected. Particle aggregation during reaction could explain the decrease in photoelectron signals, however, because the product selectivity as well as the activity remain unchanged over multiple catalyst reuses, it should be possible to conclude that no nanoparticle aggregation is taking place.[41]

Table 4.12 XPS normalised areas of samples before and after use.

Sample	Au/C	Pd/C	O/C
AuPd/HTC pH6	0.15	0.17	0.13
AuPd/HTC pH6_used	0.09	0.09	0.57
AuPd/HTC pH6 KOH	0.22	0.13	0.30
AuPd/HTC pH6 KOH_used	0.14	0.13	0.45
AuPd/HTC pH6H2O	0.05	0.04	0.17
AuPd/HTC pH6H2O_used	0.04	0.03	0.27
AuPd/ VXC72R	-	-	0.36
AuPd/ VXC72R_used	-	-	0.37

Since no direct correlation between the change in XPS peaks intensity and catalyst activity is found, whether the metallic particles are growing or are modified in any way during reaction, this is not affecting the catalytic performance for the oxidation of glycerol. In Table 4.12, the normalised areas of O are also reported. Comparing the normalised values before and after

catalyst use, an increase in O amount can be noticed. This variation could be correlated to the presence of NaOH in the basic aqueous reaction mixture. In fact, to recover the catalyst between reuses, no temperature oven drying but only a mild drying in air was applied, allowing for some species to remain on the catalysts surface. However, the weak adsorption of hydroxyl groups on the surface of the catalysts is not such to alter their activity.

Overall, the catalysts discussed here show to be stable and reusable over multiple glycerol oxidation tests, confirming that HTC materials could be applied as catalysts support.

4.3   Conclusions

During this project, a collaboration between Cardiff University and the Max-Planck Institute was established. The knowledge of our collaborators about preparation of HTCs, which are a cheap and environmentally friendly alternative to commercial carbons prepared by high energy carbonisation of non-renewable feedstock, opens up to the possibility of producing carbons bearing specific morphological, electronic and chemical properties. Various series of HTC samples were synthesised, exchanged and used as supports for AuPd catalysts, however only a fraction has been presented here for simplicity.

In this chapter, the preparation of the catalysts, their catalytic screening for the glycerol oxidation reaction and characterisation of the materials are reported and discussed. All samples were studied by N_2 physisorption, elemental analysis, XPS, XRD and SEM.

The HTC materials, used as support for AuPd nanoparticles, varied for carbon source, preparation conditions, post-treatments and annealing atmosphere, leading to carbonaceous samples differing in morphology, surface area, porosity, oxygen and nitrogen content. Overall, the variability and complexity of these materials made this study challenging. However, this gave us an initial overview on the use of alternative carbon materials to be applied as support for metallic nanoparticles, which does not seem to have been exploited so far. Carbon materials are largely applied in various applications as well as catalysts and catalysts support. Together with alumina and silica, carbon is the most used support for the preparation of industrial catalysts. It is generally considered an inert stable material, due to the graphitic character. However, we see here that a simple synthesis method can lead to a variety of carbons with different physical and chemical characteristics, of which one should take advantage to study and develop new catalytic materials.

In this work, the effect of a variety of HTC supports on the AuPd catalytic activity for the glycerol oxidation reaction was studied. Because the support is known to play an important role

in the final catalytic activity, it is important to study the possible correlation between the various material characteristics and the final catalytic performance.

From the range of HTCs presented here, we were able to obtain two main conclusions. On one side, using different carbon sources to prepare the HTCs showed to have an effect on the size of the spherical agglomerates (ranging from nm to μm) as well as on the shape of the carbon structures. The size and curvature of the carbon surface, in contact with the metal nanoparticles seems to have an effect on the final catalytic activity of these materials. In particular, the smaller the HTC particles, the more positive effect on the activity of the corresponding supported AuPd catalysts. Whereas larger or planar structures lead to overall less active catalysts. An explanation to this enhancing effect could be found in the higher amount of defects on the surface of the support together with the increased curvature of the metal-carbon interface. It is not clear how the reactivity of a nanoparticle could be affected if it is positioned on an edge plane or on a basal plane (see Figure 4.1). In fact, the surface of these carbonaceous materials could be composed of planes of condensed material or of ends of a graphitic sheets pointing out to the surface. The geometry and structure of the surface of the support could affect not only the way the nanoparticles anchor onto the support, but also interact with the reactants. However the higher activity achieved by the commercial carbon and the glucose-based HTC seem to relate to the size of their particles.

On the other side, the presence of oxygen within the carbon structure has shown to have a negative effect on the catalytic activity for the glycerol oxidation reaction. The catalysts supported on the HTC pHX KOH series and composed of *ca* .13% O achieved lower glycerol conversion compared to the corresponding catalysts supported on the HTC pHX series. Another group of materials was prepared by strong oxidation of the initial HTC pH6 achieving up to 22% O content and leading to an almost complete deactivation of the AuPd nanoparticles, reaching less than 10% glycerol conversion after 2 h reaction. These low activity results are in agreement with previous published data. The reason for such low activity has been explained as that condensed HTC materials are characterised by a system of π-electrons that are mobile and give a rather basic character to the material. The addition of oxygen groups, which are electron-withdrawing, leads to an acidification of the material which in turns affects the way the electrons are moving between the metal nanoparticle and the support during the reaction, affecting the adsorption of the hydroxyls groups, of the reactant and hence the reaction turnover.[87]
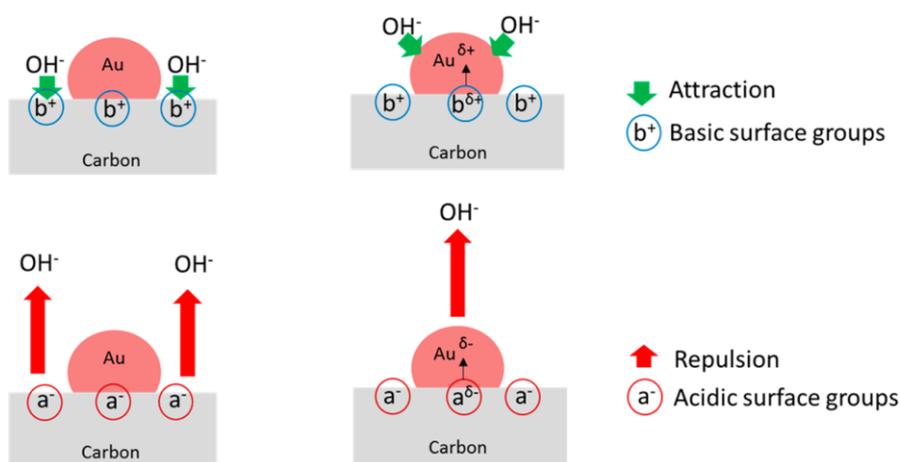
Figure 4.24 Graphical representation of the effect of the acid/base character of a carbon support on the alcohol oxidation activity of an Au-based catalyst. Taken from reference [87]

In conclusion, the use of HTC materials as catalysts support seem to be promising. The use of available starting materials such as commercial sugars or biomass waste, and the simple synthesis procedure, makes it an environmental and economically viable method to produce carbonaceous materials in laboratory as well as in larger scale. The possibility to tune, modify and overall design the desired support characteristics have here been mentioned. Because the support is known to have an effect on the catalytic activity of metal nanoparticles, it should be of interest that tailored supports could be synthesised based on necessity. The subsequent addition of catalytically active metals can follow the procedures know from literature, allowing the study on a variety of catalysts as well as the possible effect that the support has on their activity.

As for future study, the determination of the point of zero charge would be a valuable method to assess the surface characteristics of these materials as well as a useful parameter for a further rationalisation of the data collected so far. Another point that could be further addressed is the surface area analysis. We have shown how the total surface area of the samples changes upon different treatments and preparation methods, suggesting that different porous structures can arise during the preparation steps. Because a complete and detailed surface analysis was not always possible during this project, we think that a further study focussed on study the characteristics of these most certainly porous carbon materials could be of interest.

4.4   References

1.   Rodriguez-Reinoso, F. The role of carbon materials in heterogeneous catalysis. *Carbon* **1998,** *36* (3), 159-175.

2.   Geim, A. K.; Novoselov, K. S. The rise of graphene. *Nat Mater* **2007,** *6* (3), 183-91.

3.   Montes-Moran, M. A.; Suarez, D.; Menendez, J. A.; Fuente, E. On the nature of basic sites on carbon surfaces: An overview. *Carbon* **2004,** *42* (7), 1219-1225.

4.   Banks, C. E.; Davies, T. J.; Wildgoose, G. G.; Compton, R. G. Electrocatalysis at graphite and carbon nanotube modified electrodes: edge-plane sites and tube ends are the reactive sites. *Chem Commun (Camb)* **2005,** (7), 829-41.

5.   Parshetti, G. K.; Chowdhury, S.; Balasubramanian, R. Biomass derived low-cost microporous adsorbents for efficient CO_2 capture. *Fuel* **2015,** *148*, 246-254.

6.   Auer, E.; Freund, A.; Pietsch, J.; Tacke, T. Carbons as supports for industrial precious metal catalysts. *Applied Catalysis A-General* **1998,** *173* (2), 259-271.

7.   Funke, A.; Ziegler, F. Hydrothermal carbonization of biomass: A summary and discussion of chemical mechanisms for process engineering. *Biofuels Bioproducts & Biorefining-Biofpr* **2010,** *4* (2), 160-177.

8.   Hu, B.; Yu, S. H.; Wang, K.; Liu, L.; Xu, X. W. Functional carbonaceous materials from hydrothermal carbonization of biomass: an effective chemical process. *Dalton Trans* **2008,** (40), 5414-23.

9.   Kubo, S.; Demir-Cakan, R.; Zhao, L.; White, R. J.; Titirici, M. M. Porous carbohydrate-based materials via hard templating. *ChemSusChem* **2010,** *3* (2), 188-94.

10.   Baccile, N.; Laurent, G.; Babonneau, F.; Fayon, F.; Titirici, M.-M.; Antonietti, M. Structural Characterization of Hydrothermal Carbon Spheres by Advanced Solid-State MAS ^{13}C NMR Investigations. *The Journal of Physical Chemistry C* **2009,** *113* (22), 9644-9654.

11.   Titirici, M. M.; White, R. J.; Falco, C.; Sevilla, M. Black perspectives for a green future: hydrothermal carbons for environment protection and energy storage. *Energy & Environmental Science* **2012,** *5* (5), 6796-6822.

12.   Lua, A. C.; Guo, J. Preparation and characterization of activated carbons from oil-palm stones for gas-phase adsorption. *Colloids and Surfaces a-Physicochemical and Engineering Aspects* **2001,** *179* (2-3), 151-162.

13.   Unur, E.; Brutti, S.; Panero, S.; Scrosati, B. Nanoporous carbons from hydrothermally treated biomass as anode materials for lithium ion batteries. *Microporous and Mesoporous Materials* **2013,** *174*, 25-33.

14.   Sun, K.; Tang, J.; Gong, Y.; Zhang, H. Characterization of potassium hydroxide (KOH) modified hydrochars from different feedstocks for enhanced removal of heavy metals from water. *Environ Sci Pollut Res Int* **2015,** *22* (21), 16640-51.

15.   Titirici, M. M.; Antonietti, M.; Baccile, N. Hydrothermal carbon from biomass: a comparison of the local structure from poly- to monosaccharides and pentoses/hexoses. *Green Chemistry* **2008,** *10* (11), 1204-1212.

16.   Dimitratos, N.; Lopez-Sanchez, J. A.; Anthonykutty, J. M.; Brett, G.; Carley, A. F.; Tiruvalam, R. C.; Herzing, A. A.; Kiely, C. J.; Knight, D. W.; Hutchings, G. J. Oxidation of glycerol using gold-palladium alloy-supported nanocrystals. *Phys Chem Chem Phys* **2009,** *11* (25), 4952-61.

17.   Hou, W. B.; Dehm, N. A.; Scott, R. W. J. Alcohol oxidations in aqueous solutions using Au, Pd, and bimetallic AuPd nanoparticle catalysts. *Journal of Catalysis* **2008,** *253* (1), 22-27.

18.   Yang, X.; Chen, D.; Liao, S.; Song, H.; Li, Y.; Fu, Z.; Su, Y. High-performance Pd–Au bimetallic catalyst with mesoporous silica nanoparticles as support and its catalysis of cinnamaldehyde hydrogenation. *Journal of Catalysis* **2012,** *291*, 36-43.

19.   Wenhao Luo, M. S., Andrew M. Beale, Qian He, Christopher J. Kiely, Pieter C.A. Bruijnincx, Bert M. Weckhuysen. High performing and stable supported nano-alloys for the catalytic hydrogenation of levulinic acid to g-valerolactone. *Nature Communications* **2015,** *6*.

20.   Behr, A.; Eilting, J.; Irawadi, K.; Leschinski, J.; Lindner, F. Improved utilisation of renewable resources: New important derivatives of glycerol. *Green Chemistry* **2008,** *10* (1), 13-30.

21.   Pagliaro, M.; Ciriminna, R.; Kimura, H.; Rossi, M.; Della Pina, C. From glycerol to value-added products. *Angew Chem Int Ed Engl* **2007,** *46* (24), 4434-40.

22.   Carrettin, S.; McMorn, P.; Johnston, P.; Griffin, K.; Kiely, C. J.; Hutchings, G. J. Oxidation of glycerol using supported Pt, Pd and Au catalysts. *Physical Chemistry Chemical Physics* **2003,** *5* (6), 1329-1336.

23.   Landon, P.; Collier, P. J.; Papworth, A. J.; Kiely, C. J.; Hutchings, G. J. Direct formation of hydrogen peroxide from H2/O2 using a gold catalyst. *Chemical Communications* **2002,** (18), 2058-2059.

24.   Wang, D.; Villa, A.; Su, D. S.; Prati, L.; Schlögl, R. Carbon-Supported Gold Nanocatalysts: Shape Effect in the Selective Glycerol Oxidation. *ChemCatChem* **2013,** *5* (9), 2717-2723.

25.   Ketchie, W. C.; Murayama, M.; Davis, R. J. Promotional effect of hydroxyl on the aqueous phase oxidation of carbon monoxide and glycerol over supported Au catalysts. *Topics in Catalysis* **2007,** *44* (1-2), 307-317.

26.   Rodriguez, A. A.; Williams, C. T.; Monnier, J. R. Selective liquid-phase oxidation of glycerol over Au–Pd/C bimetallic catalysts prepared by electroless deposition. *Applied Catalysis A: General* **2014,** *475*, 161-168.

27.   Prati, L.; Rossi, M. Gold on carbon as a new catalyst for selective liquid phase oxidation of diols. *Journal of Catalysis* **1998,** *176* (2), 552-560.

28.   Bianchi, C.; Porta, F.; Prati, L.; Rossi, M. Selective liquid phase oxidation using gold catalysts. *Topics in Catalysis* **2000,** *13* (3), 231-236.

29.   Biella, S.; Castiglioni, G. L.; Fumagalli, C.; Prati, L.; Rossi, M. Application of gold catalysts to selective liquid phase oxidation. *Catalysis Today* **2002,** *72* (1-2), 43-49.

30.   Carrettin, S.; McMorn, P.; Johnston, P.; Griffin, K.; Hutchings, G. J. Selective oxidation of glycerol to glyceric acid using a gold catalyst in aqueous sodium hydroxide. *Chemical Communications* **2002,** (7), 696-697.

31.   Dimitratos, N.; Lopez-Sanchez, J. A.; Hutchings, G. J. Green Catalysis with Alternative Feedstocks. *Topics in Catalysis* **2009,** *52* (3), 258-268.

32.   Demirel, S.; Lehnert, K.; Lucas, M.; Claus, P. Use of renewables for the production of chemicals: Glycerol oxidation over carbon supported gold catalysts. *Applied Catalysis B-Environmental* **2007,** *70* (1-4), 637-643.

33.   Bianchi, C. L.; Canton, P.; Dimitratos, N.; Porta, F.; Prati, L. Selective oxidation of glycerol with oxygen using mono and bimetallic catalysts based on Au, Pd and Pt metals. *Catalysis Today* **2005,** *102*, 203-212.

34.   Wang, D.; Villa, A.; Porta, F.; Su, D.; Prati, L. Single-phase bimetallic system for the selective oxidation of glycerol to glycerate. *Chem Commun (Camb)* **2006,** (18), 1956-8.

35.   Ketchie, W.; Murayama, M.; Davis, R. Selective oxidation of glycerol over carbon-supported AuPd catalysts. *Journal of Catalysis* **2007,** *250* (2), 264-273.

36.   Prati, L.; Villa, A.; Porta, F.; Wang, D.; Su, D. S. Single-phase gold/palladium catalyst: The nature of synergistic effect. *Catalysis Today* **2007,** *122* (3-4), 386-390.

37.   Porta, F.; Prati, L. Selective oxidation of glycerol to sodium glycerate with gold-on-carbon catalyst: an insight into reaction selectivity. *Journal of Catalysis* **2004,** *224* (2), 397-403.

38.   Ketchie, W. C.; Fang, Y. L.; Wong, M. S.; Murayama, M.; Davis, R. J. Influence of gold particle size on the aqueous-phase oxidation of carbon monoxide and glycerol. *Journal of Catalysis* **2007,** *250* (1), 94-101.

39.   Villa, A.; Dimitratos, N.; Chan-Thaw, C. E.; Hammond, C.; Prati, L.; Hutchings, G. J. Glycerol oxidation using gold-containing catalysts. *Acc Chem Res* **2015,** *48* (5), 1403-12.

40.   Dimitratos, N.; Lopez-Sanchez, J. A.; Lennon, D.; Porta, F.; Prati, L.; Villa, A. Effect of particle size on monometallic and bimetallic (Au,Pd)/C on the liquid phase oxidation of glycerol. *Catalysis Letters* **2006,** *108* (3-4), 147-153.

41.   Chan-Thaw, C. E.; Campisi, S.; Wang, D.; Prati, L.; Villa, A. Selective Oxidation of Raw Glycerol Using Supported AuPd Nanoparticles. *Catalysts* **2015,** *5* (1), 131-144.

42.   Jennifer K. Edwards, A. F. C., Andrew A. Herzing, Christopher J. Kiely, Graham J. Hutchings. Direct synthesis of hydrogen peroxide from H_2 and O_2 using supported Au–Pd catalysts. *Faraday Discuss* **2008,** *138*, 225-239.

43.   Lu, Y. M.; Zhu, H. Z.; Li, W. G.; Hu, B.; Yu, S. H. Size-controllable palladium nanoparticles immobilized on carbon nanospheres for nitroaromatic hydrogenation. *Journal of Materials Chemistry A* **2013,** *1* (11), 3783-3788.

44.   Doke, D. S.; Umbarkar, S. B.; Gawande, M. B.; Zbori, R.; Biradar, A. V. Environmentally Benign Bioderived Carbon Microspheres-Supported Molybdena Nanoparticles as Catalyst for the Epoxidation Reaction. *Acs Sustainable Chemistry & Engineering* **2017,** *5* (1), 904-910.

45.   Demirel-Gulen, S.; Lucas, M.; Claus, P. Liquid phase oxidation of glycerol over carbon supported gold catalysts. *Catalysis Today* **2005,** *102*, 166-172.

46.   Bianchi, C. L.; Biella, S.; Gervasini, A.; Prati, L.; Rossi, M. Gold on carbon: influence of support properties on catalyst activity in liquid-phase oxidation. *Catalysis Letters* **2003,** *85* (1-2), 91-96.

47.   Sankar, M.; He, Q.; Morad, M.; Pritchard, J.; Freakley, S. J.; Edwards, J. K.; Taylor, S. H.; Morgan, D. J.; Carley, A. F.; Knight, D. W.; Kiely, C. J.; Hutchings, G. J. Synthesis of stable ligand-free gold-palladium nanoparticles using a simple excess anion method. *ACS Nano* **2012,** *6* (8), 6600-13.

48.   Casaletto, M. P.; Longo, A.; Martorana, A.; Prestianni, A.; Venezia, A. M. XPS study of supported gold catalysts: the role of Au^0 and $Au^{+\delta}$ species as active sites. *Surface and Interface Analysis* **2006,** *38* (4), 215-218.

49.   Teschner, D.; Pestryakov, A.; Kleimenov, E.; Havecker, M.; Bluhm, H.; Sauer, H.; Knop-Gericke, A.; Schlogl, R. High-pressure X-ray photoelectron spectroscopy of palladium model hydrogenation catalysts. Part 1: Effect of gas ambient and temperature. *Journal of Catalysis* **2005,** *230* (1), 186-194.

50.   Moulder, J. F.; Stickle, W. F.; Sobol, P. E.; Bomben, K. D. *Handbook of X-ray Photoelectron Spectroscopy*. Perkin-Elmer Corporation: Norwalk, CT, 1992.

51.   Biniak, S.; Szymanski, G.; Siedlewski, J.; Swiatkowski, A. The characterization of activated carbons with oxygen and nitrogen surface groups. *Carbon* **1997,** *35* (12), 1799-1810.

52.   Reiche, S.; Blume, R.; Zhao, X. C.; Su, D.; Kunkes, E.; Behrens, M.; Schlögl, R. Reactivity of mesoporous carbon against water – An in-situ XPS study. *Carbon* **2014,** *77*, 175-183.

53.   Felten, A.; Bittencourt, C.; Pireaux, J. J. Gold clusters on oxygen plasma functionalized carbon nanotubes: XPS and TEM studies. *Nanotechnology* **2006,** *17* (8), 1954-1959.

54.   Yu, L.; Falco, C.; Weber, J.; White, R. J.; Howe, J. Y.; Titirici, M. M. Carbohydrate-derived hydrothermal carbons: a thorough characterization study. *Langmuir* **2012,** *28* (33), 12373-83.

55.   Stobinski, L.; Lesiak, B.; Malolepszy, A.; Mazurkiewicz, M.; Mierzwa, B.; Zemek, J.; Jiricek, P.; Bieloshapka, I. Graphene oxide and reduced graphene oxide studied by the XRD, TEM and electron spectroscopy methods. *Journal of Electron Spectroscopy and Related Phenomena* **2014,** *195*, 145-154.

56.   Kagenda, C.; Lule, I.; Paulik, C. Improved Nitrogen-Doped Carbon Materials for High Performing Lithium Air Batteries. *South African Journal of Chemical Engineering* **2018,** *25*, 32-41.

57.   Philip, D. Green synthesis of gold and silver nanoparticles using Hibiscus rosa sinensis. *Physica E-Low-Dimensional Systems & Nanostructures* **2010,** *42* (5), 1417-1424.

58.   Pantojas, V.; Rodríguez-Vindas, D.; Morell, G.; Rivera, A.; Ortiz, C.; Santiago-Aviles, J. J.; Otano-Rivera, W. In *Synthesis of palladium with different nanoscale structures by sputtering deposition onto fiber templates*, SPIE: 2008; p 12.

59.   Zhan, G.; Huang, J.; Du, M.; Abdul-Rauf, I.; Ma, Y.; Li, Q. Green synthesis of Au–Pd bimetallic nanoparticles: Single-step bioreduction method with plant extract. *Materials Letters* **2011,** *65* (19-20), 2989-2991.

60.   Dorofeev, G. A.; Streletskii, A. N.; Povstugar, I. V.; Protasov, A. V.; Elsukov, E. P. Determination of nanoparticle sizes by X-ray diffraction. *Colloid Journal* **2012,** *74* (6), 675-685.

61.   O'Connell, K.; Regalbuto, J. R. High Sensitivity Silicon Slit Detectors for 1 nm Powder XRD Size Detection Limit. *Catalysis Letters* **2015,** *145* (3), 777-783.

62.   Maria Jesus Lazaro, L. C., Veronica Celorrio, Juan Ignacio Pardo, Siglinda Perathoner, Rafael Moliner. Study and application of Vulcan XC-72 in low temperature fuel cells. In *Carbon black production, properties and uses*, Sanders, I. J.; Peeten, T. L., Eds. Nova Science Publishers: Hauppauge, N.Y. :, 2011.

63.   Reiche, S.; Kowalew, N.; Schlögl, R. Influence of synthesis pH and oxidative strength of the catalyzing acid on the morphology and chemical structure of hydrothermal carbon. *Chemphyschem* **2015,** *16* (3), 579-87.

64.   Villa, A.; Campione, C.; Prati, L. Bimetallic gold/palladium catalysts for the selective liquid phase oxidation of glycerol. *Catalysis Letters* **2007,** *115* (3-4), 133-136.

65.   Wang, D.; Villa, A.; Porta, F.; Prati, L.; Su, D. S. Bimetallic gold/palladium catalysts: Correlation between nanostructure and synergistic effects. *Journal of Physical Chemistry C* **2008,** *112* (23), 8617-8622.

66.   Zhou, Y. K.; Neyerlin, K.; Olson, T. S.; Pylypenko, S.; Bult, J.; Dinh, H. N.; Gennett, T.; Shao, Z. P.; O'Hayre, R. Enhancement of Pt and Pt-alloy fuel cell catalyst activity and durability via nitrogen-modified carbon supports. *Energy & Environmental Science* **2010,** *3* (10), 1437-1446.

67.   Sheng, Z. H.; Gao, H. L.; Bao, W. J.; Wang, F. B.; Xia, X. H. Synthesis of boron doped graphene for oxygen reduction reaction in fuel cells. *Journal of Materials Chemistry* **2012,** *22* (2), 390-395.

68.   Chen, P.; Wang, L. K.; Wang, G.; Gao, M. R.; Ge, J.; Yuan, W. J.; Shen, Y. H.; Xie, A. J.; Yu, S. H. Nitrogen-doped nanoporous carbon nanosheets derived from plant biomass: an efficient catalyst for oxygen reduction reaction. *Energy & Environmental Science* **2014,** *7* (12), 4095-4103.

69.   Koh, K.; Meng, Y.; Huang, X.; Zou, X.; Chhowalla, M.; Asefa, T. N- and O-doped mesoporous carbons derived from rice grains: efficient metal-free electrocatalysts for hydrazine oxidation. *Chem Commun (Camb)* **2016,** *52* (93), 13588-13591.

70.   Yang, M.; Wang, Z.; Wang, W.; Liu, C. J. Synthesis of AuPd alloyed nanoparticles via room-temperature electron reduction with argon glow discharge as electron source. *Nanoscale Res Lett* **2014,** *9* (1), 405.

71.   Nowicki, P.; Pietrzak, R.; Wachowska, H. X-ray Photoelectron Spectroscopy Study of Nitrogen-Enriched Active Carbons Obtained by Ammoxidation and Chemical Activation of Brown and Bituminous Coals. *Energy & Fuels* **2010,** *24* (2), 1197-1206.

72.   Ai, K.; Liu, Y.; Ruan, C.; Lu, L.; Lu, G. M. Sp2 C-dominant N-doped carbon sub-micrometer spheres with a tunable size: a versatile platform for highly efficient oxygen-reduction catalysts. *Adv Mater* **2013,** *25* (7), 998-1003.

73.   Zhao, L.; Baccile, N.; Gross, S.; Zhang, Y. J.; Wei, W.; Sun, Y. H.; Antonietti, M.; Titirici, M. M. Sustainable nitrogen-doped carbonaceous materials from biomass derivatives. *Carbon* **2010,** *48* (13), 3778-3787.

74.   Prati, L.; Villa, A.; Chan-Thaw, C. E.; Arrigo, R.; Wang, D.; Su, D. S. Gold catalyzed liquid phase oxidation of alcohol: the issue of selectivity. *Faraday Discuss* **2011,** *152* (0), 353-65; discussion 393-413.

75.   Demir-Cakan, R.; Makowski, P.; Antonietti, M.; Goettmann, F.; Titirici, M. M. Hydrothermal synthesis of imidazole functionalized carbon spheres and their application in catalysis. *Catalysis Today* **2010,** *150* (1-2), 115-118.

76.   Staykov, A.; Ooishi, Y.; Ishihara, T. Immobilizing Metal Nanoparticles on Single Wall Nanotubes. Effect of Surface Curvature. *Journal of Physical Chemistry C* **2014,** *118* (17), 8907-8916.

77.   Antolini, E.; Passos, R. R.; Ticianelli, E. A. Effects of the carbon powder characteristics in the cathode gas diffusion layer on the performance of polymer electrolyte fuel cells. *Journal of Power Sources* **2002,** *109* (2), 477-482.

78.   Ye, J. S.; Liu, Z. T.; Lai, C. C.; Lo, C. T.; Lee, C. L. Diameter effect of electrospun carbon fiber support for the catalysis of Pt nanoparticles in glucose oxidation. *Chemical Engineering Journal* **2016,** *283*, 304-312.

79.   Yoshida, H.; Igarashi, N.; Fujita, S.; Panpranot, J.; Arai, M. Influence of Crystallite Size of TiO_2 Supports on the Activity of Dispersed Pt Catalysts in Liquid-Phase Selective Hydrogenation of 3-Nitrostyrene, Nitrobenzene, and Styrene. *Catalysis Letters* **2015,** *145* (2), 606-611.

80.   Pari, G.; Darmawan, S.; Prihandoko, B. Porous Carbon Spheres from Hydrothermal Carbonization and KOH Activation on Cassava and Tapioca Flour Raw Material. *4th International Conference on Sustainable Future for Human Security Sustain 2013* **2014,** *20*, 342-351.

81.   Rodrigues, E. G.; Pereira, M. F. R.; Chen, X. W.; Delgado, J. J.; Orfao, J. J. M. Influence of activated carbon surface chemistry on the activity of Au/AC catalysts in glycerol oxidation. *Journal of Catalysis* **2011,** *281* (1), 119-127.

82.   Wang, D.; Villa, A.; Su, D.; Prati, L.; Schlögl, R. Carbon-Supported Gold Nanocatalysts: Shape Effect in the Selective Glycerol Oxidation. *ChemCatChem* **2013,** *5* (9), 2717-2723.

83.   Leon y Leon, C. A.; Solar, J. M.; Calemma, V.; Radovic, L. R. Evidence for the protonation of basal plane sites on carbon. *Carbon* **1992,** *30* (5), 797-811.

84.   Moreno-Castilla, C.; Lopez-Ramon, M. V.; Carrasco-Marin, F. Changes in surface chemistry of activated carbons by wet oxidation. *Carbon* **2000,** *38* (14), 1995-2001.

85.   Fraga, M. A.; Jordao, E.; Mendes, M. J.; Freitas, M. M. A.; Faria, J. L.; Figueiredo, J. L. Properties of carbon-supported platinum catalysts: Role of carbon surface sites. *Journal of Catalysis* **2002,** *209* (2), 355-364.

86.   Dungen, P.; Schlögl, R.; Heumann, S. Non-linear thermogravimetric mass spectrometry of carbon materials providing direct speciation separation of oxygen functional groups. *Carbon* **2018,** *130*, 614-622.

87.   Donoeva, B.; Masoud, N.; de Jongh, P. E. Carbon Support Surface Effects in the Gold-Catalyzed Oxidation of 5-Hydroxymethylfurfural. *ACS Catalysis* **2017,** *7* (7), 4581-4591.

Chapter

5

Modification of a Pd/TiO$_2$ catalyst by addition of N-heterocyclic carbene ligands

5.1 Introduction

5.1.1 N-Heterocyclic Carbenes in heterogeneous catalysis

N-Heterocyclic Carbenes (NHC) are a class of compounds characterised by a nucleophilic carbon centre, stabilised within a 5-membered ring structure. They are two-electron σ-donor ligands with little π-accepting ability.[1] They have the ability to coordinate to both high- and low-oxidation –state transition metals and their preparation on the large scale is easier than that of another very common class of ligands, phosphines. Compared to phosphine ligands the NHC-metal bond has also been reported to be more stable. NHCs show exceptional thermal stability and their preparation allows a large versatility, achieving among others structural chirality, various functionalisation and the ability to act as anchoring site on surfaces.[1-3]
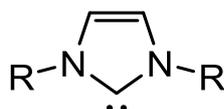
Figure 5.1 General structure of an NHC.

The research group of Glorius was the first to introduce the application of NHC decorating the surface of supported metal nanoparticles.[4] The presence of these surface modifiers has been shown to be able to improve not only the (stereo) selectivity but also the activity of the supported nanoparticles for a variety of catalytic reactions by either introducing steric hindrance that affects the interaction of the substrate with the catalytic active site or by modifying the electronic structure of the supported metal.[4-6]

5.1.1 Palladium catalysts for hydrogen peroxide synthesis

Palladium is a noble metal that presents unique catalytic properties for not only hydrogenation but also some oxidation reactions, as well as various coupling reactions and for this reason is widely used in both academia and in industrial applications.[7-8] Palladium-based catalysts are largely used in the synthesis of fine chemicals and bioactive molecules, due to their efficiency.[9] Thanks to their characteristic nature, homogeneous catalysts are most often reported

in literature, since the molecular structure and the catalytic cycle is generally easier to understand. However, for industrial applications, heterogeneous catalysts are preferred for their easy handling and recovery. Supported palladium catalysts have shown to be active materials in a variety of processes, such as hydrogenolysis,[10] C=C double bond hydrogenation[11] and carbon-carbon coupling reactions.[12-13] Other important transformations are the liquid-phase hydrogenation of aromatic nitro compounds [8, 14] and the oxidation of primary and secondary alcohols into aldehydes and ketones.[15] Another example of use of palladium containing catalysts are in the direct synthesis of hydrogen peroxide.[7]

Many industrial processes requiring oxidation steps still use stoichiometric, hence non-catalytic amounts of oxygen donors in the form of inorganic salts, organic peroxides or percarboxylic acids, overall having low atom efficiency and high waste formation.[16-18] On one side, the environmental friendly, atom efficient and available molecular oxygen is the preferred oxidant, however only few processes take advantage of this clean alternative, due to the limited amount of catalysts found active and selective when using O$_2$ under mild reaction conditions.[19] On the other side, hydrogen peroxide (H$_2$O$_2$) is a largely produced commodity chemical, showing oxidising properties and used as disinfectant and bleaching agent in large-scale processes, giving water as only decomposition product.[20] The discovery of the activity of titanium silicalite TS-1 for the oxidation of propene and the ammoxidation of cyclohexanone in the presence of hydrogen peroxide, has opened up to the study of the synthesis of fine chemicals, by use of H$_2$O$_2$ as oxidant with high reactivity and low environmental impact.[21]

Industrially, large amounts of H$_2$O$_2$ are produced *via* the subsequent process of hydrogenation/oxidation of substituted antraquinones (see Figure 5.2), this being an indirect, centralised and efficient process introduced in 1939 by Riedl and Pfleiderer of BASF.[22] The industrial approach utilises numerous distillation steps to produce highly concentrated H$_2$O$_2$ solutions, which are then transported to the end user who often requires much lower concentrations of H$_2$O$_2$. The need for H$_2$O$_2$ production on an industrial scale requires its transport and storage on-site, utilising a number of acid additives to stabilise the compound. However, these stabilising agents require downstream removal, with an associated cost for the end stage user. By comparison, the direct synthesis of diluted H$_2$O$_2$ from its components H$_2$ and O$_2$ would allow for on-site production and significant energy and costs savings with regards to the transportation, storage and dilution of industrially synthesised H$_2$O$_2$. The high flammability of the two gasses and the use of high pressures, requires to work in diluted conditions, below the flammability level (< 4 %), which allows to achieve only low H$_2$O$_2$ concentration solutions.[23-24]
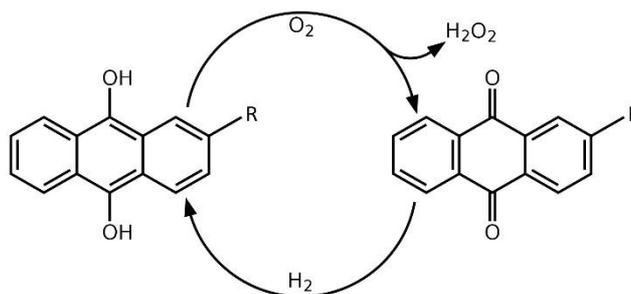
Figure 5.2 Schematic representation of the Riedl–Pfleiderer process for the antraquinone autoxidation.

Palladium based catalysts are already used for the antraquinone hydrogenation step and since the beginning of 1900s, Pd has shown to be the most active metal for the synthesis of H_2O_2.[20, 25-26]. The major drawback of Pd-based catalysts is that the species active for the synthesis are also able to facilitate the decomposition or further hydrogenation steps (Figure 5.3), leading to loss of product.[22] Although palladium based catalysts have long been studied for this reaction, the determination of the catalytic active site for the direct synthesis of H_2O_2 is still under debate. Both Pd(0) and Pd(II) have been reported to be able to catalyse the synthesis of H_2O_2. However, the former has also been found responsible for its sequential hydrogenation.[27-28] Because possible aggregation of Pd into large metallic nanoparticles during catalyst preparation or under reaction conditions could take place, forming planes of highly coordinated Pd species, the isolation of Pd(0) species needs to be maximised, by either oxidative treatments or dilution of the active metal with a secondary metal, to form an alloy. Alloy systems have shown to improve the H_2O_2 productivity and selectivity, most probably due to electronic effects arising from the alloy formation.[22]
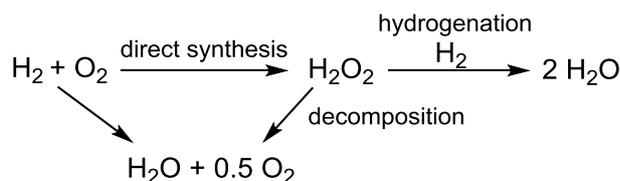
Figure 5.3 Hydrogen peroxide synthesis reaction scheme.

5.1.2 Aim of the project

Once the metal nanoparticles are formed and supported on the carrier material, they do interact with it through a bond. The support is chosen based on the final stability of the catalyst, as the metal anchors to it avoiding sintering or leaching under reaction conditions. However, the choice of support has long shown to be strongly related also to the overall performance of the final catalytic material influencing both reactivity and selectivity of the supported metal for a specific reaction.[29-32] Therefore, the support-metal chemical interaction should, in fact, be considered as a ligand-metal interaction, where the choice of ligand does affect the properties of the metal.[29] The research presented so far in this thesis on the support-metal interaction, this

chapter focusses on the influence on the structure and on the catalysis that an organic ligand could have when added to a supported metal nanoparticle. Recently, a new collaboration with the University of Münster was established aimed at studying and developing new catalytic materials.

In the past, palladium-based catalysts supported on titania (TiO₂) have been studied in the Hutchings research group for the direct synthesis of H_2O_2 from H_2 and O_2, the oxidation of benzyl alcohol and glycerol and for the hydrogenation of nitroarenes.[33-36]

Once the active metal is deposited onto an inert support, the characteristics of the nanoparticles can be tuned by an appropriate activation treatment (as also studied and discussed in Chapter 3), which has a direct effect on the oxidation state of the metal species as well as on the size of the nanoparticles.[37] In particular, metallic Pd(0) nanoparticles have been shown to be active for the reduction of the NO_2 group and for the direct synthesis of H_2O_2.[33, 36] However, selectivity issues may arise in the presence of additional reducible functional groups in the former case, and with further product decomposition in the latter case. Therefore, the role of the addition of the NHC ligands is of interest. To ensure the formation of Pd(0) nanoparticles, with a more defined structure, compared to PdO agglomerates, a reductive treatment was chosen. By impregnation of an acidified $PdCl_2$ aqueous solution (HCl, 0.58 M) onto TiO₂, followed by a reductive heat treatment, Pd(0) nanoparticles are formed achieving high dispersion of the metal and uniform particle size below 4 nm.[38]

Based on previous works, the aim of this project has been to study the addition of NHCs ligands with known electronic and steric hindrance characteristics that could modify the electronic density and covering of the supported metallic nanoparticles and hence influence the catalytic activity for different liquid phase catalytic reactions. In particular, the collaborators in Münster synthesised NHCs with various geometric as well as electronic characteristics. While in Cardiff University a 1% Pd/TiO₂ sample was prepared by modified impregnation method, based on work previously reported in the literature.[38] The monometallic sample was modified by addition of different NHCs and the modified materials were then characterised and their activity investigated for the catalytic hydrogenation of 3-nitrostyrene and the direct synthesis of hydrogen peroxide. The oxidation state and the electron density of a catalytic active site is an important parameter to consider when synthesising a catalyst, because this often dictates the reactivity towards the reactants.[37] Because the electronic characteristics of the NHCs can be tuned by changing the functional groups on the carbene ring, it is of interest to understand how electron donation or withdrawal from the ligand to the supported metal nanoparticles could affect the active species during a heterocatalytic reaction. Moreover, it was of interest to try and study how the size and possible steric hindrance of the structures of the NHC ligands could influence the selectivity and the way the substrate approaches the nanoparticle.

Since the work conducted so far on similar NHC modified heterogeneous catalysts has been performed under inert and controlled conditions typical of organic chemistry procedures,[4-6] it was of interest to determine the stability of these samples in the presence of air and moisture.

Through this project a new collaboration was established, where the knowledge of heterogeneous catalysis and ligand design in homogeneous systems could meet. NHC modified Pd/TiO₂ materials were prepared and characterised by means of surface techniques, in order to study how the initial catalyst changes upon addition of the NHC moieties. Moreover, the stability and the position of these ligands interacting with the catalysts surface was of interest. The possible use of these materials in liquid or gas phase reactions, where high temperatures and pressures may be applied, require a good stability of the catalyst.

As this is a new project and the organic-inorganic system is not well known, mainly characterisation of the new materials has been carried out as to try and better understand the features and variation of these modified catalysts compared to the usual materials prepared in the CCI laboratories. In this Chapter, the results of this initial work are reported and discussed.

5.2   Results and discussion

5.2.1   Palladium catalysts characterisation

Palladium was impregnated on TiO₂ P25 and reduced in furnace (at 400 °C for 4 h under a flow of 5% H₂/Ar) according to the procedure reported in literature.[38] The as-prepared sample was sent to our collaborators of the research group of Prof. Glorius at the Organic Chemistry Institute at the University of Münster, where the NHC ligands were added following the method previously reported.[5] In Figure 5.4 are shown the structures of the NHC ligands used to modify the 1 wt. %Pd/TiO₂ catalyst. The basic 5-membered N-heterocyclic structure (imidazolylidene) has been modified by addition of different groups at the N positions. The presence of the cyclohexane, mesityl and iso-propyl group formed the ICy, IMes and IPr NHC ligands respectively. The further modification of the latter by addition of phenyl groups in para position or on the propyl group led to formation of the large NHC ligand structures named *p*Ph-IPr and IPr* respectively.
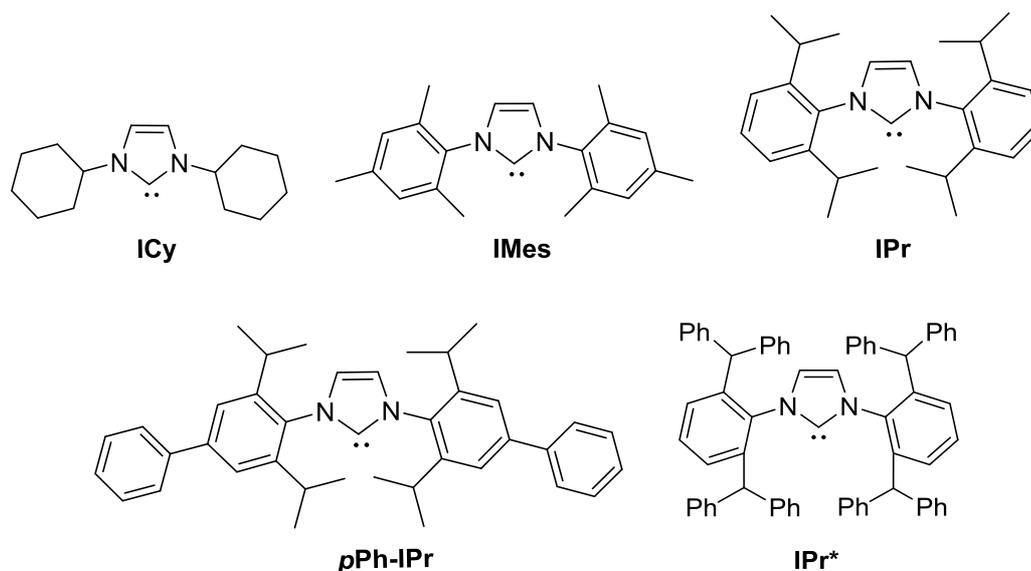
Figure 5.4 NHC ligands structures.

The non-aromatic flexible ICy and the aromatic more expanded IMes ligands were added in 1:1 molar ratio with the metal, while the IPr ligand was also added in lower to higher amount, 2:1, 1:2, 1:5 and 1:10 Pd: NHC ratio. The ICy, IMes and IPr ligands are known to have similar electronic characteristics, while the geometry and flexibility of their structures change.[39] The IPr ligand was modified not only by addition of a phenyl group in para position *p*Ph-IPr, in order to increase the aromatic system and possibly increase the stability of the structure, but also by substituting the multiple methyl groups in ortho position with phenyl rings IPr*, substantially increasing the steric hindrance of the structure. These two ligands were added to the 1% Pd/TiO₂ catalysts in 1:2 metal: NHC ratio.

From previous work in this field, as well as the initial work on this topic by the group of Glorius, the direct interaction between the carbene carbon and the noble metal is known to be formed.[40-41] The procedure applied in this project for the addition of the NHC to the supported palladium catalysts has proved formation of the NHC-metal bond by ^{13}C solid-state NMR.[5] However, it is possible that an interaction between the ligand and the catalyst support might also take place.

Once the 1% Pd/TiO₂ catalysts were modified, they were sent back to Cardiff University where characterisation was performed. The samples were also tested for the liquid phase hydrogenation of 3-nitrostyrene and the direct synthesis of hydrogen peroxide from gaseous H₂ and O₂. The results are reported in the following Sections (5.2.1.1-5.2.2.2).

5.2.1.1 X-Ray Photoelectron spectroscopy

The samples exchanged during this project were analysed by XPS as to study how the metal and the nitrogen signal would change upon addition of the NHC ligands. In Figure 5.5, the

photoelectron spectra of the Pd 3d region are shown. The initial 1% Pd/TiO₂ catalyst, its modification with various amount of IPr ligand (Figure 5.5a) and with addition of different NHC ligands (Figure 5.5b) are reported.
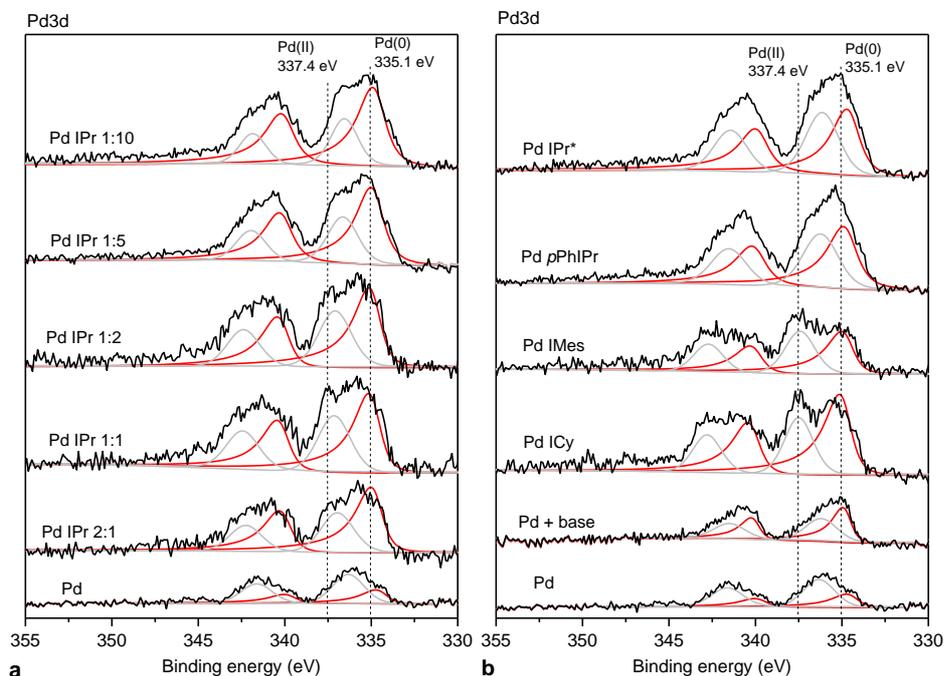
Figure 5.5 XPS analysis of palladium region of the NHC modified 1% Pd/TiO₂ samples. Deconvolution of the peaks shows presence of Pd(0) (in red) and Pd(II) (in grey).

The palladium 3d photoelectron signal is characterised by two spin-orbit components, $Pd3d_{5/2}$ at lower binding energy and $Pd3d_{3/2}$ at higher energy, separated by 5.26 eV.[42] The spectra have been deconvoluted as to better determine the different species present in the catalysts. The $Pd3d_{5/2}$ peak at 335.1 eV corresponds to metallic palladium Pd(0),[43] whereas a higher binding energy signal between *ca.* 336 and 337 eV is attributed to Pd(II).[44-45] The unmodified Pd sample shows the presence of not only Pd(0), but also a substantial amount of Pd(II) at 336.3 eV.[45] This suggests that the as-prepared 1% Pd/TiO₂ sample presents both Pd(0) and Pd(II) components, due to some surface oxidation.

After addition of the NHC ligands (ICy, IMes, IPr and its modification, also in different metal: NHC ratios), it is possible to notice the presence of Pd(0), as well as Pd(II) species, the latter found at higher binding energies compared to the as-prepared 1% Pd/TiO₂ catalyst. The Pd(II) photoelectron peak shifts to up to 337.4 eV, most probably due to an effect of the modification of the initial sample. On one side, the larger presence of a Pd(0) component could be indicating that as the carbene carbon interacts directly with the metal, donating electronic density, a shift to lower binding energy compared to the as-prepared 1%Pd /TiO₂ is achieved. On the other side, the formation of a more positively charged palladium species could be arising during addition of the NHC ligands, where strong base and solvents are used. To confirm this possibility, some of the as-prepared 1% Pd/TiO₂ sample was treated as per method used for the

NHC addition, without the actual addition of the carbene. The sample was analysed by XPS, not showing substantial variation from the untreated sample.

An explanation to the presence and binding energy shift of the Pd(II) peak after addition of the NHC could be found in the interaction of a protonated $NHCH^+$ molecule, bearing a positive charge on one of the nitrogen atoms, the imidazolium cation, and the metal nanoparticle. To confirm this hypothesis, the nitrogen region of these samples has been analysed. If a positive nitrogen species is present, the corresponding imidazolium cation $NHCH^+$ could be interacting with the palladium metal nanoparticle leading to a decrease in electron density.

In Figure 5.6a are plotted the nitrogen XPS spectra of the samples presenting an increasing amount of IPr ligand (from 2:1 to 1:10 Pd: NHC ratio), whereas in Figure 5.6b, there are shown the samples containing different NHC ligands. The nitrogen 1s photoelectron signal gives rise to only one component, whose position can fall in the range of binding energies between 398 and 403 eV, the position being dependant on the charge and oxidation state of the element. In previous works, where NHCs were added to a gold surface as well as to unsupported nanoparticles, only one peak at around 400 eV was detected by XPS, which can be assigned to the neutral nitrogen species present in the imidazolylidene ring when the carbene carbon is directly bound to the metal.[46-47] Similar results were obtained when studying Pd nanoparticles supported on Fe_3O_4 and further modified by addition of NHC ligands, the XPS analysis revealed the presence of only one N1s peak near 400 eV.[4]
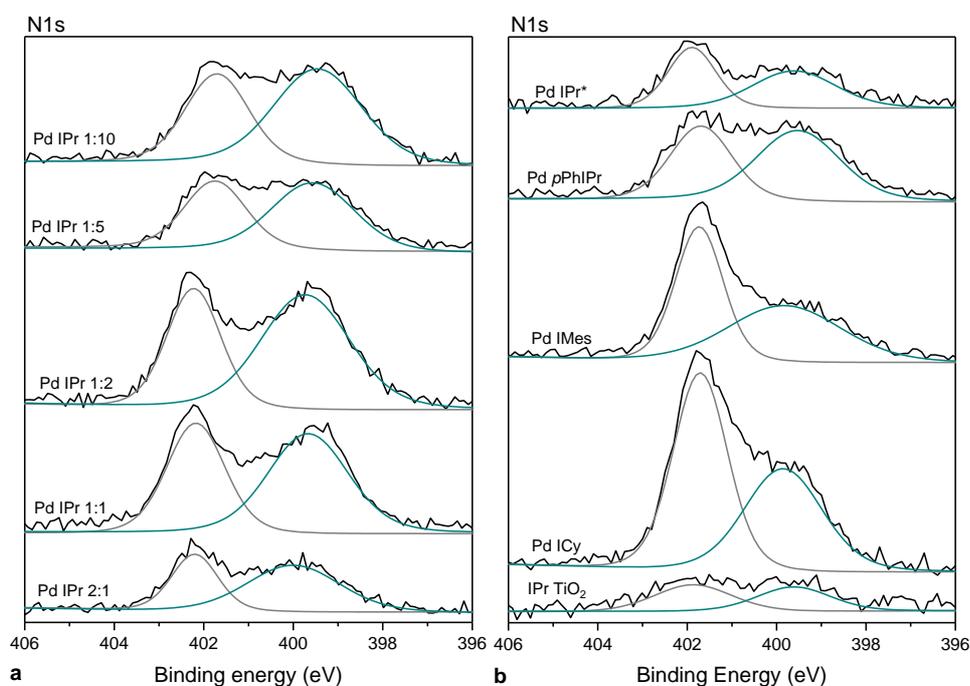

Figure 5.6 XPS analysis of the nitrogen region of NHC modified 1%Pd/TiO₂ samples. Deconvolution of the peaks indicates presence of neutral (green line) and positively charged (grey line) nitrogen species.

In contrast to what has been observed previously, after peak fitting of the XPS spectra of the NHC modified 1% Pd/TiO$_2$ samples, it is possible to notice the presence of two different nitrogen components. One is positioned at *ca.* 399.6 eV and the other is found at *ca.* 402 eV. The lower binding energy peak located at *ca.* 399.6 eV can be assigned to organic substituted neutral amino compounds C-NR$_2$, whereas the higher N1s binding energy signal near 402 eV can be assigned to protonated and positively charged nitrogen species such as an ammonium salt R$_4$-N$^+$.[42] In fact, a charged species could be arising from the protonation of the free carbene (Figure 5.7a), which leads to the formation of the imidazolium cation (Figure 5.7b).

(a)   (b)
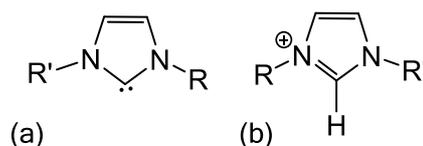
Figure 5.7 General structure of the free N-heterocyclic carbene (a) and the protonated imidazolium cation (b).

For reference, a sample of IPr imidazolium salt, IPrHBF$_4$, was exchanged with our collaborators and analysed by XPS. The nitrogen photoelectron spectrum of IPrHBF$_4$ is reported in Figure 5.8. The peak position indicates the presence of an N species with binding energy of 401.7 eV, which can be unequivocally assigned and used as reference.
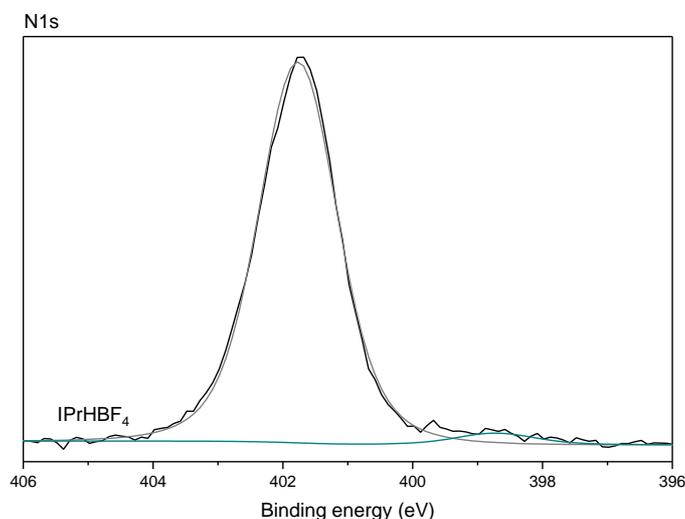
Figure 5.8 Nitrogen XPS spectrum of the IPr imidazolium salt, IPrHBF$_4$.

From here, the low binding energy peak has been assigned to the free carbene that has formed a bond directly with the metal nanoparticle, while the formation and presence in all samples of positively charged nitrogen atoms could be due to a protonation taking place during the NHC addition to the Pd catalyst. The presence of adsorbed water molecules may lead to protonation of the reactive carbene carbon.[48-49] A similar assignment has been previously suggested by the group of Glorius and co-workers, where the XPS analysis of nitrogen in the ICy imidazolium salt, the corresponding free carbene and the ICy ligand stabilising a palladium centre in solution showed

higher (401.5 eV) or lower (399.5 eV) binding energies depending on the protonation and stabilisation of the carbene species.[50]

Because the as-prepared Pd/TiO₂ sample contains 1 wt. % of metal in contrast to the large amount of support, and the vast majority of the surface of the sample is composed of the metal oxide, it should not be excluded the possibility that the NHCs interact with the support. With the purpose of having a sample to be used as reference and comparison, some bare TiO₂ support was modified by addition of the IPr ligand in the same quantity used for the Pd IPr 2:1 sample. The N1s photoelectron analysis reported at the bottom of Figure 5.6b shows two nitrogen components, however with a lower intensity, indicating that the NHC ligand does interact with the support, as it could interact in the presence of the supported metal, by presenting both the imidazolium cation and the free carbene interacting directly with the transition metal present in the oxide support.

The presence of two N1s photoelectron signals, which has not been reported in previous works on similarly prepared samples, could be ascribed to the fact that so far, these NHC/metal systems have been handled in controlled, dry and inert environments such as glove boxes and Schlenk lines, in absence of air and moisture. These precautions have only limitedly been applied during our study, as one of the interests of this project is to determine whether and how stable these samples are.

When calculating the ratio between the XPS area of a specific element and the area of titanium, which for these samples is the reference element, is possible to determine a normalised value to be used to compare the various samples discussed here. When calculating the normalised nitrogen areas for all the NHC modified Pd samples, the values reported in Table 5.1 are obtained.

As the IPr ligand added to 1% Pd/TiO₂ increases from 2:1 to 1:10, the nitrogen XPS area increases from 8.4 to 23.7, which confirms the increasing amount of NHC added. Ligands added in 1:1 molar ratio show very comparable nitrogen content around 16, while the sterically hindering NHCs added in 1:2 molar ratio seem to have more difficulties in interacting with the surface of the Pd catalyst as the structure becomes more expanded and bulkier (IPr<pPh-IPr<IPr*).

Table 5.1 Nitrogen XPS normalised areas for NHC modified palladium catalysts.

Sample	N/Ti*10⁻³
Pd IPr 2:1	8.4
Pd IPr 1:1	16.5
Pd IPr 1:2	18.7
Pd IPr 1:5	17.4
Pd IPr 1:10	23.7
Pd IPr* 1:2	8.4
Pd *p*Ph-IPr 1:2	14.7
Pd IMes 1:1	17.6
Pd ICy 1:1	17.1
IPr/TiO₂ 2:1	4.1

From the XPS analysis of the NHC modified Pd samples, it is possible to conclude that the interaction between the carbene ligands and the metal is taking place, and a substantial oxidation of the metal is occurring by presence of an imidazolium cation. It should also be underlined that the NHC ligands are not only interacting with the metal nanoparticles, but also with the support. A better understanding of which species are present in the samples, where are they located, and how stable are they on the surface of the catalysts will be attempted in the following sections.

5.2.1.2 Attenuated Total Reflectance Infrared spectroscopy

Another spectroscopic technique applied to study the NHC modified 1%Pd/TiO₂ samples was Attenuated Total Reflectance Infrared (ATR-IR) spectroscopy. By IR analysis is possible to study the vibrational modes of molecules and depending on the stretching frequency is possible to qualitatively determine the type of bonding. Typically, organic molecules show bands in the 2850-3000 cm⁻¹ arising from sp^3 C-H stretching, whereas C=C vibration within the aromatic rings are expected to give multiple bands between 1500-1600 cm⁻¹.

As with XPS analysis, the NHC modified Pd catalysts were compared to two reference samples, the IPr modified TiO₂ and the imidazolium salt IPrHBF₄. The initial 1% Pd/TiO₂ sample, the reference samples and the variously NHC modified 1% Pd/TiO₂ samples were measured by ATR-IR spectroscopy and the transmittance spectra are plotted in Figure 5.9. Figure 5.9a shows the samples containing NHC IPr in different metal to ligand ratio and as well as the reference samples, IPrHBF₄ and IPrTiO₂. In Figure 5.9b there are plotted the spectra of the as-prepared 1% Pd/TiO₂ sample and its modification with various NHC ligands.
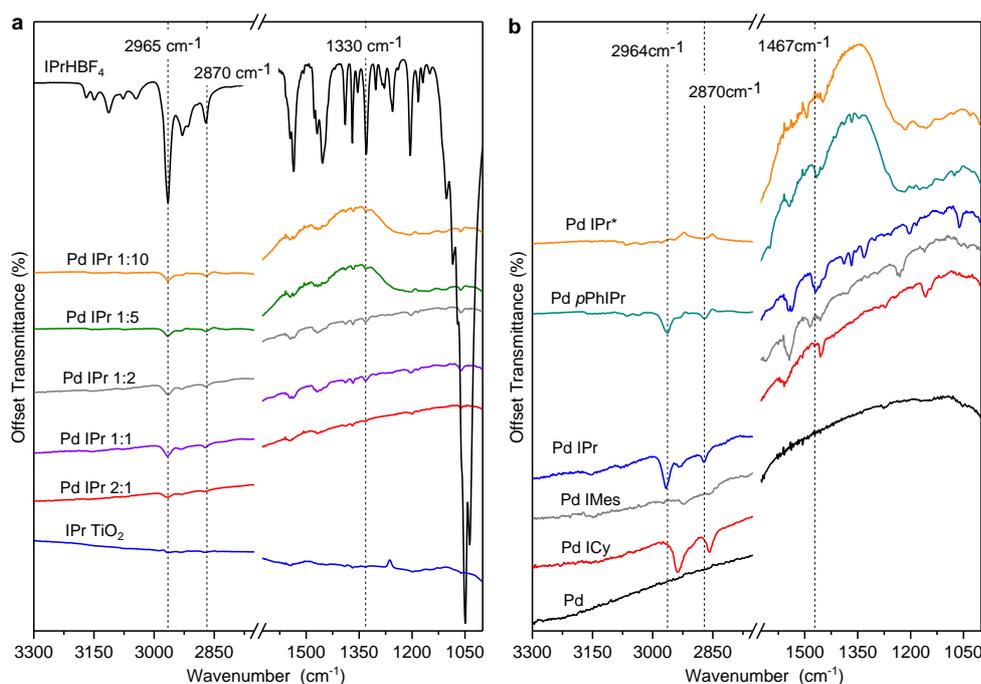
Figure 5.9 ATR-IR spectra of the reference and the NHC modified Pd samples.

In previous work performed by Ranganath *et al.* the IR technique was used to confirm the presence of the NHC on the surface of the catalyst and found that around 2900 and 1300 cm⁻¹ there is the presence of bands that can be attributed to the ligands,[4] as has been highlighted by dotted lines in the spectra plotted in Figure 5.9. This is further confirmed by comparison with the pure imidazolium salt, IPrHBF₄. The very high intensity peak of the imidazolium salt spectrum is due to the concentration of the sample, compared to the low percentages of ligand added to the supported Pd catalyst. It is, however, possible to notice the presence of well comparable bands between the imidazolium salt, containing the protonated NHC, and the NHC modified Pd catalyst, presenting the free carbene (as well as its protonated counterpart) attached to the metal nanoparticles. On the contrary, the as-prepared 1% Pd/TiO₂ catalyst does not show any band in the range considered, once more, confirming that the signals observed here are due to the addition of the ligands.

In the wavenumber region between 2850-3000 cm⁻¹, two main bands arise, and they are present in all NHC modified samples apart from the Pd IMes and the Pd IPr* samples, whereas the Pd ICy shows a shift of the two bands towards lower wavenumbers. Similar behaviour is found in the fingerprint region between 1100 and 1550 cm⁻¹, where mainly bands arising from bending vibrations are detected. In this region, the Pd IMes sample does show some defined bands that could be assigned to the aromatic rings.

In conclusion, it is possible to confirm that the analysis of the different NHC ligands show not only specific bands depending on their molecular structures, but also that bands are highly comparable and reproducible between samples containing the same ligand, which makes IR a good technique for study and identify such complex structures.

5.2.1.3 Thermogravimetric analysis

Thermogravimetric analysis (TGA) was necessary to assess the thermal stability of the NHC ligands on the surface of the samples. Moreover, it was performed in order to confirm the presence and amount of ligand added to the as-prepared 1% Pd/TiO₂ catalyst.

Initially, the thermal stability of the NHC modified 1% Pd/TiO₂ samples was measured performing experiments in air as previously done by Ernst *et al.*[5] Because during treatment in air uncontrolled combustion may take place, the samples were also analysed in a flow of He. During such treatment, decomposition rather than combustion of the ligand should occur, leading to a more detailed analysis.

In Figure 5.10, the PdICy sample TGA results obtained in air and in He flow are shown as example. Comparing the mass losses achieved during the experiments under different atmospheres (Figure 5.10a), higher mass loss is observed during treatment in presence of oxygen. The corresponding first derivative plots are shown in Figure 5.10b. While during treatment in air, very close vicinity of the two peaks maxima (at 300 and 350 °C) are observed; during treatment in He two different mass losses (at 300 and above 400 °C) took place. The presence of two mass losses may correlate with the presence of two nitrogen signals as seen in the XPS analysis, which were attributed to the imidazolium cation NHCH⁺ and the carbene ligand NHC.
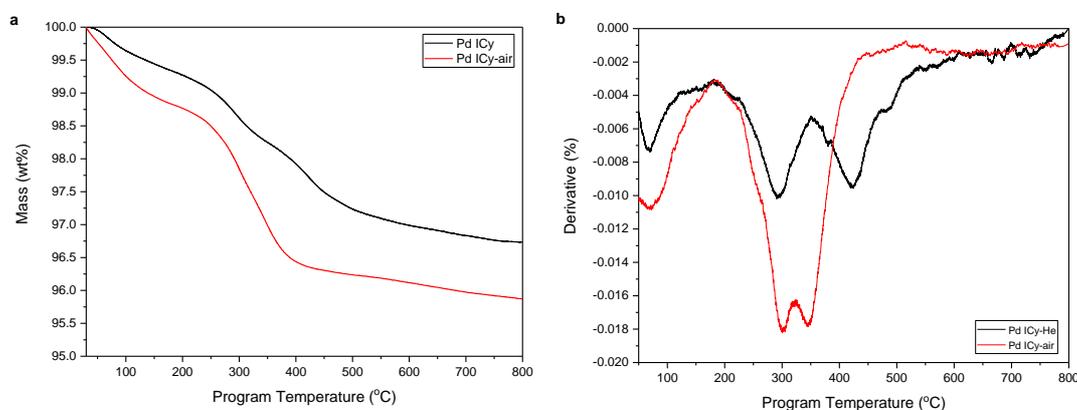
Figure 5.10 TGA mass loss (a) and first derivative (b) plots comparing the experiments performed on Pd ICy in air and in He.

Since the treatment in He leads to decomposition rather than combustion and shows better resolved mass losses, it should also be more suitable for the study of the stability (as bond strength) of the carbene interacting with the palladium catalyst. For this reason, the following TGA were performed under He flow.

In Figure 5.11 there are shown the results of the IPr modified Pd samples, bearing an increasing amount of ligand (from 2:1 to 1:10, Pd: NHC ratio).
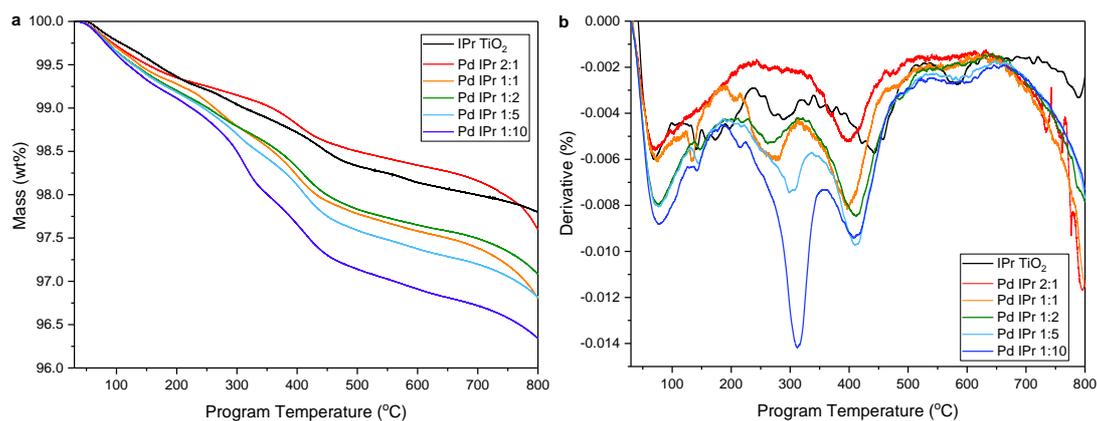
Figure 5.11 TGA mass loss and first derivative plots of the samples containing increasing amount of IPr ligand.

When comparing the first derivative plots of the Pd samples to which increasing amounts of IPr ligand were added (Figure 5.11b), it is possible to notice that the sample containing the least amount of ligand Pd IPr 2:1 shows only one peak at about 400 °C, while higher amount of ligand leads to formation of a second peak at lower temperatures (around 280 °C). It should particularly be noted that as the amount of ligand added to the catalyst increases, the peak at 280 °C becomes more intense, while the peak at 400 °C remains quite stable as os saturation has been reached. This shows that two different NHC species are at the surface of the catalyst, bonded with different strength to the metal and to the support. Therefore, it is possible to deduce that a strongly bonded NHC species, stable on the surface of the supported catalyst up to 400 °C, reaches full capacity as the amount of ligand increases. After that a less stable interaction between the NHC and the catalyst is formed, leading to thermal decomposition at around 280 °C.

Because the Pd metal loading is the same for all samples, it should be possible to hypothesise that the high temperature mass loss peak associates with the carbene ligand interacting directly with the metal nanoparticles and forming a bond stable up to 400 °C. Once the surface of the metal is saturated with the NHC, at NHC: metal ratio of 1:1 and higher, the exceeding ligand starts bounding to the support, allowing higher ligand additions, which are less stable on the surface of the samples and come off at around 300 °C. Moreover, the possible protonation of part of the NHC (as detected by XPS) might lead to species loosely bound to the surface by electrostatic interaction, which are decomposed at around 280 °C.

In the derivative plot of Figure 5.11, also the reference IPr sample added to the TiO₂ has been plotted and shows the same mass losses of the other Pd IPr modified samples. The presence of two species correlates with the presence of two nitrogen species as detected by XPS for the same sample and should suggest that NHC molecules interacts in similar ways whether there is the presence of the noble metal or not.

The mass loss and the corresponding first derivative plots of the Pd catalyst modified with variously structured NHC ligands are reported in Figure 5.12.
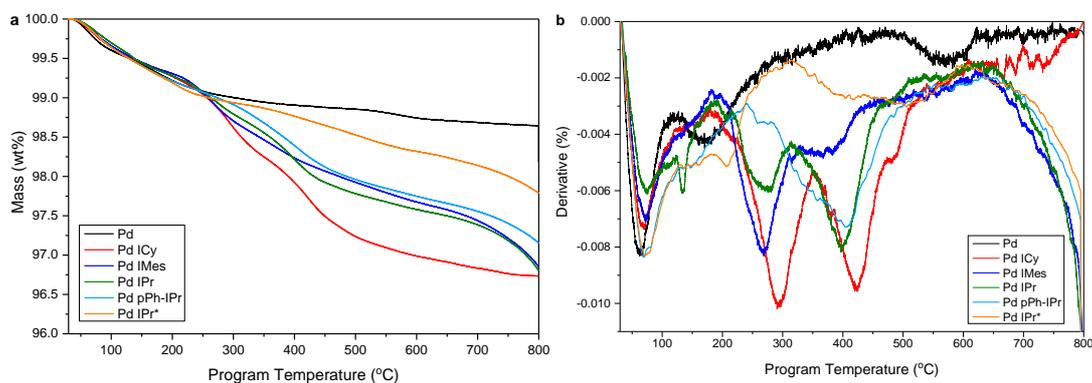
Figure 5.12 TGA mass loss and first derivative plots of the 1%Pd/TiO₂ samples containing differently structured NHC ligand.

For the ICy, IMes and IPr modified Pd samples, it is possible to see that two mass losses are occurring at comparable temperatures around 280 and 380 °C. However, for the larger *p*Ph-IPr and IPr* NHC modified samples, the derivative plots suggest a less uniform decomposition of the ligand, although its loss is taking place at high temperatures, above 380 °C. In fact, the plot assigned to *p*Ph-IPr shows a broad and asymmetric peak shape, while a very weak and broad mass loss peak of the IPr* modified sample suggests very low concentration of the added ligand.

In a similar way to the normalised nitrogen areas calculated from the XPS results (see Table 5.1), the mass loss values tabulated in Table 5.2 could be used to compare and partially quantify the differently modified Pd samples. As mentioned before, the amount of ligand added is calculated in a molar ratio to respect with the metal, while the molar weight of the carbene ligands changes depending on the substitution. Hence, in Table 5.2, the mass loss values determined by TGA were divided by the molecular weight of ligand present in the sample and defined as a normalised mass loss.

Table 5.2 Mass loss percentages from TGA and corresponding normalised values of the NHC modified 1%Pd/TiO₂ samples.

Sample	NHC MW [g/mol]	Mass loss [%]	Normalised mass loss [10^{-3}]
1%Pd/TiO₂	-	1.36	0
IPr TiO₂	388.6	2.20	14.0
PdIPr 2:1	388.6	2. 40	6.2
PdIPr 1:1	388.6	3.20	8.2
PdIPr 1:2	388.6	2.92	7.5
PdIPr 1:5	388.6	3.19	8.2
PdIPr 1:10	388.6	3.67	9.4
PdICy 1:1	232.4	3.26	14.0
PdIMes 1:1	304.4	3.15	10.4
Pd pPh-IPr 1:2	540.8	2.84	5.3
Pd IPr* 1:2	885.2	2.21	2.5

The data regarding the samples prepared adding increasing amount of IPr ligand, from 2:1 to 1:10, confirm that more ligand has actually been deposited on the palladium catalyst during modification, with a normalised mass loss increase from 6.2 to 9.4. Comparing the samples with 1:1 = NHC: Pd ratio, it is possible to notice that as the size of the ICy, IMes and IPr ligands increases, the normalised mass determined from TGA decreases, from 14.0 to 8.2, indicating that the size of the NHC affects the amount of ligand that can be actually added to the supported material. In a similar manner, by comparing the samples with 1:2 = ligand:metal ratio, IPr, pPh-IPr and IPr*, it is possible to see how the large and bulky NHCs are only present in small quantities, with normalised mass losses as low as 2.5. The bulkier the functionalisation of the 1, 3-position of the imidazolylidene ring and hence the steric hindrance of the NHC ligand, the less bonding to the surface takes place. This last consideration about the Pd IPr* sample goes also well in accordance with the low nitrogen amount as determined by XPS and the low intensity of the stretching and bending vibrations detected by IR spectroscopy.

These results seem to indicate that during addition of the ligand to the as-prepared 1% Pd/TiO₂ catalyst an incomplete ligand addition takes place, possibly due to the difficult interaction of large and hindering NHC structures with the Pd catalyst.

One of the main features of the results obtained from thermogravimetric analysis is that two species are decomposed during the treatment and this reflects the XPS analysis discussed in

Section 5.2.1.1, where the nitrogen region showed presence of two different nitrogen species. For this reason, a selective thermal decomposition of the IPr ligand from the surface of the sample was performed, at different temperatures under inert conditions, to further study and assign to specific NHC species the peaks previously observed.

5.2.1.4 Study of the stability of different NHC species at the surface

Since two NHC species are bound in different ways to the palladium catalyst, as determined not only by XPS analysis, but also by TGA, it was decided to investigate further to try assign each peak to a specific ligand speciation.

One approach was to perform two TGA heat treatments at 300 and 500 °C respectively, using the Pd IPr 1:2 sample in order to selectively eliminate the less strongly bound species detected at *ca.* 280 °C and then study the sample once both mass losses occurred.

Another approach was to determine whether the materials change upon the presence of organic solvents. In fact, because these modified Pd samples could be used as catalysts in liquid phase reactions in the presence of an organic solvent, Pd IPr 1:1 was stirred in toluene at a temperature of 40 °C for 30 min. The solid was recovered by filtration, washed with acetone and let to dry. These specific conditions were applied based on the fact that the catalytic performance of these materials would later be tested for the hydrogenation of 3-nitrostyrene, requiring these parameters.

The IR and XPS spectra of the samples before and after the heat treatments or the washing step are plotted in Figure 5.13 and 5.14 respectively.
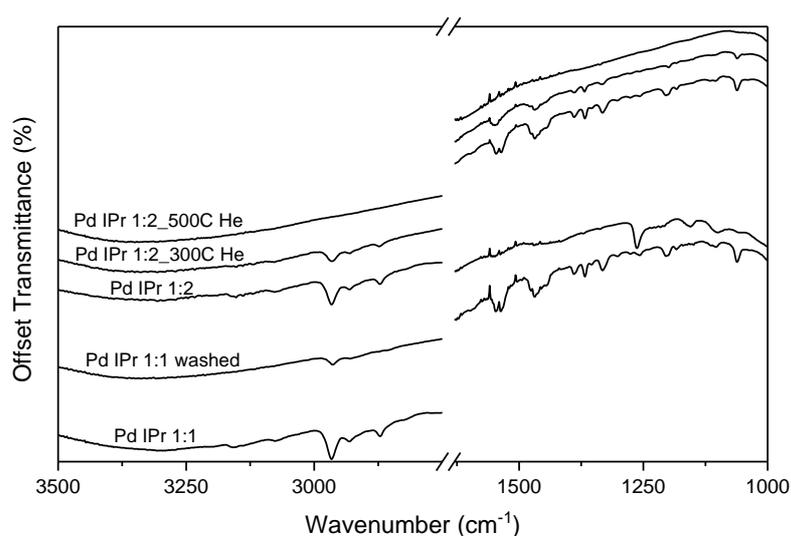
Figure 5.13 ATR-IR spectra of the 1% Pd/TiO₂ sample and of the heat treated PdIPr 1:2 samples.

The ATR-IR spectra of the Pd IPr samples after treatment at 300 °C and after being washed in toluene, still show stretching bands well comparable to the initial samples and assignable to the ligands. However, the intensity of all the signals are much decreased, suggesting that some of the NHC has either decomposed or leached, leaving less ligand present after the treatment. After the TGA at 500 °C no C-H stretching bands are visible in the ATR-IR spectrum, confirming that both the low and high temperature mass losses took place.
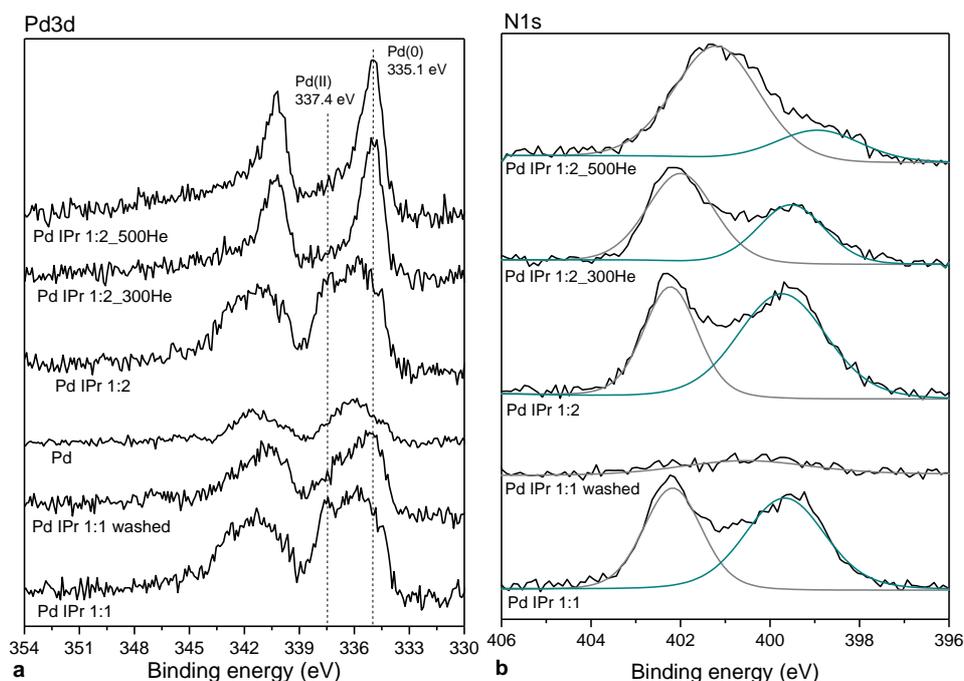
Figure 5.14 XPS spectra of the palladium and nitrogen region.

From the XPS analysis of the palladium region (data reported in Table 5.3), the amount of metal remains mostly unchanged during the stability experiments, but more interestingly an overall increase in Pd(0) component is noticed after both gas and liquid treatments (Figure 5.14a). The heat treatment in inert atmosphere leads to a strong sharpening and formation of only Pd(0), characterised by asymmetric photoelectron peaks, which occurs already after the treatment at 300 °C, with the complete disappearance of Pd(II) species.

In contrast to what was expected, the XPS analysis of the nitrogen region (Figure 5.14b) gave opposite results to the ATR-IR ones. After toluene washing, the samples show no nitrogen signal, suggesting that all the ligand has leached in the organic environment, contrary to what was detected by IR analysis. However, it is possible to confirm that the slight oxidation of the palladium as seen in the XPS spectra (as well as more in detail in Section 5.2.1.1) was due to the addition of the NHC ligand, and that once the ligand leaves the surface of the sample, the palladium XPS signal returns similar to that of the initial 1% Pd/TiO$_2$ sample.

Table 5.3 Ratios of the nitrogen peaks at 402 and 399 eV, nitrogen and palladium normalised areas of IPr modified samples treated for stability study.

Samples	N1s peaks area ratio	Normalised N1s area [10^3]	Normalised Pd3d area [10^3]
PdIPr 1:1	0.81	16.5	25.6
Pd IPr 1:1 washed	-	2.3	22.6
PdIPr 1:2	0.64	18.7	30.3
Pd IPr 1:2 300He	1.50	14.4	26.8
Pd IPr 1:2 500He	3.59	14.3	27.5

By gas chromatography coupled with mass spectrometry (GC-MS), it was possible to confirm the presence of the NHC in the toluene solution after washing, as the molecular fragment of the IPr free carbene was detected at a 388 m/z value. The inert conditions under which our collaborators work require the use of freshly-distilled, high purity solvents, to decrease the contamination and the presence of water. Dry toluene has been used by our collaborators as solvent of choice during the addition of the NHCs to the 1% Pd/TiO$_2$ catalyst. Therefore, using low purity and possibly water containing toluene during the tests performed in Cardiff, led to fast dissolution of the ligand in the liquid phase. From this is possible to conclude that the organic liquid environment dissolves the ligand in solution, not affecting the metal speciation.

The samples that underwent heat treatments at 300 and 500 °C seem to lead to a rearrangement of the nitrogen species rather than a decrease. In fact, these samples still have very comparable normalised nitrogen areas, as determined by XPS analysis and reported in Table 5.3. After the treatment at 500 °C no clear transmission bands were visible by ATR-IR, suggesting that the C-H bearing part of the IPr ligand might be decomposed during the heat treatment in He, while the nitrogen is somehow retained on the surface. The amount of nitrogen determined by XPS remains constant whether the Pd IPr 1:2 sample is heated up to 300 or 500 °C. However, the XPS signal (Figure 5.14b) changes quite substantially, with the peak at lower binding energy strongly decreasing in intensity, while the high binding energy peak broadens and shifts of almost 1 eV towards lower binding energy. Overall the spectrum of the samples treated at 500 °C shows one broad asymmetric nitrogen photoelectron peak with a maximum positioned at 401.2 eV, which is a value somehow in between the two peaks previously observed.

By coupling a temperature programmed setup with a mass spectrometer, it was possible to follow the evolution of the outlet gas, but it was not possible to detect the NHC molecular fragments as the concentration of the ligands were too low.

Overall, these behaviours seem to indicate that the ligands are strongly bound, as high temperatures are required to achieve their decomposition, however the presence of organic solvents may be detrimental, due to NHC solubility. The constant presence of nitrogen after heat treatment suggests that the ligands decompose and the functional groups of the imidazole rings are broken, leaving nitrogen species behind.

From the evidences reported in these sections, it seems possible to conclude that the carbene ligands interact in various modes to the surface of the catalysts as well as with the bare support. For this reason, it is difficult to assign a definitive speciation to each peak or signal detected by the characterisation techniques used in this study.

During this project, various NHC ligands were used, featuring increasing size. Overall, it has been observed that the size of the NHC ligand plays an important role in the interaction between the ligand and the supported metal catalyst, with smaller NHC structures more abundantly interacting with the starting material.

It should be possible to say that both, the neutral carbene and the imidazolium cation, bound to the metal nanoparticle and lead to a stronger interaction compared to the molecules bound to the support, this conclusion being drawn from the TGA analysis that shows the saturation of the mass loss at 400 °C as the ligand addition increases.

5.2.2   Catalytic testing

After discussing the characterisation of the NHC modified materials, here are reported the results of some of them for different catalytic reactions, to see whether the presence of a ligand on the metallic nanoparticle could affect the reactivity of the catalyst by blocking the active sites or facilitating reactants adsorption.

5.2.2.1 3-Nitrostyrene hydrogenation

The synthesis of ammino compounds is important because these molecules are used in the industrial production of dyes, pharmaceuticals, fertilisers and plastics.[51] As discussed in the Introduction Chapter 1 and in Chapter 3, 3-nitrostyrene (3-NS) is a model substrate used for the study of the selective hydrogenation of nitrocompounds including multiple reducible functional groups. Aiming to use pure H₂ as atom efficent reducing agent, activated by a selective heterogeneous catalyst, this field of research is of interest, since industrial production is often applying steichiometric amounts of salts mixtures, forming large amount of waste and requiring multiple purification steps.[52] Moreover, unselective reactions may lead to formation of undesired hydroxylamine compouds, which are unstable and explosive. Gold, platinum and palladium based catalysts have been reported to be active for the reduction of nitrocompounds, however achieveng

both activity, selectivity and stability is still under development.[8, 53-54] Moreover, the products selectivity during reaction can be tuned by a combination of metal, support and dispersion of the metal.[55]

The presence of both the nitrogroup and the C=C double bond on 3-NS makes it a suitable subtrate to study the selectivity of a catalyst. In Chapter 3, the study of platinum catalysts was reported, showing the favourable hydrogenation of the nitrogroup, leading to the synthesis of the desired product 3- vinylaniline (3-VA, see Figure 5.15). Palladium-based catalysts are well known to be highly active towards hydrogenation of C=C double bonds, nitro and carbonyl groups, due to their ability to coordinate the substrate through the π-system as well as to adsorb and split H_2 molecules.[8-9, 56-57]
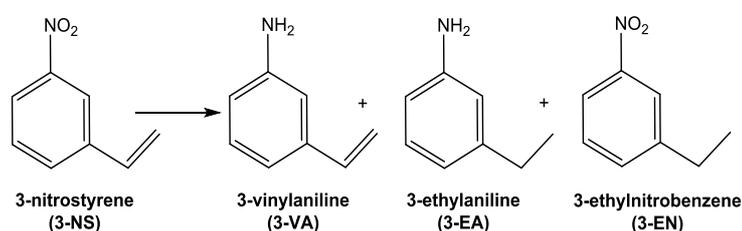
Figure 5.15 3-Nitrostyrene hydrogenation reaction scheme.

As the 1% Pd/TiO₂ catalyst was expected to be active for this reaction, in order to see whether the presence of the NHC ligands on the Pd catalyst could affect the activity or selectivity of the hydrogenation of 3-NS, the as-prepared 1% Pd/TiO₂ sample and the ICy, IMes and IPr in different ratios modified Pd catalysts were tested.

The catalytic results reported in Table 5.4 indicate that Pd was very selective in reducing preferentially the C=C double bond, forming 3-ethylnitrobenzene (3-EN)[57]. As previously experienced and discussed in Chapter 3, once 60 % 3-NS conversion has been achieved, the formation of the fully hydrogenated 3-ethylaniline (3-EA) is observed. For this reason, it is possible to say that no major variation in the selectivity are observed between the samples tested here and 3-EN is the main product.

Table 5.4 Activity and selectivity data of the 3-nitrostyrene hydrogenation reaction using NHC modified Pd catalysts.

Sample	Time (min)	3-NS Conv (%)	Selectivity (%)		
			3-VA	3-EA	3-EN
Pd	15	67	0	12	88
	30	100	0	17	83
Pd ICy	15	31	0	0	100
	30	51	0	0	100
Pd IMes	15	40	0	0	100
	30	54	0	0	100
PdIPr 2:1	15	62	0	4	96
	30	90	0	6	94
PdIPr 1:1	15	58	0	4	96
	30	89	0	8	92
PdIPr 1:2	15	65	0	5	95
	30	88	0	8	92

However, even if selectivity was comparable between catalysts, different activities were observed as reported in Figure 5.16. It is possible to notice how the smaller, more flexible and non-aromatic ICy modified palladium sample led to the strongest deactivation, while by adding bigger and planar ligands, the activity is only slightly lower than that of the as-prepared 1% Pd/TiO₂ catalyst. The catalysts modified with NHC IPr in different amounts showed only *ca.* 12 % lower conversions compared to the unmodified catalyst. Moreover, the amount of ligand (from 2:1 to 1:2, NHC: Pd ratio) did not seem to play a role.
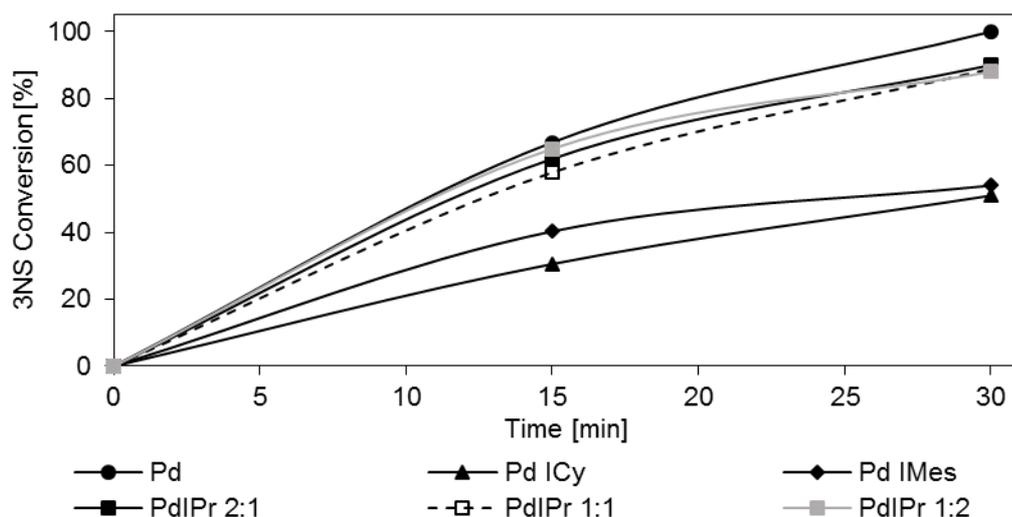
Figure 5.16 Comparison of the time-on-line data of the 3-NS hydrogenation reaction using NHC modified Pd catalysts.

In the previous Section 5.2.1.3 discussing the thermogravimetric experiments on these NHC modified catalysts, it was found that the smaller the structure of the ligand, the higher amount of it was actually attached and interacting with the material during modification. Hence, the normalised amount of ligand as determined by TGA followed the trend ICy > IMes > IPr. Therefore, it suggests that the smaller the NHC structure, the more ligand is present on the surface of the catalyst, possibly blocking reactive catalytic sites and decreasing the catalytic capacity of the initial 1% Pd/TiO₂ material that shows the highest 3-NS conversions. In addition, the Pd catalysts modified with different IPr amounts (between 2:1 and 1:2, NHC: Pd ratio) did not show strong variation in normalised thermogravimetric mass loss (between 6.2 and 8.2, see Table 5.2), which in turn, can explain the similar conversions achieved during the 3-NS hydrogenation reaction. At last, as mentioned before, the selectivity is not affected, indicating that the substrate interacts in the same way with the active site on the palladium nanoparticle, despite the presence of the ligand.

In the previous Section 5.2.1.4, washing the NHC modified Pd catalyst with toluene led to strong leaching of the ligand in solution. The 3-NS hydrogenation reaction is carried out at 40 °C using toluene as solvent, hence these results should reflect the activity of the modified catalysts before the ligands are dissolved in the reaction medium.

5.2.2.2 Hydrogen peroxide synthesis

The synthesis of H_2O_2 is of interest since low concentration of this compounds act as mild oxidant, with bleaching and disinfectant effects, giving water as decomposition product (Figure 5.17).[20, 58] It is produced in large-scale quantity via the antraquinone indirect process, however for transportation, safety and handling of high concentrated H_2O_2 solutions, a centralised industrial production is less desirable.[58] Therefore, the direct synthesis from its components H_2 and O_2 would be an ideal and cost effective solution. Palladium catalysts are active for the synthesis of

H₂O₂ from its elements, but often decomposition of the products due to instability or further hydrogenation can occur on many of these materials, leading to low selectivity and low yields.[58-59] In particular, compared to Pd(II), Pd(0) is reported to be more active in the hydrogenation of H₂O₂.[28]
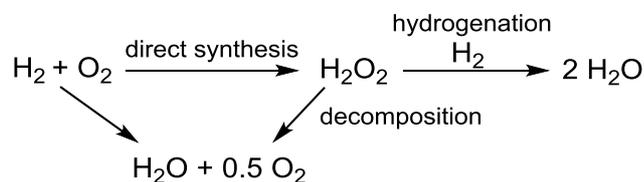
Figure 5.17 Hydrogen peroxide synthesis reaction scheme.

The addition of the NHC ligands to the metal nanoparticle could block the rather extended Pd(0) surface, considered responsible for the hydrogenation of synthesised H₂O₂ similarly to what was previously reported for the reduction of substituted benzene rings.[5]

In Section 5.2.1.1, where XPS results were discussed, it was observed how the presence of the ligand, possibly in the cationic form, could induce a shift of the Pd binding energy towards higher values, as partial oxidation of the metal occurred. However, addition of the ligand could also lead to a shielding of the nanoparticle, hindering it from the reactants, as seen for the 3-NS hydrogenation reaction.

The NHC modified 1% Pd/TiO₂ samples were tested for both the hydrogen peroxide synthesis and degradation (combined decomposition and hydrogenation) reactions. From the productivity results reported in Table 5.5, it is possible to see that the presence of the carbene ligands affected the activity of the catalyst also for this reaction.

Table 5.5 H₂O₂ synthesis reaction using NHC modified Pd catalysts.

Catalyst	H₂O₂ productivity [mol$_{H2O2}$ kg$_{cat}^{-1}$ h^{-1}]	H₂O₂ degradation [mol$_{H2O2}$ kg$_{cat}^{-1}$ h^{-1}]

1%Pd/TiO$_2$	95	362
Pd IPr 2:1	110	266
Pd IPr 1:1	127	235
Pd IPr 1:2	133	338
Pd IPr 1:5	125	268
Pd IPr 1:10	122	266
Pd ICy 1:1	110	264
Pd IMes 1:1	109	237
Pd *p*Ph-IPr 1:2	84	236
Pd IPr* 1:2	67	236

Reaction conditions: 0.01 g catalyst, 2.9 g H$_2$O, 5.6 ml MeOH, 420 psi 5 %H$_2$/CO$_2$, 160 psi 25 %O$_2$/CO$_2$, 2 °C, 1200 rpm, 30 min.

On one side, it could be noticed that increasing the amount of IPr ligand from 2:1 to 1:5 has a positive effect on the productivity, with an increase from 110 to up to 125 mol$_{H2O2}$ kg$_{cat}^{-1}$ h^{-1} respectively, while Pd IPr 1:10 sample shows a comparable productivity to the latter, if not a decrease, suggesting that the enhancement had reached a volcano top. On the other side, the unmodified 1% Pd/TiO$_2$ catalyst showed a productivity of 95 mol$_{H2O2}$ kg$_{cat}^{-1}$ h^{-1} and by adding 1:1 molar ratio of NHC ligand, as aromaticity is introduced to the system changing ligand from ICy to IPr, the amount of H$_2$O$_2$ formed is higher. At last, very sterically hindering NHC ligands such *p*Ph-IPr and IPr* added in 1:2 molar ratio, seem to mainly screen the nanoparticles and their active sites, leading to a general drop in peroxide productivity from 95 to 84 and 67 mol$_{H2O2}$ kg$_{cat}^{-1}$ h^{-1} respectively. Because from the characterisation study discussed in the previous sections is known that only a limited amount of these large ligands has actually bound to the surface of the catalyst, it may indicate that such small presence is enough to lead to a strong deactivation.

The degradation activity, determined by reacting H$_2$O$_2$ in the presence of hydrogen, and reported in the same table, does not change significantly by modifying the type and amount of NHC added to the 1% Pd/TiO$_2$ catalyst. These results evidence that only the productivity changes, without the undesired decomposition pathway being affected. The enhanced activity of the IPr modified catalysts is not coupled to a higher product decomposition, suggesting the possibility that the presence of the ligand passivates the surface of the metal as well as of the support, both known for their ability to decompose H$_2$O$_2$. In conclusion, a H$_2$O$_2$ productivity improvement is observed as more ligand is added to the as-prepared 1% Pd/TiO$_2$ catalyst, which suggests that the NHC ligands might facilitate the interaction between the reactants and the catalyst.

From the XPS analysis of the Pd region of the samples discussed in this chapter it was noticed an oxidation of the metal after addition of the NHC ligands, as well as an increase in Pd(0) contribution, possibly due to the electronic donation from the carbene carbon to the metal centre. As previously mentioned, both oxidation states are active for the production of H_2O_2, therefore it might be possible to correlate the presence with both metallic and oxidised palladium species with an improved activity.

5.3   Conclusions and further work

The possibility of synthesising heterogeneous catalysts bearing the features of homogeneous catalysts is of great advantage for improving chemical processes and manufacture. These initial steps into this new field of study has given us the chance to learn new methodologies. With the knowledge acquired during this project, we can now set a more focussed research, aiming to achieve those structure-activity relationships that are the base of our research. To do this, definite materials characteristics should be obtain by careful preparation and a specific test reaction should be used to confirm such materials features.

During this project, a series of monometallic 1% Pd/TiO₂ catalysts modified with different NHC ligands were prepared and characterised by XPS, ATR-IR and TGA. The presence of the ligand on the surface of the catalyst, both on the metallic particle as well as on the support itself was confirmed. Moreover, the ligand was found not only in the form of neutral carbene (NHC) but also protonated to form the imidazolium cation (NHCH⁺), leading to partial oxidation of the metal. The as-prepared 1% Pd/TiO₂ sample seemed to mainly undergo partial oxidation due to the protonation of the NHC ligands, however NHC-metal interaction and electron donation is also present. This can be inferred from the fact that a more defined Pd(0) component is present after ligand addition, and from thermogravimetric analysis showing saturation of a mass loss peak as the amount of ligand is increased.

These samples have been tested for different catalytic test reactions and showed interesting results for the hydrogenation of 3-NS and in the direct synthesis of H_2O_2. From the results of the former it was observed a deactivation of the catalysts as more and larger ligands were added to the initial Pd catalyst. Although a negative result, this is another indication of the direct interaction between the NHC and the nanoparticles, as the active sites are blocked. An opposite behaviour was observed for the latter test reaction, were an increase in H_2O_2 productivity was observed taking place in samples with increasing amount of IPr ligand, however similarly to the previous case, large NHC structures deactivate the catalysts, indicating that these large molecules are indeed obstructing the interaction between the reactants and the nanoparticles. A possible explanation is that small molecules such H_2 and O_2 can still reach the surface of the supported metal, whereas larger substrates find more difficulties. It should be noted that the thermal stability of the ligands

on the surface of the catalysts reached temperature as high as 400 **°C**, suggesting the possible use of these modified materials for gas phase reactions.

After this initial part of the project, we have achieved a better knowledge of the carbene-supported metal system and new approaches and structures could be studied in the future. For instance, since an electronic donation is at the basis of the interaction, the use of NHC ligands presenting strong electron donating and electron withdrawing groups could change the metal properties. These electronic modifications of the nanoparticles could potentially give a better insight into the determination of the active species for specific reactions, as well as improve the activity of inactive metals, similarly to an alloying procedure. Another approach could be that of preparing supported metal catalysts, presenting highly dispersed small metal particles (clusters or single atoms), in order to fully exploit the metal-carbene interaction and avoid loss of electronic donation due to presence of bulk metal, were electronic changes are less noticeable.

5.4 References

1.   Herrmann, W. A. N-heterocyclic carbenes: a new concept in organometallic catalysis. *Angew Chem Int Ed Engl* **2002,** *41* (8), 1290-309.

2.   Arduengo, A. J.; Harlow, R. L.; Kline, M. A stable crystalline carbene. *Journal of the American Chemical Society* **1991,** *113* (1), 361-363.

3.   Herrmann, W. A.; Köcher, C. N-Heterocyclic Carbenes. *Angewandte Chemie International Edition in English* **1997,** *36* (20), 2162-2187.

4.   Kalluri V. S. Ranganath, J. K., Andreas H. Schaefer, Frank Glorius. Asymmetric Nanocatalysis: N-Heterocyclic Carbenes as Chiral Modifiers of Fe₃O₄/Pd nanoparticles. *Angewandte Chemie International Edition in English* **2010,** (49), 7786 –7789.

5.   Johannes B. Ernst, S. M., Fei Wang, Mizuki Tada, Frank Glorius. Tunable Heterogeneous Catalysis: NHeterocyclic Carbenes as Ligands for Supported Heterogeneous Ru/K-Al₂O₃ Catalysts To Tune Reactivity and Selectivity. *Journal of the American Chemical Society* **2016,** (138), 10718−10721.

6.   Ernst, J. B.; Schwermann, C.; Yokota, G. I.; Tada, M.; Muratsugu, S.; Doltsinis, N. L.; Glorius, F. Molecular Adsorbates Switch on Heterogeneous Catalysis: Induction of Reactivity by N-Heterocyclic Carbenes. *J Am Chem Soc* **2017,** *139* (27), 9144-9147.

7.   Landon, P.; Collier, P. J.; Carley, A. F.; Chadwick, D.; Papworth, A. J.; Burrows, A.; Kiely, C. J.; Hutchings, G. J. Direct synthesis of hydrogen peroxide from H₂ and O₂ using Pd and Au catalysts. *Physical Chemistry Chemical Physics* **2003,** *5* (9), 1917-1923.

8.   Figueras, F.; Coq, B. Hydrogenation and hydrogenolysis of nitro-, nitroso-, azo-, azoxy- and other nitrogen-containing compounds on palladium. *Journal of Molecular Catalysis a-Chemical* **2001,** *173* (1-2), 223-230.

9.   Blaser, H. U.; Indolese, A.; Schnyder, A.; Steiner, H.; Studer, M. Supported palladium catalysts for fine chemicals synthesis. *Journal of Molecular Catalysis a-Chemical* **2001,** *173* (1-2), 3-18.

10.   Urbano, F. J.; Marinas, J. M. Hydrogenolysis of organohalogen compounds over palladium supported catalysts. *Journal of Molecular Catalysis a-Chemical* **2001,** *173* (1-2), 329-345.

11.   Kang, J. H.; Shin, E. W.; Kim, W. J.; Park, J. D.; Moon, S. H. Selective hydrogenation of acetylene on TiO₂-added Pd catalysts. *Journal of Catalysis* **2002,** *208* (2), 310-320.

12.   Yin, L.; Liebscher, J. Carbon-carbon coupling reactions catalyzed by heterogeneous palladium catalysts. *Chem Rev* **2007,** *107* (1), 133-73.

13.   Corma, A.; Garcia, H.; Leyva, A. Catalytic activity of palladium supported on single wall carbon nanotubes compared to palladium supported on activated carbon Study of the Heck and Suzuki couplings, aerobic alcohol oxidation and selective hydrogenation. *Journal of Molecular Catalysis a-Chemical* **2005,** *230* (1-2), 97-105.

14.   Rylander, P. *Catalytic hydrogenation over platinum metals*. Elsevier: 1967.

15.   Kakiuchi, N.; Maeda, Y.; Nishimura, T.; Uemura, S. Pd(II)−Hydrotalcite-Catalyzed Oxidation of Alcohols to Aldehydes and Ketones Using Atmospheric Pressure of Air. *The Journal of Organic Chemistry* **2001,** *66* (20), 6620-6625.

16.   Mckillop, A.; Sanderson, W. R. Sodium Perborate and Sodium Percarbonate - Cheap, Safe and Versatile Oxidizing-Agents for Organic-Synthesis. *Tetrahedron* **1995,** *51* (22), 6145-6166.

17.   Wadhwani, P.; Mukherjee, M.; Bandyopadhyay, D. The prime reactive intermediate in the iron(III) porphyrin complex catalyzed oxidation reactions by tert-butyl hydroperoxide. *J Am Chem Soc* **2001,** *123* (49), 12430-1.

18.   Ebrahimi, F.; Kolehmainen, E.; Oinas, P.; Hietapelto, V.; Turunen, I. Production of unstable percarboxylic acids in a microstructured reactor. *Chemical Engineering Journal* **2011,** *167* (2-3), 713-717.

19.   Michèle Besson, P. G. Selective oxidation of alcohols and aldehydes on metal catalysts. *Catalysis Today* **2000,** *57*, 127–141.

20.   Campos-Martin, J. M.; Blanco-Brieva, G.; Fierro, J. L. G. Hydrogen Peroxide Synthesis: An Outlook beyond the Anthraquinone Process. *Angewandte Chemie International Edition* **2006,** *45* (42), 6962-6984.

21.   Lu, X. Q.; Wu, H. H.; Jiang, J. G.; He, M. Y.; Wu, P. Selective synthesis of propylene oxide through liquid-phase epoxidation of propylene with H₂O₂ over formed Ti-MWW catalyst. *Journal of Catalysis* **2016,** *342*, 173-183.

22.   Edwards, J. K.; Hutchings, G. J. Palladium and gold-palladium catalysts for the direct synthesis of hydrogen peroxide. *Angew Chem Int Ed Engl* **2008,** *47* (48), 9192-8.

23.   Gaikwad, A. G.; Sansare, S. D.; Choudhary, V. R. Direct oxidation of hydrogen to hydrogen peroxide over Pd-containing fluorinated or sulfated Al₂O₃, ZrO₂, CeO₂, ThO₂, Y₂O₃ and Ga₂O₃ catalysts in stirred slurry reactor at ambient conditions. *Journal of Molecular Catalysis a-Chemical* **2002,** *181* (1-2), 143-149.

24.   Melada, S.; Pinna, F.; Strukul, G.; Perathoner, S.; Centi, G. Palladium-modified catalytic membranes for the direct synthesis of H₂O₂: preparation and performance in aqueous solution. *Journal of Catalysis* **2005,** *235* (1), 241-248.

25.   Burch, R.; Ellis, P. R. An investigation of alternative catalytic approaches for the direct synthesis of hydrogen peroxide from hydrogen and oxygen. *Applied Catalysis B-Environmental* **2003,** *42* (2), 203-211.

26.   Choudhary, V. R.; Sansare, S. D.; Gaikwad, A. G. Direct Oxidation of H₂ to H₂O₂ and Decomposition of H₂O₂ Over Oxidized and Reduced Pd-Containing Zeolite Catalysts in Acidic Medium. *Catalysis Letters* **2002,** *84* (1/2), 81-87.

27.   Lewis, R. J.; Hutchings, G. J. Recent Advances in the Direct Synthesis of H₂O₂. *ChemCatChem* **2019,** *11* (1), 298-308.

28.   Edwards, J. K.; Pritchard, J.; Piccinini, M.; Shaw, G.; He, Q.; Carley, A. F.; Kiely, C. J.; Hutchings, G. J. The effect of heat treatment on the performance and structure of carbon-supported Au–Pd catalysts for the direct synthesis of hydrogen peroxide. *Journal of Catalysis* **2012,** *292*, 227-238.

29.   Argo, A. M.; Odzak, J. F.; Lai, F. S.; Gates, B. C. Observation of ligand effects during alkene hydrogenation catalysed by supported metal clusters. *Nature* **2002,** *415*, 623.

30.   Choudhary, V. R.; Dhar, A.; Jana, P.; Jha, R.; Uphade, B. S. A green process for chlorine-free benzaldehyde from the solvent-free oxidation of benzyl alcohol with molecular oxygen over a supported nano-size gold catalyst. *Green Chemistry* **2005,** *7* (11), 768.

31.   Mironenko, R. M.; Belskaya, O. B.; Gulyaeva, T. I.; Nizovskii, A. I.; Kalinkin, A. V.; Bukhtiyarov, V. I.; Lavrenov, A. V.; Likholobov, V. A. Effect of the nature of carbon support on the formation of active sites in Pd/C and Ru/C catalysts for hydrogenation of furfural. *Catalysis Today* **2015,** *249*, 145-152.

32.   Liu, J. Advanced Electron Microscopy of Metal–Support Interactions in Supported Metal Catalysts. *ChemCatChem* **2011,** *3* (6), 934-948.

33.   Edwards, J.; Solsona, B.; Landon, P.; Carley, A.; Herzing, A.; Kiely, C.; Hutchings, G. Direct synthesis of hydrogen peroxide from H2 and O2 using TiO2-supported Au–Pd catalysts. *Journal of Catalysis* **2005,** *236* (1), 69-79.

34.   Enache, D. I.; Barker, D.; Edwards, J. K.; Taylor, S. H.; Knight, D. W.; Carley, A. F.; Hutchings, G. J. Solvent-free oxidation of benzyl alcohol using titania-supported gold–palladium catalysts: Effect of Au–Pd ratio on catalytic performance. *Catalysis Today* **2007,** *122* (3-4), 407-411.

35.   Dimitratos, N.; Lopez-Sanchez, J. A.; Anthonykutty, J. M.; Brett, G.; Carley, A. F.; Tiruvalam, R. C.; Herzing, A. A.; Kiely, C. J.; Knight, D. W.; Hutchings, G. J. Oxidation of glycerol using gold-palladium alloy-supported nanocrystals. *Phys Chem Chem Phys* **2009,** *11* (25), 4952-61.

36.   Qu, R.; Macino, M.; Iqbal, S.; Gao, X.; He, Q.; Hutchings, G. J.; Sankar, M. Supported Bimetallic AuPd Nanoparticles as a Catalyst for the Selective Hydrogenation of Nitroarenes. *Nanomaterials (Basel)* **2018,** *8* (9).

37.   Cuenya, B. R. Synthesis and catalytic properties of metal nanoparticles: Size, shape, support, composition, and oxidation state effects. *Thin Solid Films* **2010,** *518* (12), 3127-3150.

38.   Sankar, M.; He, Q.; Morad, M.; Pritchard, J.; Freakley, S. J.; Edwards, J. K.; Taylor, S. H.; Morgan, D. J.; Carley, A. F.; Knight, D. W.; Kiely, C. J.; Hutchings, G. J. Synthesis of stable ligand-free gold-palladium nanoparticles using a simple excess anion method. *ACS Nano* **2012,** *6* (8), 6600-13.

39.   Dorta, R.; Stevens, E. D.; Scott, N. M.; Costabile, C.; Cavallo, L.; Hoff, C. D.; Nolan, S. P. Steric and electronic properties of N-heterocyclic carbenes (NHC): a detailed study on their interaction with Ni(CO)₄. *J Am Chem Soc* **2005,** *127* (8), 2485-95.

40.   Lara, P.; Rivada-Wheelaghan, O.; Conejero, S.; Poteau, R.; Philippot, K.; Chaudret, B. Ruthenium Nanoparticles Stabilized by N-Heterocyclic Carbenes: Ligand Location and Influence on Reactivity. *Angewandte Chemie* **2011,** *123* (50), 12286-12290.

41.   Richter, C.; Schaepe, K.; Glorius, F.; Ravoo, B. J. Tailor-made N-heterocyclic carbenes for nanoparticle stabilization. *Chemical Communications* **2014,** *50* (24), 3204-3207.

42.   Moulder, J. F.; Stickle, W. F.; Sobol, P. E.; Bomben, K. D. *Handbook of X-ray Photoelectron Spectroscopy.* Perkin-Elmer Corporation: Norwalk, CT, 1992.

43.	Powell, C. J. Recommended Auger parameters for 42 elemental solids. *Journal of Electron Spectroscopy and Related Phenomena* **2012,** *185* (1-2), 1-3.

44.	Teschner, D.; Pestryakov, A.; Kleimenov, E.; Havecker, M.; Bluhm, H.; Sauer, H.; Knop-Gericke, A.; Schlogl, R. High-pressure X-ray photoelectron spectroscopy of palladium model hydrogenation catalysts. Part 1: Effect of gas ambient and temperature. *Journal of Catalysis* **2005,** *230* (1), 186-194.

45.	Kim, K. S.; Gossmann, A. F.; Winograd, N. X-ray photoelectron spectroscopic studies of palladium oxides and the palladium-oxygen electrode. *Analytical Chemistry* **2002,** *46* (2), 197-200.

46.	Crudden, C. M.; Horton, J. H.; Ebralidze, II; Zenkina, O. V.; McLean, A. B.; Drevniok, B.; She, Z.; Kraatz, H. B.; Mosey, N. J.; Seki, T.; Keske, E. C.; Leake, J. D.; Rousina-Webb, A.; Wu, G. Ultra stable self-assembled monolayers of N-heterocyclic carbenes on gold. *Nat Chem* **2014,** *6* (5), 409-14.

47.	Man, R. W. Y.; Li, C. H.; MacLean, M. W. A.; Zenkina, O. V.; Zamora, M. T.; Saunders, L. N.; Rousina-Webb, A.; Nambo, M.; Crudden, C. M. Ultrastable Gold Nanoparticles Modified by Bidentate N-Heterocyclic Carbene Ligands. *J Am Chem Soc* **2018,** *140* (5), 1576-1579.

48.	Amyes, T. L.; Diver, S. T.; Richard, J. P.; Rivas, F. M.; Toth, K. Formation and stability of N-heterocyclic carbenes in water: the carbon acid pKa of imidazolium cations in aqueous solution. *J Am Chem Soc* **2004,** *126* (13), 4366-74.

49.	Droge, T.; Glorius, F. The measure of all rings N-heterocyclic carbenes. *Angew Chem Int Ed Engl* **2010,** *49* (39), 6940-52.

50.	Ruhling, A.; Schaepe, K.; Rakers, L.; Vonhoren, B.; Tegeder, P.; Ravoo, B. J.; Glorius, F. Modular Bidentate Hybrid NHC-Thioether Ligands for the Stabilization of Palladium Nanoparticles in Various Solvents. *Angew Chem Int Ed Engl* **2016,** *55* (19), 5856-60.

51.	Song, J. J.; Huang, Z. F.; Pan, L.; Li, K.; Zhang, X. W.; Wang, L.; Zou, J. J. Review on selective hydrogenation of nitroarene by catalytic, photocatalytic and electrocatalytic reactions. *Applied Catalysis B-Environmental* **2018,** *227*, 386-408.

52.	Bellamy, F. D.; Ou, K. Selective Reduction of Aromatic Nitro-Compounds with Stannous Chloride in Non-Acidic and Non-Aqueous Medium. *Tetrahedron Letters* **1984,** *25* (8), 839-842.

53.	Corma, A.; Serna, P. Chemoselective hydrogenation of nitro compounds with supported gold catalysts. *Science* **2006,** *313* (5785), 332-4.

54.	Corma, A.; Serna, P.; Concepcion, P.; Calvino, J. J. Transforming nonselective into chemoselective metal catalysts for the hydrogenation of substituted nitroaromatics. *Journal of the American Chemical Society* **2008,** *130* (27), 8748-53.

55.	Vile, G.; Albani, D.; Almora-Barrios, N.; Lopez, N.; Perez-Ramirez, J. Advances in the Design of Nanostructured Catalysts for Selective Hydrogenation. *ChemCatChem* **2016,** *8* (1), 21-33.

56.	Sen, A.; Lai, T. W. Mechanism of palladium(II)-catalyzed carbon-carbon double bond isomerization in olefins. *Inorganic Chemistry* **1984,** *23* (20), 3257-3258.

57.	Molnár, Á.; Sárkány, A.; Varga, M. Hydrogenation of carbon–carbon multiple bonds: chemo-, regio- and stereo-selectivity. *Journal of Molecular Catalysis A: Chemical* **2001,** *173* (1-2), 185-221.

58.	Edwards, J. K.; Hutchings, G. J. Palladium and Gold–Palladium Catalysts for the Direct Synthesis of Hydrogen Peroxide. *Angewandte Chemie International Edition* **2008,** *47* (48), 9192-9198.

59.   Choudhary, V. R.; Sansare, S. D.; Gaikwad, A. G. Direct Oxidation of H2 to H2O2 and Decomposition of H2O2 Over Oxidized and Reduced Pd-Containing Zeolite Catalysts in Acidic Medium. *Catalysis Letters* **2002,** *84* (1), 81-87.

Chapter

6

Summary and conclusion

6.1   Work summary

Heterogeneous catalysts are complex structures, in which many parameters such as the choice of metal and of support, the preparation method and the particle size play an important role in the formation of the final material bearing the desired characteristics.

For long time the development of catalysts has been based on a trial and error method. Where systematic changes were applied to study, improve and design materials that were found active for specific or for group of reactions.

With the background knowledge achieved so far, and with the help of computational chemistry, nowadays the research in heterogeneous catalysis is moving towards the design of materials with desired properties based on predictions. Moreover, the ability of calculating and determining the energy profiles of a reaction using rare metal catalysts, opens up to the possibility of using alternative, cheaper and more abundant starting materials that would mimic and match the calculated energetic requirements. Otherwise, because catalysts often contain expensive rare metals, whose availability and activity should be maximised in order to minimise the presence of inactive species, achieving structure-activity correlations is of great interest for understanding how a catalyst work and use this insight knowledge for developing new materials.

On one side, a variety of experimental approaches has been attempted for improving known systems, such as minimising the particle size distribution and maximising the metal dispersion, alloying metals, using different supports or performing an activation treatment. On the other side, the outcome of the modification in the preparation of such small-scale materials requires a thorough characterisation study as well as the improvement in the techniques used, leading to the definition and establishment of new standardised procedures and patterns.

From this background, the aims of this PhD work were to investigate how the reactivity of catalytically active supported metal nanoparticles could be modified by using different strategies. And in particular to try and draw conclusions on the relationship between the structural characteristics and the observed catalytic performances. Therefore, based on previous literature, the effect that heat treatments, support characteristics and addition of ligands have on catalysts has been explored.

Gold, palladium and platinum-based supported catalysts have been prepared by the modified impregnation method and tested for both hydrogenation and oxidation liquid phase reactions. Since for each series of materials presented in the discussion Chapters 3-5 a variety of catalytic activity were found, characterisation of the materials became necessary to try and draw structure-activity correlations for the different behaviours observed.

With the help of a variety of spectroscopic and microscopic characterisation techniques, probing different aspects of a catalyst, qualitative and quantitative information were gathered, reaching a deeper understanding of the structure of the samples and in some cases allowing to find a trend between the chemico-physical characteristics of the materials and their catalytic properties.

The research work conducted during these years and presented in this thesis, has been divided into three parts. Here follows a brief summary of the work performed and the main results obtained for each of the project undertaken.

6.1.1.   Chapter 3 - Pt/TiO$_2$ catalysts for selective 3-NS hydrogenation

Inspired by the work previously reported by Corma's research group,[1] the Pt/TiO$_2$ system for the selective hydrogenation of the model compound 3-NS has been studied.

If in previous reports, the chemoselective reduction of the nitro group showed to be an issue, the focus of this work was to study the formation of the active species and improve the catalytic activity of an already highly selective catalyst.

To achieve this, a systematic study of monometallic Pt/TiO$_2$ samples with different metal loadings were prepared and activated at 450 °C, which has previously been shown to produce highly selective catalysts. However, in this project not only a reductive step, but also a combination of calcination followed by reduction at 450 °C was attempted. After catalytic testing, this series of catalysts showed to lead to a variety of intrinsic hydrogenation activities, suggesting that both the metal loading and the heat treatment induced a variation in the rate of the reduction of the NO$_2$ group. Therefore, a series of characterisation analysis such as XPS, STEM, CO chemisorption, XANES and EXAFS allowed to determine that the particle size, the platinum local environment and the metal dispersion are crucial parameters that need to be controlled.

The combination of high metal loading (0.2 and 0.5 %Pt) and reductive treatment of the as-prepared catalyst tends to lead to metal sintering, by forming rather large and inhomogeneous particles and Pt-Pt species. It is also possible that metal particle decoration occurs by the oxide support, that grows and partly covers the Pt agglomerates, however a definitive proof of that was not obtained. As a consequence, very low TOF values are achieved by these reduced materials

(up to 1380 h^{-1}). Whereas, by a combination of calcination and reduction heat treatments, clusters and nanoparticles (*ca.* 1 nm) with substantial presence of Pt-O sites and with small particle size distribution, led to extremely high hydrogenation activities (up to 5660 h^{-1}), the highest so far ever reported in literature.

As the initial metal concentration decreases (0.05 and 0.08 %Pt), good metal dispersion can easily be obtained, however leading to intermediate 3-NS turnovers (up to 4100 h^{-1}), probably due to the low amount of active metal.

The approximation of the amount of Pt peripheral and surface sites has shown to correlate well with the intrinsic activity of the samples only for the former case, confirming that the Pt-TiO$_2$ species are fundamental not only for the selectivity but also for the activity of the catalysts. Although the close vicinity of the metal and the support, in the form of Pt-O sites, favours the catalytic performance, a reductive step leading to Pt(0) is required in order to observe any substrate conversion.

Therefore, during this project it was possible to determine that the quantity of the metal used during impregnation and the activation step are crucial parameters that need to be taken into consideration in order to achieve not only the most active catalyst, but also the most metal efficient one. A delicate balance between metal loading and heat treatment has been found, shining more light on the structure-activity relationship present in this system.

Future work

Even if substantial testing, characterisation and study was required for these materials, to allow the understanding of the behaviour of the catalytic system, there are still some questions that could be addressed and explore in the future.

Although these Pt catalysts have shown to be extremely active and highly selective for the hydrogenation of 3-NS, they were not reusable after recovery from the reaction medium, therefore these issue should be addressed as to improve and attempt to optimise the whole process. To do this, a new recovery procedure might be developed, in order to maintain – unchanged- the active species. Otherwise, a re-activation procedure step could be tried in order to re-gain the initial activity.

Since the most active 0.2 %Pt/TiO$_2$ calcined and reduced catalyst could reach exceptionally high TOF, another approach could be to keep the catalyst in the reaction environment and study how it would perform if tested in a flow reactor.

The effect of the support in this catalytic system is known to affect not only the activity but also the product selectivity, with the choice of TiO$_2$ being beneficial as it suppresses the formation

of hydroxylamines.[1] Because the interaction between the metal oxide and the supported metal has shown to be fundamental for the enhancement in catalytic performance, it would be of interest to study the effect of other metal oxides, reducible like CeO_2 and not reducible like Al_2O_3, as well as inert materials like carbon.

Environmental, health, safety and economic issues are crucial points that should be taken under consideration when developing a potentially industrially relevant process. Reactions were performed under mild conditions of temperature and pressure, however the use of a less harmful solvent than toluene, such as ethanol, would be highly desirable. Moreover, use of a cheaper and readily available metal, would be advantageous and highly desirable. For example, after high temperature treatment, also Ni has been found active for the hydrogenation of 3-NS, which could be worth further exploring.

In previous literature, the different Pt site present on the surface of Pt/TiO_2 catalysts were investigated by mean of IR spectroscopy using CO as probe molecule. This work could use such insight knowledge and CO DRIFT technique could be applied.

In-situ and *in-operando* characterisation techniques are a developing field in catalysis because great insight knowledge can be obtained by study a process while it takes place. Following the interactions of molecules during a reaction or the changes occurring during formation of a material allow to obtain fundamental information. Therefore, it would be challenging but interesting to study how the structure develops and what kind of modification undergoes the 0.5 %Pt/TiO_2 during reduction at 450 °C, compared to the sample undergoing calcination and then reduction under the same conditions.

6.1.2. Chapter 4 – HTCs as support for AuPd nanoparticles

The focus of the work discussed in Chapter 4 has been the study of the effect of a variety of hydrothermal carbons (HTC) as supports for bimetallic AuPd catalysts.

A large amount of literature is available already where the use of biomass feedstocks is applied for the synthesis of carbon materials to be used in various fields. Tailored materials with porous structures can be prepared by a simple and environmentally friendly process. The characteristics of the final material can be tuned by modifying the synthesis process, making it an appealing method to achieve the desired material.[2]

However, so far, little has been reported on the use of hydrothermal carbons to be used as support for metal nanoparticles. The collaborators in this project, supplied us with a variety of HTCs synthesised by a solvothermal process by use of sugars as carbon source. By modification of the synthesis conditions, the final material could achieve different characteristics.

Alloying two metals, to form bimetallic nanoparticles has been shown to lead to improved reactivity compared to the monometallic counterparts. This has been the case of AuPd supported catalyst for the selective oxidation of glycerol in basic aqueous medium. For this same reaction, multiple studies have reported to use carbon as support of choice.[3] Because the metal nanoparticles and the support are in close contact, the structure of the latter can influence the characteristic of the former. Hence, the study of the effect of different carbons on the final activity of AuPd catalysts was attempted.

Multiple series of 0.5% AuPd/HTC (1:1, mol: mol) catalysts were prepared by the modified impregnation method and tested for the glycerol oxidation reaction with addition of base. Although the products selectivity showed to be extremely comparable between the samples, a large variety in glycerol conversions was observed. This behaviour suggests that the substrate interacts with the catalyst and the reactants in a similar fashion in all cases, leading to the same proportion of products, however some catalysts show a higher affinity to glycerol adsorption and products desorption, leading to higher reaction turnovers and improved glycerol conversions. To try correlate the activity with the structure of the various supported samples, elemental analysis, XPS, XRD, SEM and N_2 physisorption experiments were used to characterise the catalysts.

From the variety of samples taken into consideration it was possible to draw some conclusions that follow.

By SEM extremely large metal agglomerates were detected, the presence of which were confirmed by XRD particle size analysis. From XPS analysis all the metal nanoparticles were found to be composed of Au and Pd in the metallic form and information on the metal dispersion could qualitatively be obtained. It has been noticed that the size of the nanoparticles did not directly correlate with the catalytic activity. In addition, the surface area of the supports, which usually relates to the possible dispersion of the deposited metal, and hence to its exposure and availability, did not show an effect of the glycerol conversion. Both these features suggest that the reaction is either not particle size dependant, or that there are catalytically active species not detectable by XRD, but partly quantifiable by XPS.

Overall, the results and trends observed from testing the AuPd/HTC catalysts showed an agreement with previous literature. For example, catalysts supported on HTCs bearing substantial amount of oxygen in their structures showed to lead to lower glycerol conversions and the reason for this has been ascribed to the acidity that the oxygen-containing functional groups bring to the material, leading to a possible modification of the electrons movement during reaction.

The increasing glycerol conversions for catalysts supported on HTCs formed of smaller carbon spheres, suggested that the surface roughness and the proportion of carbon sheets exposed

affect the activity of the supported metal species, by applying strain and by affecting the faceting of the nanoparticles.

To assess the stability of the catalysts, reusability tests were performed, revealing that the catalysts could be easily recovered by a simple method and reused for up to 3 times, showing almost no loss in glycerol oxidation activity, nor in metal content.

Future work

The HTC supported AuPd catalysts showed a variety of catalytic activities, some of which led to considerable glycerol conversion during the reaction time. Because the presence of base is known to enhance the formation of the oxidation products, it would be of interest to test these catalysts for the glycerol oxidation without addition of base.

The utilisation of HTC materials as catalyst supports has not yet been largely exploited, but the materials discussed in Chapter 4 have overall shown to be valuable as potential support of choice. However, further testing for different catalytic reactions is required in order to establish the applicability of these materials in a wider range of processes.

One of the appealing features of commercial carbon materials is their high surface area, which comprehends also large presence of microporosity. Quite unexpectedly, many of the HTCs samples discussed here revealed extraordinary low surface areas, hence the study focussed on those preliminary results. However, now that a deeper insight has been achieved about HTCs, a detailed study of the pore structure could be of interest.

In the discussion Chapter 4, the charge of the carbon supports in solution was questioned multiple times as responsible for the variation in glycerol conversion during oxidation reactions, therefore the determination of the isoelectric point could shine a light on the state of the surface of the HTCs in the reaction medium.

6.1.3. Chapter 5 - NHC modified Pd/TiO$_2$ catalysts

On one hand, NHCs comprise a group of compounds featuring variability in both structural and electronic characteristics. They are ligands largely used in organometallic chemistry for a wide variety of reactions.[4] On the other hand, supported Pd/TiO$_2$ catalysts have shown to be stable and reactive for a range of reactions.

In recent years, NHCs have been reported to be potential modifiers of supported metal nanoparticles, being able to enhance the activity and direct the selectivity towards the desired products in catalytic reactions.[5] Therefore, the intent and aims of the work discussed in Chapter 5 were to investigate the effect of the presence of NHC ligands on the surface of Pd nanoparticles

supported on TiO_2. Another focus of the project has been the determination of the stability of the ligands on the surface of the samples, under thermal and reaction conditions as well as in the absence of controlled storage conditions.

NHCs have been synthesised by collaborators and used to decorate Pd nanoparticles supported on TiO_2. The resultant samples were characterised by means of XPS, TGA and ATR-IR techniques and tested for the hydrogenation of 3-NS and for the direct synthesis of H_2O_2.

The combination of characterisation techniques confirmed the addition of the NHCs on the Pd/TiO_2 catalyst. In particular, the results obtained from both XPS and TGA analysis detected the presence of two species, suggesting that the NHC ligands are existing on the sample in both free carbene and protonated imidazolium cation forms.

Moreover, the XPS analysis of the NHC modified Pd samples showed presence of both Pd(0) and Pd(II) species, which suggests that the carbene interacts with the metal nanoparticle donating electron density, whereas the cationic NHC leads to a partial oxidation.

From TGA analysis, the NHC-Pd system has been found to be thermally stable upon thermal treatment in inert conditions up to 200 °C, with the second temperature mass loss at *ca.* 380 °C. In particular, the two mass losses were assigned to the protonated (low temperature) and to the neutral carbene (high temperature) decomposing from the surface. Further TGA data analysis allowed to determine that the smaller the structure of the NHC, the higher the amount of ligand actually present on the sample. On the contrary, the ligands seem to easily leave the surface once the samples are added to the liquid reaction solutions. Therefore it might be preferable to study these materials in gas phase reactions.

The modifications have found to directly affect the reactivity of these NHC-Pd catalysts. On one side the presence of the ligands leads to a decrease in 3-NS conversions, with stronger deactivation the larger the structure of the ligand, suggesting a block of the reactive metal surface.

On the other side, the presence of ligands was able to enhance the H_2O_2 productivity, a possible reason behind this being the presence of both the Pd(0) and Pd(II) components.

Future work

During this project an initial assessment and understanding of the NHC-supported metal system has been developed. However from here some points and explanation remain open as future research interests.

One main unclear fact that would require further exploring is the origin and formation of the imidazolium cation. XPS and TGA analysis were performed in close vicinity to the arrival of the

samples, but a repetition of the analysis at various length of time could show how the two carbene species develop over time.

In this field of study a very common analysis useful for the detection of the carbene-metal bond is ^{13}C-NMR. This could be applied for these samples, not only to compare previous works, but also to see if the presence of the imidazolium salt can be confirmed by solid state ^{13}C-NMR.

The evident instability of the NHC on the surface of the Pd/TiO$_2$ catalyst in toluene indicated the loss of the ligand during reaction. Hence, a more in depth and systematic study of the dissolution of the NHCs under reaction conditions and with use of different solvents and temperatures would allow to assess which are the possible conditions under which to study and test these modified catalysts.

6.2 References

1. Corma, A.; Serna, P.; Concepcion, P.; Calvino, J. J. Transforming nonselective into chemoselective metal catalysts for the hydrogenation of substituted nitroaromatics. *Journal of the American Chemical Society* **2008,** *130* (27), 8748-53.

2. Titirici, M.-M.; Antonietti, M. Chemistry and materials options of sustainable carbon materials made by hydrothermal carbonization. *Chem Soc Rev* **2010,** *39* (1), 103-116.

3. Carrettin, S.; McMorn, P.; Johnston, P.; Griffin, K.; Kiely, C. J.; Hutchings, G. J. Oxidation of glycerol using supported Pt, Pd and Au catalysts. *Physical Chemistry Chemical Physics* **2003,** *5* (6), 1329-1336.

4. Matthew N. Hopkinson, C. R., Michael Schedler, Frank Glorius. An overview of N-heterocyclic carbenes. *Nature* **2014,** *510*, 485-496.

5. Johannes B. Ernst, S. M., Fei Wang, Mizuki Tada, Frank Glorius. Tunable Heterogeneous Catalysis: NHeterocyclic Carbenes as Ligands for Supported Heterogeneous Ru/K-Al$_2$O$_3$ Catalysts To Tune Reactivity and Selectivity. *Journal of the American Chemical Society* **2016,** (138), 10718−10721.